ERDC/CHL TR-15-13

US Army Corps
of Engineers®
Engineer Research and
Development Center

ERDC
INNOVATIVE SOLUTIONS
for a safer, better world

# Point Judith, Rhode Island, Breakwater Risk Assessment

Jeffrey A. Melby, Norberto C. Nadal-Caraballo,
and John Winkelman

August 2015


Coastal and Hydraulics Laboratory

# Report Documentation Page

*Form Approved*
*OMB No. 0704-0188*



| 1. REPORT DATE | 2. REPORT TYPE | 3. DATES COVERED |
|---|---|---|
| **AUG 2015** | | **00-00-2015 to 00-00-2015** |

| 4. TITLE AND SUBTITLE | 5a. CONTRACT NUMBER |
|---|---|
| **Point Judith, Rhode Island, Breakwater Risk Assessment** | 5b. GRANT NUMBER |
| | 5c. PROGRAM ELEMENT NUMBER |
| 6. AUTHOR(S) | 5d. PROJECT NUMBER |
| | 5e. TASK NUMBER |
| | 5f. WORK UNIT NUMBER |
| 7. PERFORMING ORGANIZATION NAME(S) AND ADDRESS(ES) **Coastal and Hydraulics Laboratory,,U.S. Army Engineer and Development Center,,3090 Halls Ferry Road,,Vicksburg,,MS, 39180** | 8. PERFORMING ORGANIZATION REPORT NUMBER |
| 9. SPONSORING/MONITORING AGENCY NAME(S) AND ADDRESS(ES) | 10. SPONSOR/MONITOR'S ACRONYM(S) |
| | 11. SPONSOR/MONITOR'S REPORT NUMBER(S) |

12. DISTRIBUTION/AVAILABILITY STATEMENT
**Approved for public release; distribution unlimited**

13. SUPPLEMENTARY NOTES

14. ABSTRACT

**Point Judith breakwaters were built between 1891 and 1914. Three structures provide shelter for refuge, search and rescue operations, a commercial harbor, and a sandy, recreational shoreline. The Main breakwater is presently in a severely damaged state, and its functional efficiency compared to the as-built condition is unknown. This report provides a summary of a life-cycle risk assessment of the Point Judith Main breakwater. The report summarizes the Point Judith breakwater history, the present condition, the historical offshore wave climate in the area, nearshore wave and water level climate, probabilistic characteristics of the historical wave and water level climate, simulated breakwater damage and wave overtopping transmission, and resulting wave climate in the protected bay. Future sea level rise and its implications on structure performance are analyzed. Several rehabilitation alternatives are designed and then subjected to life cycles of storms with and without sea level rise. The results of the life-cycle study are discussed in the context of the future performance with and without rehabilitation.**

15. SUBJECT TERMS

| 16. SECURITY CLASSIFICATION OF: | | | 17. LIMITATION OF ABSTRACT | 18. NUMBER OF PAGES | 19a. NAME OF RESPONSIBLE PERSON |
|---|---|---|---|---|---|
| a. REPORT | b. ABSTRACT | c. THIS PAGE | | | |
| **unclassified** | **unclassified** | **unclassified** | **Same as Report (SAR)** | **188** | |

**The U.S. Army Engineer Research and Development Center (ERDC)** solves the nation's toughest engineering and environmental challenges. ERDC develops innovative solutions in civil and military engineering, geospatial sciences, water resources, and environmental sciences for the Army, the Department of Defense, civilian agencies, and our nation's public good. Find out more at www.erdc.usace.army.mil.

To search for other technical reports published by ERDC, visit the ERDC online library at http://acwc.sdp.sirsi.net/client/default.

ERDC/CHL TR-15-13
August 2015

# Point Judith, Rhode Island, Breakwater Risk Assessment

Jeffrey A. Melby and Norberto C. Nadal-Caraballo

*Coastal and Hydraulics Laboratory*
*U.S. Army Engineer Research and Development Center*
*3909 Halls Ferry Road*
*Vicksburg, MS 39180-6199*

John Winkelman

*U.S. Army Engineer District, New England*
*CENAE-EP-WM*
*696 Virginia Road*
*Concord, MA 01742-2751*

Final report



Prepared for U.S. Army Engineer District, New England
696 Virginia Road
Concord, MA 01742-2751

# Abstract

Point Judith breakwaters were built between 1891 and 1914. Three structures provide shelter for refuge, search and rescue operations, a commercial harbor, and a sandy, recreational shoreline. The three breakwaters consist of the offshore Main breakwater and two shore-connected breakwaters, all built as conventional multilayered rubble mound structures. The breakwaters have been rehabilitated a number of times, with the last construction in 1984. The Main breakwater is presently in a severely damaged state, and its functional efficiency compared to the as-built condition is unknown. This report provides a summary of a rigorous life-cycle analysis of the Point Judith Main breakwater. The study was conducted during the period 2011–2014 by the U.S. Army Engineer Research and Development Center, Coastal and Hydraulics Laboratory, Vicksburg, MS, in cooperation with the U.S. Army Engineer District, New England. The report summarizes the Point Judith breakwater history, the present condition, the historical offshore wave climate in the area, nearshore wave and water level climate, probabilistic characteristics of the historical wave and water level climate, simulated breakwater damage and wave overtopping transmission, and resulting wave climate in the protected bay. Future sea level rise and its implications on structure performance are analyzed. Several rehabilitation alternatives are designed and then subjected to life cycles of storms with and without sea level rise. The results of the life-cycle study are discussed in the context of the future performance with and without rehabilitation.

# Contents

# Figures and Tables

## Figures

## Tables

# Preface

The study summarized in this report was conducted at the request of the New England District (NAE), U.S. Army Corps of Engineers (USACE). John Winkelman was the primary engineering point of contact at NAE, and Michael Walsh was the Program Manager at NAE. The Economics lead was Janet Patev. The portion of the study reported herein was funded by NAE and primarily conducted at the Engineering Research and Development Center (ERDC), Coastal and Hydraulics Laboratory (CHL), Vicksburg, MS, during the period January 2011–May 2014.

This report was prepared by Dr. Jeffrey A. Melby and Dr. Norberto Nadal-Caraballo, Harbors, Entrances, and Structures (HES) Branch, CHL, and Winkelman, USACE District, New England.

Drs. Melby and Nadal-Caraballo were under the general supervision of Dr. Donald Ward, Acting Chief, HES Branch. HES Branch was under the general supervision of Dr. Jackie Pettway, Chief, Navigation Division. José E. Sánchez was Director, CHL, and Dr. Kevin Barry was Deputy Director, CHL.

At the time of publication, LTC John T. Tucker III was the Acting Commander of ERDC. Dr. Jeffery P. Holland was Director.

# Unit Conversion Factors

A sponsor requirement for this study was the use of English Customary units of measurement. Most measurements and calculations were done in International System (SI) units and then converted to English Customary. The following table can be used to convert back to SI units.

| Multiply | By | To Obtain |
|---|---|---|
| feet | 0.3048 | meters |
| cubic feet | 0.02831685 | cubic meters |
| pounds (force) | 4.448222 | newtons |
| square feet | 0.09290304 | square meters |

# 1 Introduction

## 1.1 Background

This report provides a life-cycle analysis of the Point Judith Main breakwater. The study was conducted during 2011–2014 by the NAE, with a majority of the modeling outlined herein conducted by the ERDC, CHL. This report summarizes the Point Judith breakwater history, the present condition, the historical offshore wave and water level climate in the area, nearshore wave and water level climate, joint probabilistic characteristics of the historical wave and water level climate, simulated breakwater damage and wave overtopping transmission, and resulting wave climate in the sheltered bay. The implications of sea level rise are analyzed. Several alternative breakwater rehabilitations are designed and then subjected to life cycles of storms with and without sea level rise to assess their reliability and functional performance. Finally, the results of the life-cycle study are discussed in the context of the future performance with and without rehabilitation.

## 1.2 Point Judith breakwater history

Between 1891 and 1914, three rubble mound breakwaters were constructed to provide a sheltered area for a harbor of refuge (HoR) south of Point Judith, RI (Figures 1 and 2). The 6,970-foot (ft)-long, L-shaped Main breakwater was constructed offshore. The two other structures were the 3,640 ft long West Shore Arm and the 2,240 ft long East Shore Arm. The structures had variable slopes and crown widths (Figure 4). Structure repair began before the structures were completed, and repairs were made periodically through 1950, primarily to the east arm of the Main breakwater and the East Shore Arm breakwater. The rehabilitation in 1950 included armor stone weights of 1–6 tons, stone quantity of 19,090 tons, crest elevation of 10 ft mean lower low water (mllw), crest width of 20 ft, seaside slope of 1 vertical:2 horizontal (1V:2H), and leeside slope of 1V:1H. A rehabilitation in 1961–1963 had the following characteristics: stone weight = 12–15 tons, stone quantity = 119,000 tons, crest elevation = 10 ft mllw, crest width = 20 ft, seaside slope = 1V:2H, and leeside slope = 1V:1H. A rehabilitation in 1983–1984 had the following characteristics: stone weight = 12–15 tons, stone quantity = 20,275 tons (including new stone and reset old stone), crest elevation = 10 ft mllw, and crest width = 20 ft. The contract

Figure 1. Regional map.

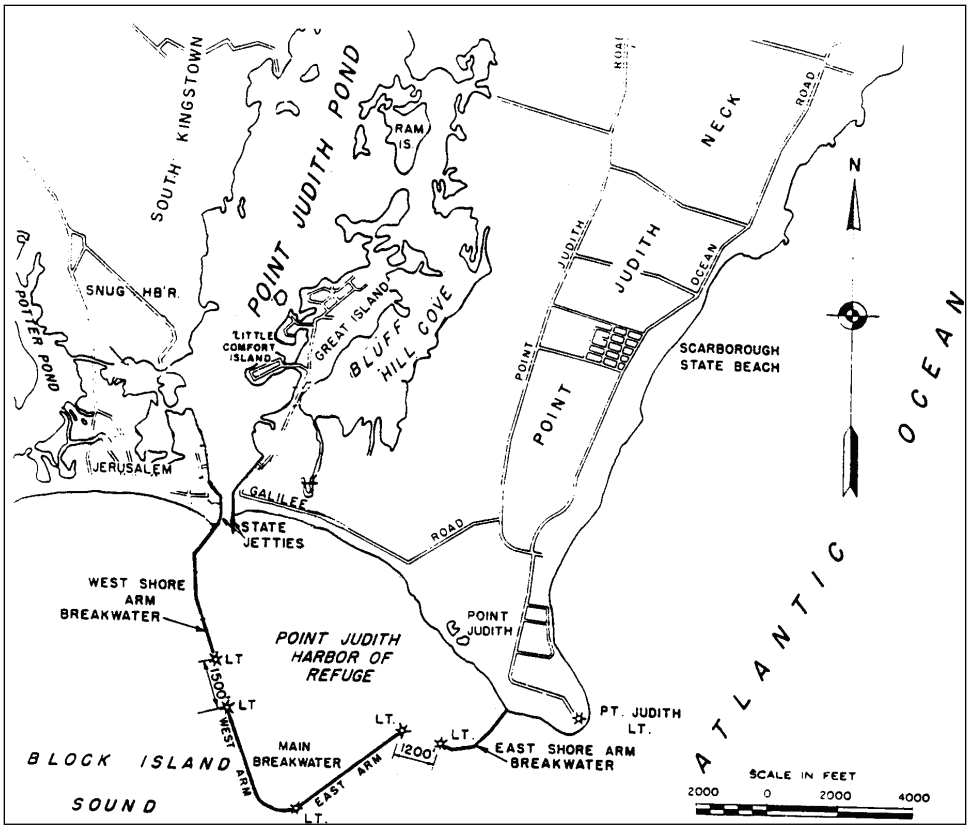


Figure 2. Regional aerial photograph from CorpsGlobe.

called for placing 57,600 tons of stone, but the contractor defaulted, and rehabilitation was not completed. The rehabilitation characteristics included the following:

Sta 0+00 to 20+34: seaside slope = 1V:1.5H; leeside slope = 1V:1.5H

Sta 20+34 – 67+25: seaside slope = 1V:2H; leeside slope = 1V:2H

Main breakwater stationing is shown in Figure 3. Note that Sta 0+00 is at the north end of the west leg of the Main breakwater while station 67+25 is at the east end of east arm. The majority of the Main breakwater was constructed with side slopes of 1V:2H. The original design cross sections are shown in Figure 4 while the 1984 rehabilitation sections are shown in Figure 5. The armor stone conditions for the 1984 repair are listed in Table 1, referenced to mean sea level (MSL).

Figure 3. Approximate stationing for Main breakwater. West leg is 0+00 – 22+00, bend is 22+00 – 34+00, and east leg is 34+00 – 67+00.

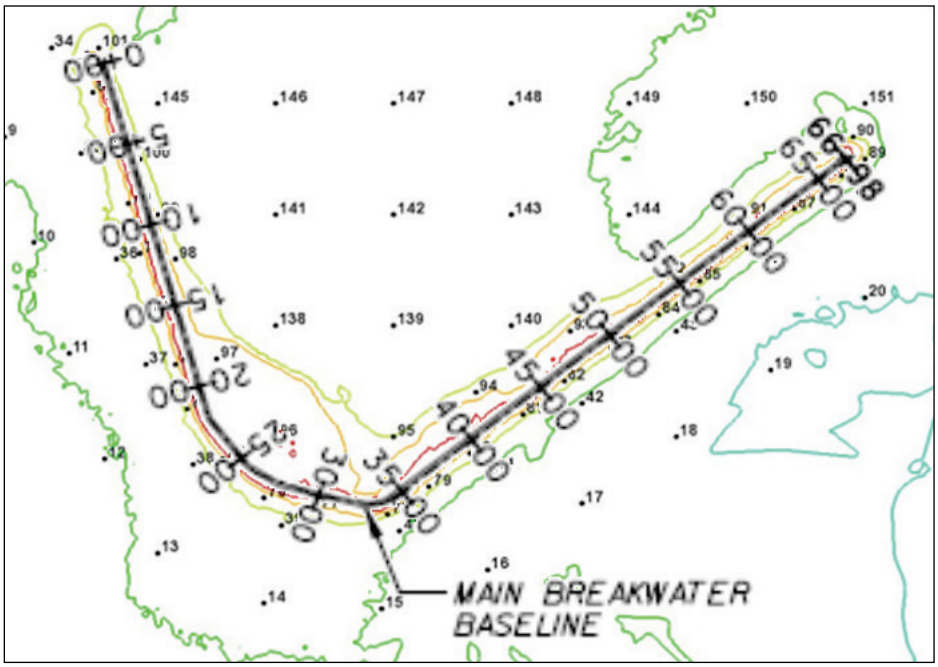

Figure 4. Original as-built cross sections.

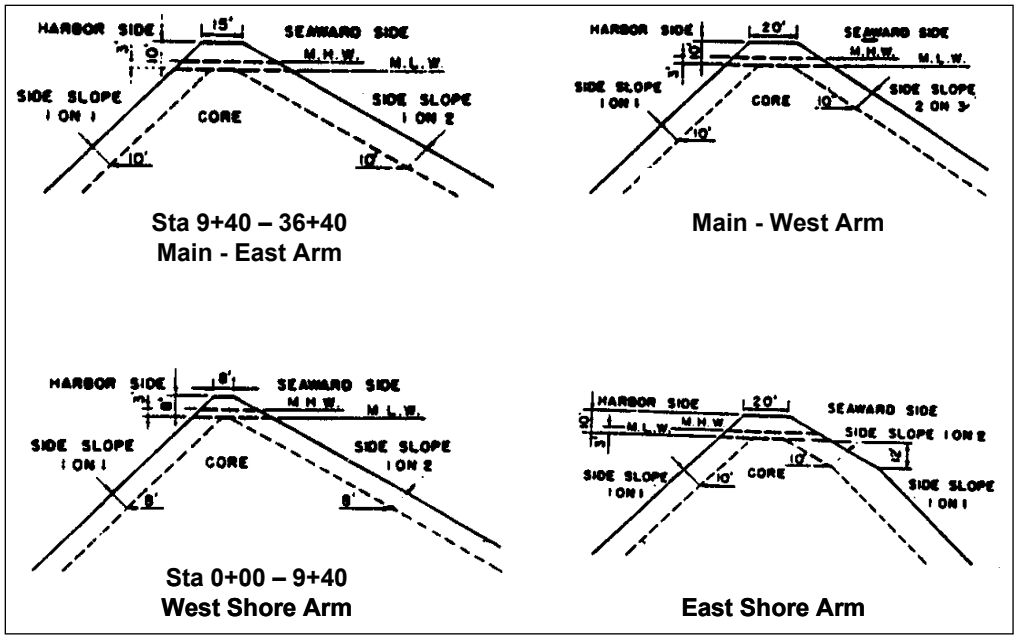


Figure 5. 1984 rehabilitation cross sections of Main breakwater.

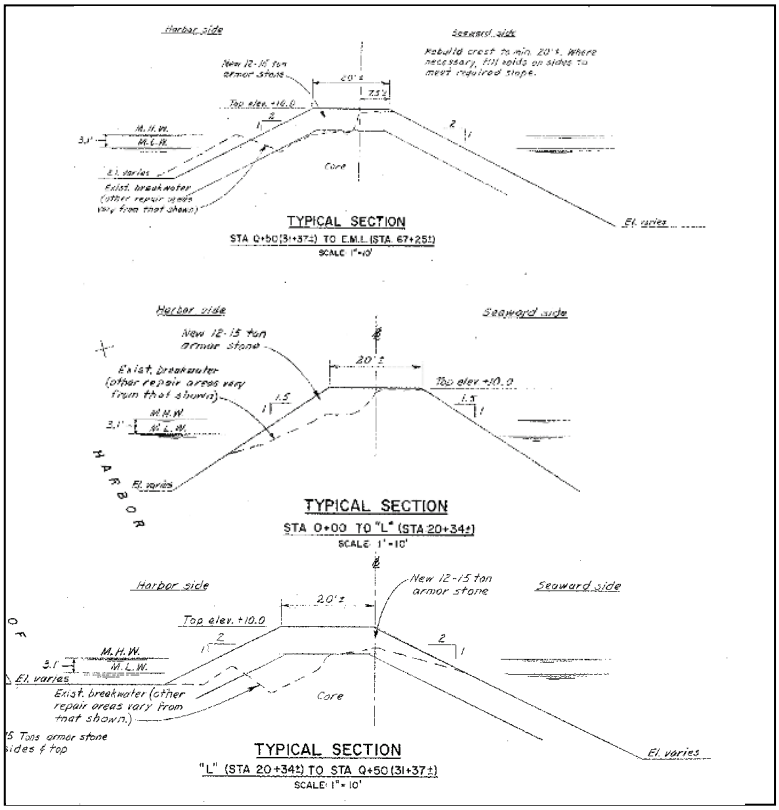

Table 1. Rehabilitation in 1984 as-built section properties for 500 ft reaches.

| Reach | Start, ft | End, ft | Beginning Crest Height, ft, MSL | Beginning Crest Width, ft | Seaside Slope | Leeside Slope | Armor Stone Size, ton | Wave Input Station | Depth, ft, MSL |
|---|---|---|---|---|---|---|---|---|---|
| 1 | 0 | 5+00 | 8.26 | 20 | 1.5 | 1.5 | 13.5 | 35 | 22.9 |
| 2 | 5+00 | 10+00 | 8.26 | 20 | 1.5 | 1.5 | 13.5 | 36 | 21.2 |
| 3 | 10+00 | 15+00 | 8.26 | 20 | 1.5 | 1.5 | 13.5 | 36 | 21.2 |
| 4 | 15+00 | 20+00 | 8.26 | 20 | 1.5 | 1.5 | 13.5 | 37 | 22.9 |
| 5 | 20+00 | 25+00 | 8.26 | 20 | 2.0 | 2.0 | 13.5 | 38 | 22.2 |
| 6 | 25+00 | 30+00 | 8.26 | 20 | 2.0 | 2.0 | 13.5 | 39 | 20.6 |
| 7 | 30+00 | 35+00 | 8.26 | 20 | 2.0 | 2.0 | 13.5 | 39 | 20.6 |
| 8 | 35+00 | 40+00 | 8.26 | 20 | 2.0 | 2.0 | 13.5 | 40 | 27.7 |
| 9 | 40+00 | 45+00 | 8.26 | 20 | 2.0 | 2.0 | 13.5 | 41 | 30.6 |
| 10 | 45+00 | 50+00 | 8.26 | 20 | 2.0 | 2.0 | 13.5 | 42 | 31.2 |
| 11 | 50+00 | 55+00 | 8.26 | 20 | 2.0 | 2.0 | 13.5 | 43 | 31.6 |

The east leg of the Main breakwater is presently in a severely damaged condition as shown in Figures 6 and 7. Figures 8–16 show cross sections spaced at 200 ft along the entire breakwater, obtained from a lidar survey conducted in March 2010. The only profiles near the original design crest elevation of 10 ft mllw (8.26 MSL) are on the west and east ends. The remainder of the structure shows significant damage with shallower slopes on the seaside and leeside, narrowed crest widths, lowered crest elevations, and significant debris accumulation on the leeside. On much of the east leg, the crest has been translated shoreward as well. The maximum elevations of all profiles plotted in Figures 8–16 are listed in Table 2.

To determine characteristic crest elevations for reaches, the maximum elevations every 20 ft along the breakwater were sampled, and these are plotted in Figure 17. The average of the top five maximum points were averaged along uniform 200 ft long reaches in order to define characteristic reach elevations, and these are also plotted in Figure 17. The green line (higher) shows the results of averaging the top five points along each 500 ft reach. The orange line shows the results of computing the average + standard deviation of all points in each 500 ft reach. After comparing these characteristic surfaces to the breakwater, it was found that the green surface best characterizes the breakwater crest elevation, and it is used to describe reach crest elevations when evaluating structure performance.

Figure 6. Recent aerial photograph of Main breakwater.

Figure 7. Close-up photograph of damaged section on Main breakwater.

Figure 8. Condition in 2010 of profiles of Stations 16, 18, and 20 with leeside on left and seaside on right. Elevations are in feet relative to mllw, and stationing is in feet.

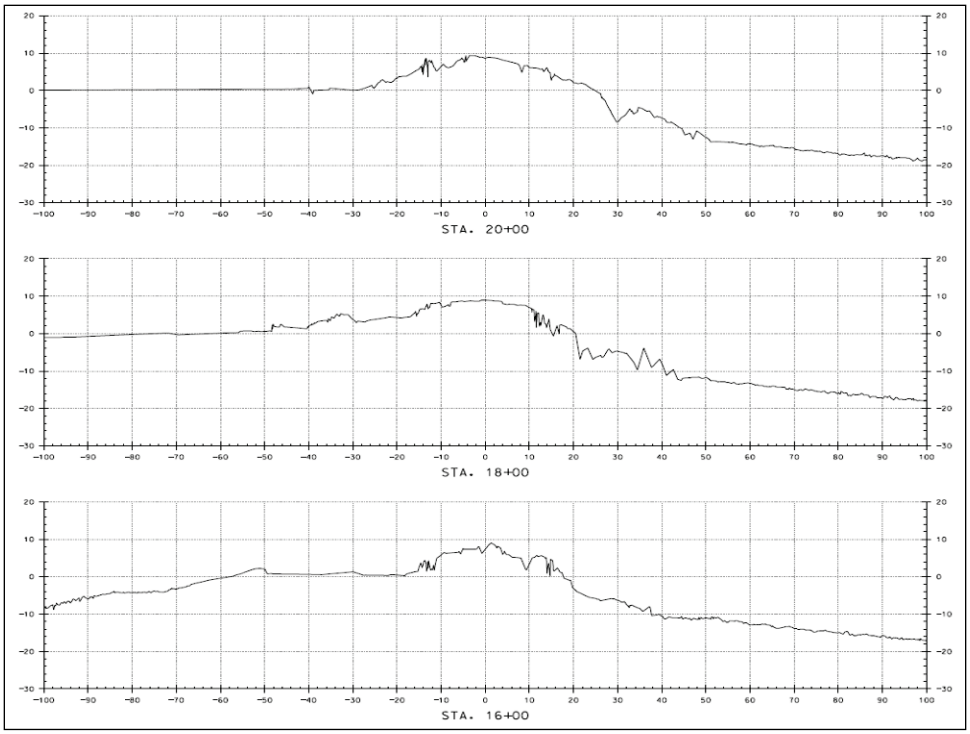


Figure 9. Condition in 2010 of profiles of Stations 22, 24, and 26 with leeside on left and seaside on right. Elevations are in feet relative to mllw, and stationing is in feet.

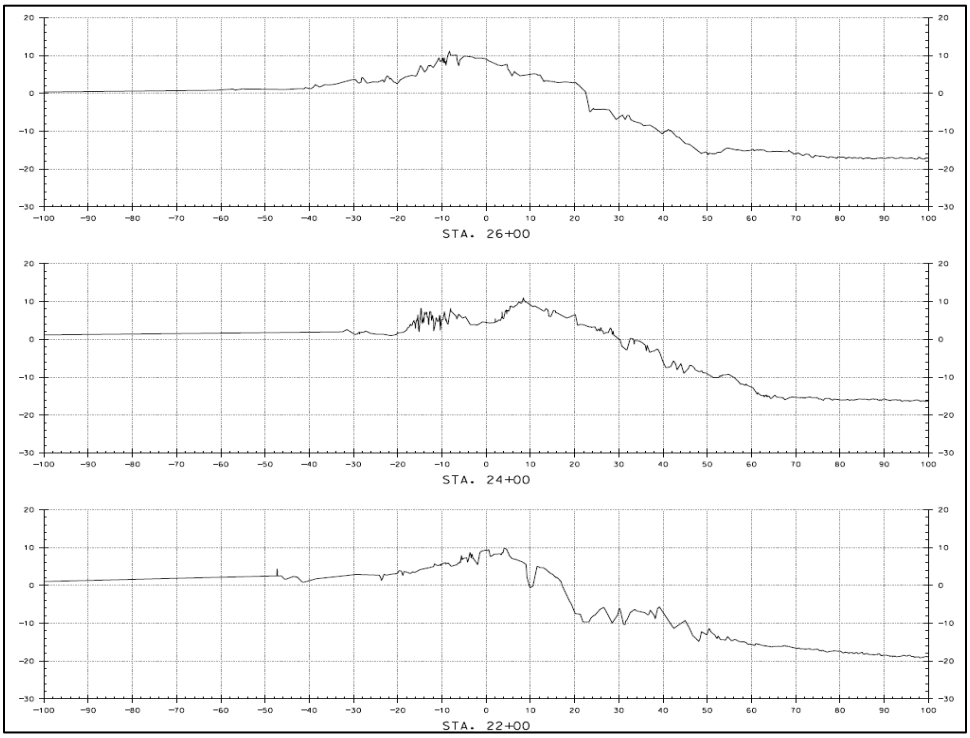

Figure 10. Condition in 2010 of profiles of Stations 28, 30, and 32 with leeside on left and seaside on right. Elevations are in feet relative to mllw, and stationing is in feet.

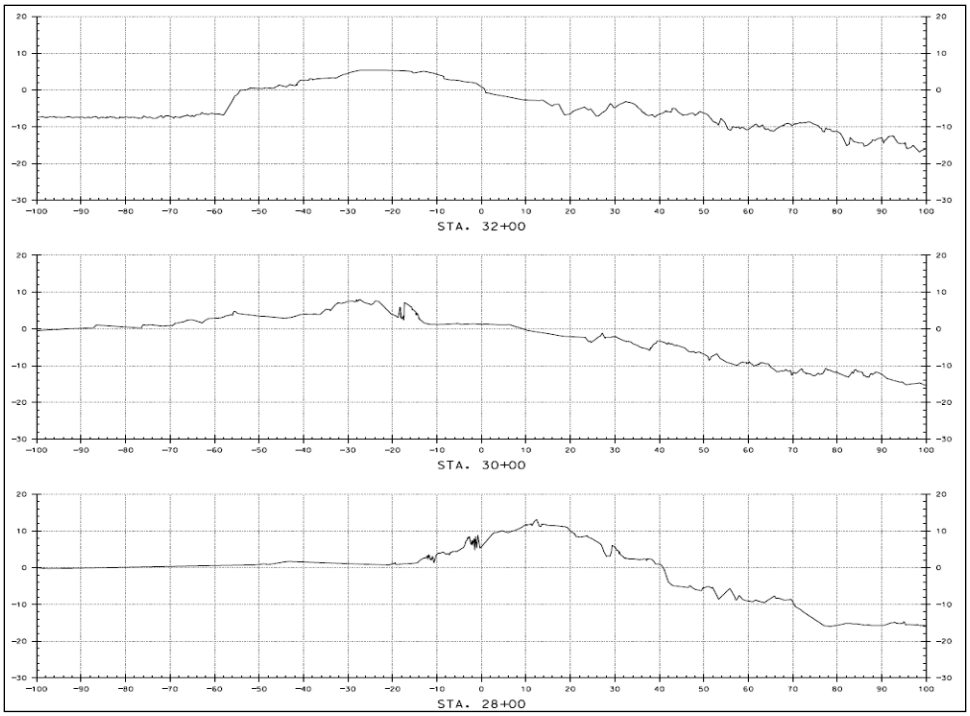


Figure 11. Condition in 2010 of profiles of Stations 34, 36, and 38 with leeside on left and seaside on right. Elevations are in feet relative to mllw, and stationing is in feet.

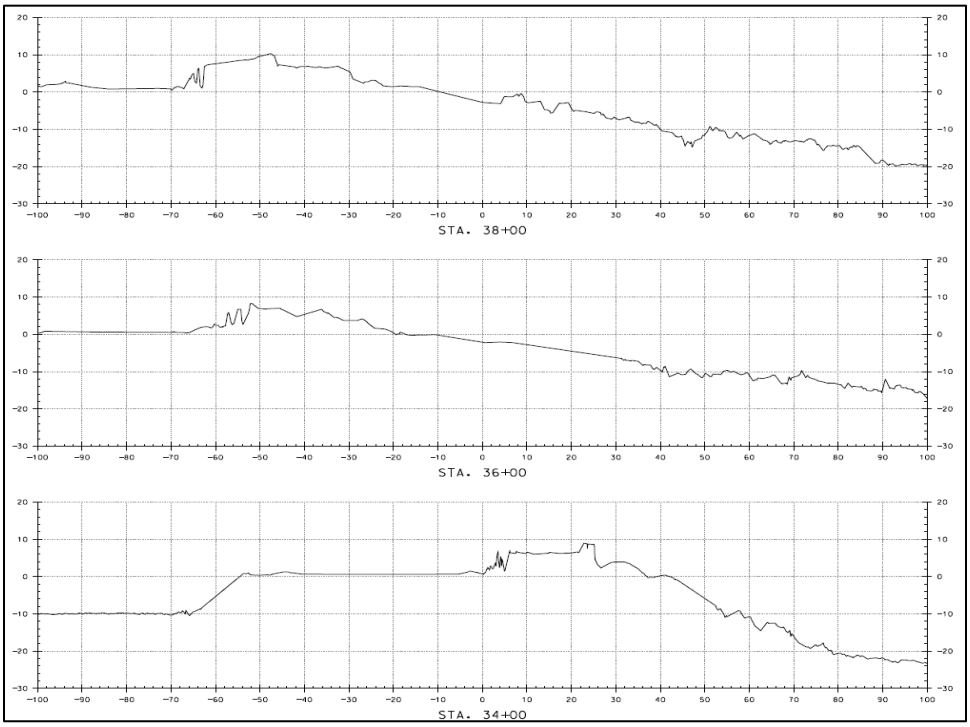

Figure 12. Condition in 2010 of profiles of Stations 40, 42, and 44 with leeside on left and seaside on right. Elevations are in feet relative to mllw, and stationing is in feet.

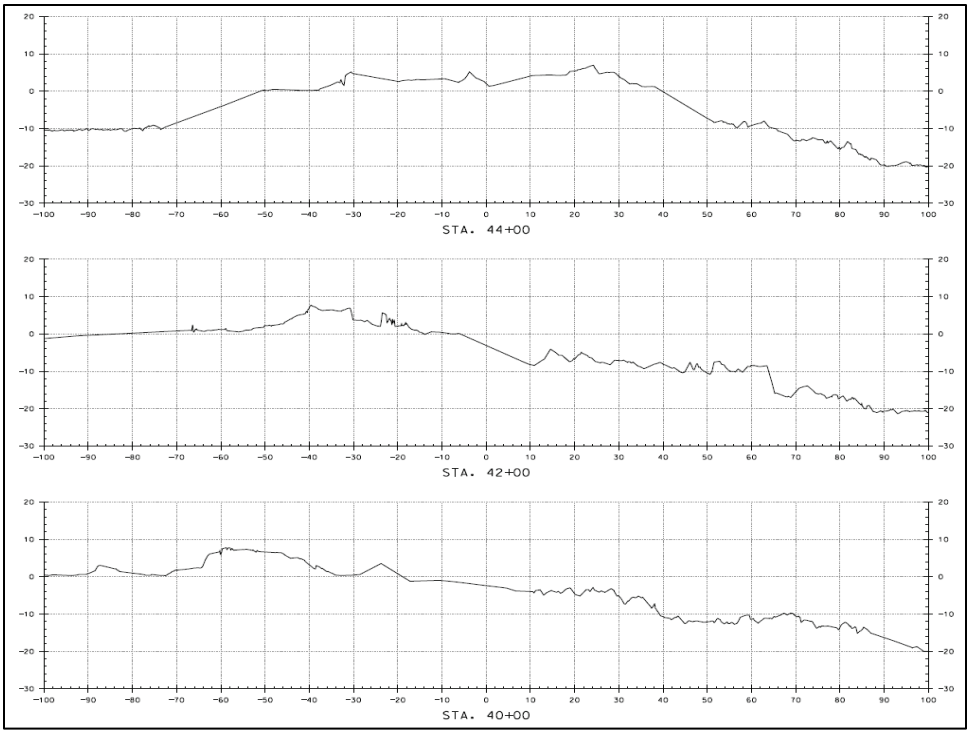


Figure 13. Condition in 2010 of profiles of Stations 46, 48, and 50 with leeside on left and seaside on right. Elevations are in feet relative to mllw, and stationing is in feet.

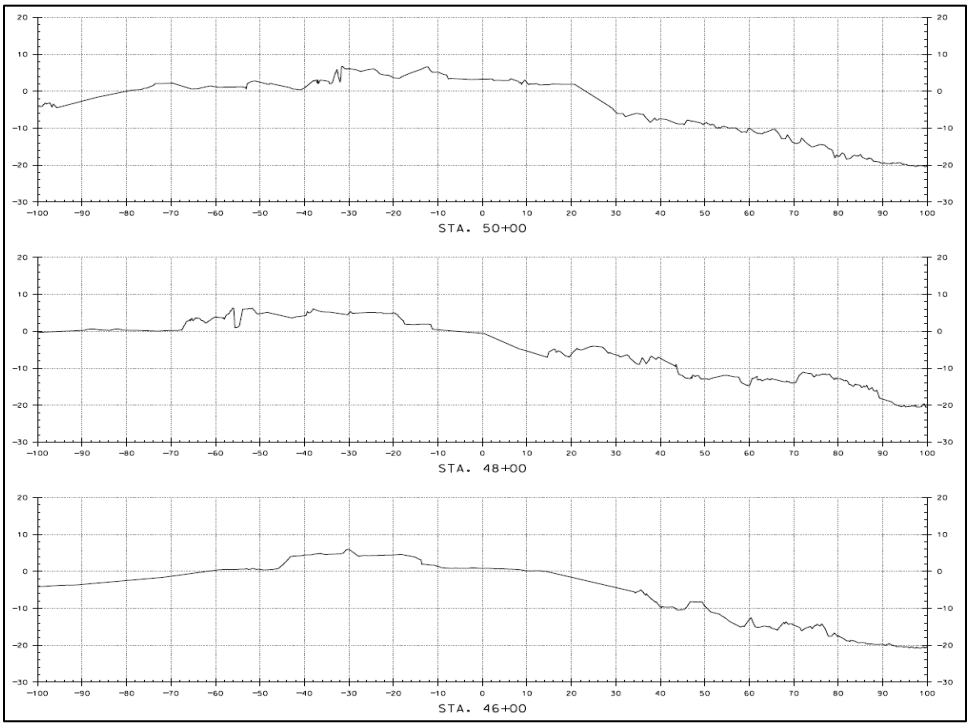

Figure 14. Condition in 2010 of profiles of Stations 52, 54, and 56 with leeside on left and seaside on right. Elevations are in feet relative to mllw, and stationing is in feet.

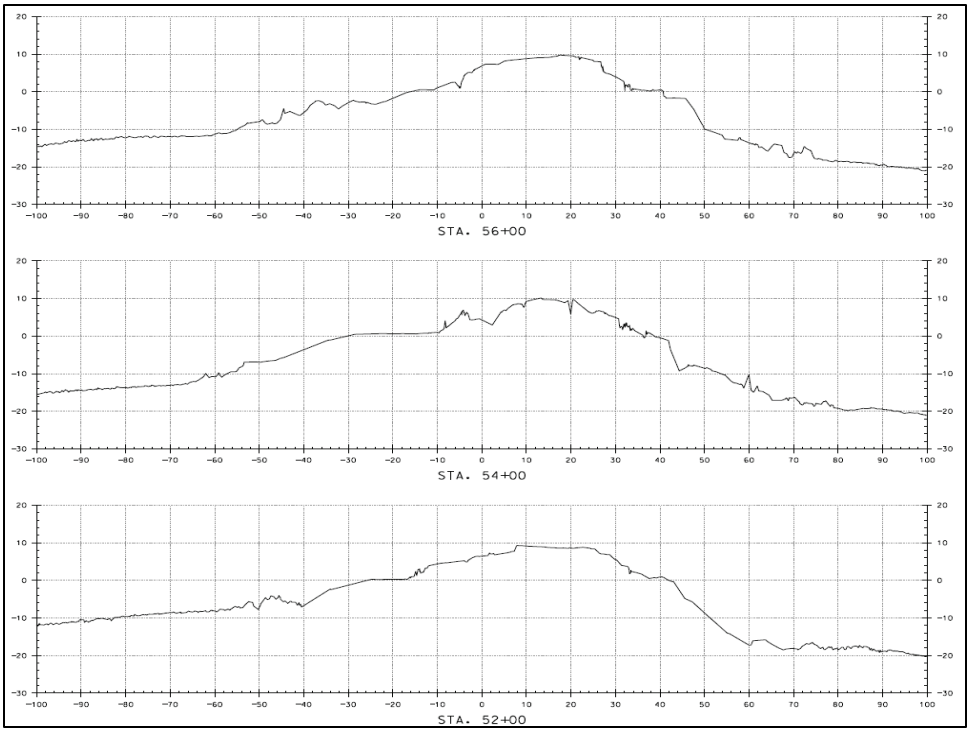


Figure 15. Condition in 2010 of profiles of Stations 58, 60, and 62 with leeside on left and seaside on right. Elevations are in feet relative to mllw, and stationing is in feet.

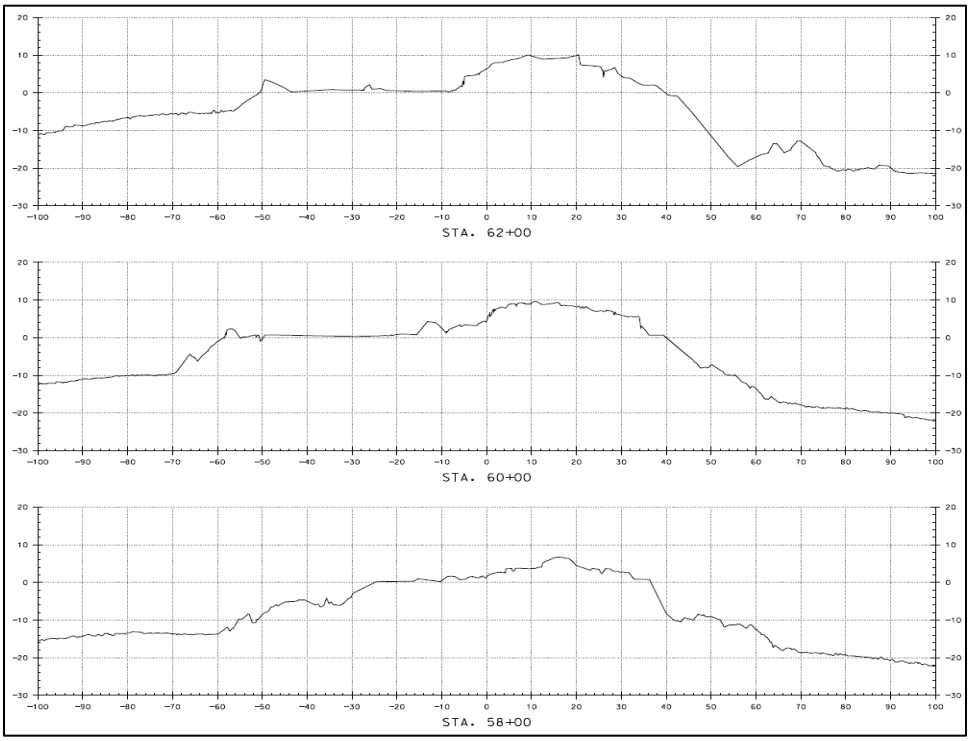

Figure 16. Condition in 2010 of profiles of Stations 64, 66 with leeside on left and seaside on right. Elevations are in feet relative to mllw, and stationing is in feet.

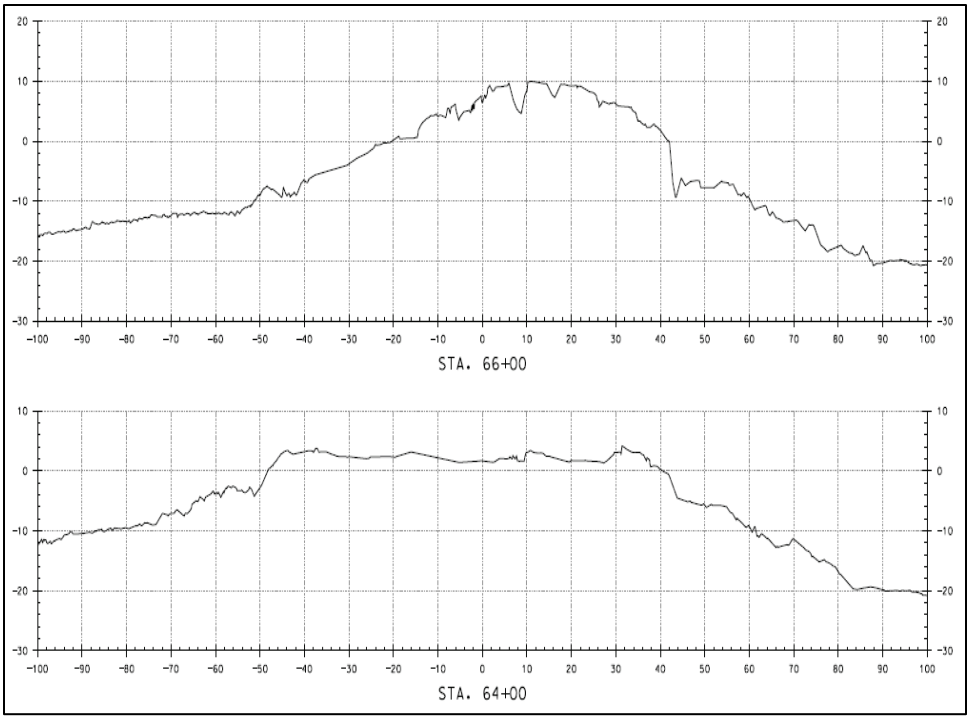


Figure 17. Profile maximums (points) and averages of maximum crest elevations (horizontal colored lines) along Main breakwater from 2003 and 2007 lidar surveys.

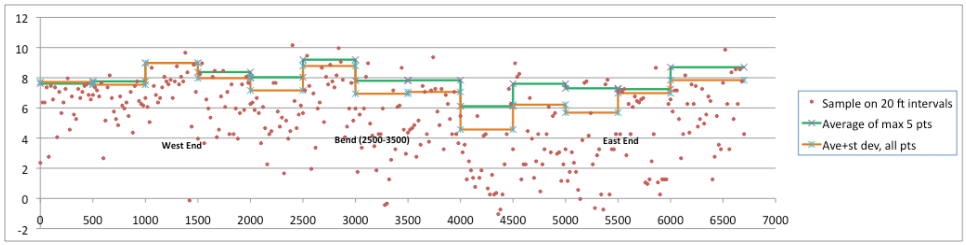

Table 2. Maximum crest heights of Main breakwater profiles.

| Beginning Station | Maximum Crest Height, ft, MSL | Beginning Station | Maximum Crest Height, ft, MSL |
|---|---|---|---|
| 0 | 10.3 | 42+00 | 5.2 |
| 2+00 | 7.5 | 44+00 | 4.2 |
| 4+00 | 8.0 | 46+00 | 4.6 |
| 6+00 | 6.2 | 48+00 | 5.0 |
| 8+00 | 6.7 | 50+00 | 7.5 |
| 10+00 | 8.0 | 52+00 | 8.4 |
| 12+00 | 10.0 | 54+00 | 8.0 |
| 14+00 | 7.3 | 56+00 | 5.0 |
| 16+00 | 7.3 | 58+00 | 7.8 |
| 18+00 | 7.6 | 60+00 | 8.4 |
| 20+00 | 8.0 | 62+00 | 2.4 |
| 22+00 | 9.2 | 64+00 | 8.2 |
| 24+00 | 9.4 | 66+00 | 8.2 |
| 26+00 | 11.4 | | |
| 28+00 | 6.2 | | |
| 30+00 | 3.6 | | |
| 32+00 | 7.2 | | |
| 34+00 | 6.6 | | |
| 36+00 | 8.5 | | |
| 38+00 | 6.1 | | |
| 40+00 | 6.0 | | |

# 2 Summary of Storm Forcing

## 2.1 Overview

Waves and water levels constitute the primary forcing for the breakwater and the protected elements. Waves can cause damage to the breakwater and may be depth limited. Depth-limited breaking waves can be more damaging than nonbreaking waves. If the water levels are high enough, waves can overtop the breakwater crest causing damage to the crest and leeside of the breakwater. As noted by Melby (2009, 2010), leeside damage development is more aggressive than seaside damage and is more likely to result in crest height reduction. Crest height reduction leads to increased wave transmission over the structure and more wave energy in the protected areas. For a severely damaged outer breakwater, lesser storms may become significant events inside the protected area, from both operational and shoreline damage perspectives. Waves may limit navigation in the channel and may cause erosion of the beach and shoreline areas. Water levels driven by storm surge, tide, and wave setup may also cause flooding. This chapter contains a summary of the detailed analysis of the historical storms. Additional details are contained in the appendices.

Wave transformation is dependent on bathymetry, so a separate study was conducted to define the bathymetry using high-fidelity lidar measurements. This is described in Appendix A. In this study, high-fidelity wave generation and transformation models were used to accurately determine historical storm wave conditions near the structures and in the HoR. These models and their application are described in Appendix B. Measurements from a local water level gage were used to define historical water levels.

## 2.2 Offshore wave hindcast

The offshore wave conditions are based on the Global Reanalysis of Ocean Waves Fine Atlantic Basin (GROW-FAB), a service provided by Oceanweather, Inc. (2011). This is a 57-year (yr) hindcast with numerically calculated wave information at 3-hour (hr) intervals from 1954 through 2010. The directional wave spectra were also provided for an internal 30-minute (min) grid at Station (Sta) 373 (40.9 degrees [deg] North Latitude, 71.2 deg West Longitude), located approximately 45 miles south of Point

Judith Harbor offshore at 173.2 ft depth. The spectral GROW wave hindcast was used as the offshore wave input in the numerical wave transformation modeling study.

As described in Appendix C, 225 storms with peak significant wave heights greater than 15.1 ft were selected from the GROW hindcast for this wave modeling study using the peaks-over-threshold method. The storms are listed, ranked by wave height, in Table C1. This sample includes an average of four storms per year. For each storm, the modeled storm hydrograph duration was approximately 36 hr with 18 hr before and after the peak wave height. This resulted in transformation of 2,301 wave conditions to the project site.

## 2.3 Wave transformation

Offshore waves for the 225 most intense storms were transformed to nearshore using the spectral wave transformation model Coastal Modeling System-Wave (CMS-Wave) (Lin et al. 2008) as described in Appendix B. Waves for the most severe 20 storms were propagated into the sheltered HoR using the time-domain, phase-resolving wave model BOUSS-2D (Nwogu and Demirbilek 2001, 2006) to calculate the interaction of nearshore waves with the channels, breakwaters, and surrounding land features. This very high-fidelity modeling is also described in Appendix B. The BOUSS-2D modeling was used to validate surrogate models described in Appendix C. The 20 most severe storms are listed in Table B3.

## 2.4 The storms

An extremal statistical analysis was conducted of the offshore GROW wave conditions as discussed in Appendix C. Storm peak values of wave height, wave period, storm power, wave direction, surge, and total water level are listed in Table C1 with storm peaks ranked by wave height from highest to lowest. The seven most significant storms from Table C1 are listed in Table 3.

The most significant storms from a storm surge perspective were included in the modeled 225 storms. For example, the top four storms ranked by surge are also within the top five storms ranked by wave height. The top two events by wave height, hurricanes Bob and Carol, were ranked the top two by surge and the top two by total water level. These two storms were the storms of record for Point Judith. The *perfect storm* with peak wave

height on 31 October 1991, made famous by the novel and feature movie, was ranked 15th for wave height but ranked 5th by surge. The maximum tidal range in the area of the HoR is 6.04 ft (difference between the highest and lowest astronomical tides) while the diurnal range is 3.85 ft (difference between mean higher high water [mhhw] and mllw). Tides have a significant influence on storm water level and can raise the significance of many moderate wave and surge events from a project performance perspective.

Table 3. Most extreme storms from Table C1 ranked by offshore wave height.

| Storm Name | Peak Date | Peak $H_{m0}$ in feet | Peak Surge in feet |
|---|---|---|---|
| Hurricane Bob | 8/19/1991 | 33.0 | 5.1 |
| Hurricane Carol | 8/31/1954 | 27.9 | 7.9 |
| Hurricane Edna | 9/11/1954 | 27.6 | N/A |
| Hurricane Donna | 9/12/1960 | 27.3 | 4.4 |
| Hurricane Gloria | 9/27/1985 | 27.2 | 4.4 |
| Hurricane Esther | 9/21/1961 | 25.6 | 2.3 |
| Not Named | 12/12/1992 | 24.6 | 2.8 |

The modeled storms constitute a wide range of conditions, varying from the most significant historical events down to storm events that occur on a monthly basis. This range is important. The most significant events will cause damage to the breakwater and may cause damage and flooding to the protected areas. However, the navigation operational limit states are far less severe and can occur on a monthly frequency in the stormy winter months. The offshore limit state for navigation is a significant wave height of approximately $H_{m0}$ = 10 ft, and as can be seen in Table C1, this occurs frequently. A life-cycle modeling strategy to model the significant processes over the entire life of the project has been constructed. This life cycle of storm events includes both the extreme damaging events as well as the operational events that limit safe navigation.

## 2.5 Wave and water level extremal statistical analysis

The detailed extremal statistical analysis is described in Appendix C. A joint probability analysis was conducted on storm response parameters related to waves and water levels to establish a basis for design alternatives and for conducting a Monte Carlo simulation of synthetic life cycles of storm events.

The joint probabilistic model was used to develop design alternatives for the breakwater. Table C3 lists the CMS-Wave stations and associated datum depths that are opposite the 500 ft long reaches shown in Figure 3. The wave and water level conditions associated with the various return periods for the CMS-Wave stations along the seaward side of the Main breakwater are listed in Appendix D. For the conditions listed, the wave height was chosen from the wave height marginal distribution; then the other parameters were selected as mean values associated with each return period from the bivariate normal distribution. Water level was selected slightly differently. For water level, three different values corresponding to varied quartiles were selected: $\mu$, $\mu+\sigma$, and $\mu+2\sigma$, where $\mu$ is the mean and $\sigma$ is the standard deviation. In this way, the sensitivity of the design to varied water levels could be ascertained. Note that return period conditions were only used to establish trial alternatives. The alternatives were then exposed to the life cycles of storms to determine the relative performance of each alternative. Using this method, return periods provide an arbitrary way to characterize alternatives. Other methods are equally viable because the final preferred alternative decision is based on functional performance.

## 2.6 Sea level rise

An analysis of the structure response to historical wave and water level conditions with sea level rise (SLR) was conducted. In this case, the surrogate wave transformation model was used to transform the GROW offshore historical waves to nearshore with five different SLR trends (USACE 2011) as follows, including three National Research Council (NRC) curves:

1. No SLR
2. Linear SLR trend extending the historical trend measured at Newport tide gage
3. NRC I
4. NRC II
5. NRC III

SLR is computed using the equation

$$E(t_2) - E(t_1) = 0.0017(t_2 - t_1) + b\left(t_2^{\,2} - t_1^{\,2}\right)$$

where $t_2$-$t_1$ is the time from 1992 and $E(t_2)$-$E(t_1)$ is the difference in water levels. The coefficient of 0.0017 meters (m) is the global mean SLR. The coefficient $b$ is the only difference between the curves and is 2.71e-5, 7.00e-5, and 1.13e-4 for NRC-I, NRC-II, and NRC-III, respectively. The SLR scenarios are shown in Figure 18. In this case, the curves were normalized to begin at SLR = 0 in 2013, so $t_2 = t_n - 1992$ and $t_1 = 2013 - 1992$, where $t_n$ is the year for which the calculation prediction is being made.

Figure 18. Sea level rise scenarios used in this study.

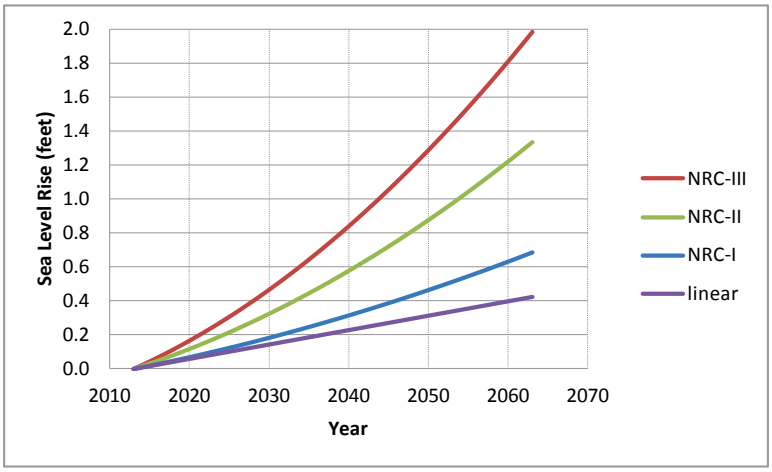


Comparing Figure 18 to the results of Church and White (2011) and Houston (2013), the NRC-II prediction corresponds to a probability of exceedence of 0.05 while the NRC-I prediction has a probability of exceedance of approximately 0.6. The NRC-I curve is slightly below the present exponential long-term SLR projection using the global MSL data from Church and White (2011) extending back to 1860. The NRC-I prediction, which is SLR scenario 3 herein, is a reasonable approximation of the most likely SLR scenario, and the NRC-II is a reasonable upper bound.

# 3 Breakwater Design Alternatives and Breakwater Damage and Consequences for Historical Wave Conditions

## 3.1 Breakwater Simulation

An engineering software suite called Breakwater Simulation (BWSim) (Melby 2010, developed at ERDC-CHL, was used for analyzing the structural and functional performance of the Main breakwater. The model consists of a suite of Matlab scripts to compute structure damage progression, wave transmission by overtopping, and wave transmission into the protected embayment. The computational methods are described in Appendix E.

## 3.2 Repair alternatives

### 3.2.1 Cross-section design

Four repair alternatives were proposed by the NAE, and these are listed in Table 4 and shown in Figures 19–22.

Table 4. Repair alternatives.

| | Seaside Slope | Leeside Slope | Crest Height (ft, MSL, MLLW) | Crest Width (ft) |
|---|---|---|---|---|
| Alternative 1 | 1V:2H | 1V:2H | 8.26, 10.0 | 20 |
| Alternative 2 | 1V:3H | 1V:2H | 8.26, 10.0 | 20 |
| Alternative 3 | 1V:2H | 1V:2H | 14.26, 16.0 | 20 |
| Alternative 4 | 1V:3H | 1V:2H | 14.26, 16.0 | 20 |

Figure 19. Alternative 1 idealized cross sections on existing damaged sections. Elevations are in feet relative to mllw, and stationing along the horizontal axis is in feet.

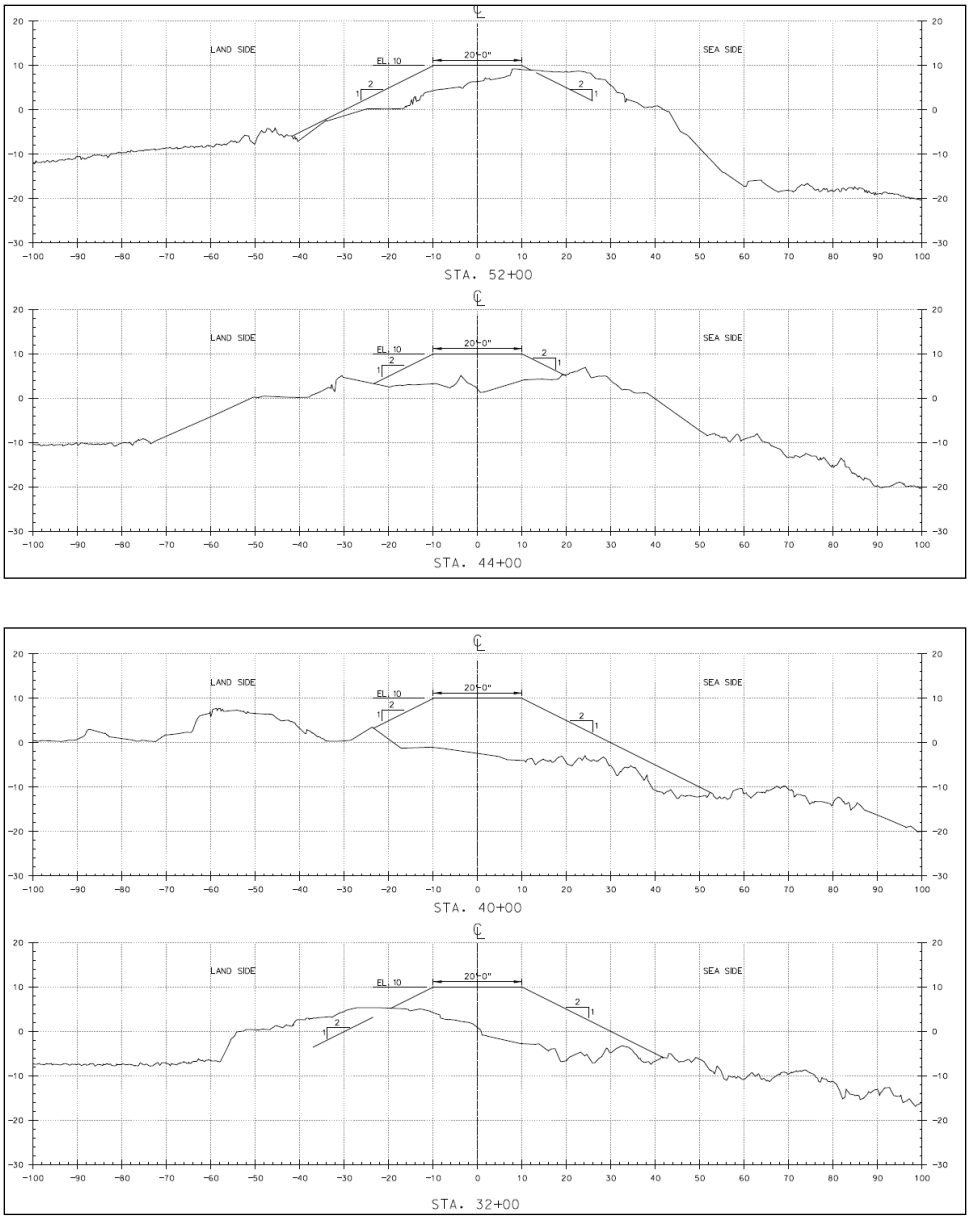

Figure 20. Alternative 2 idealized cross sections on existing damaged sections. Elevations are in feet relative to mllw, and stationing along the horizontal axis is in feet.

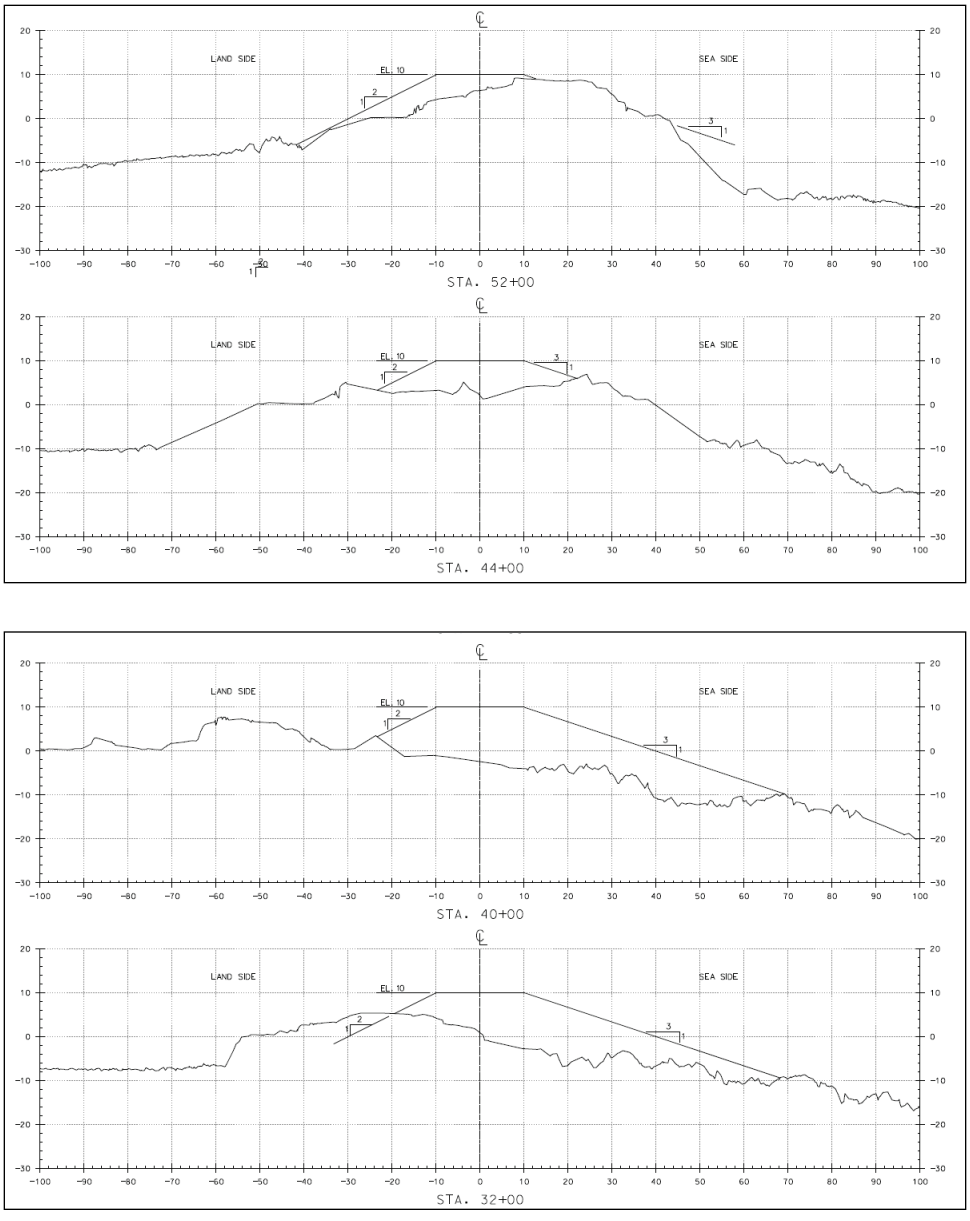

Figure 21. Alternative 3 idealized cross sections on existing damaged sections. Elevations are in feet relative to mllw, and stationing along the horizontal axis is in feet.

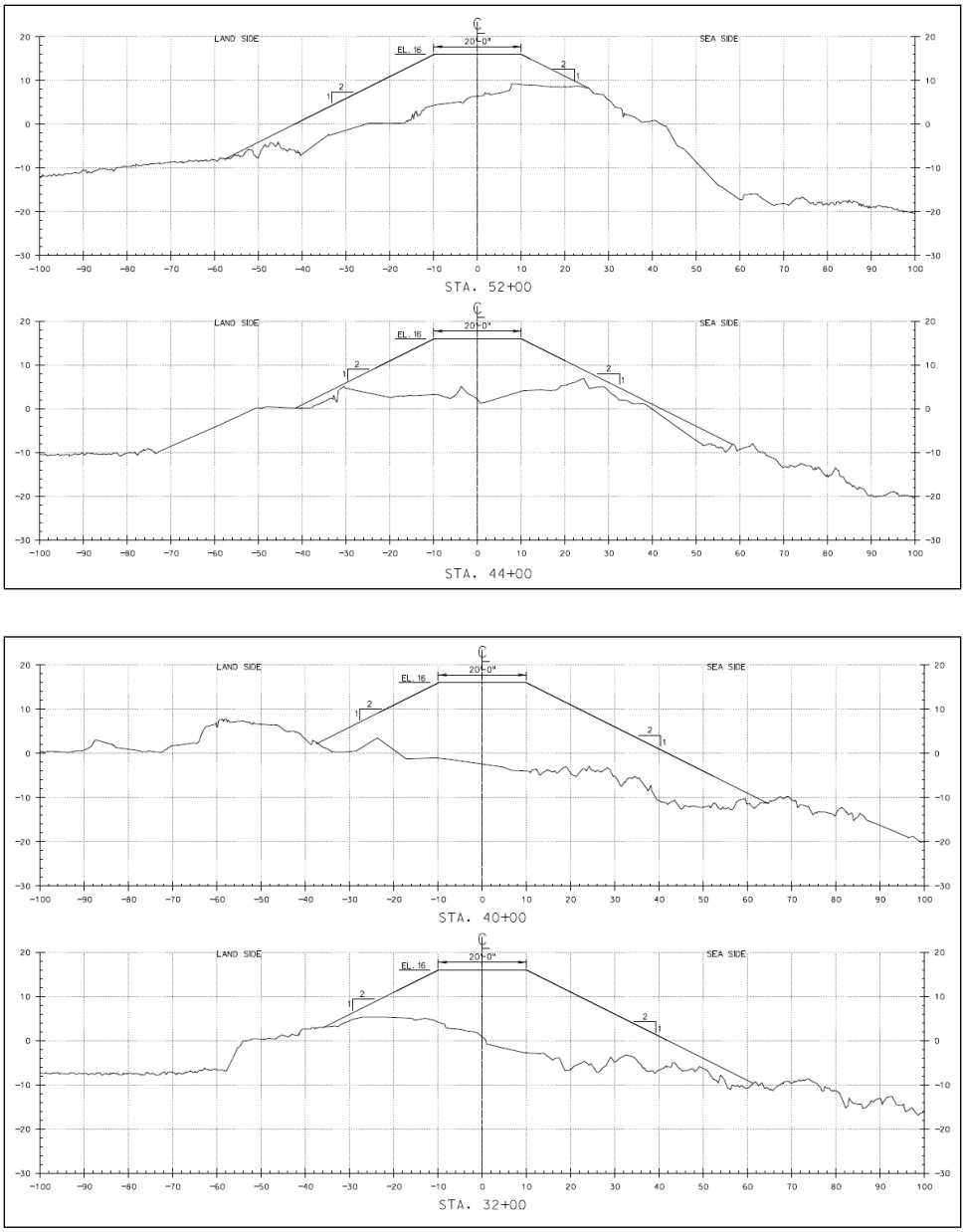

Figure 22. Alternative 4 idealized cross sections on existing damaged sections. Elevations are in feet relative to mllw, and stationing along the horizontal axis is in feet.

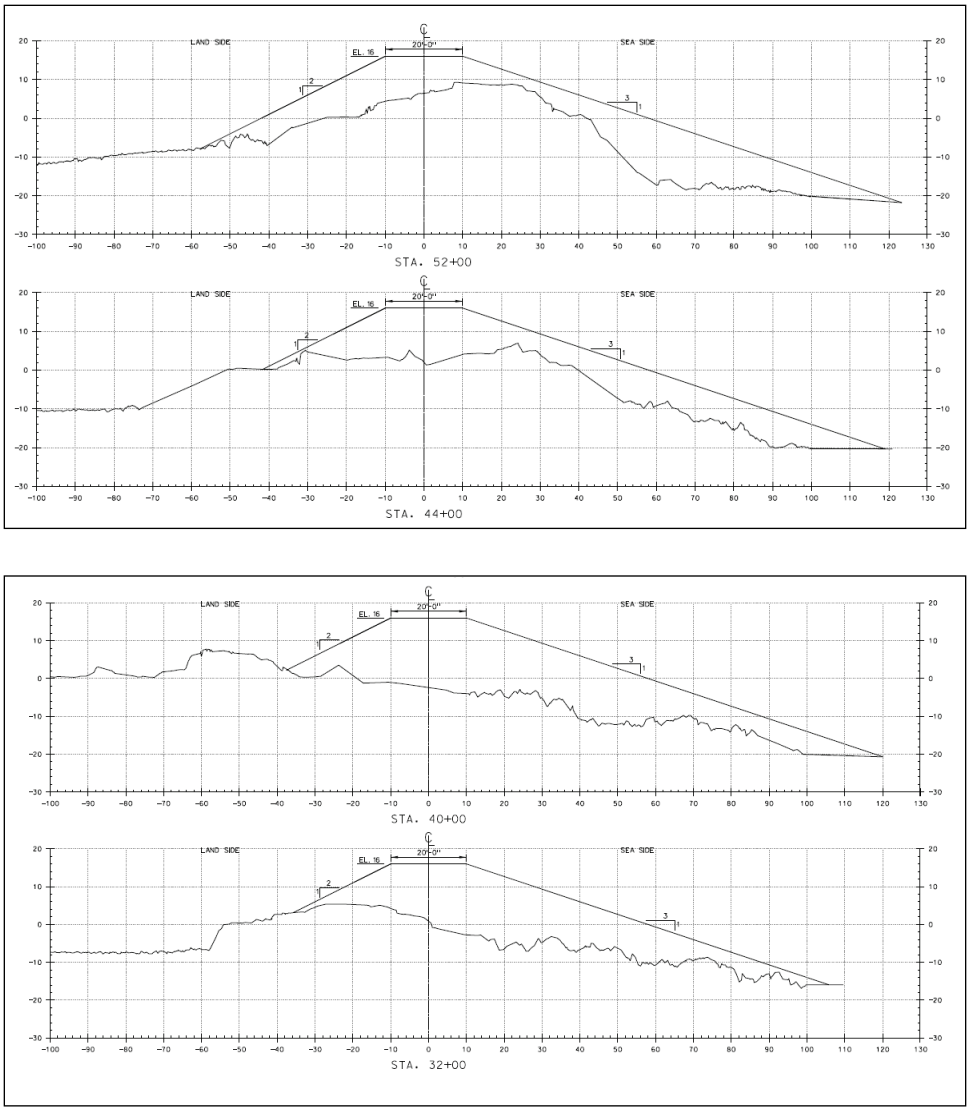


### 3.2.2 Stable seaside armor size

Stable armor stone size is computed here using empirical equations developed by Melby and Kobayashi (2011) as described in Appendix E. The design is based on the joint probability of wave and water level parameters for discrete levels of exceedance probability. For the armor stone sizing, the return period values from tables in Appendix D were used. The wave height corresponding to each return period was selected from the marginal wave height distribution, and the other parameters were selected as mean values from the joint probability distributions. The exception is the water level which was selected as the mean plus two standard deviations in order to achieve a conservative stone size. For each return period, a wide range

of armor sizes was computed over the structure length because the wave and water level values vary along the structure. The number of armor weights along the structure was reduced to two for each alternative corresponding to the maximum stone weights for west and east legs. The final list of seaside armor sizes is listed in Table 5. Note that later in the report, there is reference to the alternatives as 1.1 through 1.8, 2.1 through 2.8, etc., with the first digit indicating the cross section and the second indicating the return period for armor stone sizing. For these calculations, granite armor stone specific gravity is $S_a$ = 2.76, corresponding to a specific weight of 172.2 pounds per cubic feet (lb/ft$^3$) and zero damage is $S$ = 2. $S$ is defined in Figure 23 as the cross-sectional damage normalized by the nominal stone dimension squared. In this respect, $S$ is of similar order of magnitude to the number of stones displaced (Melby and Kobayashi 2011). The stable stone sizes are generally greater than the existing 12–15 ton armor stone used on the last two rehabilitations.

Note that the empirical stability equations used herein are derived from mean fits to data and are not necessarily conservative. For these large USACE projects, the goal is typically identification of the alternative that maximizes net economic benefits. Therefore, these stone sizes are somewhat arbitrary and are simply inputs to the risk analysis. In this type of analysis, the wave and water level return period simply provides some context for the alternative but is not a primary design condition. That is, the goal here is not to design to a specific return period, such as 50 or 100 yr. The goal is to determine which of these alternatives has the lowest risk and produces the highest net benefits. Herein, risk is defined as the product of the probability of consequences and the cost of those consequences.

Table 5. Seaside median stone weights in tons for various alternatives and return periods for mean plus two standard deviation water level.

| Alternative | BW Reach | Return Period (Years) | | | | | | | |
|---|---|---|---|---|---|---|---|---|---|
| | | 5 | 10 | 25 | 50 | 75 | 100 | 200 | 500 |
| 1 | 0+00 – 20+00 | 7 | 8 | 9 | 10 | 10 | 10 | 11 | 12 |
| | 20+00 – 67+00 | 16 | 18 | 20 | 21 | 22 | 23 | 24 | 25 |
| 2 | 0+00 – 20+00 | 4 | 5 | 5 | 6 | 6 | 6 | 6 | 7 |
| | 20+00 – 67+00 | 9 | 10 | 11 | 12 | 12 | 12 | 13 | 14 |
| 3 | 0+00 – 20+00 | 7 | 8 | 9 | 10 | 10 | 10 | 11 | 12 |
| | 20+00 – 67+00 | 16 | 18 | 20 | 21 | 22 | 23 | 24 | 25 |
| 4 | 0+00 – 20+00 | 4 | 5 | 5 | 6 | 6 | 6 | 6 | 7 |
| | 20+00 – 67+00 | 9 | 10 | 11 | 12 | 12 | 13 | 13 | 14 |

Figure 23. Illustration of damage parameters.

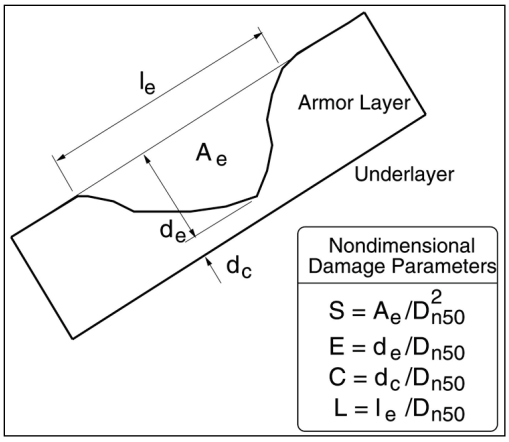


### 3.2.3 Stable leeside armor size

Historically, leeside armor sizing and damage prediction have not been a major study focus for rubble mound structures. However, for breakwaters like Point Judith, with a relatively low crest, leeside armor stability can be the most critical failure mode. In addition, leeside damage progression can be much more aggressive than seaside. For this study, leeside armor sizes were computed using the methods described in Appendix E. The stable leeside armor sizes for the return period conditions summarized in Appendix D are listed in Table 6. The mean plus two standard deviation water level was selected for design to achieve a conservative leeside stone size that would not be at risk of catastrophic failure. The leeside stone weights are significantly greater than historically used on the structure for most alternatives. This is a consequence of the relatively low crest height. The importance of the leeside armor stone will be shown in following sections.

Table 6. Leeside median stone weights in tons for various alternatives and return periods for mean plus two standard deviation water level.

| Alternative | BW Reach | Return Period (Years) | | | | | | | |
|---|---|---|---|---|---|---|---|---|---|
| | | 5 | 10 | 25 | 50 | 75 | 100 | 200 | 500 |
| 1 | 0+00 – 20+00 | 9 | 11 | 14 | 17 | 18 | 19 | 22 | 25 |
| | 20+00 – 67+00 | 22 | 29 | 39 | 47 | 52 | 56 | 65 | 77 |
| 2 | 0+00 – 20+00 | 6 | 8 | 10 | 12 | 13 | 14 | 16 | 18 |
| | 20+00 – 67+00 | 16 | 21 | 28 | 35 | 38 | 41 | 48 | 57 |
| 3 | 0+00 – 20+00 | 4 | 5 | 7 | 9 | 10 | 10 | 12 | 14 |
| | 20+00 – 67+00 | 12 | 17 | 23 | 28 | 31 | 33 | 39 | 48 |
| 4 | 0+00 – 20+00 | 3 | 3 | 5 | 6 | 6 | 7 | 8 | 9 |
| | 20+00 – 67+00 | 8 | 11 | 15 | 19 | 21 | 23 | 27 | 33 |

Note that the leeside stone sizes for high return periods are unreasonably large and would not be expected to be chosen for design. They are shown only to illustrate the relative range of stable sizes.

## 3.3 Historical damage — model validation

Seaside and leeside breakwater damage accumulation as well as crest height reduction over the life cycle are modeled herein using the methods of Melby (2009, 2010) and Melby and Kobayashi (2011) described in Appendix E. Life-cycle simulation methods are further described in Males and Melby (2012). The empirical damage accumulation process models are coded into the BWSim software. For validation, the historical damage since 1954, including the repair in 1984, was modeled.

Table 7 lists hindcast damage simulation results using BWSim for historical storms over the 57 yr period 1954–2010. In this case, the structure was exposed to storms in Table C1, and seaside, leeside, and crest damage computed. The structure was repaired during the summer of 1984. The detailed profile of the postrepair structure is unknown. Herein a uniform postrepair damage level of $S = 2$ is assumed, corresponding to slight damage, because the contractor defaulted and had significant problems during construction. The damage values given are mean + standard deviation where the quartile quantifies the along-shore spatial variability of damage. This statistic better represents the progression to failure in a reasonably conservative way, particularly without a physical model to validate the numerical model. Seaside damage progression is shown in Figure 24, leeside in Figure 25, and crest height reduction in Figure 26. Reaches from 0 – 25+00 are not shown because they do not exhibit significant damage. This is because the severe storm waves are primarily from the south and do not directly attack the west leg of the outer breakwater. Wave save stations are the same for some reaches, so some lines overlap on the plots.

The damage on both the seaside and leeside at the end of the historical simulation period is severe. However, the crest height reduction is a result of leeside damage because seaside did not progress to a level that would cause crest height reduction. The leeside damage dominates for conditions where there is a low crest and undersized armor stone as summarized by Melby (2009, 2010). Reaches near the middle of the east leg suffer the most damage with the most exposed station being 40 - 45. The crest height at the end of the simulation is lowered by approximately one stone

dimension. However, because there has been so much damage and repair over the century since original construction, there is a very wide mound of stone that still dissipates considerable wave energy.

Table 7. Predicted damage from BWSim over period 1954–2010 for historical wave and water level conditions with repair in summer 1984.

| Reach | Start, ft | End, ft | Beginning Crest Height, ft, MSL | Seaside S+sd | Leeside S+sd | Predicted Ending Crest Height, ft, MSL | Actual Ending Crest Height, ft, MSL |
|---|---|---|---|---|---|---|---|
| 6 | 25+00 | 30+00 | 8.3 | 5 | 14 | 8.3 | 9.2 |
| 7 | 30+00 | 35+00 | 8.3 | 7 | 15 | 7.8 | 7.8 |
| 8 | 35+00 | 40+00 | 8.3 | 8 | 18 | 7.8 | 7.8 |
| 9 | 40+00 | 45+00 | 8.3 | 8 | 18 | 6.1 | 6.1 |
| 10 | 45+00 | 50+00 | 8.3 | 7 | 16 | 7.6 | 7.6 |
| 11 | 50+00 | 55+00 | 8.3 | 7 | 16 | 7.3 | 7.3 |
| 12 | 55+00 | 60+00 | 8.3 | 6 | 13 | 7.2 | 7.2 |
| 13 | 60+00 | 67+00 | 8.3 | 5 | 12 | 8.3 | 8.7 |

Figure 24. BWSim modeled seaside damage as a function of time for outer reaches.

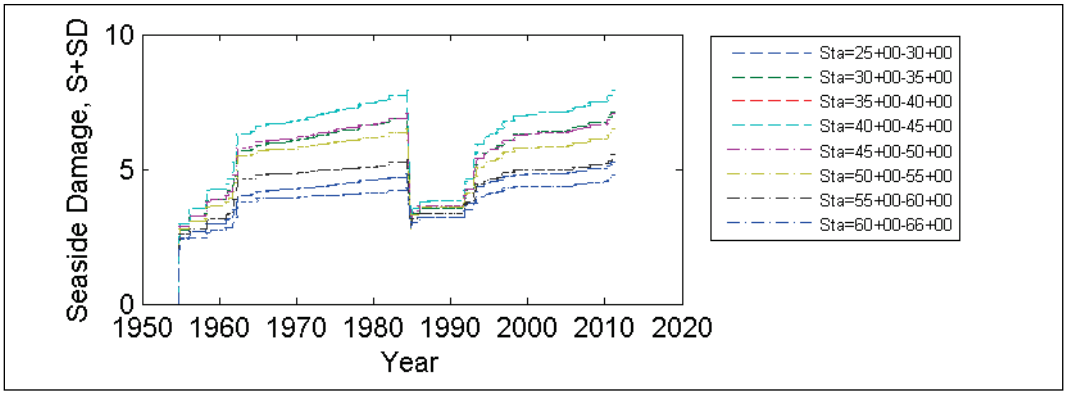


Figure 25. BWSim modeled leeside damage as a function of time for outer reaches.

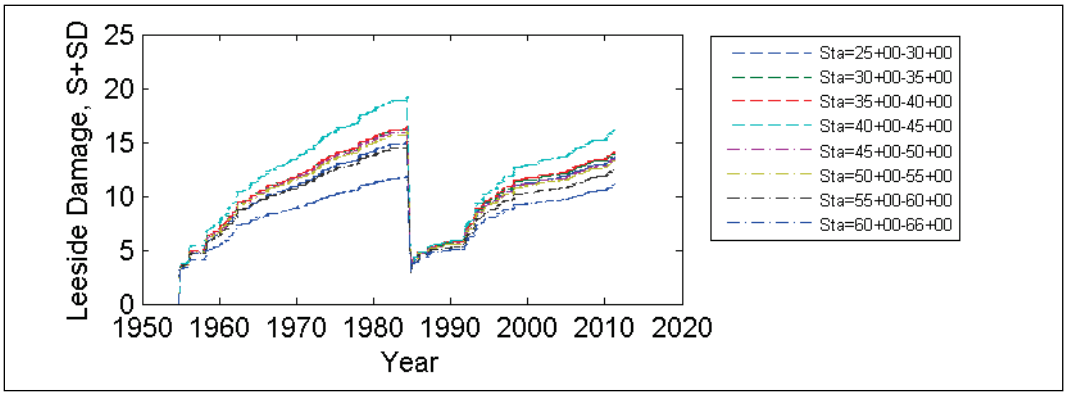

Figure 26. BWSim modeled crest height as a function of time for outer reaches.

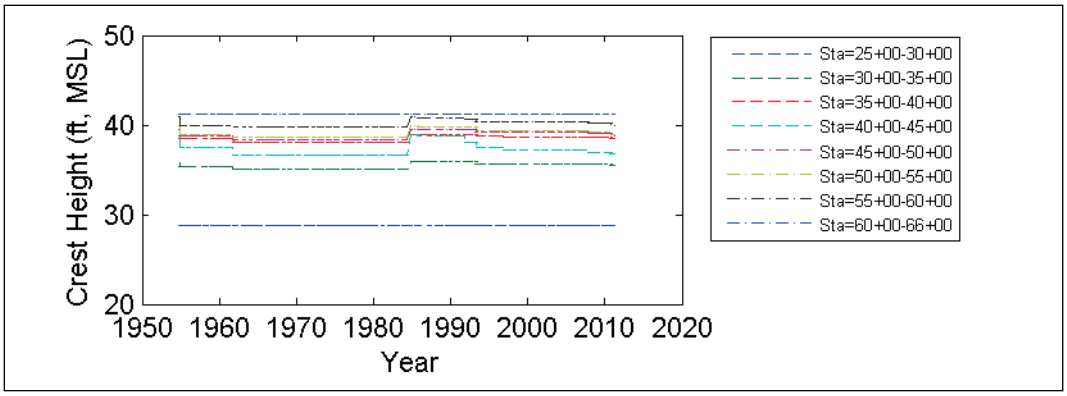


From discussion in Chapter 1 related to Figure 17, the 2010 reach crest elevations were computed from lidar data as the average of the highest five points. The BWSim modeled average crest elevations for each reach are listed in Table 7 along with the actual crest elevations in 2010. The model results agree well with the measured values with an average error of -2%.

## 3.4 Wave transmission

### 3.4.1 Wave overtopping

For a low-crested structure like the Point Judith Main breakwater, wave transmission from wave overtopping is common. Wave overtopping transmission is worse for heavily damaged sections that have lowered crest elevations. Wave overtopping transmission describes the transformation of spectral wave height from the seaside of the breakwater, $(H_{mo})_i$, to the leeside of the structure, $(H_{mo})_t$. Overtopping transmission $C_t = (H_{mo})_t/(H_{mo})_i$ is computed using the methods in Appendix E.

### 3.4.2 Wave diffraction

The wave energy that passes over and through the structures and through the inlets will propagate to the consequence locations. The areas of particular interest are the navigation channel along the West Shore Arm breakwater, the mooring area in the lee of the Main breakwater, and the shoreline that may be exposed to erosionary conditions. For most projects, computation of this wave transmission is done using a physical model or a computationally costly numerical wave transformation/diffraction model. However, for risk-based studies, this high-fidelity modeling can be too expensive and time consuming due to the number of events that are required to be transformed. A practical alternative is to precompute the

wave transmission for a wide variety of cases, construct a surrogate model, and then use this surrogate model in the simulation to transform the wave energy. As discussed in Appendix C, a Boussinesq wave model was used to compute the diffracted wave transmission for the 20 worst-case storms. In addition, a separate study was done to compute wave diffraction through an idealized gap for a wide variety of structure configurations and wave and water level conditions. These data were used to develop a generalized diffraction surrogate model based on a lookup table with gap width, location behind structure, water depth, wave height, wave period, and wave direction as the parameters of interest.

### 3.4.3 Wave transmission to consequence locations

Within the simplified approach in BWSim, the transmitted wave height for each structure reach and the incident wave at the inlets are assumed to all be independent. Each transmitted wave condition on the leeward side of each breakwater reach as well as the wave conditions just inside of each inlet are all diffracted independently to each consequence location using the diffraction surrogate model, and then the wave energies are summed. This method provides a reasonable indication of the total wave energy reaching consequence locations as a function of structure condition for life-cycle investigations.

### 3.4.4 Validation of wave transmission for historical storms

The overtopping transmission and surrogate diffraction method was validated for the 20 top storms using the BOUSS-2D results. The wave transmission was computed for 22 save points scattered uniformly throughout the HoR as shown in Figure 27. The numbers displayed in Figure 27 are %error = $(H_{mo\text{-}surr}\text{-}H_{mo\text{-}Bouss})/H_{mo\text{-}Bouss}$*100%, where $H_{mo\text{-}surr}$ is the surrogate significant wave height from a summation of wave energies and $H_{mo\text{-}Bouss}$ is the BOUSS-2D modeled transmitted significant wave height. Figure 27 shows that the surrogate model produced quite a large variability of accuracy over the protected region. However, the poor predictions are at locations that would be expected to have large uncertainty. For example, Save Point 129 has consistently large error because it is located in an area with wave reflection that would be represented in the Boussinesq model but not in the surrogate model. Similarly, all save points close to the shore exhibited larger errors primarily because these include not only reflection but wave refraction, shoaling, and breaking, processes not represented in the surrogate model.

As such, the points along the shore and Save Point 129 are excluded from the consequence analysis. Over the 15 remaining save points, the surrogate model with energy summation method produced an average error in transmitted $H_{mo}$ of 4% with a standard deviation of error of 17%. This is quite a good result and is comparable to wave modeling errors for more detailed and computationally intensive wave models.

Figure 27. Average percent difference between diffraction surrogate model and BOUSS-2D for top 20 storms over all save points.

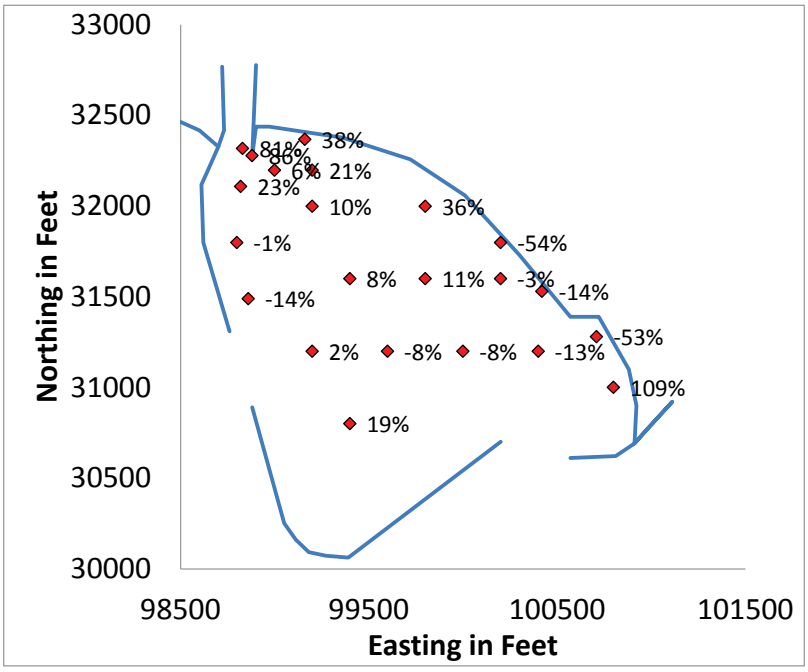


As an additional validation, it was noted that the BOUSS-2D model was relatively sensitive to local bathymetry and other harbor configuration effects. As such, the BOUSS-2D results were averaged into groups of four neighboring save points. The above comparison was repeated with grouped BOUSS-2D results, and the result was a reduction of the standard deviation of errors to less than 10%.

Figures 28 and 29 show the wave heights throughout the HoR for the mean of all historical storm peaks and for Hurricane Bob, respectively. These figures illustrate that the regions with highest waves in the HoR are located near the east entrance while the second highest regions are inside the west entrance and in the outer reach of the navigation channel. This is a result of the waves penetrating through the entrance and then propagating down the relatively deep channel. The area in the direct lee of the breakwater is the most sheltered region. Figures 30 and 31 show the wave

overtopping only. In this case, the wave energy through the inlets was set to zero. For the mean, the breakwater still provides significant sheltering in a deteriorated state with very little wave energy throughout the HoR. Comparing Figures 29 and 31 illustrates that the wave energy in the navigation channel and along the shoreline contains significant contribution from overtopping for Hurricane Bob because of the elevated water levels. For extreme storms like Bob, the breakwater still provides protection even in a deteriorated state.

Figure 28. Mean of all peak historical storm transmitted significant wave heights from 1954 through 2010 throughout HoR.

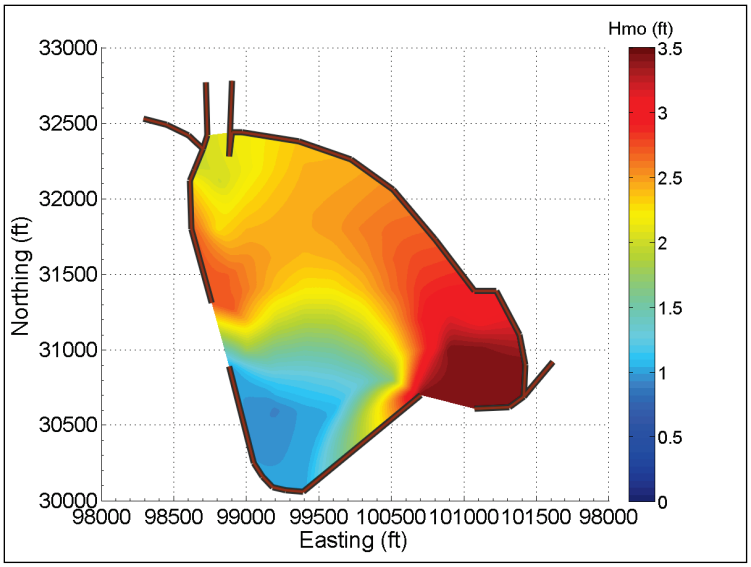


Figure 29. Peak transmitted significant wave height throughout HoR for Hurricane Bob in August 1991.

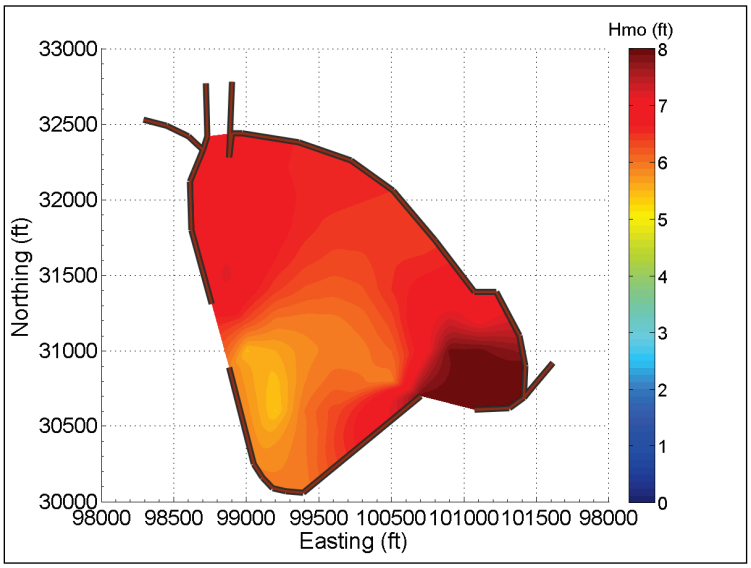

Figure 30. Mean historical storm transmitted significant wave height throughout HoR for wave overtopping only.

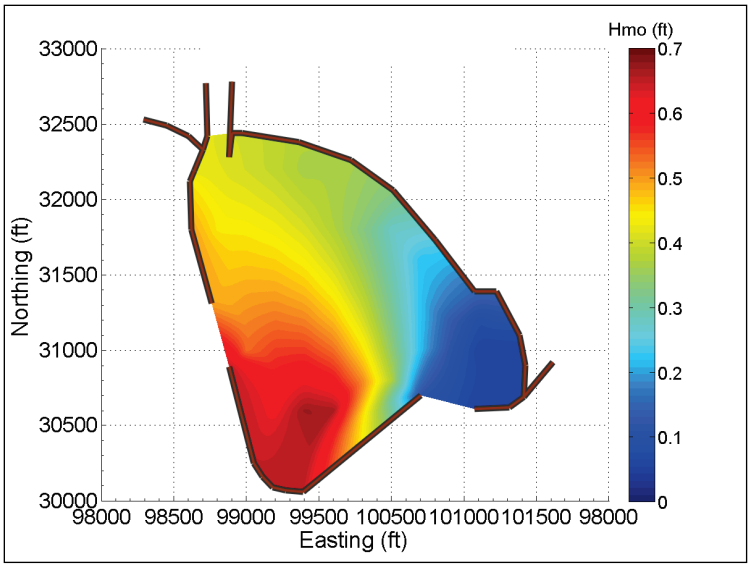


Figure 31. Peak transmitted significant wave height throughout HoR for Hurricane Bob for wave overtopping only.

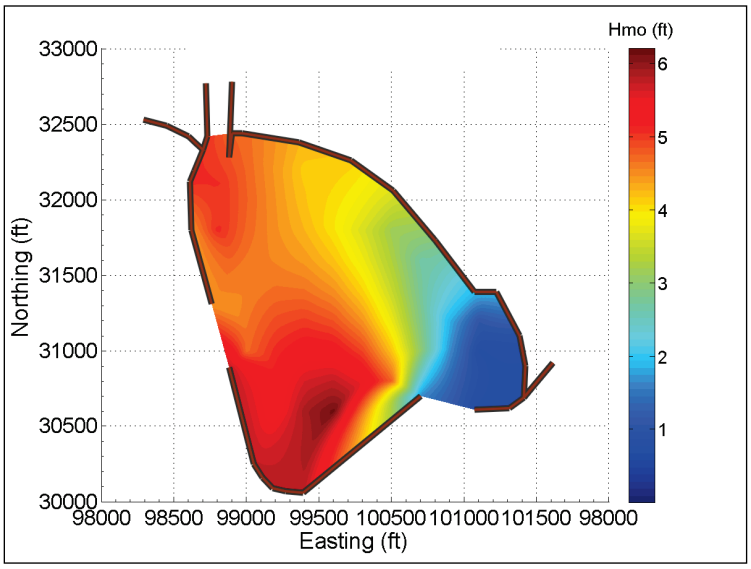


### 3.4.5 Wave transmission for navigation limit state

In order to define consequences, the response in the HoR was organized into separate regions by grouping save stations. The regions are shown in Figure 32 and are defined as follows:

- Group 1 – Mooring Area; Sta 141, 142, 143, 146, 147, 148, 149, 150, 155, 156, 157, 158, 159, 168, 169
- Group 2 – Back Bay; Sta 196, 202, 203, 204

- Group 3 – Mid Bay; Sta 154, 166, 167, 170, 177, 178, 179, 180, 185, 186, 187, 188, 190, 191, 192, 193, 194, 195, 197, 198, 199
- Group 4 – West Navigation Channel; Sta 129, 132, 135, 136
- Group 5 – West Entrance; Sta 165, 175, 176, 183, 184
- Group 6 – East Entrance; Sta 160, 161, 162, 171, 172, 173, 181, 189

Figure 32. Save station groups in harbor of refuge.

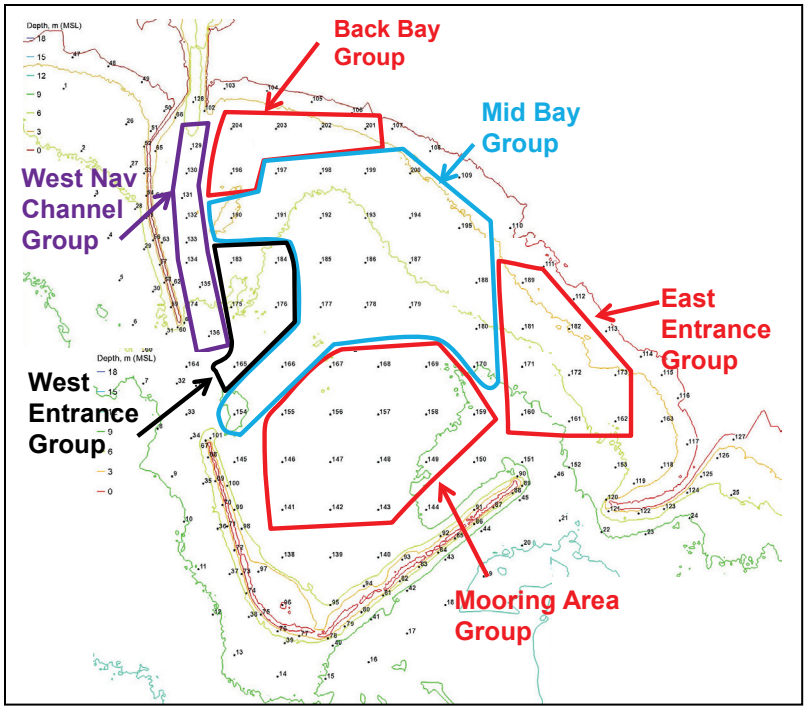


It is unknown what the exact conditions are that result in cessation of navigation of the commercial fishing fleet, the ferries, the recreational fishing fleet, and other navigation traffic. However, a survey of the commercial fleet by NAE suggested limiting significant wave heights outside the bay of $H_{mo}$ = 10 ft and inside the HoR of $H_{mo}$ = 4 ft. Figure 33 shows the exceedances-of-limit state of $H_{mo}$ = 4 ft in various regions in the harbor for historical wave and water level conditions with repair in 1984. The vertical blue lines are simply occurrences defined as any save station registering a significant wave height in excess of 4 ft for a given storm.

The results illustrate that there were roughly one to two events per year where the significant wave height exceeded 4 ft in the navigation channel or the west entrance while the east entrance had closer to three exceedance events per year illustrating the southern exposure.

Figure 33. Exceedance of $H_{m0}$ = 4 ft limit state for historical wave and water level conditions and historical breakwater conditions with repair in 1984.

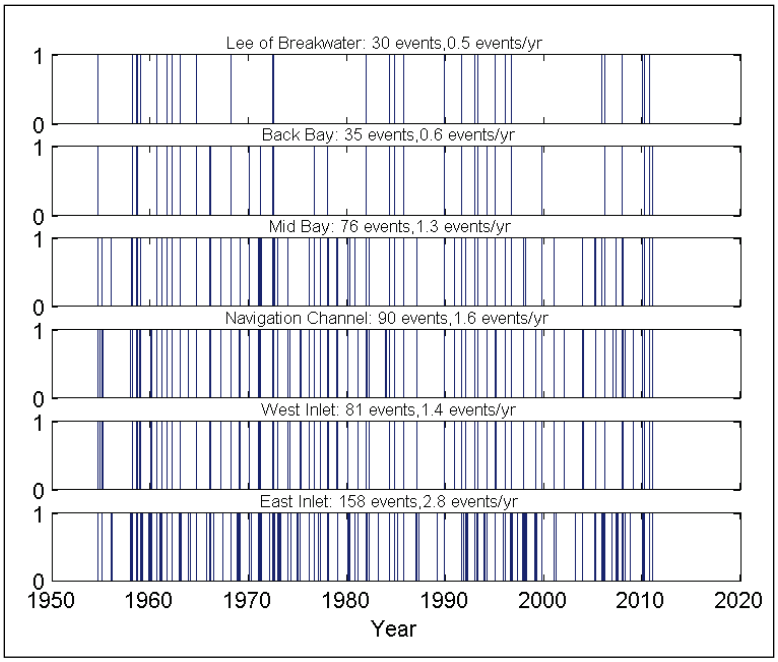


Table 8 lists the historical exceedances over the 57 yr historical life cycle for the various save station groups for the HoR limit state of 4 ft. For comparison, there were 71 events that exceeded the offshore wave height limit state wave height of 10 ft. The offshore representative location was save station 205 at latitude 41.343098° and longitude -71.522701°. This point is 1 mile southwest of the outer breakwater bend. Table 8 also lists the number of events that are common between the offshore and HoR limit state exceedances. Only the HoR events that are unique from the offshore exceedances are meaningful from a consequence point of view because the offshore limit state exceedances are unaffected by any breakwater remediation measures. Of the 90 exceedance events in the navigation channel over the life cycle, 55 were unique, or just under 1 per year. When the performance of the alternatives in the next chapter is evaluated, this is the number expected to decrease for the breakwater repair alternatives or increase if no remediation measures are implemented.

Table 8. Wave height limit state exceedances for historical wave and water level conditions.

| Save Station Group | 1 | 2 | 3 | 4 | 5 | 6 |
|---|---|---|---|---|---|---|
| Inside events that exceeded 4 ft | 30 | 35 | 76 | 90 | 81 | 158 |
| Number of common events | 27 | 26 | 46 | 35 | 35 | 68 |

# 4 Results of Life Cycle Simulation of Future Response

Up to this point, aspects primarily discussed have been high-fidelity hydrodynamic modeling and BWSim modeling of historical wave and water level conditions and the corresponding breakwater and HoR response to validate the models and to illustrate past performance. BWSim was also run for the life cycle of historical storm events for the five sea level rise scenarios for a range of breakwater repair alternatives that were summarized in Chapter 2. This chapter summarizes the results of those simulations. In this analysis, there is no maintenance to the structure during the life cycle.

## 4.1 Without-project alternative

The same analysis discussed in Chapter 3 was completed for the *without-project* alternative. In this case, the simulation starts in 2014 and runs 57 yr until the beginning of 2071 but uses the historical events. The starting breakwater condition used for the without-project alternative is the ending condition from the historical simulation which matched the lidar surveys from 2010. Figure 34 shows the time-series of simulated seaside, leeside, and crest damage for all reaches for SLR 1. The results show fairly clearly that, for the without-project alternative, the damage to the breakwater will continue to escalate while the crest height only decreases slightly. Other SLR scenarios produce similar plots.

Figure 35 and Table 9 present the exceedances of the navigability limit states within the HoR. Recall that there were 71 exceedances offshore for the historical storms. Comparing Figure 35 and 33 suggests increasing impacts to navigation as a result of not repairing the breakwater. Subtracting the number of unique events between Tables 8 and 9 illustrates the impact on functional performance between the historical and the future with no repair. In particular, there is an increase in frequency of exceedance of the navigability limit state of 4 ft in the channel from 55 unique events to 67 unique events between the historical and the future for SLR1. For SLR2 and SLR3, the increase is from 55 to 68. The exceedances increase to 69 and 70 in the future for SLR4 and SLR5,

respectively. This difference range is 12 to 15 exceedances over the 57 yr life cycle or approximately one additional exceedance every 4–5 yr over the historical performance if there is no repair in the future life cycle.

Figure 34. Without-project damage to breakwater for historical conditions for SLR 1.

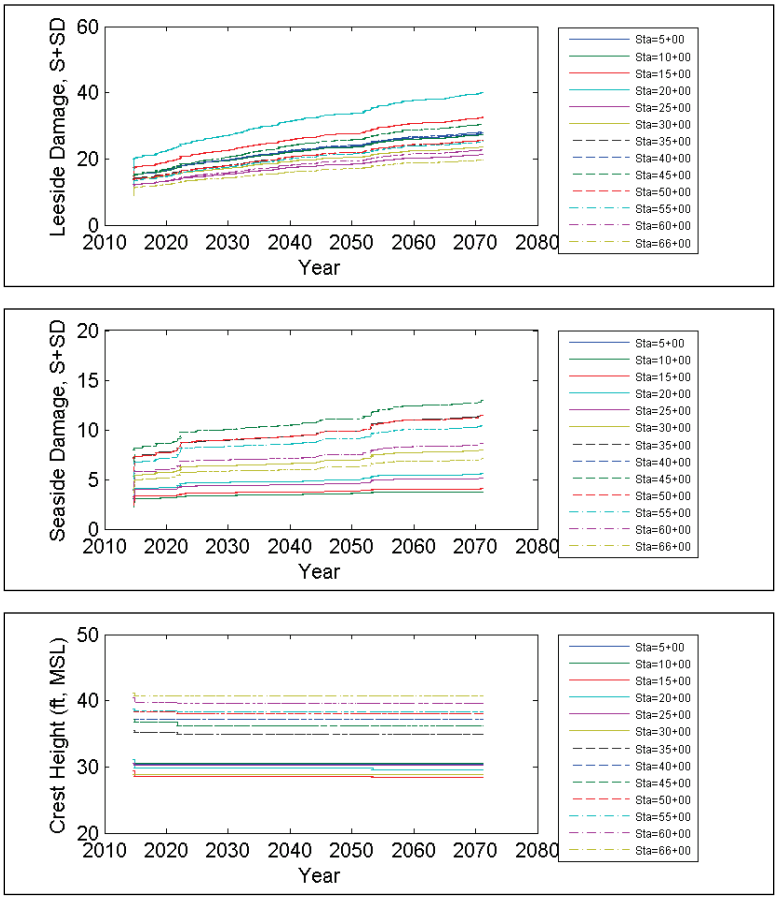


Figures 36 and 37 show the wave heights throughout the HoR for the mean of all historical storm peaks and for Hurricane Bob, respectively, for the without-project alternative and SLR3. These figures can be compared with Figures 28 and 29. Both sets of Figures illustrate that the highest waves in the HoR are located near the east entrance while the second highest regions are inside the west entrance and in the outer reach of the navigation channel. Figures 36 and 37 also show that there is little change in mean or maximum peak storm wave conditions over the historical conditions and that the breakwater still provides significant sheltering in a deteriorated state. The two sets of figures show that the mean peak storm wave height in the navigation channel is approximately 3 ft, and the maximum peak storm wave height for Hurricane Bob in the navigation channel is 7–8 ft for both the historical and the without-project alternatives.

Figure 35. Exceedance of $H_{m0}$ = 4 ft limit state for historical wave and water level conditions, without-project structure conditions, and SLR 1.

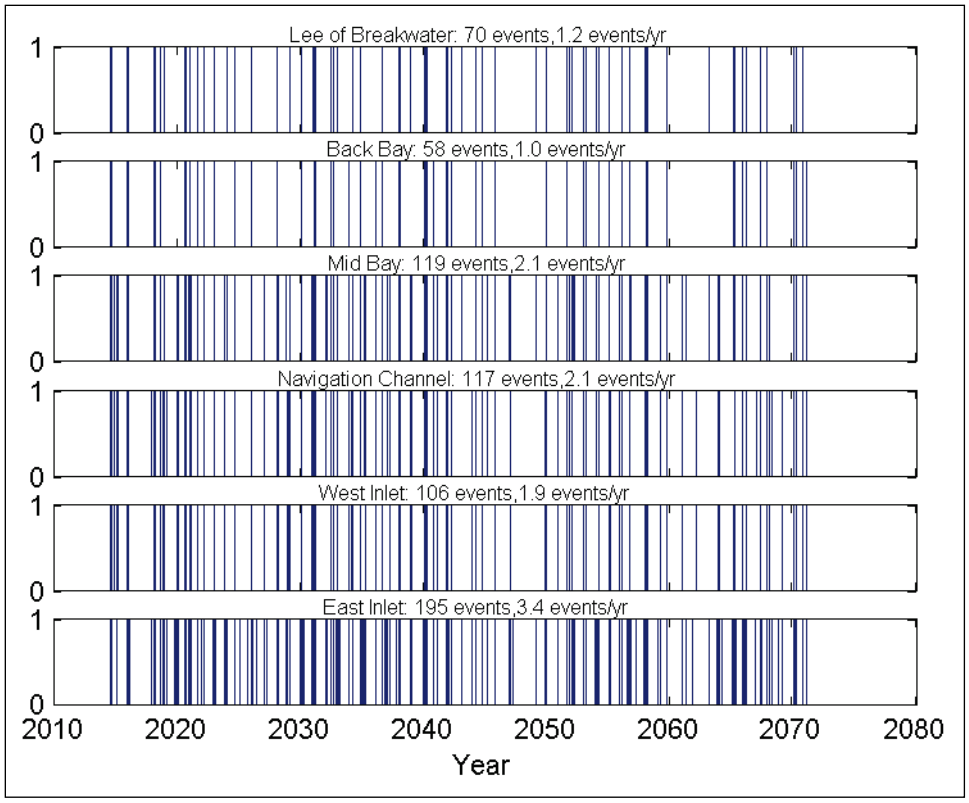


Table 9. Wave height limit state exceedances for without-project alternative exposed to historical wave and water level conditions with SLR.

| SLR | Save Station Group | 1 | 2 | 3 | 4 | 5 | 6 |
|---|---|---|---|---|---|---|---|
| 1 | Inside events that exceeded 4 ft | 70 | 58 | 119 | 117 | 106 | 195 |
| 1 | Number of common events | 59 | 43 | 66 | 50 | 49 | 70 |
| 2 | Inside events that exceeded 4 ft | 70 | 60 | 119 | 118 | 107 | 194 |
| 2 | Number of common events | 59 | 43 | 66 | 50 | 49 | 70 |
| 3 | Inside events that exceeded 4 ft | 71 | 62 | 122 | 118 | 109 | 194 |
| 3 | Number of common events | 60 | 44 | 66 | 50 | 49 | 70 |
| 4 | Inside events that exceeded 4 ft | 77 | 60 | 122 | 120 | 109 | 194 |
| 4 | Number of common events | 64 | 42 | 65 | 51 | 50 | 70 |
| 5 | Inside events that exceeded 4 ft | 78 | 64 | 123 | 120 | 113 | 193 |
| 5 | Number of common events | 64 | 44 | 66 | 50 | 52 | 70 |

Figure 36. Mean of all peak transmitted storm wave heights for without-project alternative using historical storms but run from 2014 through 2070 with no breakwater repair and initial condition of damaged structure in 2010. NRC Curve I SLR scenario was used.

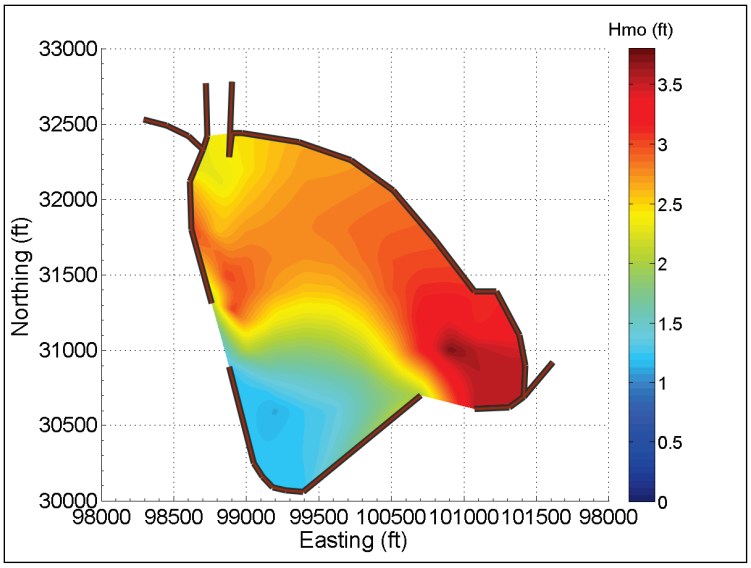


Figure 37.Peak transmitted storm wave heights for without-project alternative for Hurricane Bob occurring 37 yr into life cycle that begins in 2014. Damage on breakwater at time of hurricane is computed with no breakwater repair and initial condition of damaged structure in 2010. NRC Curve I SLR scenario was used.

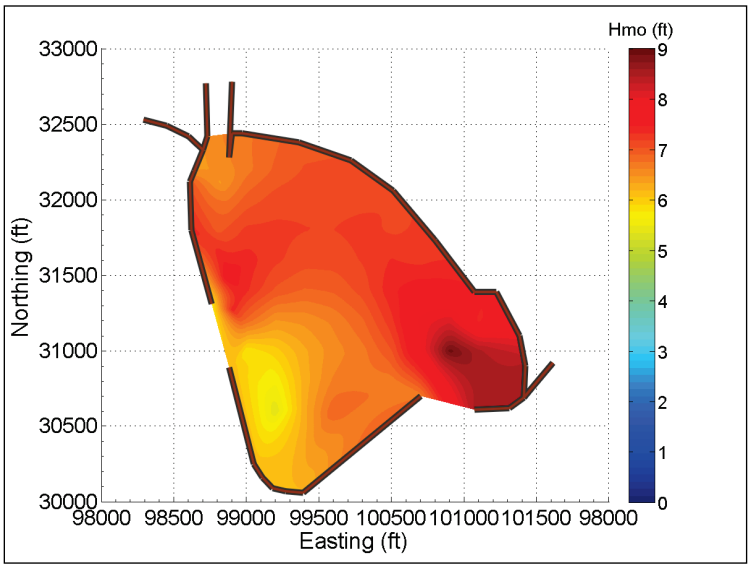


## 4.2 Breakwater damage for repair alternatives

Tables F1–F15 in Appendix F contain the results of simulations using BWSim for historical waves and water levels with the five SLR scenarios

shown in Figure 18. The tables contain results for the four cross-sectional alternatives with eight different return period armor stone sizes. Separate tables are given for seaside damage, leeside damage, and remaining freeboard at the end of each 57 yr life-cycle simulation. All simulations start with the repaired cross sections shown in Figures 19–22.

These tables indicate that all alternatives sustain little damage because the structure was designed for relatively conservative wave and water level conditions. The impact of the higher crest can be seen by comparing the low-crested Alternatives 1–2 with the higher-crested Alternatives 3–4. The leeside damage is less with the higher crest.

The reach 35+00–45+00 sustains the most damage for all alternatives and all SLR scenarios. This is due to there being larger waves seaward of this section for most storms. This is consistent with the historical damage along the structure with this area being more severely damaged.

The results of the simulations summarized in Appendix F suggest that the damage decreases with increasing armor stone size uniformly across all alternatives and all SLR scenarios, as expected. There is very little crest erosion for all Alternatives.

As discussed above, SLR scenario 3 (NRC-I) is the most likely scenario, so attention can be focused on Tables F7–F9. Looking at the damage levels for Alternatives 1 and 3, seaside damage for 50–75 yr return period stone sizes (Alternatives 1.4–1.5 and 3.4–3.5) is in the range of $S = 2 - 4$, only slightly above the no-damage criterion of $S = 2$. This is a level of damage considered to be in the serviceable range and is likely to not require major maintenance. For leeside damage, the damage is in the range $S = 0 - 5$ for all alternatives. This is also in an acceptable range that would not require maintenance.

The question remains: even if the damage to the structure was substantial or the structure was not rehabilitated, what is the impact to the protected areas? This question will be addressed in the following chapter.

## 4.3 Wave transmission

The resulting wave heights within the HoR at select save stations are listed in Tables F16 through F25 in Appendix F. Tables F16 through F20 list the *mean* peak storm significant wave heights ($H_{mo}$) computed across all

storms for each station, and Tables F21 through F25 list the *maximum* peak storm wave heights. The tables indicate that the wave heights in the lee of the structure are not overly sensitive to damage or sea level rise.

Generally, the peak transmitted wave height is not a function of armor stone size. In addition, comparing across all Figures, SLR has very little effect on overall peak transmitted wave heights.

Figures 38 and 39 show the transmitted wave heights for the with-project condition, similar to the previous two figures. In this case, the wave heights are shown for Alternative 1, 75 yr return period armor stone size and SLR scenario 3. The figures are similar to the without-project alternative illustrating that there is little difference in mean or peak transmitted wave heights between the with- and without-project alternatives.

To demonstrate the changes resulting from a repaired breakwater, difference plots between the with-project and without-project alternatives are shown in Figures 40 through 45 for various alternatives and SLR scenarios. In all cases, the 75 yr return period stone size is used. For Figures 40 and 41, the mean of all storm peaks and Hurricane Bob transmission are shown, respectively, for the NRC Curve I SLR scenario and Alternative 1. Figures 42 and 43 are similar except that Alternative 3 is shown (higher crest than Alternative 1). Figures 44 and 45 are similar to 40 and 41 except that the highest SLR scenario was used, NRC Curve III. As with the other figures, the increases in wave heights between the with- and without-project alternatives are minimal and generally less than 0.5 ft in the areas of concern and are less than 2 ft in the navigation channel for the storm of record. This demonstrates that the structure in a deteriorated condition along with increased sea levels will remain relatively effective at reducing wave heights in the HoR.

Finally shown in the ERDC modeling effort is that a majority of the wave energy entering the HoR impacting navigation and the shoreline does so through the east and west entrances in the breakwater complex. Shown in Figure 46 is a plot of wave height difference between the existing conditions with both gap and overtopping energy vs. just the gap transmission. As shown, the increase in wave height from overtopping is less than 0.5 ft, indicating a majority of the energy is entering through the breakwater gaps and not over the damaged structure. The gaps are constructed features and are part of the authorized project, so closing the two entrance gaps was not considered during this study.

Figure 38. Mean transmitted wave height for life cycle from 2014 through 2070 with no repair. With-project alternative is Alternative 1 using 75 yr return period and NRC Curve I.

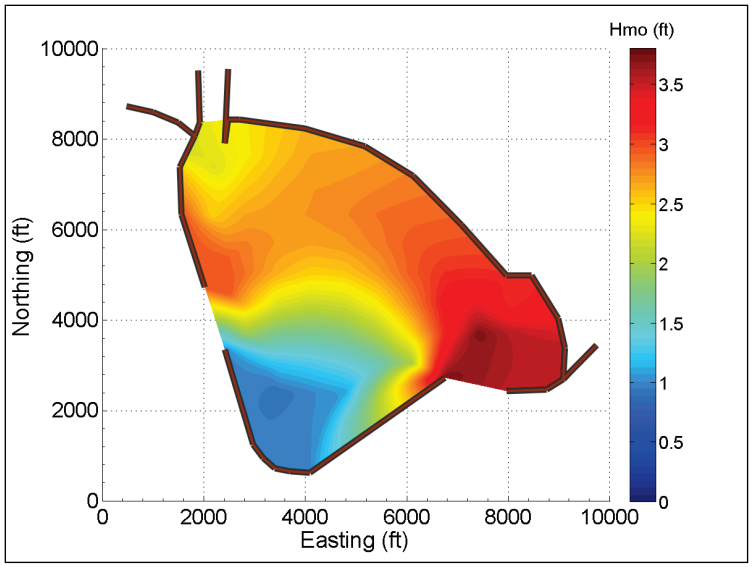


Figure 39. Peak transmitted storm wave heights for Hurricane Bob occurring 37 years into life cycle that begins in 2014. Damage on breakwater at time of hurricane is computed with no breakwater repair and initial condition of damaged structure in 2010. With-project alternative is Alternative 1 using 75 yr return period and NRC Curve I.

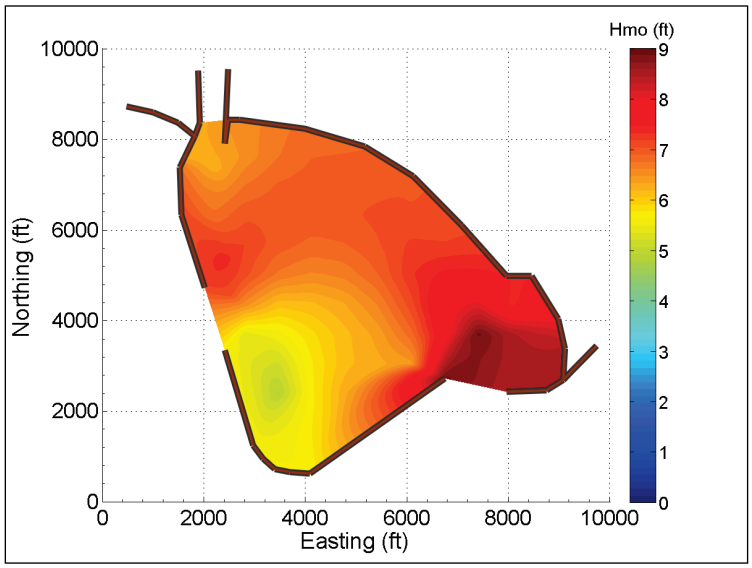

Figure 40. Difference of mean of storm peak transmitted wave height between with-project and without-project alternatives for life cycle from 2014 through 2070 with no repair. With-project Alternative 1 using 75 yr return period and NRC Curve I.

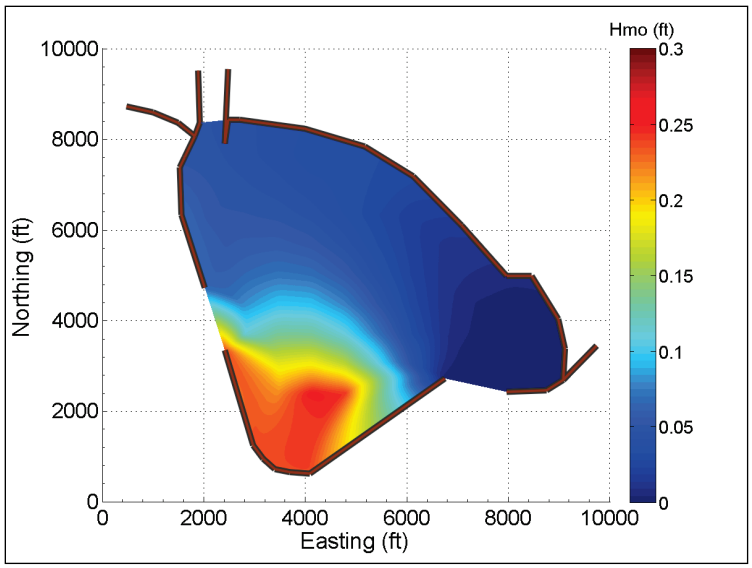


Figure 41. Difference of peak transmitted wave height between with-project and without-project alternatives for Hurricane Bob occurring 37 yr into life cycle that begins in 2014. Damage on breakwater at time of Hurricane Bob is computed with no breakwater repair and initial condition of damaged structure in 2010. With-project alternative is Alternative 1 using 75 yr return period and NRC Curve I.

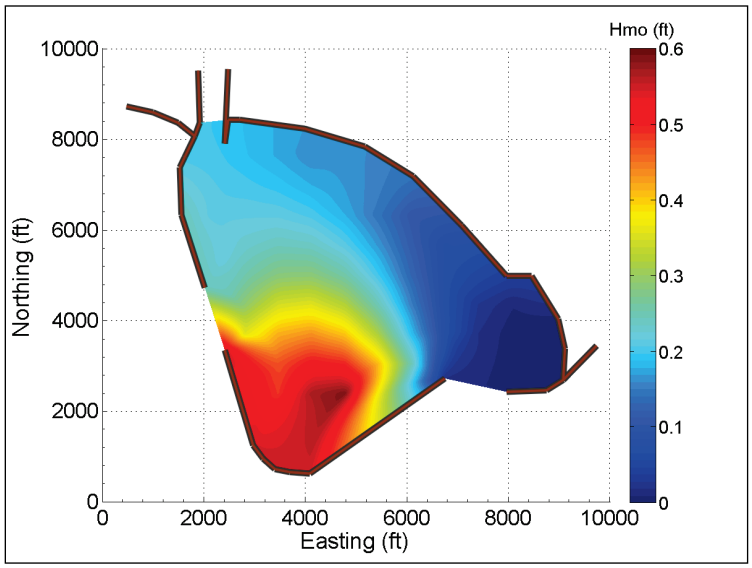

Figure 42. Difference of mean of storm peak transmitted wave height between with-project and without-project alternatives for life cycle from 2014 through 2070 with no repair. With-project Alternative 3 using 75 yr return period and NRC Curve I.

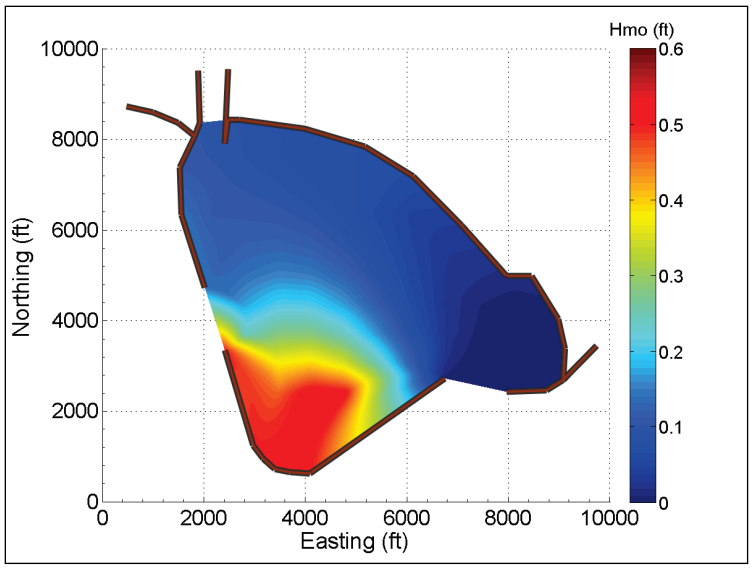


Figure 43. Difference of peak transmitted wave height between with-project and without-project alternatives for Hurricane Bob occurring 37 yr into life cycle that begins in 2014. Damage on breakwater at time of Hurricane Bob is computed with no breakwater repair and initial condition of damaged structure in 2010. With-project alternative is Alternative 3 using 75 yr return period and NRC Curve I.

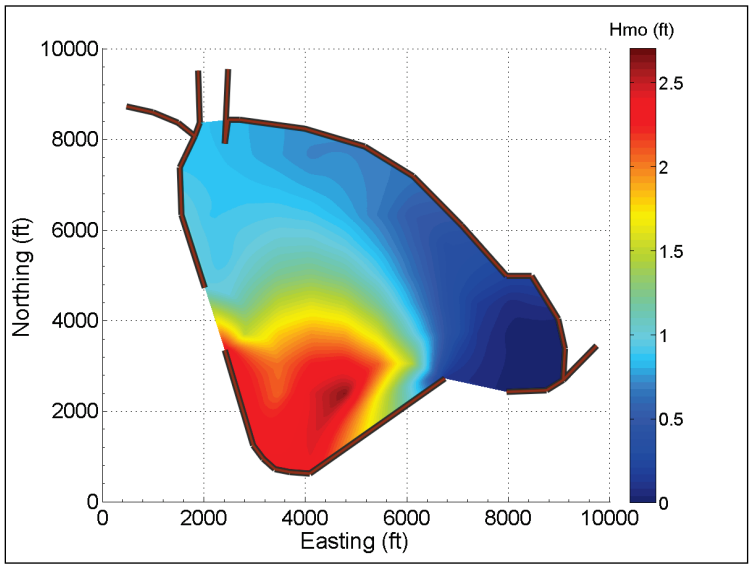

Figure 44. Difference of mean of storm peak transmitted wave height between with-project and without-project alternatives for life cycle from 2014 through 2070 with no repair. With-project Alternative 1 using 75 yr return period and NRC Curve III.

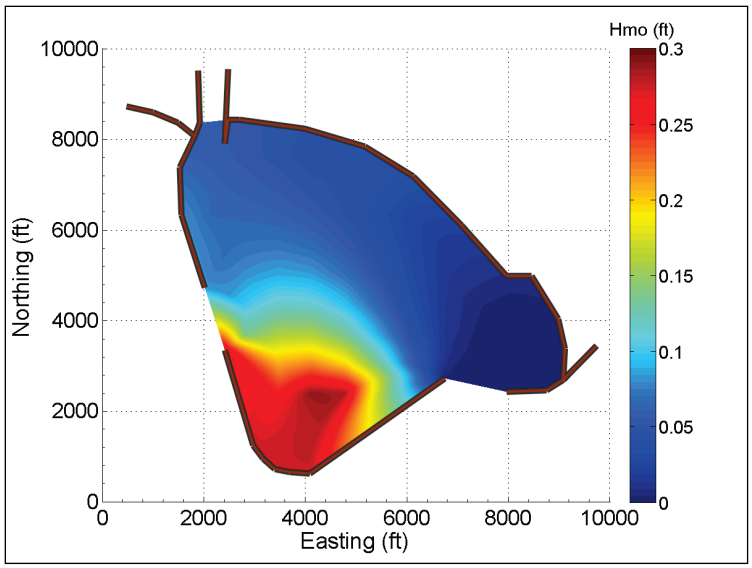


Figure 45. Difference of peak transmitted wave height between with-project and without-project alternatives for Hurricane Bob occurring 37 yr into life cycle that begins in 2014. Damage on breakwater at time of Hurricane Bob is computed with no breakwater repair and initial condition of damaged structure in 2010. With-project alternative is Alternative 1 using 75 yr return period and NRC Curve III.

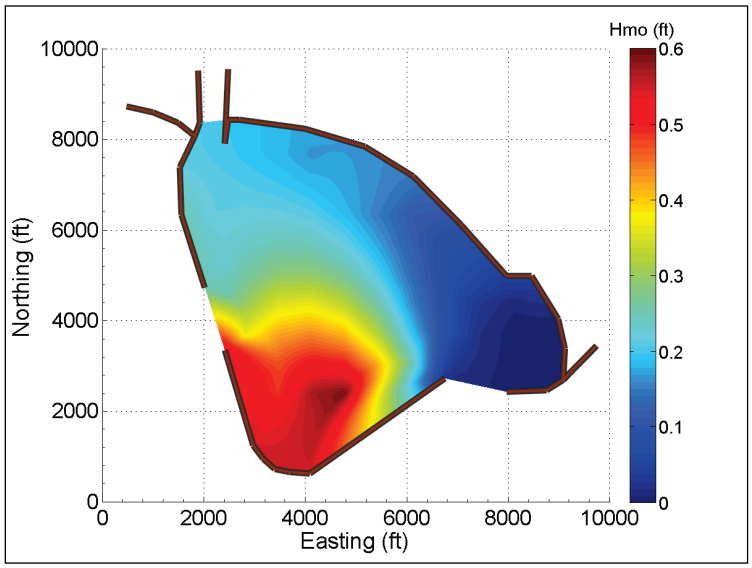

Figure 46. Difference of mean transmitted wave height between with-project and without-project where with-project alternative does not allow overtopping transmission or damage for life cycle from 2014 through 2070. With-project Alternative 1 using 75 yr return period under NRC Curve I.

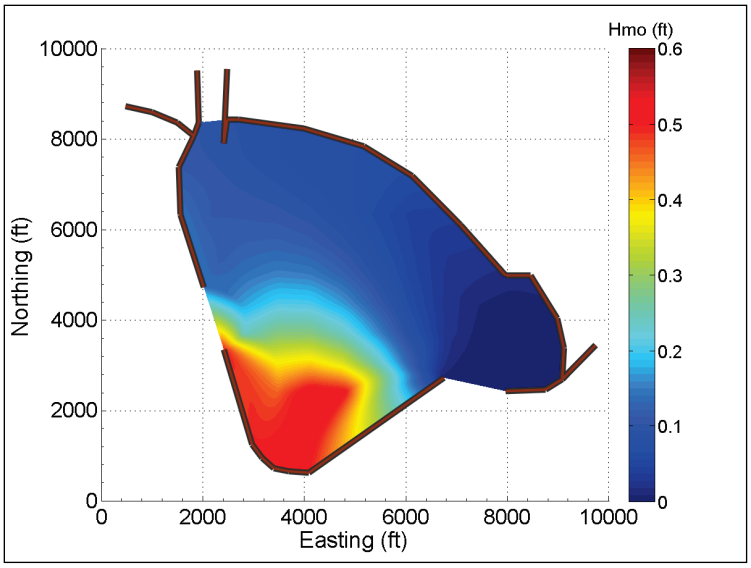


## 4.4 Navigation impacts — days closed

Given the minor change in wave heights shown in the previous section for the structure in various states of repair and even with significant SLR, it was predicted that the impacts to navigation would be minimal, and this was confirmed through the following analysis. The full set of historical storms from the past 57 yr was modeled with the 1984 repaired cross section of the breakwater in place (similar to Alternative 1). The repaired condition was used to set a benchmark for comparison using the wave height limits discussed above. Recall that the limiting significant wave height outside the HoR was $H_{mo}$ = 10 ft and inside the HoR was $H_{mo}$ = 4 ft. Using these limits along with the wave modeling discussed previously, an analysis was performed to determine how often the navigation limits were exceeded for various repair/damage states of the breakwater by running the full set of storms for the 57 yr period of wave data.

In the 57 yr historical record, there were 71 cases of the exterior wave condition exceeding $H_{mo}$ of 10 ft. Also from the modeling, the number of occurrences within the harbor exceeding $H_{mo}$ of 4 ft was determined. For the West Navigation Channel Group within the HoR (Figure 32), the 4 ft limit was exceeded 90 times, and for the East Entrance Group the 4 ft limit was exceeded 158 times. The fact that the east entrance exceeded the west

entrance is not surprising since most storm waves approach from the south-to-southeast direction, which aligns better with the east entrance.

The wave modeling and results were further screened, and it was determined that there were 55 exceedance events over 57 yr that occurred in the West Navigation Channel area that were exclusive of an outside closure. That meant that during the 57 yr time period, there were 55 times that boats could not make it out of the Point Judith Harbor at Galilee because conditions within the HoR would not allow transit to the open ocean, but if they could have made it to the ocean, the waves would have been less than the 10 ft navigation threshold, and the ocean would have been *open* to navigation. For the east side entrance, that number was 90 events. Once again, the larger number is logical since there is more direct exposure to the predominant storm wave direction at the East Entrance. Considering the higher exposure and the more frequent closure of the East Entrance, the main focus of this effort was placed on the West Entrance since vessels trying to transit out of the harbor under storm conditions would do so at the West Entrance. Also, if the West Navigation Channel was closed, this would prevent vessels from leaving port or entering port since vessels coming through the East Entrance would still have to use the West Navigation Channel. The benchmark comparing the various with- and without-project conditions for navigation into and out of the HoR and Point Judith Harbor was set at 55 exclusive events over the 57 yr storm record period at the west channel. This averages just less than one closure event per year. Once again, this was for the 57 yr historical life cycle, with a repair in 1984.

A second measure of navigational impacts was the effect on the actual designed function of providing shelter during storms. As shown in Figure 32, the area designated as the Mooring Area Group would be the area where vessels would anchor. It was uncertain what the wave height threshold would be for a vessel on anchorage seeking shelter from a storm. This would depend on vessel size. For consistency, the 4 ft threshold and the associated number of events were used as a relative comparison for the future with- and without-project conditions. For the historical life cycle, with a repair in 1984, there were 30 events in the 57 yr storm record that exceeded the 4 ft threshold.

To determine the change in navigation days, and therefore the impact to navigation, Table 10 was developed listing the number of exclusive

navigation closure days for the West Navigation Channel and the number of anchorage days in the Mooring Area for the with- and without-project alternatives and for the range of SLR.

Table 10. Number of navigation closure days within the HoR.

| BW Condition | West Navigation Channel | | Mooring Area | |
|---|---|---|---|---|
| | 57 yr record | days/yr | 57 yr record | days/yr |
| Historical | 91 | 1.6 | 29 | 0.5 |
| W/O Proj SLR 2 | 118 | 2.1 | 70 | 1.2 |
| W/O Proj SLR 3 | 118 | 2.1 | 70 | 1.2 |
| W/O Proj SLR 5 | 120 | 2.1 | 78 | 1.4 |
| Alt 1, SLR2 | 112 | 2.0 | 67 | 1.2 |
| Alt 1, SLR3 | 112 | 2.0 | 67 | 1.2 |
| Alt 1, SLR5 | 112 | 2.0 | 72 | 1.3 |
| Alt 3, SLR2 | 96 | 1.7 | 55 | 1.0 |
| Alt 3 SLR3 | 96 | 1.7 | 55 | 1.0 |
| Alt 3 SLR5 | 96 | 1.7 | 58 | 1.0 |

## 4.5 Navigation impacts — sediment transport into channel

The leading cause of sediment transport along most open ocean coasts is wave energy. Waves breaking on a shoreline generate longshore currents and also suspend sediment from the wave-breaking action. The suspended sediment is then transported alongshore. By reducing the wave energy within the HoR, sediment transport must be reduced as well. Therefore, if wave energy within the HoR increased significantly due to the deterioration of the breakwater, it could be inferred that sediment transport would increase, leading to increased shoaling rates within the channels. This would potentially require increased dredging. As shown in the prior sections, wave energy will not increase significantly for the no-repair alternative.

To help further illustrate the minor increase in wave energy that results from the breakwater deterioration, the number-of-navigable-days metric was once again used. While the 4 ft threshold was set for safe navigation, it was also considered a metric for determining overall increase in wave height within the HoR and in the near-shoreline beach region of the HoR. Back Bay and Mid Bay Areas were used to develop metrics similar to what was done for navigation (Table 10). The total number of days with wave heights above 4 ft was used to determine the increased wave energy from a

deteriorated structure and to measure the reduction that would result from repairing the structure. As presented in Table 11, the 4 ft wave height exceedance decreases from 1.0–1.1 days/yr to 0.7–0.9 days/yr between without-project and with-project alternatives for the Back Bay area, depending on the SLR scenario. Similarly, for the Mid Bay Area, the 4 ft exceedance decreases from 2.1–2.2 to 1.9–2.1 days/yr. This decrease is not statistically significant, and therefore, the increase in potential sediment transport within the HoR is likely not significant.

Table 11. Number of days waves exceed 4 ft within HoR.

| BW Condition | Back Bay | | Middle Bay | |
|---|---|---|---|---|
| | 57 yr record | days/yr | 57 yr record | days/yr |
| Historical | 35 | 0.6 | 76 | 1.3 |
| W/O Proj SLR 1 | 58 | 1.0 | 119 | 2.1 |
| W/O Proj SLR 3 | 60 | 1.1 | 119 | 2.1 |
| W/O Proj SLR 5 | 63 | 1.1 | 123 | 2.2 |
| Alt 1, SLR1 | 52 | 0.9 | 113 | 2.0 |
| Alt 1, SLR3 | 53 | 0.9 | 117 | 2.1 |
| Alt 1, SLR5 | 53 | 0.9 | 119 | 2.1 |
| Alt 3, SLR1 | 42 | 0.7 | 107 | 1.9 |
| Alt 3, SLR3 | 43 | 0.8 | 109 | 1.9 |
| Alt 3, SLR5 | 42 | 0.7 | 110 | 1.9 |

## 4.6 Alternative analysis — beach storm performance evaluation

As discussed above, the benefits/impacts to navigation of not repairing the breakwater are minimal. Also, due to the very small increase in wave height in the HoR, it was concluded that longshore transport of beach sediment and harbor sediment would not be increased significantly, and therefore, it is not likely that there would be a significant increase in the shoaling rate of the navigation channel into Galilee Harbor. An analysis of the beach erosion was conducted to determine the impacts of the with- and without-project alternatives.

### 4.6.1 Historical shoreline change

As part of the initial reconnaissance level study, maps were developed using aerial photography from the State of Rhode Island GIS web portal, historical shoreline data from the State of Rhode Island that spanned 1939 to 2004, and two lidar data sets from 2000 and 2007. Based on the

information in that analysis, it was concluded that the long-term trend (1939 to 2004) in shoreline movement within the HoR was generally stationary to slightly accretionary. The exception to this was at the eastern end of the HoR at the area north of the eastern entrance. This is due to wave energy coming through the gap in the breakwaters. It was also shown that, between 2000 and 2007, the shoreline was generally stable with small areas of minor erosion and accretion. However, the east end of the HoR showed continued erosion.

The short-term shoreline mapping effort was updated with the addition of the 2010 lidar data set. With the addition of the 2010 shoreline, most of the HoR shoreline switched to an erosionary trend. This indicates that during the time period between 2007 and 2010, there was erosion because during the time period of 2000 to 2007 there was no erosion. This 3 yr period cannot be taken as the new trend since it is a very short period of time. It is also understood that the shoreline has likely eroded since 2010 due to Hurricanes Irene and Sandy. These more rare events are anomalous. The recent general erosion cannot be connected to the increased damage of the Main Breakwater. The short-term erosion signal is of interest and certainly warrants monitoring. This could be done by the State, Town of Narragansett, or through the use of the USACE lidar data flights, which are flown every 5 yr.

### 4.6.2 SBEACH modeling overview

SBEACH is an empirically based numerical model used for simulating 2D, cross-shore beach morphology change under hydrodynamic loading. The model was initially formulated using data from prototype-scale laboratory experiments and further developed and verified based on field measurements (Larson and Kraus 1990).

To run the SBEACH model, two basic pieces of information are needed, and those are beach profiles for the beach of interest and time-series storm data (water level, wave height, wave period, wave direction). These data were available for the beach within the HoR from the various lidar mapping efforts and the wave modeling described earlier. The SBEACH model setup consisted of importing the profiles to be modeled and developing the storm time-series.

As discussed, the beach profiles lengths were adjusted to match the wave model output locations. The grain size was set based on the collected grain size data from the USACE. The rest of the parameters were left at a default.

### 4.6.3 Beach profiles

The profiles considered for SBEACH modeling were taken from the lidar mapping completed by USACE in 2010. As shown in Figure 47, five profile lines were considered covering the two beach zones and to be coincident with the wave model output stations. Beach zones considered included the sandy beach to the west side of the HoR, which had significant dune features and was fronting residences, and the more rocky/cobble shoreline on the east side of the HoR. The profile names were designated by the nearest wave output stations at the seaward end of the profiles. From the five profiles that were extracted, only Profile 16 was modeled using SBEACH. Profile 16 (Figure 48) was representative of the sandy beach area. The cobble beach area was exposed to waves approaching directly from the eastern entrance and so would not be sensitive to the proposed structure repair alternatives.

Figure 47. Beach profiles within HoR taken from 2010 NCMP lidar data set.

Figure 48. 2010 beach profiles.

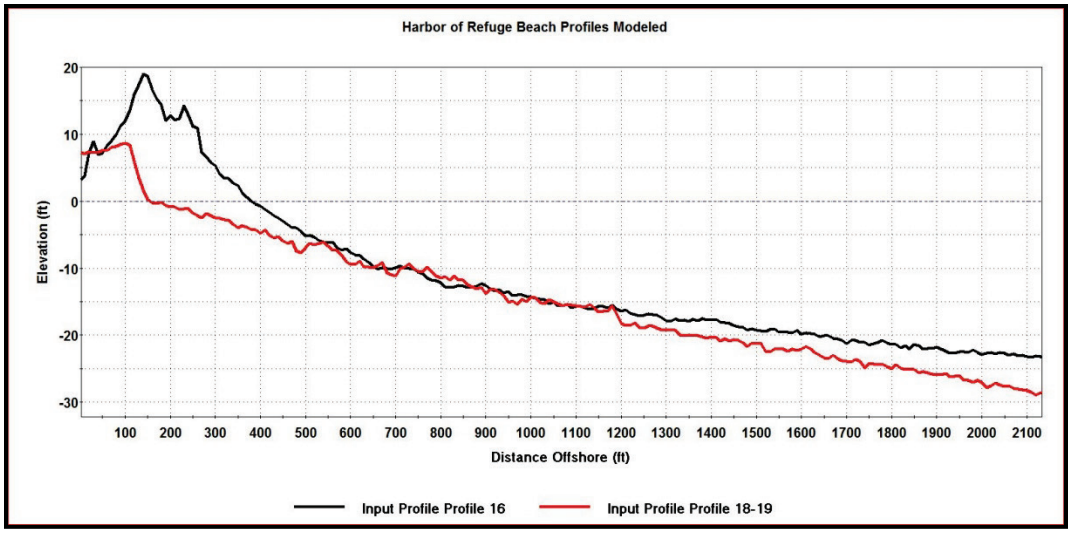


### 4.6.4 Storms for beach modeling

The storms used in the modeling were a subset of the historical storms used during the storm damage breakwater life-cycle modeling effort. Ranking the storms within this set by maximum offshore wave height and maximum water level allowed the selection of the worst storms and also lesser historic storms. Table 12 lists storms used in this effort. Within the table is a brief description of the storm and why it was selected.

Table 12. Historical storms modeled in SBEACH.

| Storm Dates | Storm Name/Description | Wave Height $H_{m0}$ (ft) | Max. Water Level ft-MSL |
|---|---|---|---|
| 8/31/1954 | Hurricane Carol (Highest Water Level) | 10.2 | 8.5 |
| 3/6/1962 | Ash Wednesday Storm (Highest Wave Height) | 17.1 | 3.8 |
| 2/6/1978 | Blizzard of '78 | 15.3 | 4.6 |
| 8/19/1991 | Hurricane Bob | 12.0 | 5.8 |
| 10/31/1991 | Perfect Storm /Halloween Storm | 9.0 | 5.3 |
| 1/23/2005 | Typical Nor'Easter | 13.2 | 2.8 |

The storms for the with- and without-project conditions were run with the historic rate of SLR and the USACE high rate (NRC III curve) of SLR. Since the storms were run in the CHL analysis with the 57 yr storm historic record, the time at which the storm occurred determined the water level due to SLR. Storms early in the record, such as Hurricane Carol, occurred with very little increase in SLR. However, storms later in the

record, such as Hurricane Bob (the Perfect Storm) and the Typical Nor'easter, occurred on a higher level of SLR due to the later occurrence in the storm record.

There was little difference between the with- and without-project wave conditions. There was a maximum increase of less than 0.30 ft in wave height between with- and without-project conditions.

### 4.6.5 SBEACH modeling results

The SBEACH results are plotted in Figures 49 through 54 for various with- and without-project conditions. Each plot shows the initial beach profile, representing year 2010, and the minimum most-eroded profile for each storm.

As anticipated, the differences between with- and without-project profiles were undetectable for the three *smaller* storms and only small differences were observed for the three *largest* storms: Hurricane Carol, Hurricane Bob, and the Perfect Storm. There are noticeable differences in profiles for the historic and high SLR rates. However, these differences are relatively small and independent of the with- and without-project conditions. With this information it was demonstrated that repairing the East Arm of the Main Breakwater did not significantly benefit the shoreline for a broad range of storm events.

Figure 49. Beach profile change for Hurricane Carol for the with- and without-project conditions.

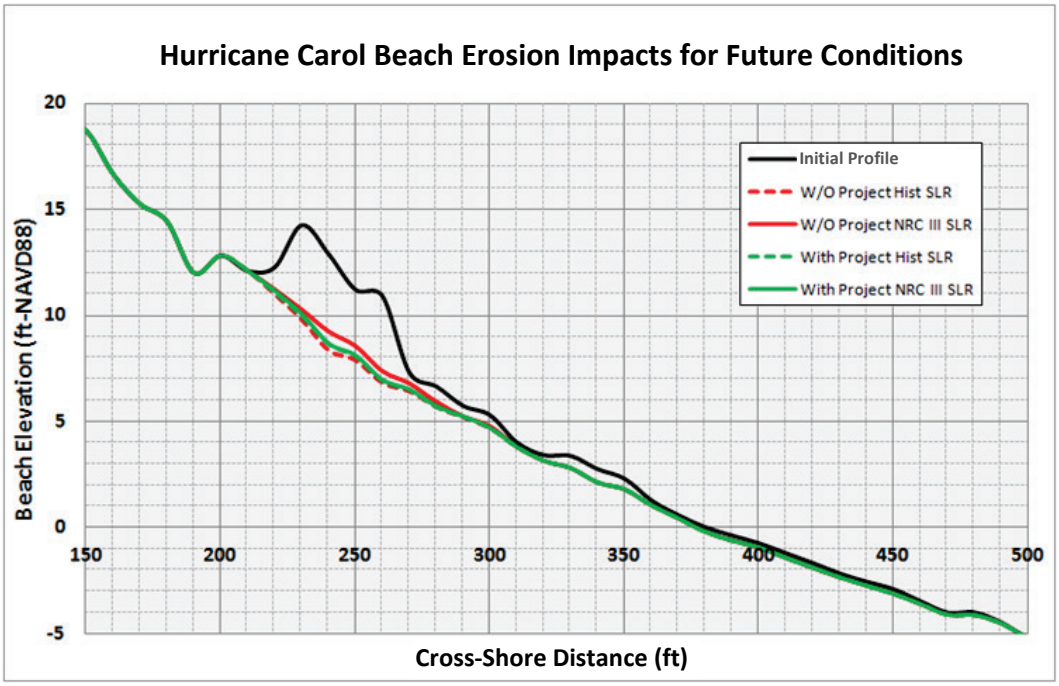


Figure 50. Beach profile change for Ash Wednesday storm for the with- and without-project conditions.

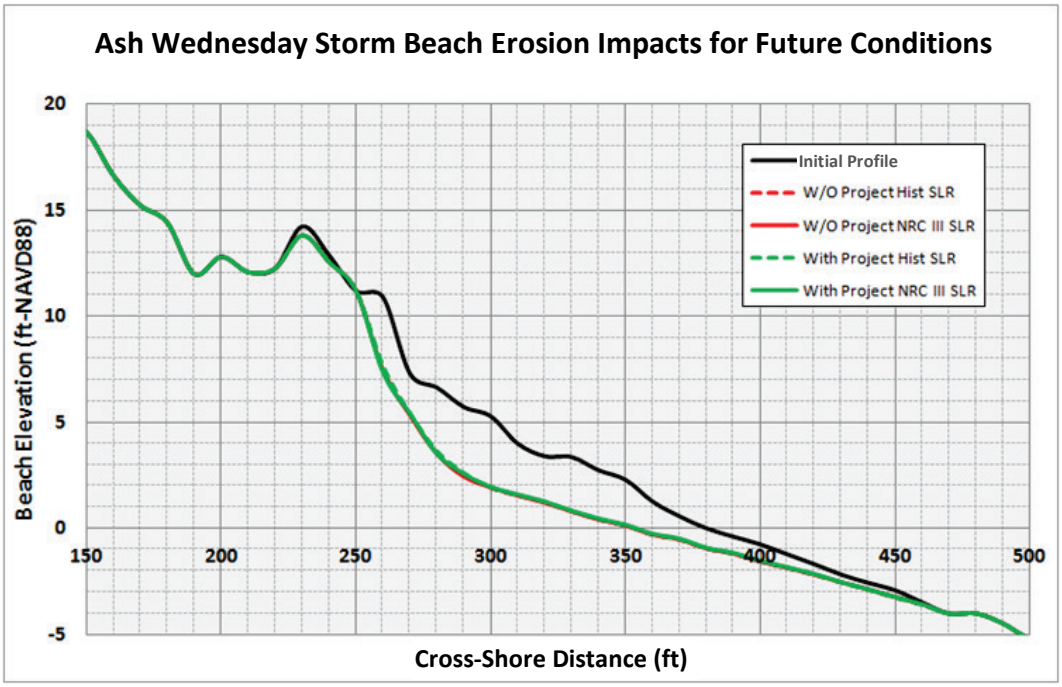

Figure 51. Beach profile change for Blizzard of 1978 for the with- and without-project conditions.

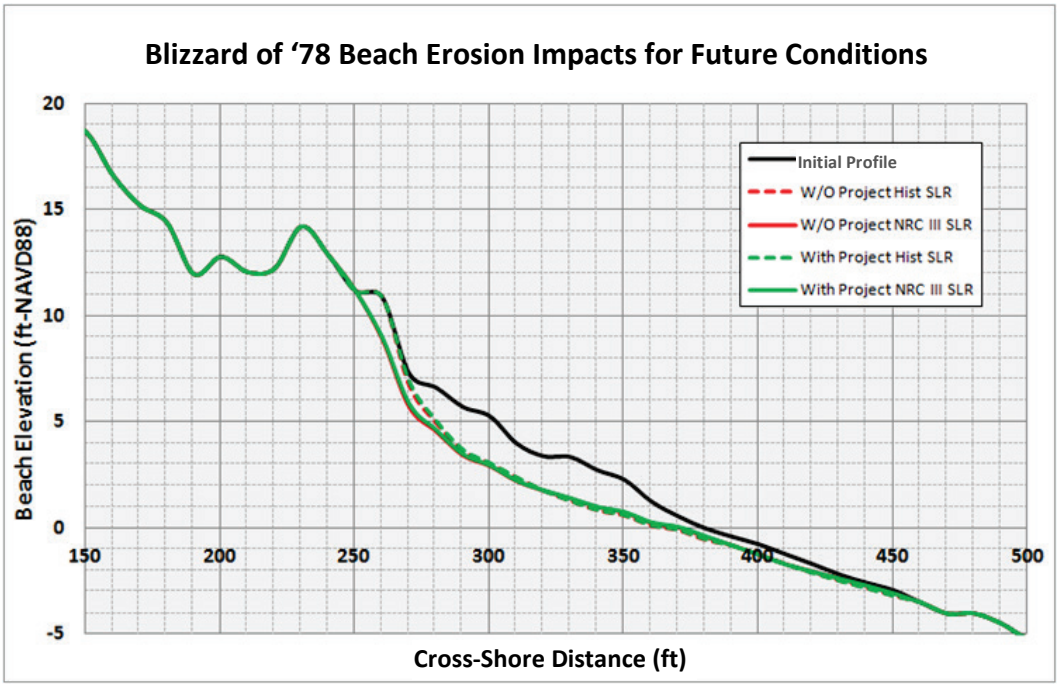


Figure 52. Beach profile change for Hurricane Bob for the with- and without-project conditions.

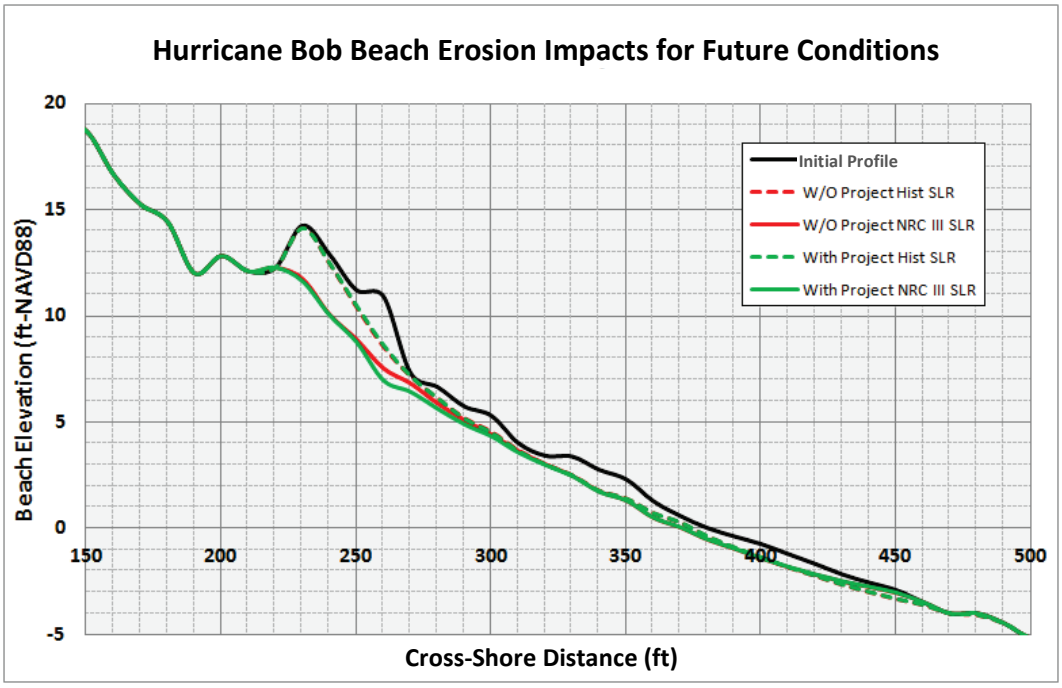

Figure 53. Beach profile change for the Perfect Storm for the with- and without-project conditions.

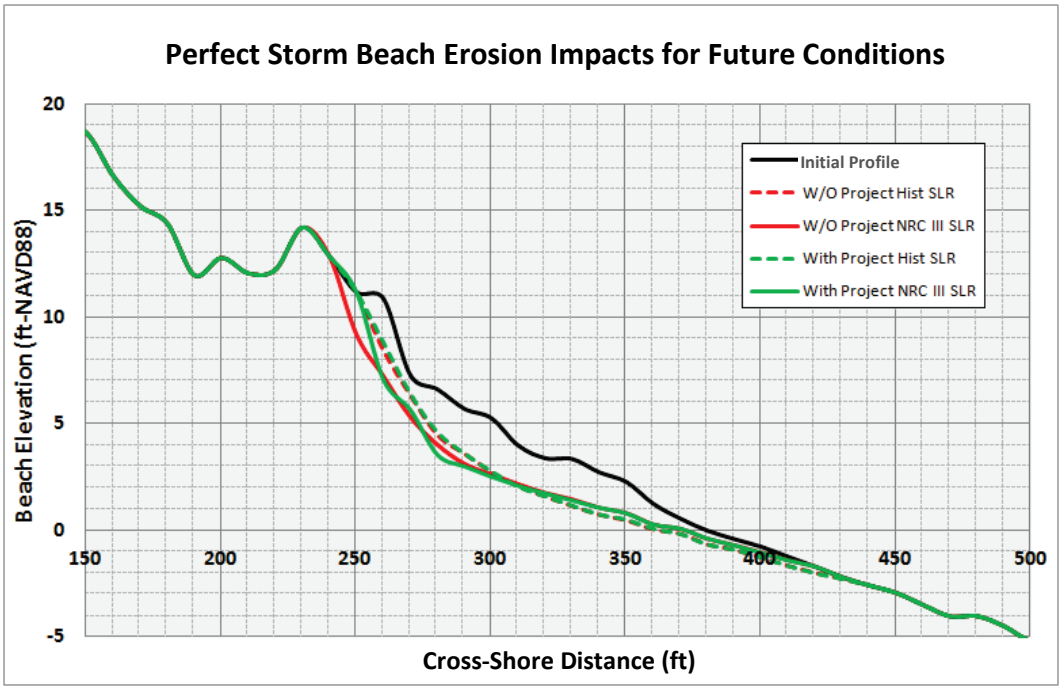


Figure 54. Beach profile change for the typical Nor'easter for the with- and without-project conditions.

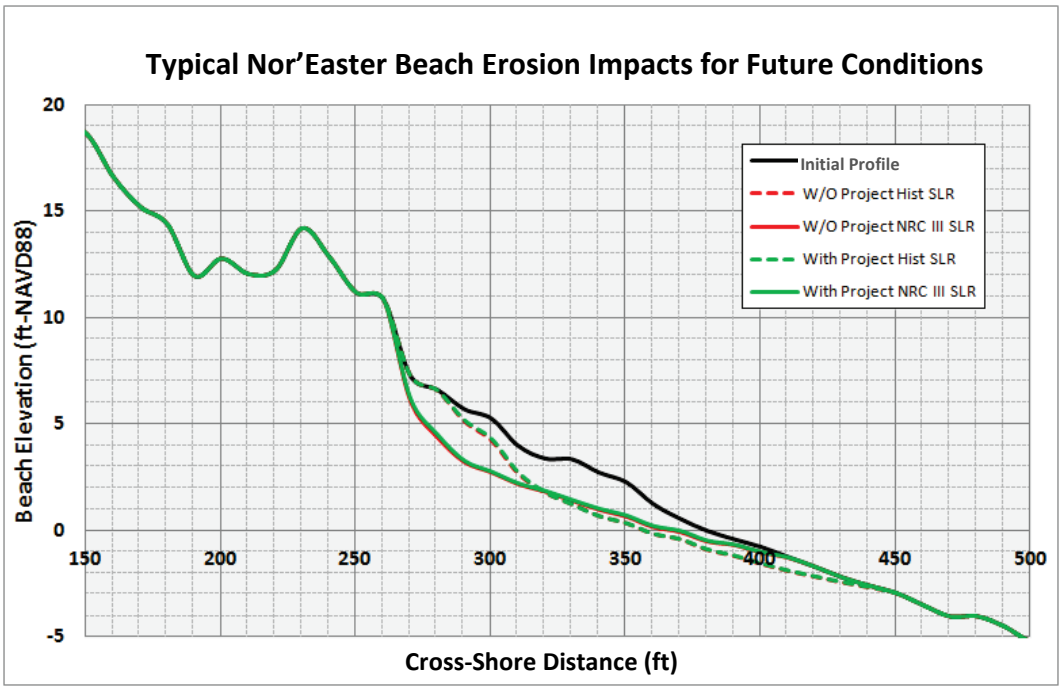

# 5 Summary and Conclusions

A detailed analysis was performed of the benefits to navigation from repairing the Main Breakwater of the Point Judith HoR. Detailed wave modeling, coastal structure design, and coastal structure life-cycle deterioration modeling were performed as part of this study. An investigation of the waves in the protected region was conducted. The impacts of the with- and without-project alternatives on navigation and sheltering were determined. Additionally, the benefits of the breakwater related to storm-induced erosion were investigated.

Based on the presented analysis, it was shown that there will be negligible impacts to the HoR function and to navigation transiting to and from Galilee Harbor by constructing the breakwater alternatives investigated herein. It was also shown that the impacts to storm damage protection are minimal if the breakwater is not repaired. Based on these two findings, it was concluded and recommended that the Main Breakwater should not be repaired. If the short-term erosion problem identified between 2007 and 2010 persists, then additional study could be performed with the likely recommendation that the most cost-effective way to address the erosion problem would be to fill the beach with dredged sand from federal navigation channel-maintenance cycle.

# References


Ahrens, J. P. 1989. Stability of reef breakwaters. *Journal of Waterway, Port, Coastal, and Ocean Engineering* 115(2):221–234.

Church, J. A., and N. J. White. 2011. Sea-level rise from the late 19th to the early 21st century. *Surveys in Geophysics*. doi:10.1007/s10712-011-9119-1

Houston, J. 2013. Global sea level projections to 2100 using methodology. *Journal of Waterway, Port, Coastal, and Ocean Engineering* 139:82–87.

Hudson, R. Y. 1959. Laboratory investigation of rubble-mound breakwaters. *Journal of the Waterways and Harbor Division, ASCE* 85(WW3):93–121.

Lang, M., T. B. M. J. Ouarda, and B. Bobée. 1999. Towards operational guidelines for over-threshold modeling. *Journal of Hydrology* 225:103–117.

Larson, M., and Kraus, N. C. 1990. *SBEACH: Numerical model for simulating storm-induced beach change, report 2: Numerical formulation and model tests.* Technical Report CERC-89-9. Vicksburg, MS: U.S. Army Engineer Waterways Experiment Station.

Lin, L., Z. Demirbilek, R. Thomas, and J. Rosati. 2011. *Verification and validation of the Coastal Modeling System, Report 2: CMS-Wave*. ERDC/CHL TR-11-10. Vicksburg, MS: U.S. Army Corps of Engineers Research and Development Center.

Lin, L., Z. Demirbilek, and F. Yamada. 2008. *CMS-Wave: A nearshore spectral wave processes model for coastal inlets and navigation projects*. ERDC/CHL TR-08-13. Vicksburg, MS: U.S. Army Engineer Research and Development Center.

Luceño, A., M. Menéndez, and F. J. Méndez. 2006. The effect of temporal dependence on the estimation of the frequency of extreme ocean climate events. *Proceedings of the Royal Society Academy* 462:1683–1697.

Melby, J. A. 1999. *Damage progression on rubble-mound breakwaters*. Technical Report CHL-99-17. Vicksburg, MS: U.S. Army Engineer Waterways Experiment Station, Coastal and Hydraulics Laboratory.

Melby, J. A. 2009. Time-dependent life-cycle analysis of coastal structures. In *Proceedings of Coastal Structures 2007,* 1842–1853. Singapore: World Scientific.

Melby, J. A. 2010. Time-dependent life-cycle analysis of breakwaters. In *IAHR Congress Proceedings, 4th International Short Course/Conference on Applied Coastal Research, IAHR*, 46–64.

Melby, J. A., and S. A. Hughes. 2004. Armor stability based on wave momentum flux. In *Proceedings of Coastal Structures 2003*, 53–65. Reston, VA: ASCE.

Melby, J. A., and N. Kobayashi. 1998. Progression and variability of damage on rubble mound breakwaters. *Journal of Waterway, Port, Coastal, and Ocean Engineering* 124(6):286–294.

Melby, J. A., and N. Kobayashi. 1999. Damage progression and variability on breakwater trunks. In *Proceedings of Coastal Structures '99*, 309–316. Rotterdam: Balkema.

Melby, J. A., and N. Kobayashi. 2011. Stone armor damage initiation and progression. *Journal of Coastal Research* 27(1):110–119.

Males, R. M., and J. A. Melby. 2012. Monte Carlo simulation model for economic evaluation of rubble mound breakwater protection in harbors. *Frontiers of Earth Science Journal, Springer* 5(4):432–441.

Melby, J. A., N. C. Nadal-Caraballo, and B. A. Ebersole. 2012. *Wave height and water level variability on Lakes Michigan and St. Clair*. ERDC/CHL TR-12-23. Vicksburg, MS: U.S. Army Engineer Research and Development Center.

Melby, J. A., and N. C. Nadal-Caraballo. 2009. *StormSim: Wave statistical modeling and simulation environment*. Draft Technical Report. Vicksburg, MS: U.S. Army Engineer Research and Development Center, Coastal and Hydraulics Laboratory.

Nwogu, O., and Z. Demirbilek. 2006. Nonlinear wave interaction with submerged and surface-piercing porous structures. In *Proceedings, 30th International Conference on Coastal Engineering*, 287–299. San Diego, CA.

Nwogu, O., and Z. Demirbilek. 2001. *BOUSS-2D: A Boussinesq wave model for coastal regions and harbors*. ERDC/CHL TR-01-25. Vicksburg, MS: U.S. Army Corps of Engineers Research and Development Center.

Oceanweather Inc. 2011. Global Reanalysis of Ocean Waves Fine Atlantic Basin (GROW-FAB) Project Description. http://www.oceanweather.com/

Scheffner, N. W., D. J. Mark, C. A. Blain, J. J. Westerink, and R. A. Luettich, Jr. 1994. *ADCIRC: An advanced three-dimensional circulation model for shelves coasts and estuaries, report 5: A tropical storm database for the East and Gulf of Mexico Coasts of the United States*. Dredging Research Program Technical Report DRP-92-6. Vicksburg, MS: U.S. Army Engineers Waterways Experiment Station.

U.S. Army Corps of Engineers (USACE). 2002. *Coastal engineering manual*. Engineer Manual EM 1110-2-1100. Washington, DC: U.S. Army Corps of Engineers.

———. 2011. *Sea-level change considerations for civil works programs*. USACE Circular No. 1165-2-211. Washington, DC: U.S. Army Corps of Engineers.

Van Gent, M. R. A., and B. Pozueta. 2004. Rear-side stability of rubble mound structures. In *Proceedings, ICCE 2004, ASCE* (4):3481–3493. Reston, VA.

# Appendix A: Analysis of Bathymetric Data[1]

## A.1 Overview

An analysis of the bathymetric data was performed to ensure the accuracy of bathymetric data being used in the wave modeling for the Point Judith Harbor. The bathymetry data analyzed for this project site were acquired from five sources listed below. Details of data set analysis are described in this appendix. The term *original data* refers to the bathymetric data provided by the NAE that had been preprocessed and not the raw data. In the present analysis, the raw data were used and combined to develop a bathymetric surface for the project.

The five original data sources, dates, and their respective vertical datums are as follows:

- Lidar2010 – NAVD88
- Lidar2007 – NAVD88
- CHL2010 (multibeam) – MLLW
- NAE2010 – MLLW
- GeoDas – MLLW (MLW prior to 1980)

Spatial/temporal characteristics and area coverage of these data sets were analyzed in an attempt to determine the most appropriate bathymetry to use in numerical models. A detailed comparison of data sets was conducted in 16 subarea polygons chosen inside and outside the harbor complex. Because the extent of spatial coverage and density of data points varied between data sets, the analysis was made within the polygons where two or more data sets overlap.

It is noted that the 3 sec arc GeoDas data are sparse but have the widest coverage. Lidar 2010 data set has some gaps but generally covers the entire harbor and outside areas of interest. The Lidar2007 data set, as well as the CHL multibeam and NAE surveys, are dense along the coast, generally covering the northern interior part of the harbor. The majority of polygons have been placed around the perimeter of breakwaters and inside the harbor where the main project interests are. Only two outside polygons

[1] Authored by Zeki Demirbilek, Lihwa Lin, and Jeffrey Melby

are located far from the breakwaters. All data points contained in each polygon have been analyzed to determine the relative vertical datum differences between the overlapping data sets.

## A.2 Analysis method

The primary reason for the analysis was to determine vertical offsets (or differences) in depth or elevation between any two overlapping data sets in each polygon area, with an ultimate objective of developing an accurate combined bathymetric data set from all five data sets. The approach used in the analysis is (1) compare mean differences of unadjusted polygon depth, (2) apply a conversion to reference data sets to a consistent common vertical datum (MSL), and (3) combine the data sets into one scatter set. Note that the mean depth is based on the original datum of each data set shown above. In this analysis, the Newport, RI, water level gage (http://www.tidesandcurrents.noaa.gov/) is used as a benchmark reference for adjusting the vertical datums from mllw to MSL. Table A1 shows the various tidal datums for the Newport gage, and Figure A1 shows the location of the gage.

### A.2.1 Dataset coverage and associated subarea polygons (graphics)

Figures A2 through A7 show the extent of coverage for five data sets with sample locations plotted as scatter plots and the subarea polygons 1 through 16.

Table A1. Tidal datums for Newport tide gage.

| | MLLW feet |
|---|---|
| Mean higher high water (MHHW) | 3.852 |
| Mean high water (MHW) | 3.606 |
| North American Vertical Datum-1988 (NAVD) | 2.041 |
| Mean tide level (MTL) | 1.873 |
| Mean sea level (MSL) | 1.736 |
| Mean low water (MLW) | 0.138 |
| Mean lower low water (MLLW) | 0.000 |

Figure A1. Location of NOS Water Level Station 8452660, Newport, RI.


Figure A2. Lidar2010 coverage with subarea polygons 1 through 13.

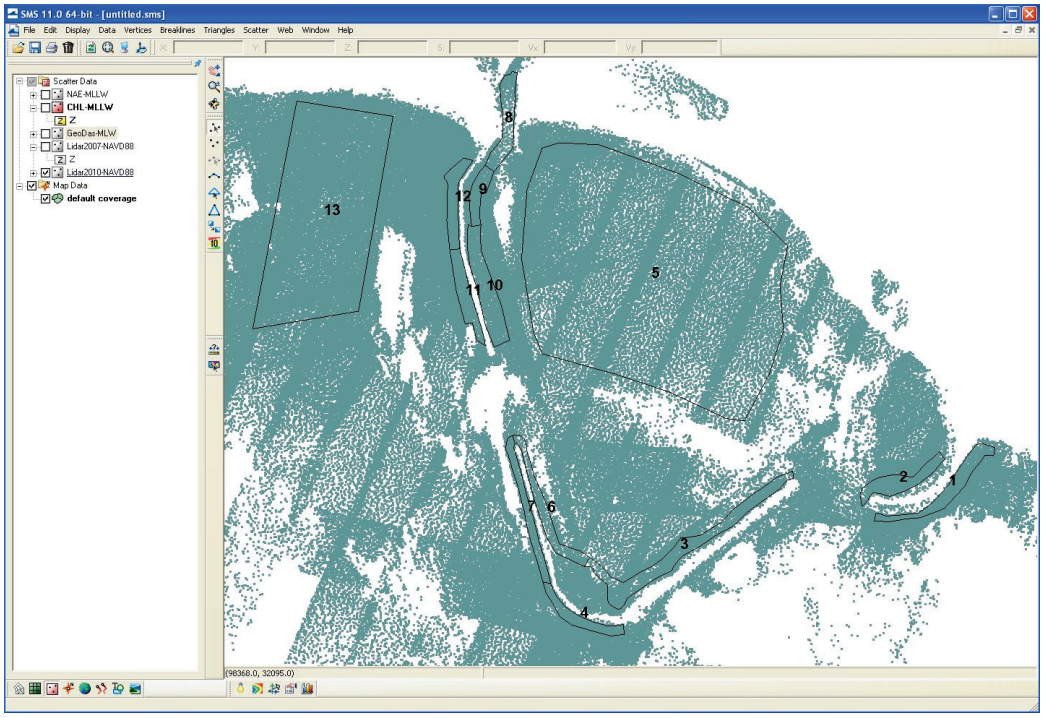

Figure A3. Lidar2010 coverage with subarea Polygons 14, 15, and 16.

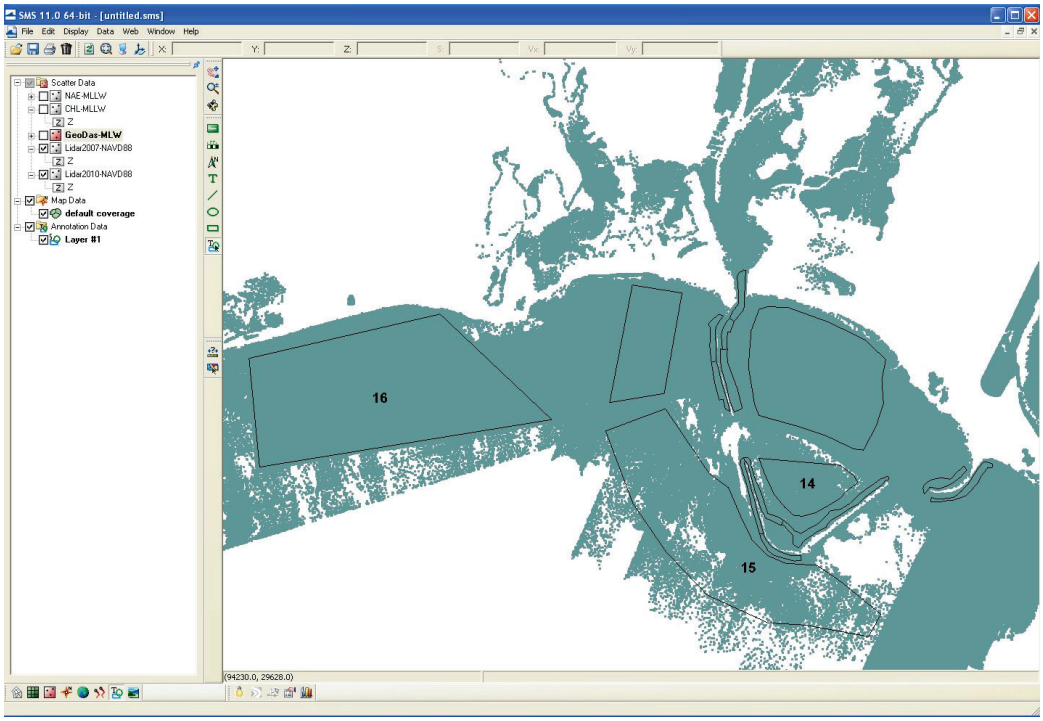


Figure A4. Lidar2007 coverage and associated polygons.

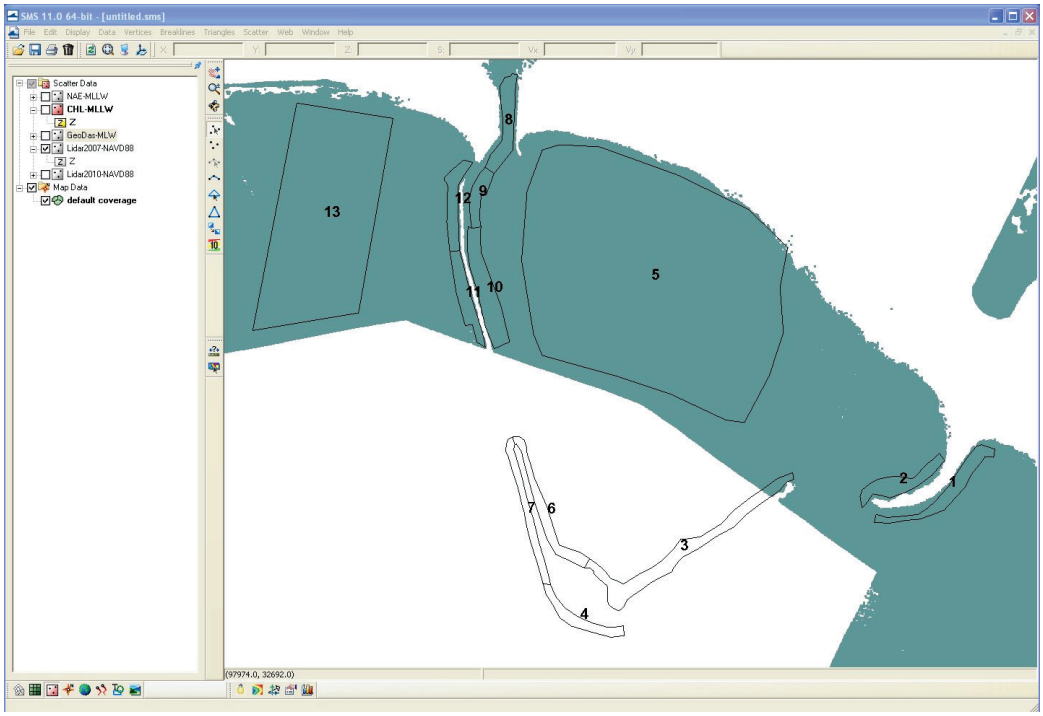

Figure A5. CHL2010 multibeam coverage and associated polygons.

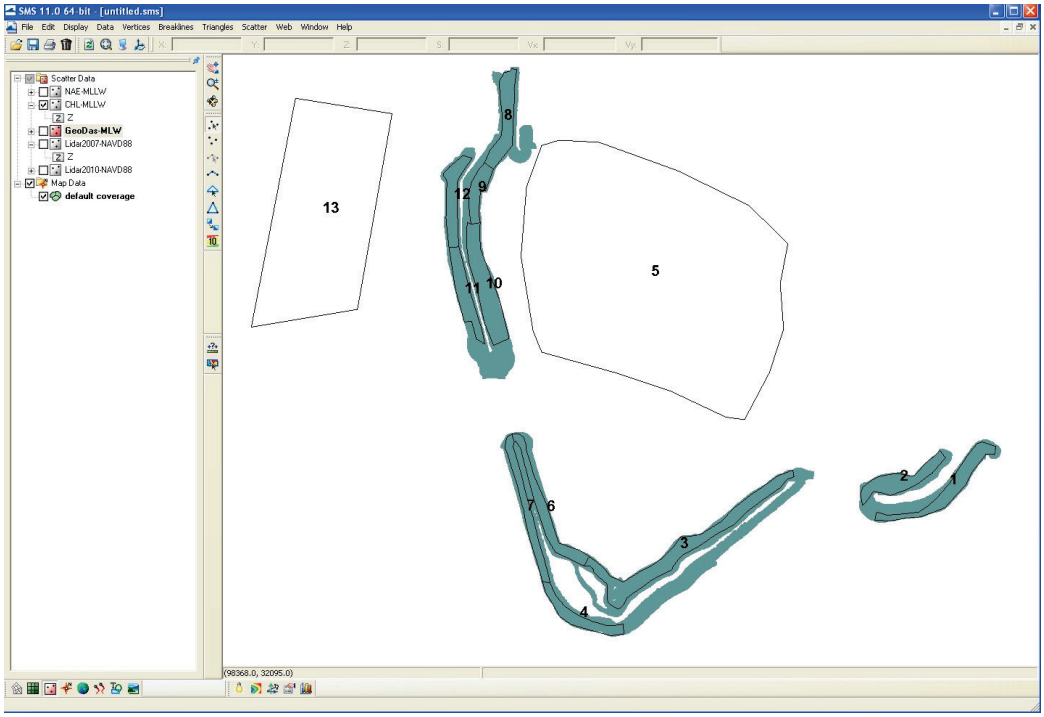


Figure A6. NAE2010 survey coverage and associated polygons.

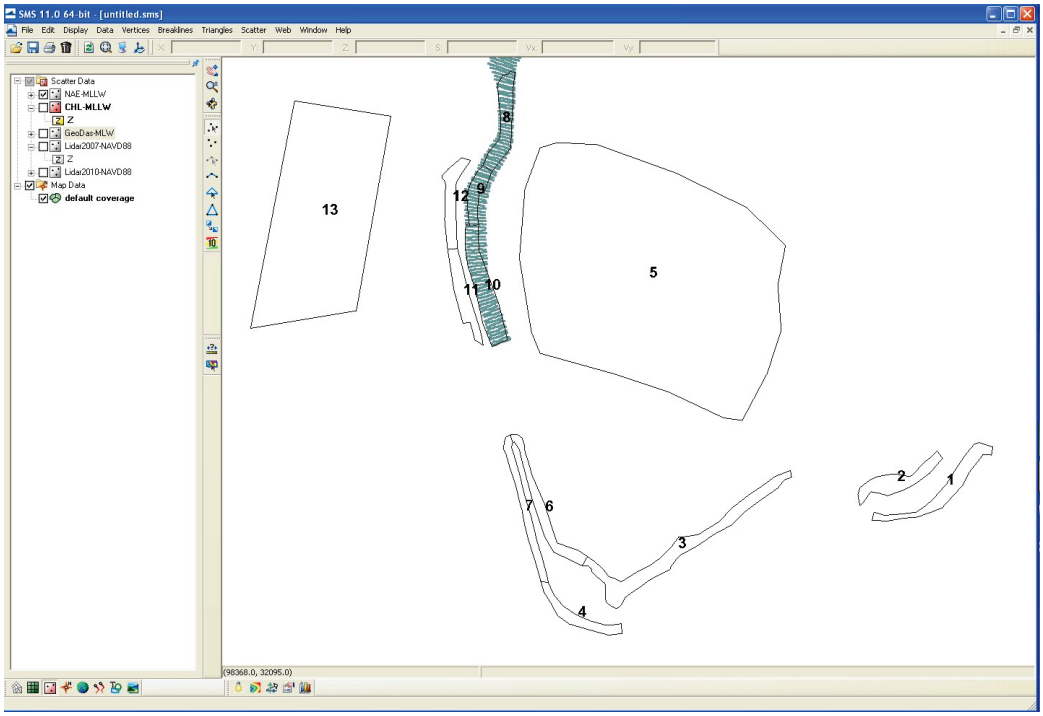

Figure A7. GeoDas coverage and associated polygons.

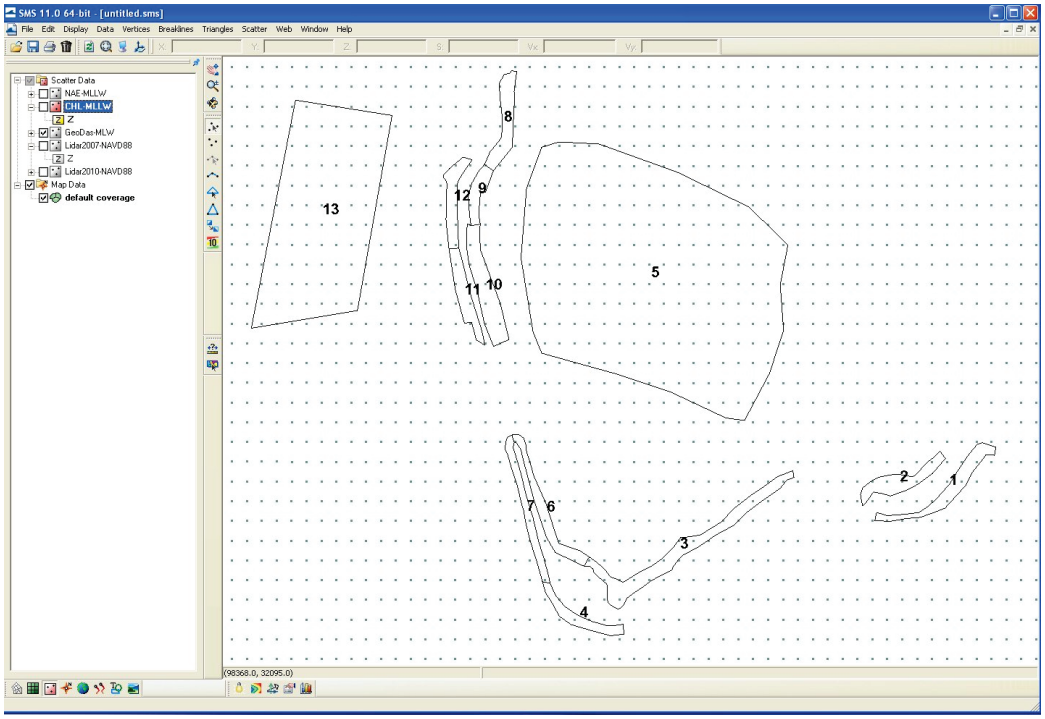


## A.2.2 Data set coverage and associated subarea polygons: Tabulated results

Tables A2 through A9 provide the mean depth value in each polygon area for different data sets.

Table A2. Data comparison for subarea polygons 1 and 2.

| Data | Subarea Polygon | Total Pts | Mean (ft) | Subarea Polygon | Total Pts | Mean (ft) |
|---|---|---|---|---|---|---|
| Lidar2010 (NAVD88) | 1 | 1738 | 21.75 | 2 | 1359 | 14.93 |
| Lidar2007 (NAVD88) | 1 | 4489 | 19.16 | 2 | 3397 | 15.45 |
| CHL2010 (MLLW) | 1 | 21617 | 15.45 | 2 | 239455 | 13.42 |
| NAE2010 (MLLW) | 1 | ---------- | ---------- | 2 | ---------- | ---------- |
| GeoDas (MLLW) | 1 | 4 | 17.06 | 2 | 5 | 17.19 |

Table A3. Data comparison for subarea polygons 3 and 4.

| Data | Subarea Polygon | Total Pts | Mean (ft) | Subarea Polygon | Total Pts | Mean (ft) |
|---|---|---|---|---|---|---|
| Lidar2010 (NAVD88) | 3 | 2635 | 22.70 | 4 | 1468 | 23.88 |
| Lidar2007 (NAVD88) | 3 | ---------- | ---------- | 4 | ---------- | ---------- |
| CHL2010 (MLLW) | 3 | 261118 | 18.54 | 4 | 57658 | 19.19 |
| NAE2010 (MLLW) | 3 | ---------- | ---------- | 4 | ---------- | ---------- |
| GeoDas (MLLW) | 3 | 11 | 24.41 | 4 | 1 | 19.69 |

Table A4. Data comparison for subarea polygons 5 and 6.

| Data | Subarea Polygon | Total Pts | Mean (ft) | Subarea Polygon | Total Pts | Mean (ft) |
|---|---|---|---|---|---|---|
| Lidar2010 (NAVD88) | 5 | 24456 | 19.98 | 6 | 708 | 20.14 |
| Lidar2007 (NAVD88) | 5 | 103140 | 19.91 | 6 | ---------- | ---------- |
| CHL2010 (MLLW) | 5 | ---------- | ---------- | 6 | 123236 | 15.39 |
| NAE2010 (MLLW) | 5 | ---------- | ---------- | 6 | ---------- | ---------- |
| GeoDas (MLLW) | 5 | 184 | 14.45 | 6 | 5 | 16.47 |

Table A5. Data comparison for subarea polygons 7 and 8.

| Data | Subarea Polygon | Total Pts | Mean (ft) | Subarea Polygon | Total Pts | Mean (ft) |
|---|---|---|---|---|---|---|
| Lidar2010 (NAVD88) | 7 | 1018 | 21.72 | 8 | 582 | 7.15 |
| Lidar2007 (NAVD88) | 7 | ---------- | ---------- | 8 | 3459 | 23.46 |
| CHL2010 (MLLW) | 7 | 91717 | 16.86 | 8 | 350321 | 22.38 |
| NAE2010 (MLLW) | 7 | ---------- | ---------- | 8 | 536 | 19.03 |
| GeoDas (MLLW) | 7 | 3 | 20.01 | 8 | ---------- | ---------- |

Table A6. Data comparison for subarea polygons 9 and 10.

| Data | Subarea Polygon | Total Pts | Mean (ft) | Subarea Polygon | Total Pts | Mean (ft) |
|---|---|---|---|---|---|---|
| Lidar2010 (NAVD88) | 9 | 1023 | 19.55 | 10 | 2032 | 19.95 |
| Lidar2007 (NAVD88) | 9 | 2148 | 17.03 | 10 | 4404 | 17.55 |
| CHL2010 (MLLW) | 9 | 88674 | 14.99 | 10 | 249830 | 15.58 |
| NAE2010 (MLLW) | 9 | 278 | 13.98 | 10 | 732 | 32.81 |
| GeoDas (MLLW) | 9 | 3 | 8.73 | 10 | 9 | 13.45 |

Table A7. Data comparison for subarea polygons 11 and 12.

| Data | Subarea Polygon | Total Pts | Mean (ft) | Subarea Polygon | Total Pts | Mean (ft) |
|---|---|---|---|---|---|---|
| Lidar2010 (NAVD88) | 11 | 1332 | 21.72 | 12 | 2481 | 16.77 |
| Lidar2007 (NAVD88) | 11 | 2327 | 19.98 | 12 | 3281 | 15.52 |
| CHL2010 (MLLW) | 11 | 170169 | 16.73 | 12 | 156944 | 13.37 |
| NAE2010 (MLLW) | 11 | ---------- | ---------- | 12 | ---------- | ---------- |
| GeoDas (MLLW) | 11 | 3 | 19.26 | 12 | 5 | 13.71 |

Table A8. Data comparison for subarea polygons 13 and 14.

| Data | Subarea Polygon | Total Pts | Mean (ft) | Subarea Polygon | Total Pts | Mean (ft) |
|---|---|---|---|---|---|---|
| Lidar2010 (NAVD88) | 13 | 21863 | 25.59 | 14 | 7439 | 28.12 |
| Lidar2007 (NAVD88) | 13 | 39656 | 23.36 | 14 | ---------- | ---------- |
| CHL2010 (MLLW) | 13 | ---------- | ---------- | 14 | ---------- | ---------- |
| NAE2010 (MLLW) | 13 | ---------- | ---------- | 14 | ---------- | ---------- |
| GeoDas (MLLW) | 13 | 72 | 20.11 | 14 | 49 | 25.72 |

Table A9. Data comparison for subarea polygons 15 and 16.

| Data | Subarea Polygon | Total Pts | Mean (ft) | Subarea Polygon | Total Pts | Mean (ft) |
|---|---|---|---|---|---|---|
| Lidar2010 (NAVD88) | 15 | 28214 | 36.35 | 16 | 18581 | 27.76 |
| Lidar2007 (NAVD88) | 15 | ---------- | ---------- | 16 | 158548 | 28.81 |
| CHL2010 (MLLW) | 15 | ---------- | ---------- | 16 | ---------- | ---------- |
| NAE2010 (MLLW) | 15 | ---------- | ---------- | 16 | ---------- | ---------- |
| GeoDas (MLLW) | 15 | 284 | 31.36 | 16 | 145 | 25.03 |

## A.3 Results and conclusions

The details of comparison between five data sets are listed in Table A10, which provides specifics of data contained in each 16-polygon area. The key findings of the analysis are summarized in this section.

CHL2010 and NAE2010 data sets show similar mean depths in the polygons where both data sets overlap. The mean difference is less than 0.5 ft. These two data sets are considered ground-truth in this analysis in calculating the offset between Lidar2007 and Lidar2010 data sets. Because the GeoDas data set has a low (3 sec arc) resolution, it is only used as the background bathymetry.

The analysis results indicated a depth offset of 4.5 ft between Lidar2010 data and CHL2010 surveys. In the polygons where these two data sets overlapped, the Lidar2010 mean depth value was 4.5 ft greater (i.e., deeper) than the mean depth from CHL2010 surveys, without vertical offset adjustment.

In the numerical hydrodynamic modeling described in Appendix B, MSL is used as the vertical datum. Note the difference between MLLW and MSL datums at Newport gage is 1.74 ft. Based on mean depth differences between Lidar2010 and CHL2010 data sets, and using the Newport gage vertical datum information shown in Table A1, the following adjustments were determined for the Lidar2010 data set:

- Lidar2010 depths (NAVD88) – 4.50 ft = Lidar2010 depths (MLLW)
- Lidar2010 depths (NAVD88) – 2.76 ft = Lidar2010 depths (MSL) (where -2.76 = -4.50 ft + 1.74 ft)

Table A10. The relative mean depth (ft) difference among five data sets for 16 subarea polygons.

| Subarea Polygon # | Lidar2010 – Lidar2007 | Lidar2010 – CHL2010 | Lidar2007 – CHL2010 | CHL2010 – NAE2010 | Lidar2010 - GeoDas | Lidar2007 - GeoDas |
|---|---|---|---|---|---|---|
| 1 | 2.59 | 6.30 | 3.71 | ---------- | 4.69 | 2.10 |
| 2 | -0.52 | 1.51 | 2.03 | ---------- | -2.26 | -1.74 |
| 3 | ---------- | 4.17 | ---------- | ---------- | -1.71 | ---------- |
| 4 | ---------- | 4.72 | ---------- | ---------- | 4.20 | ---------- |
| 5 | 0.07 | ---------- | ---------- | ---------- | 4.53 | 4.46 |
| 6 | ---------- | 4.76 | ---------- | ---------- | 3.67 | 0.00 |
| 7 | ---------- | 4.86 | ---------- | ---------- | 1.71 | ---------- |
| 8 | 1.08 | 4.43 | 3.35 | -0.30 | ---------- | ---------- |
| 9 | 2.53 | 4.56 | 2.03 | 1.02 | 10.83 | 8.30 |
| 10 | 2.40 | 4.36 | 1.97 | 0.46 | 6.50 | 4.10 |
| 11 | 1.74 | 4.99 | 3.25 | ---------- | 0.82 | 0.72 |
| 12 | 1.25 | 3.71 | 2.46 | ---------- | 3.05 | 1.80 |
| 13 | 2.23 | ---------- | ---------- | ---------- | 5.48 | 3.25 |
| 14 | ---------- | ---------- | ---------- | ---------- | 2.40 | ---------- |
| 15 | ---------- | ---------- | ---------- | ---------- | 4.99 | ---------- |
| 16 | -1.05 | ---------- | ---------- | ---------- | 2.40 | 3.77 |
| Max | 2.59 | 6.30 | 3.71 | 1.02 | 10.83 | 8.30 |
| Min | -1.05 | 1.51 | 1.97 | -0.30 | -2.26 | -1.74 |
| Mean* | 1.35 | 4.49 | 2.62 | 0.46 | 3.28 | 2.89 |

*Excludes max and min values.

Likewise, based on the mean depth differences between Lidar2007 and CHL2010 data sets, the following adjustments to Lidar2007 data set were determined:

- Lidar2007 depths (NAVD88) – 2.63 ft = Lidar2007 depths (MLLW)
- Lidar2007 depths (NAVD88) – 0.89 ft = Lidar2007 depths (MSL)

The following adjustments of CHL2010 and NAE2010 surveys are made for conversion to MSL:

- CHL2010 depths (MLLW) + 1.74 ft = CHL2010 depths (MSL)
- NAE2010 depths (MLLW) + 2.20 ft = NAE2010 depths (MSL)
- GeoDas depths (MLLW) + 1.28 ft = GeoDas depths (MSL)

Table A10 provides the mean depth differences between five data sets in each 16 subarea polygons. The three largest differences are (a) 4.50 ft between the Lidar2010 and CHL2010, (b) 3.28 ft between Lidar2010 and GeoDas, and (c) 2.89 ft between Lidar2007 and GeoDas. The smallest difference is 0.46 ft between CHL2010 and NAE2010.

Note that the differences in Table A10 are without a vertical datum conversion between the raw data sets. After determining the offsets between the overlapping data sets in each polygon, a conversion was applied to bring all data sets to a unified vertical datum (MSL).

A revised bathymetric data set was assembled from the combination of five data sets analyzed. For reference, the spatial differences between the revised bathymetric data set and the original data set are shown in Figures A8 and A9 based on two different color contouring schemes. The range of difference between the revised and original bathymetry is set to -9.84 to 9.84 ft in both figures. Inside the harbor in the water area, the difference is generally less than 8.20 ft, and around the structures it varies from -3.28 to -8.20 ft.

Figure A8. Difference between the original and revised bathymetries (display in color code 1).

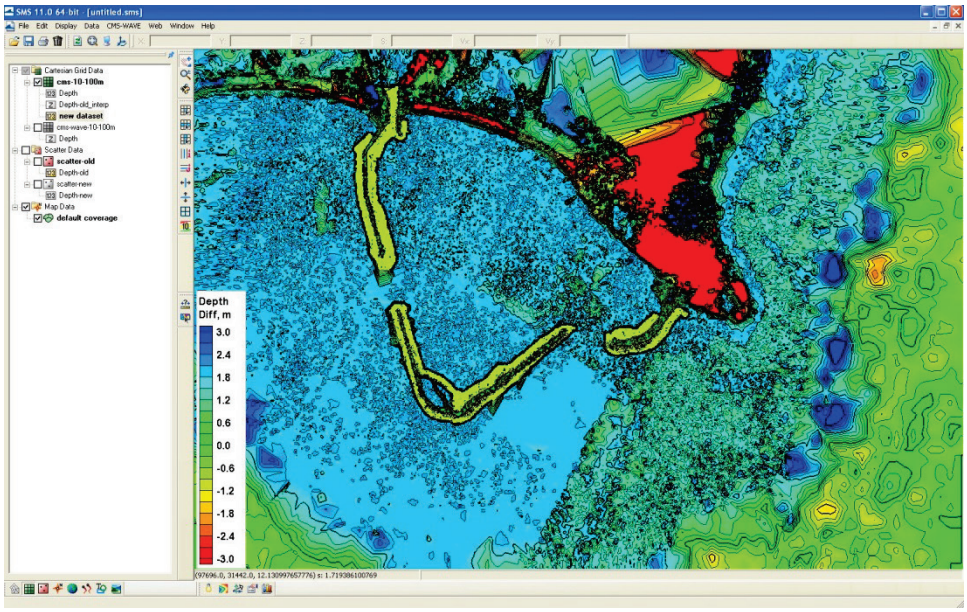

Figure A9. Difference between the original and revised bathymetries (display in color code 2).

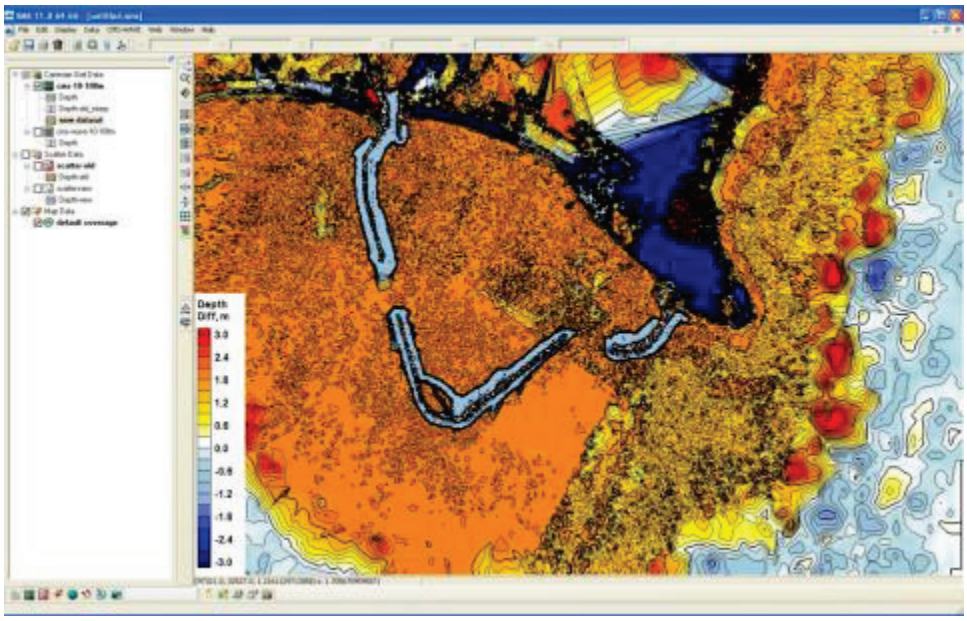


Eight transects were selected to investigate depth differences between original unadjusted and adjusted bathymetric data in different parts of the harbor. Figures A10a and A10b show the location of Transects T1 through T8. Figures A11a and A11b show comparison of the original and revised bathymetries in the harbor and vicinity. Figure A11a shows a sharp drop in the transition areas between CHL2010 and Lidar2010 (e.g., on the seaward side of the Main breakwater). Figure A11b shows the revised bathymetry where the dramatic changes in depth around the breakwaters have been eliminated.

Eight transects were selected to further evaluate the depth differences as depicted in Figures A8, A9, and A10a and A10b. Figures A12 through A19 show a comparison of the depth data from the original and revised bathymetries (MSL) along Transects T1 through T8, respectively. It is evident that the old and new bathymetries are different not only from one transect to next but also in the areas that are outside the breakwaters, across different sections of the breakwaters, and in the interior areas. The largest mean depth difference is 6.56 ft to 8.20 ft, occurring along the Transects T6, T7, and T8.

Figure A10. (a) Transects T1 through T5 displayed with the original bathymetry. (b) Transects T6, T7, and T8 displayed with the revised bathymetry.

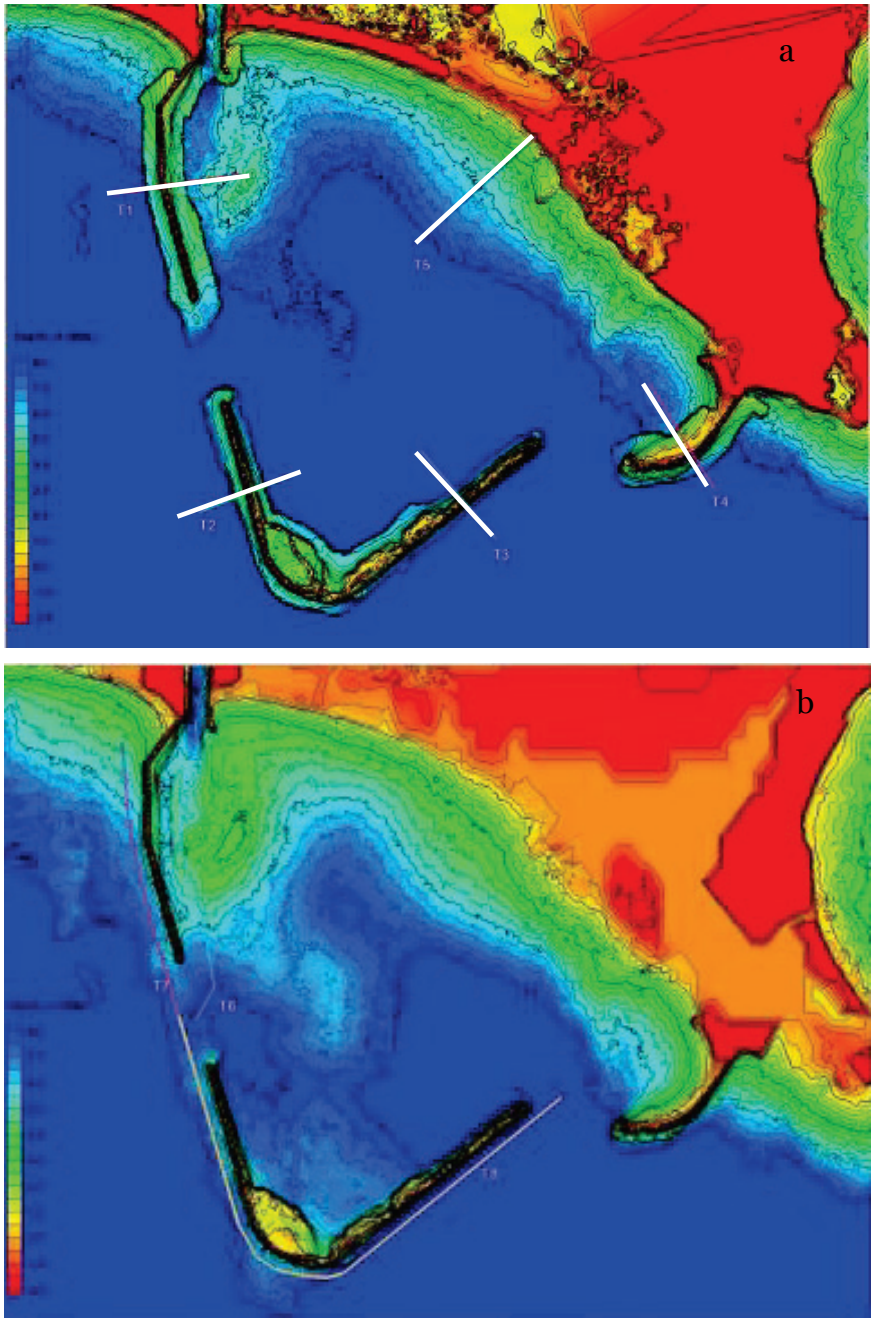

Figure A11. (a) Color-shaded plot of the original bathymetry with a sharp drop in the transition zone between CHL2010 and Lidar2010 data sets. (b) Color-shaded plot of the revised bathymetry without any noticeable drop in the transition zone between CHL2010 and Lidar2010 data sets.

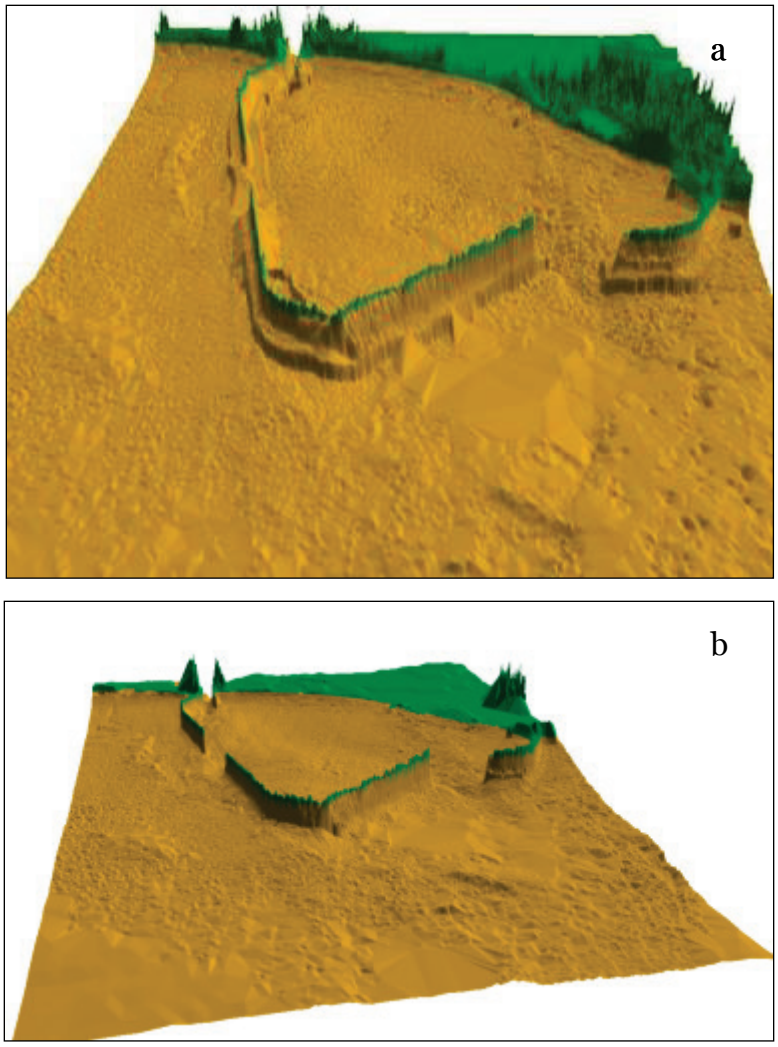

Figure A12. Comparison of original and revised depths along Transect T1


Figure A13. Comparison of original and revised depths along Transect T2.

Figure A14. Comparison of original and revised depths along Transect T3.

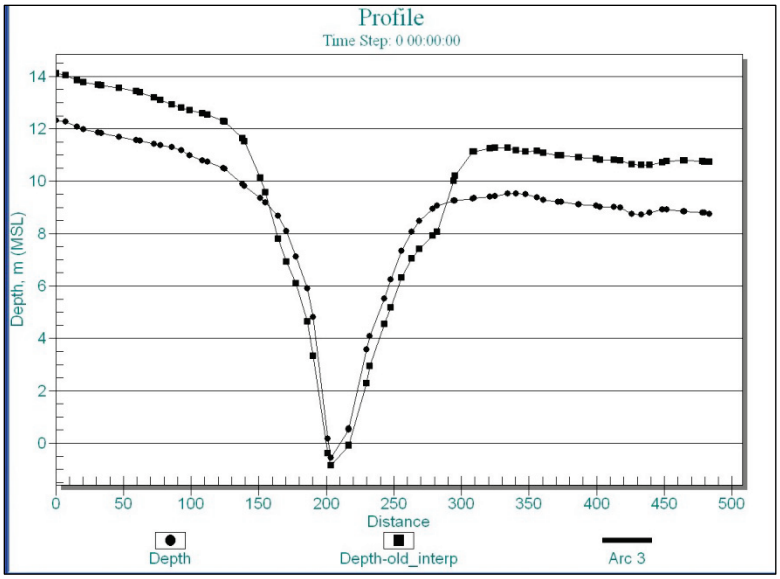


Figure A15. Comparison of original and revised depths along Transect T4.

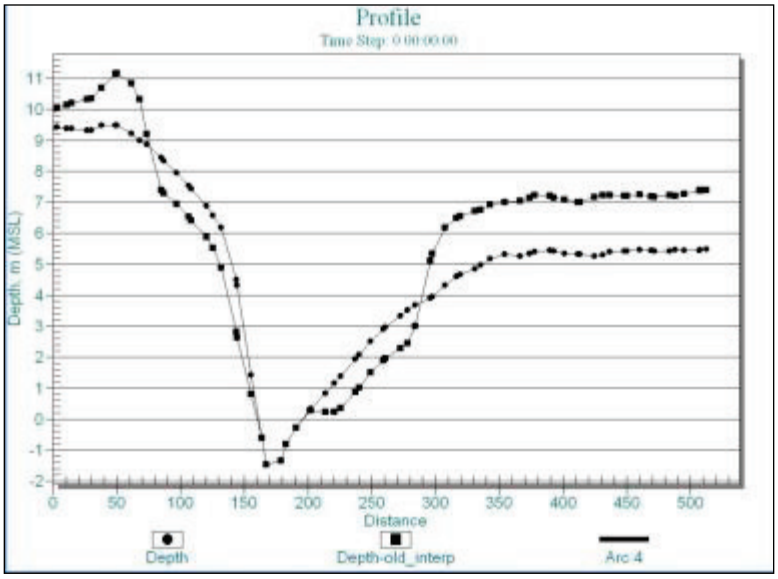

Figure A16. Comparison of original and revised depths along Transect T5.

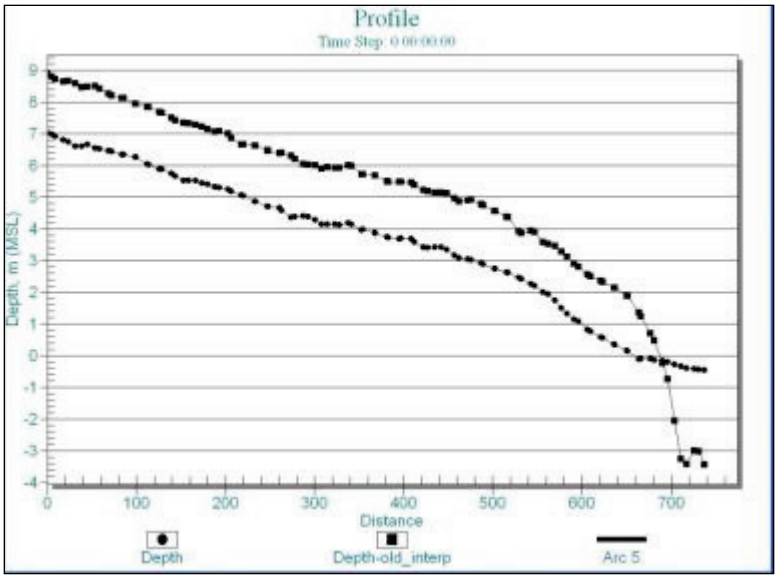


Figure A17. Comparison of original and revised depths along Transect T6.

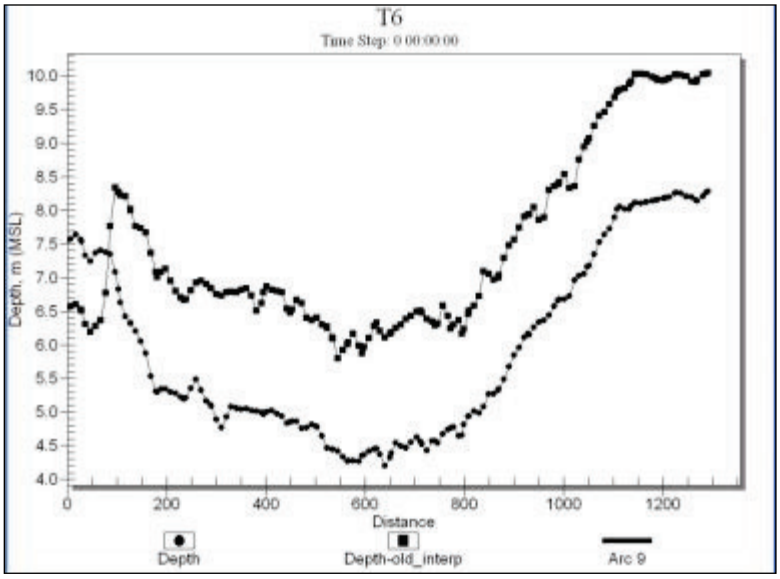

Figure A18. Comparison of original and revised depths along Transect T7.

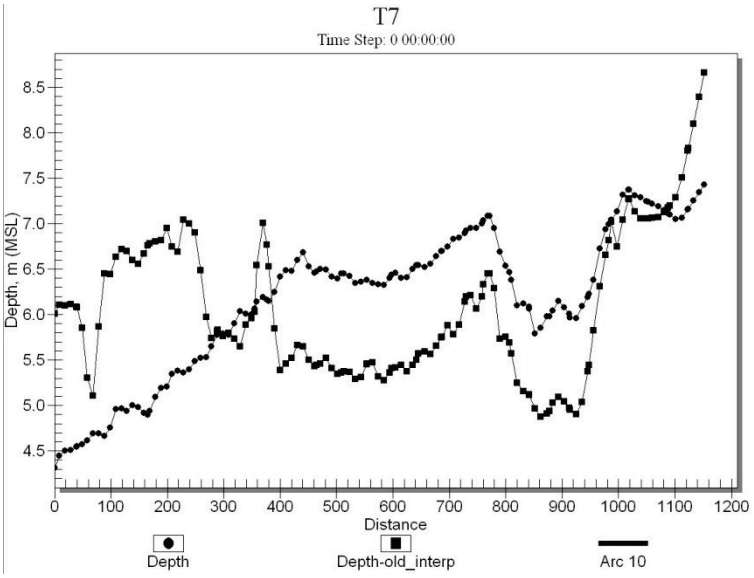


Figure A19. Comparison of original and revised depths along Transect T8.

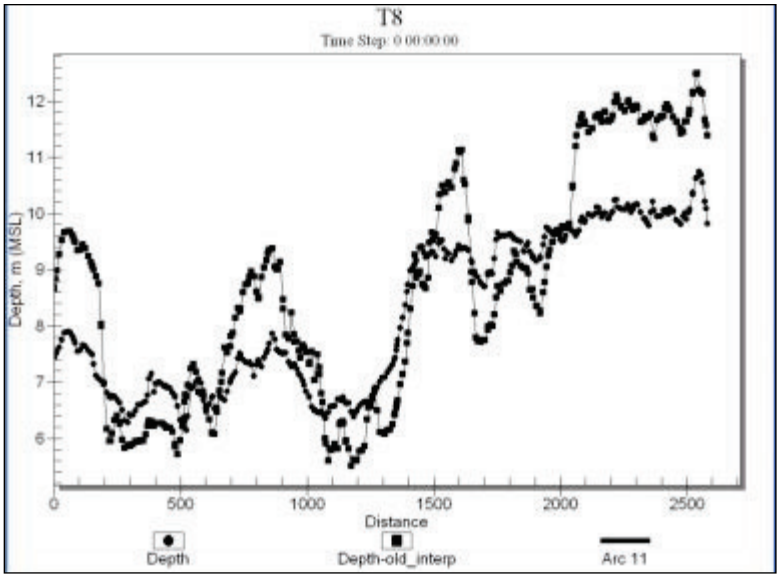

# Appendix B: Wave Modeling for Point Judith Harbor[1]

## B.1 Overview

High-fidelity wave modeling for this study consisted of three parts: (1) long-term continuous hindcast of historical offshore wave conditions, (2) transformation of the significant storm deepwater waves to project site area, and (3) transformation of waves for 20 most significant storms over damaged breakwaters and through gaps into the harbor. The first task involved analysis of offshore wave conditions from the long-term GROW hindcast. This was followed by transformation of offshore waves to nearshore using the spectral-wave transformation model CMS-Wave. Last, waves for the most severe 20 storms were propagated into the sheltered HoR using the time-domain, phase-resolving wave model BOUSS-2D to calculate the interaction of nearshore waves with the channels, breakwaters, and surrounding land features, and to validate surrogate models described in Appendix C.

CMS-Wave is a two-dimensional (2D), steady-state spectral wave model (Lin et al. 2011, 2008) capable of simulating wave processes with ambient currents at coastal inlets and navigation channels. The model can be used either in half-plane or full-plane mode for wave transformation, and it is based on the wave-action balance equation that includes wave propagation, refraction, shoaling, diffraction, reflection, breaking, and dissipation. The half-plane mode is default, and in this mode, CMS-Wave can run more efficiently as waves are transformed primarily from the seaward boundary toward shore.

BOUSS-2D is a 2D, fully-nonlinear Boussinesq-type model for waves propagating in water of variable depth (Nwogu and Demirbilek 2001, 2006). It is capable of simulating various wave phenomena including refraction, shoaling, diffraction, reflection, breaking, wave runup and overtopping coastal structures, nonlinear wave-wave interaction, and wave-induced currents (circulation). BOUSS-2D can simulate unidirectional or multidirectional seas and wave-current interaction and

[1] Authored by Zeki Demirbilek, Lihwa Lin, and Jeffrey Melby

other nonlinear wave processes such as wave-wave interaction, wave diffraction, wave-induced turbulence and dissipation, wave overtopping porous structures, infragravity waves that occur over reefs, and complex waves in coastal inlets and in ports/harbors.

## B.2 Analysis of offshore wave data

The offshore wave conditions are based on the GROW-FAB, a service provided by Oceanweather Inc (2011). This is a 57 yr hindcast that uses a 6 min grid resolution, and provides numerically calculated wave information at 3 hr intervals from 1954 through 2010. The directional wave spectra were also provided for an internal 30 min grid at Sta 373 (40.9 deg N, 71.2 deg W), located approximately 45 miles south of Point Judith Harbor offshore at 173.2 ft depth. The spectral wave data at Sta 373 were used as the offshore wave input in this numerical wave modeling study.

Figure B1 shows the GROW-FAB 6 min grid and 30 min spacing wave locations in the Rhode Island and Massachusetts coastal region. As described in Appendix C, 225 storms with peak significant wave height greater than 15.1 ft were selected for this wave modeling study using the peaks-over-threshold method. For each storm, the modeled storm hydrograph duration was 36 hr with 18 hr before and after the peak wave height. This resulted in transformation of 2,301 wave conditions to the project site.

As a check of the offshore hindcast data, the GROW-FAB Sta 373 hindcast wave conditions were compared with a nearby Coastal Data Information Program (CDIP) Buoy 154 (40.97 deg N, 71.13 deg W) during December 2010. The comparison is shown in Figure B2. Both hindcast wave height and direction from GROW-FAB are in good agreement with the CDIP buoy data. Note that the hindcast short wave periods (seas) matched better than the periods for long waves (swell). Overall, there was good agreement between hindcast and buoy data.

## B.3 Transformation of offshore waves to nearshore

CMS-Wave was used to transform deepwater offshore waves from the GROW-FAB Sta 373 project site. The wave modeling was performed using a parent grid covering the offshore of the Rhode Island coast. The CMS-Wave child grid covered the nearshore region of Rhode Island centered on Point Judith Harbor. Figure B3 shows the parent and child grid domains.

Figure B1. Location map of GROW-FAB 6 min grid stations in blue dots. Sta 373 is circled in red. Stations with 30 min spacing are shown in red dots covering Rhode Island and Massachusetts coastal areas.

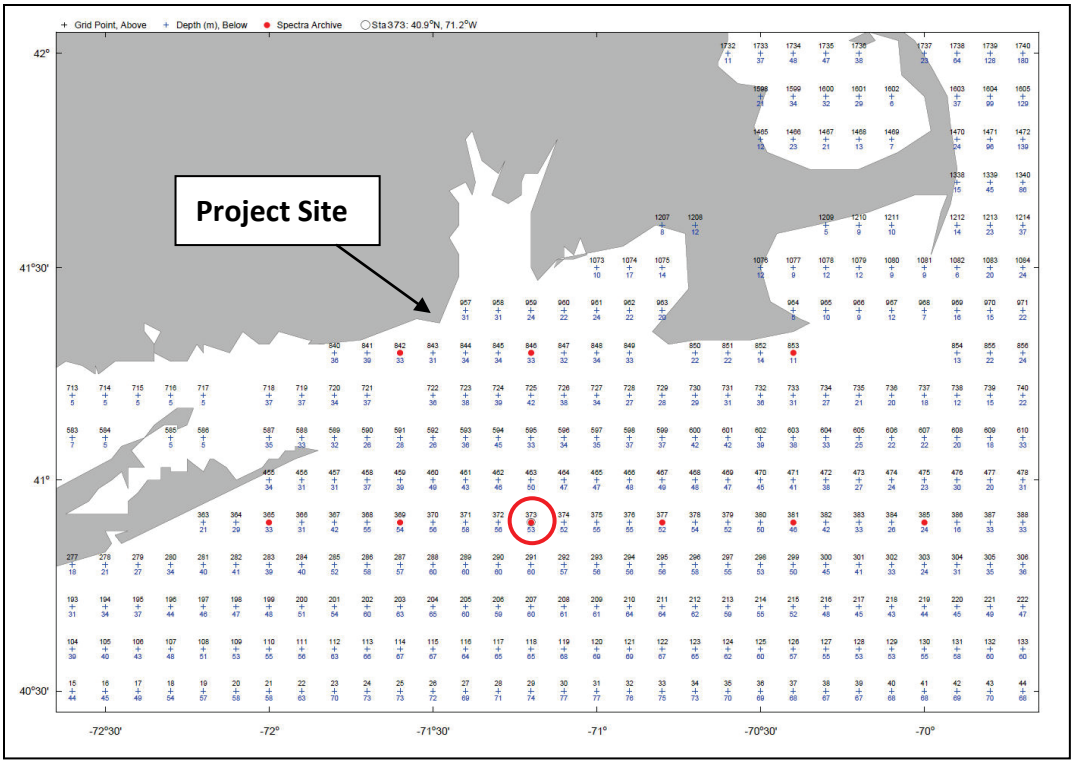


Figure B2. Comparison of GROW-FAB Sta 373 with CDIP 154 wave buoy data.

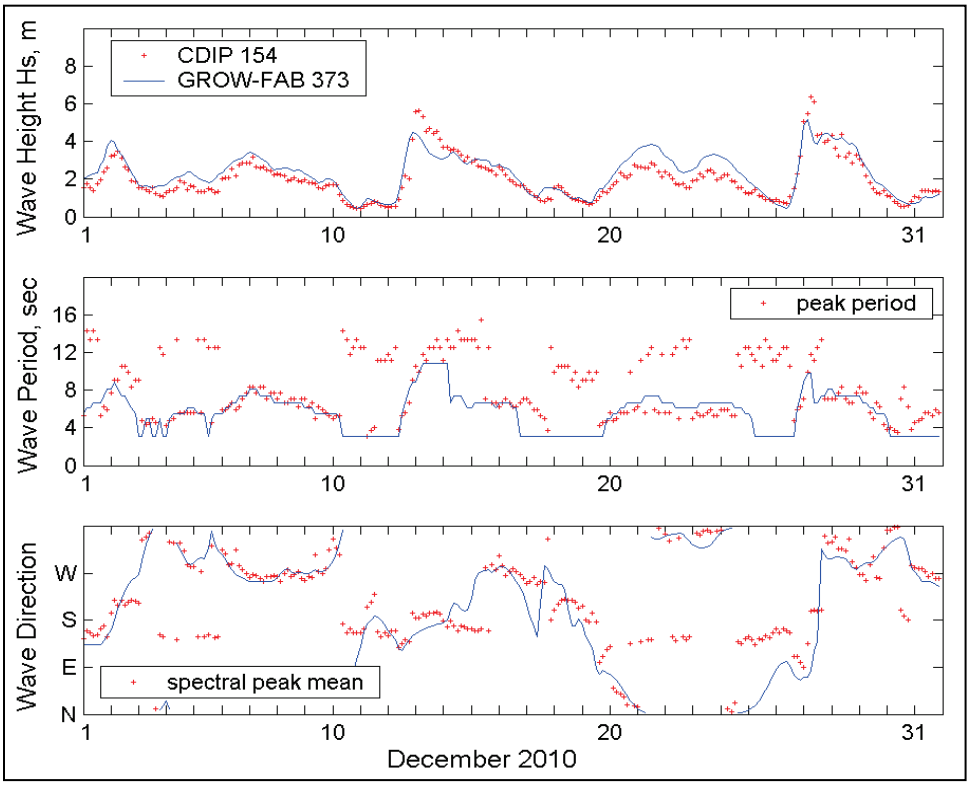

Figure B3. Spatial domain of the CMS-Wave parent and child grids.

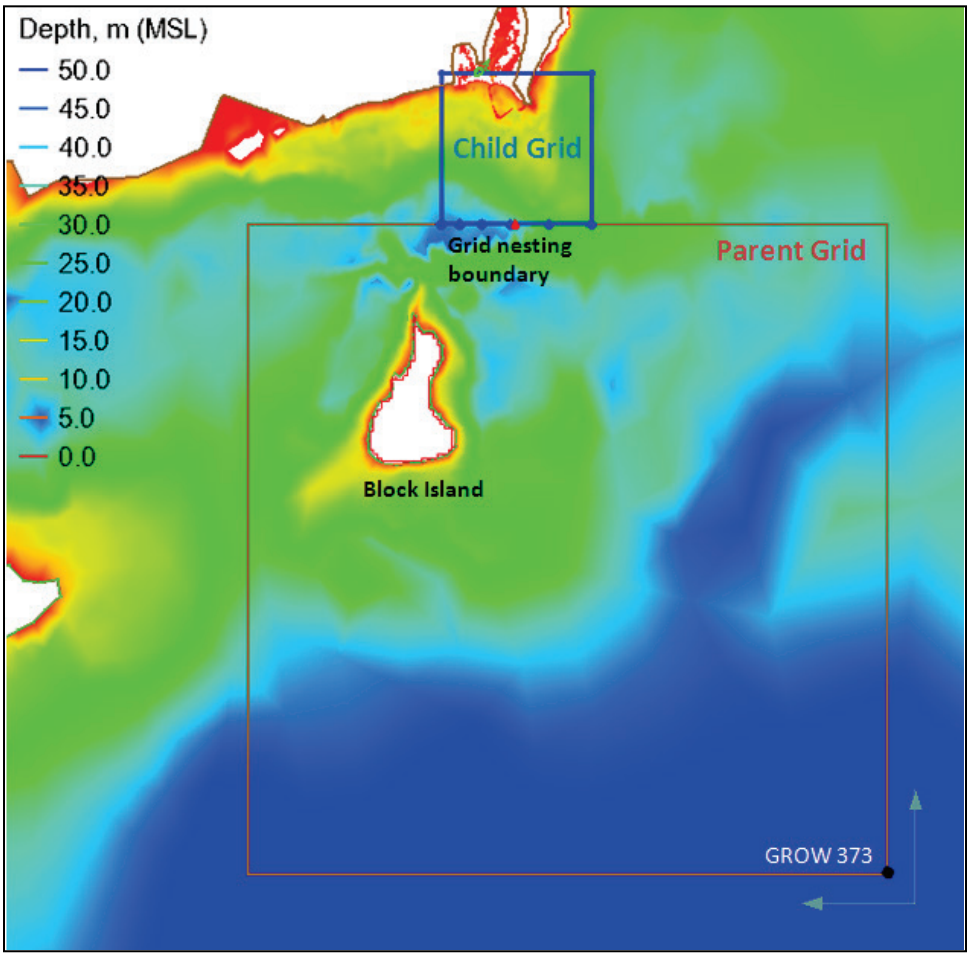


The GROW-FAB Sta 373 wave spectra were specified as the incident wave conditions at the seaward boundary of the parent grid. The parent grid model results were saved along the shoreward boundary of the grid and used as wave input conditions to the CMS-Wave child grid. Included in these wave transformation calculations were the long-term water levels from the nearest NOAA coastal station at Newport, RI.

The parent grid consisted of 171 by 174 grid cells, with a constant cell size of 820 ft. The grid covered a rectangular area of 27 miles alongshore and 27 miles cross-shore from the 180 ft depth contour offshore to 115 ft depth nearshore. The child grid had a square area of 6.2 miles by 6.2 miles and a constant cell size of 33 ft in the breakwater area and variable cell size of 33 to 330 ft elsewhere. Bathymetric data for both grids (parent and child) were as discussed in Appendix A.

Deepwater spectral waves were transformed with CMS-Wave using full- and half-plane mode. Both results were similar, and full-plane model results are used in this study. These simulations were made with a 5 deg directional resolution for a total of 35 directional bins, 30 frequency bins (0.04 to 0.24 Hz, with a 0.007 Hz increment). Wave shoaling, refraction, diffraction, reflection, runup processes, and wind input were included in CMS-Wave model simulations.

Results from the child grid were output at 204 nearshore *save* locations, numbered from 1 to 204 along transects seaward and shoreward of the breakwaters as shown in Figures B4 through B8. Table B1 provides the coordinates of save stations in Rhode Island State Plane and water depth (MSL). Of the 204 save points, 25 were located between 30 and 40 ft depth contours, 21 along approximately 20 ft contour, 20 were around the West Shore Arm breakwater near the 10 ft contour, 35 were near the 10 ft contour around the Main breakwater, 26 were near the 10 ft contour along the shoreline and East Shore Arm breakwater, 10 were along the channel centerline near the East Shore Arm breakwater, and 67 were on a gridded-network inside the breakwater-protected area.

Figure B4. CMS-Wave child grid save locations along transects positioned in and around Point Judith Harbor.

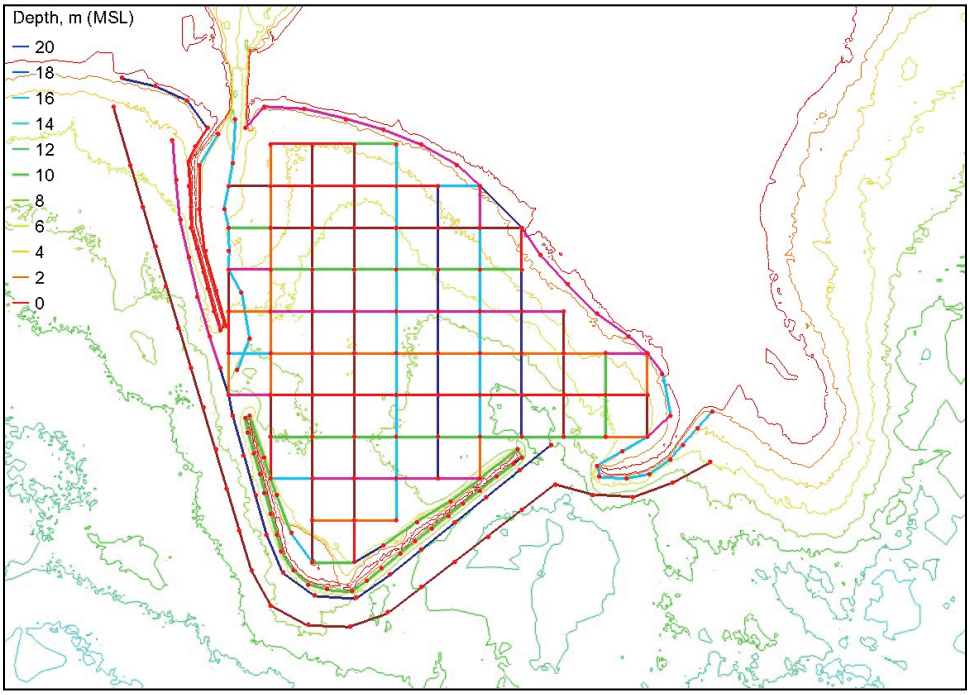

Figure B5. CMS-Wave child grid save locations placed around the East Shore Arm breakwater.

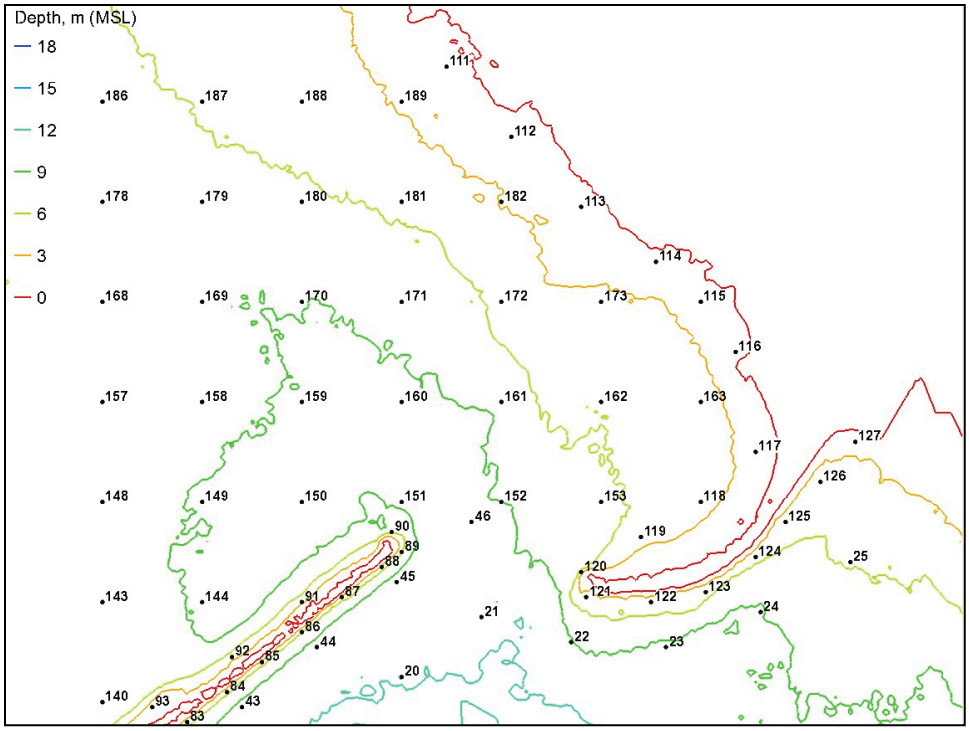


Figure B6. CMS-Wave child grid save locations around the West Shore Arm breakwater.

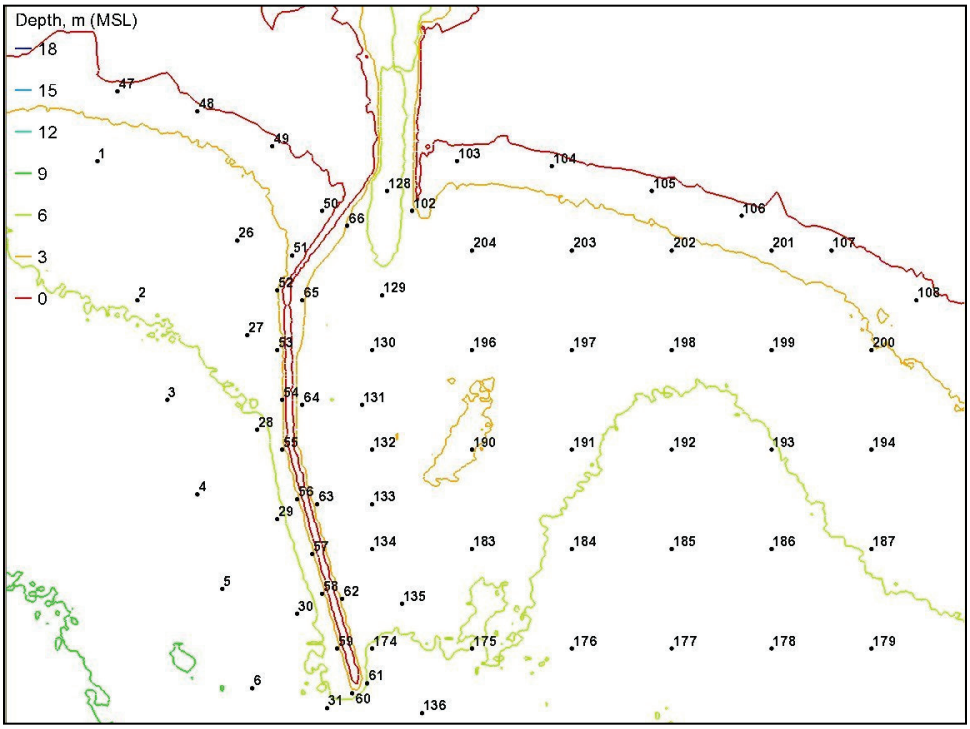

Figure B7. CMS-Wave child grid save locations near Main breakwater.

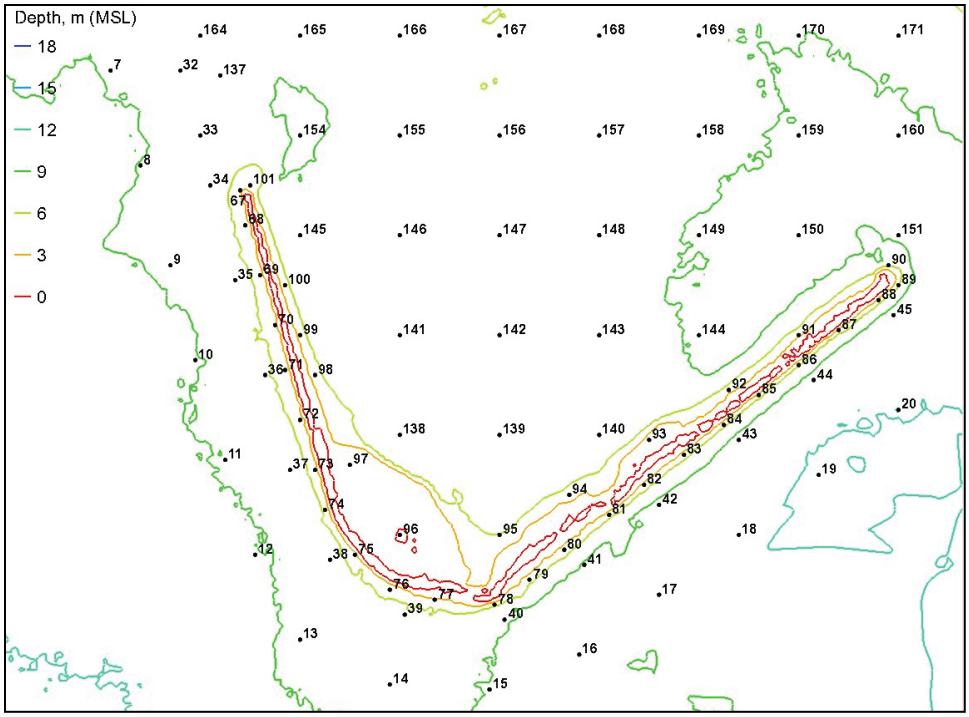


Figure B8. CMS-Wave child grid save locations inside the harbor.

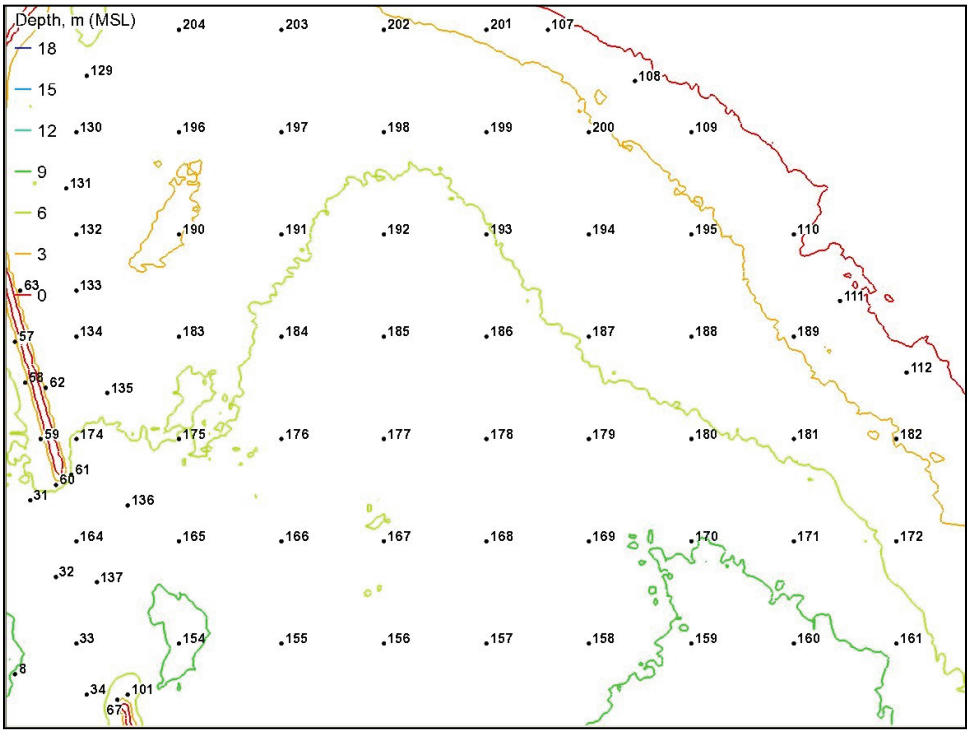

Table B1. List of CMS-Wave nearshore wave output locations.

| Location | Easting, ft | Northing, ft | Depth, ft (MSL) |
|---|---|---|---|
| 1 | 322342.78 | 106224.84 | 13.81 |
| 2 | 322605.25 | 105308.53 | 18.27 |
| 3 | 322802.10 | 104654.04 | 23.92 |
| 4 | 322998.92 | 104032.25 | 25.33 |
| 5 | 323162.96 | 103410.47 | 26.05 |
| 6 | 323359.81 | 102755.97 | 27.46 |
| 7 | 323556.66 | 102134.19 | 27.20 |
| 8 | 323753.48 | 101512.40 | 28.71 |
| 9 | 323950.33 | 100857.91 | 27.72 |
| 10 | 324114.37 | 100236.12 | 29.92 |
| 11 | 324311.22 | 99581.63 | 29.07 |
| 12 | 324508.07 | 98959.84 | 30.05 |
| 13 | 324803.31 | 98403.51 | 25.85 |
| 14 | 325393.86 | 98108.99 | 25.75 |
| 15 | 326050.03 | 98076.25 | 30.15 |
| 16 | 326640.58 | 98305.35 | 30.91 |
| 17 | 327165.55 | 98698.03 | 32.91 |
| 18 | 327690.49 | 99090.72 | 37.76 |
| 19 | 328215.42 | 99483.43 | 40.26 |
| 20 | 328740.35 | 99908.86 | 39.50 |
| 21 | 329265.29 | 100301.54 | 37.53 |
| 22 | 329855.84 | 100137.93 | 30.28 |
| 23 | 330479.20 | 100105.18 | 31.23 |
| 24 | 331102.56 | 100334.25 | 30.58 |
| 25 | 331693.11 | 100661.48 | 18.93 |
| 26 | 323261.42 | 105701.25 | 14.40 |
| 27 | 323327.03 | 105079.46 | 16.77 |
| 28 | 323392.62 | 104457.68 | 20.21 |
| 29 | 323523.85 | 103868.64 | 20.77 |
| 30 | 323655.09 | 103246.85 | 23.29 |
| 31 | 323851.94 | 102625.07 | 21.39 |
| 32 | 324015.98 | 102134.19 | 23.56 |
| 33 | 324147.21 | 101708.76 | 24.57 |
| 34 | 324212.80 | 101381.53 | 22.47 |
| 35 | 324376.84 | 100759.74 | 22.90 |

| Location | Easting, ft | Northing, ft | Depth, ft (MSL) |
|---|---|---|---|
| 36 | 324573.69 | 100137.96 | 21.16 |
| 37 | 324737.73 | 99516.17 | 22.90 |
| 38 | 325000.20 | 98927.13 | 22.24 |
| 39 | 325492.32 | 98567.16 | 20.57 |
| 40 | 326148.49 | 98534.42 | 27.66 |
| 41 | 326673.43 | 98894.39 | 30.64 |
| 42 | 327165.55 | 99287.07 | 31.20 |
| 43 | 327690.49 | 99712.50 | 31.63 |
| 44 | 328182.61 | 100105.22 | 32.64 |
| 45 | 328707.55 | 100530.61 | 32.91 |
| 46 | 329199.67 | 100923.33 | 32.22 |
| 47 | 322474.02 | 106683.20 | 2.82 |
| 48 | 322998.95 | 106552.10 | 3.90 |
| 49 | 323491.08 | 106323.00 | 4.66 |
| 50 | 323819.16 | 105897.57 | 2.62 |
| 51 | 323622.31 | 105603.05 | 8.92 |
| 52 | 323523.88 | 105373.98 | 12.27 |
| 53 | 323523.88 | 104981.27 | 15.85 |
| 54 | 323556.69 | 104654.04 | 13.35 |
| 55 | 323556.66 | 104326.77 | 15.32 |
| 56 | 323655.09 | 103999.54 | 14.53 |
| 57 | 323753.51 | 103639.53 | 15.94 |
| 58 | 323819.13 | 103377.76 | 16.96 |
| 59 | 323917.55 | 103017.78 | 15.72 |
| 60 | 324015.98 | 102723.23 | 18.11 |
| 61 | 324114.40 | 102788.68 | 20.64 |
| 62 | 323950.36 | 103345.01 | 14.01 |
| 63 | 323786.32 | 103966.80 | 16.83 |
| 64 | 323687.93 | 104621.29 | 13.52 |
| 65 | 323687.93 | 105308.53 | 8.07 |
| 66 | 323983.20 | 105799.41 | 10.50 |
| 67 | 324409.65 | 101348.79 | 12.73 |
| 68 | 324442.45 | 101119.72 | 15.58 |
| 69 | 324540.88 | 100792.45 | 15.26 |
| 70 | 324639.30 | 100465.19 | 13.98 |
| 71 | 324704.92 | 100170.67 | 15.88 |

| Location | Easting, ft | Northing, ft | Depth, ft (MSL) |
|---|---|---|---|
| 72 | 324803.35 | 99843.44 | 14.47 |
| 73 | 324901.77 | 99516.17 | 15.94 |
| 74 | 324967.39 | 99254.36 | 17.72 |
| 75 | 325164.24 | 98959.84 | 15.55 |
| 76 | 325393.90 | 98730.77 | 17.29 |
| 77 | 325689.17 | 98665.32 | 10.47 |
| 78 | 326082.87 | 98632.58 | 17.13 |
| 79 | 326312.53 | 98796.23 | 13.88 |
| 80 | 326542.19 | 98992.55 | 12.04 |
| 81 | 326837.47 | 99221.62 | 15.26 |
| 82 | 327067.13 | 99417.98 | 11.98 |
| 83 | 327329.59 | 99614.34 | 14.86 |
| 84 | 327592.06 | 99810.66 | 17.19 |
| 85 | 327821.72 | 100007.02 | 11.38 |
| 86 | 328084.19 | 100203.38 | 20.14 |
| 87 | 328346.65 | 100432.45 | 14.70 |
| 88 | 328609.12 | 100628.81 | 13.55 |
| 89 | 328740.35 | 100726.97 | 19.46 |
| 90 | 328674.74 | 100857.87 | 23.43 |
| 91 | 328084.19 | 100399.74 | 12.83 |
| 92 | 327624.87 | 100039.76 | 15.45 |
| 93 | 327099.93 | 99712.50 | 4.99 |
| 94 | 326575.00 | 99352.53 | 15.91 |
| 95 | 326115.68 | 99090.75 | 19.55 |
| 96 | 325459.51 | 99090.75 | -1.31 |
| 97 | 325131.43 | 99548.92 | 1.61 |
| 98 | 324901.77 | 100137.96 | 16.67 |
| 99 | 324803.35 | 100399.77 | 13.45 |
| 100 | 324704.92 | 100727.00 | 15.75 |
| 101 | 324475.26 | 101381.50 | 15.35 |
| 102 | 324409.71 | 105897.57 | 13.55 |
| 103 | 324704.99 | 106224.84 | 4.99 |
| 104 | 325328.35 | 106192.09 | 4.63 |
| 105 | 325984.51 | 106028.44 | 4.69 |
| 106 | 326575.07 | 105864.83 | 4.00 |
| 107 | 327165.62 | 105635.76 | 4.69 |

| Location | Easting, ft | Northing, ft | Depth, ft (MSL) |
|---|---|---|---|
| 108 | 327723.36 | 105308.50 | 4.04 |
| 109 | 328084.25 | 104981.23 | 5.28 |
| 110 | 328740.39 | 104326.74 | 1.38 |
| 111 | 329035.66 | 103901.31 | 2.26 |
| 112 | 329462.17 | 103443.14 | 4.63 |
| 113 | 329921.49 | 102985.01 | 4.23 |
| 114 | 330413.62 | 102625.03 | 1.97 |
| 115 | 330708.89 | 102363.22 | 4.92 |
| 116 | 330938.55 | 102035.96 | 4.92 |
| 117 | 331069.75 | 101381.46 | 4.20 |
| 118 | 330708.86 | 101054.20 | 12.80 |
| 119 | 330315.16 | 100825.13 | 13.85 |
| 120 | 329921.46 | 100596.06 | 15.45 |
| 121 | 329954.27 | 100432.45 | 11.88 |
| 122 | 330380.77 | 100399.70 | 16.17 |
| 123 | 330741.67 | 100465.16 | 12.60 |
| 124 | 331069.75 | 100694.23 | 17.42 |
| 125 | 331266.60 | 100923.29 | 14.60 |
| 126 | 331496.26 | 101185.10 | 12.27 |
| 127 | 331725.92 | 101446.92 | 6.66 |
| 128 | 324245.67 | 106028.48 | 25.92 |
| 129 | 324212.86 | 105341.24 | 17.45 |
| 130 | 324147.24 | 104981.27 | 16.60 |
| 131 | 324081.63 | 104621.29 | 16.27 |
| 132 | 324147.21 | 104326.77 | 11.94 |
| 133 | 324147.21 | 103966.80 | 13.48 |
| 134 | 324147.21 | 103672.28 | 15.98 |
| 135 | 324344.06 | 103312.30 | 17.29 |
| 136 | 324475.30 | 102592.32 | 25.03 |
| 137 | 324278.44 | 102101.48 | 26.74 |
| 138 | 325459.51 | 99745.24 | 22.67 |
| 139 | 326115.68 | 99745.24 | 22.15 |
| 140 | 326771.85 | 99745.24 | 22.44 |
| 141 | 325459.51 | 100399.74 | 23.65 |
| 142 | 326115.68 | 100399.74 | 23.46 |
| 143 | 326771.85 | 100399.74 | 25.66 |

| Location | Easting, ft | Northing, ft | Depth, ft (MSL) |
|---|---|---|---|
| 144 | 327428.02 | 100399.74 | 30.31 |
| 145 | 324803.35 | 101054.27 | 25.59 |
| 146 | 325459.51 | 101054.27 | 26.61 |
| 147 | 326115.68 | 101054.23 | 25.20 |
| 148 | 326771.85 | 101054.23 | 27.40 |
| 149 | 327428.02 | 101054.23 | 30.25 |
| 150 | 328084.19 | 101054.23 | 31.43 |
| 151 | 328740.35 | 101054.23 | 31.59 |
| 152 | 329396.52 | 101054.23 | 29.56 |
| 153 | 330052.69 | 101054.20 | 21.59 |
| 154 | 324803.38 | 101708.76 | 30.58 |
| 155 | 325459.55 | 101708.76 | 23.75 |
| 156 | 326115.72 | 101708.76 | 20.44 |
| 157 | 326771.88 | 101708.73 | 25.85 |
| 158 | 327428.05 | 101708.73 | 28.02 |
| 159 | 328084.22 | 101708.73 | 30.64 |
| 160 | 328740.39 | 101708.73 | 32.25 |
| 161 | 329396.56 | 101708.73 | 27.36 |
| 162 | 330052.72 | 101708.73 | 19.03 |
| 163 | 330708.89 | 101708.69 | 13.12 |
| 164 | 324147.21 | 102363.25 | 22.87 |
| 165 | 324803.38 | 102363.25 | 24.18 |
| 166 | 325459.55 | 102363.25 | 22.15 |
| 167 | 326115.72 | 102363.25 | 20.21 |
| 168 | 326771.88 | 102363.25 | 25.20 |
| 169 | 327428.05 | 102363.25 | 27.89 |
| 170 | 328084.22 | 102363.22 | 28.87 |
| 171 | 328740.39 | 102363.22 | 26.18 |
| 172 | 329396.56 | 102363.22 | 17.65 |
| 173 | 330052.72 | 102363.22 | 11.88 |
| 174 | 324147.21 | 103017.78 | 20.51 |
| 175 | 324803.38 | 103017.75 | 19.82 |
| 176 | 325459.55 | 103017.75 | 21.65 |
| 177 | 326115.72 | 103017.75 | 23.52 |
| 178 | 326771.88 | 103017.75 | 24.90 |
| 179 | 327428.05 | 103017.75 | 25.59 |

| Location | Easting, ft | Northing, ft | Depth, ft (MSL) |
|---|---|---|---|
| 180 | 328084.22 | 103017.75 | 21.59 |
| 181 | 328740.39 | 103017.72 | 17.16 |
| 182 | 329396.56 | 103017.72 | 9.28 |
| 183 | 324803.38 | 103672.28 | 16.14 |
| 184 | 325459.55 | 103672.24 | 20.67 |
| 185 | 326115.72 | 103672.24 | 24.57 |
| 186 | 326771.88 | 103672.24 | 23.00 |
| 187 | 327428.05 | 103672.24 | 18.47 |
| 188 | 328084.22 | 103672.24 | 15.06 |
| 189 | 328740.39 | 103672.24 | 8.66 |
| 190 | 324803.38 | 104326.77 | 9.28 |
| 191 | 325459.55 | 104326.77 | 18.57 |
| 192 | 326115.72 | 104326.74 | 22.11 |
| 193 | 326771.88 | 104326.74 | 20.08 |
| 194 | 327428.05 | 104326.74 | 14.07 |
| 195 | 328084.22 | 104326.74 | 11.91 |
| 196 | 324803.41 | 104981.27 | 11.71 |
| 197 | 325459.58 | 104981.27 | 15.75 |
| 198 | 326115.75 | 104981.27 | 17.62 |
| 199 | 326771.92 | 104981.27 | 15.91 |
| 200 | 327428.08 | 104981.27 | 10.89 |
| 201 | 326771.92 | 105635.76 | 7.55 |
| 202 | 326115.75 | 105635.76 | 12.47 |
| 203 | 325459.58 | 105635.76 | 12.50 |
| 204 | 324803.41 | 105635.76 | 12.04 |
| 205 | 321850.56 | 94648.88 | 54.07 |
| 206 | 326312.50 | 94416.86 | 47.41 |
| 207 | 329921.42 | 95138.75 | 45.05 |

## B.4 BOUSS-2D wave modeling for Point Judith Harbor

### B.4.1 BOUSS-2D grids

Three BOUSS-2D grids were generated to model waves approaching Point Judith Harbor from three different direction sectors: (1) “S grid” for waves incident from 165 to 195 deg sector, (2) “SE grid” for waves incident from 130 to 165 deg sector, and (3) “SW grid” for waves incident from 195 to 230 deg sector. The 20 most intense storms were simulated with these

grids. Table B2 lists additional information about these three BOUSS-2D grids and wave selection criteria. Table B3 lists the 20 historical storms selected for BOUSS-2D simulation. Figures B9 through B11 show the BOUSS-2D grid domains that were driven with the CMS-Wave output locations 205 to 207.

Table B2. Specifics of three BOUSS-2D grids used in this study.

| Name of Grid | Save Station ID | Direction Sector (deg from) | Station XYZ cords (in State Plane, ft) | No. of Storms Modeled |
|---|---|---|---|---|
| S grid | 206 | 165-195 | 326312, 94416, 52 | 3 |
| SE Grid | 207 | 130-165 | 329921, 95138, 49 | 16 |
| SW Grid | 205 | 195-230 | 321850, 94649, 54 | 1 |

Table B3. Twenty historical storms and associated peak wave and water levels simulated with BOUSS-2D model.

| Storm ID | Date | GROW Offshore Wave Height $H_{m0}$, ft | BOUSS Input Wave Height, $H_{m0}$, ft | BOUSS Input Wave Period, $T_p$, s | BOUSS Input Wave Angle θ, deg Az | SWL, ft | Offshore Grid Point |
|---|---|---|---|---|---|---|---|
| 1 | 8/31/1954 | 27.87 | 10.50 | 10.8 | 173 | 6.36 | 206 |
| 2 | 9/11/1954 | 27.63 | 16.37 | 15.9 | 154 | -1.51 | 207 |
| 13 | 3/20/1958 | 21.21 | 17.42 | 9.8 | 129 | 2.00 | 206 |
| 15 | 8/29/1958 | 16.56 | 13.19 | 9.8 | 156 | 0.16 | 207 |
| 26 | 9/12/1960 | 27.34 | 10.89 | 10.8 | 166 | 0.26 | 206 |
| 32 | 9/21/1961 | 25.55 | 18.54 | 10.8 | 136 | 3.67 | 207 |
| 34 | 3/7/1962 | 23.68 | 18.70 | 11.9 | 131 | 3.77 | 207 |
| 44 | 9/24/1964 | 16.09 | 13.39 | 14.4 | 146 | 2.07 | 207 |
| 76 | 3/5/1971 | 22.06 | 11.91 | 5.5 | 227 | -2.66 | 205 |
| 129 | 11/16/1981 | 17.10 | 14.93 | 11.9 | 137 | 0.89 | 207 |
| 137 | 3/29/1984 | 20.86 | 14.80 | 11.9 | 130 | 1.51 | 207 |
| 141 | 9/27/1985 | 27.24 | 11.55 | 14.4 | 171 | 1.74 | 206 |
| 153 | 8/19/1991 | 33.01 | 16.34 | 11.9 | 157 | 5.84 | 207 |
| 160 | 12/12/1992 | 24.62 | 16.44 | 11.9 | 131 | 0.66 | 207 |
| 177 | 9/2/1996 | 17.60 | 13.71 | 14.4 | 146 | 2.69 | 207 |
| 207 | 10/25/2005 | 19.01 | 15.22 | 9.8 | 134 | 1.48 | 207 |
| 210 | 2/12/2006 | 17.80 | 16.44 | 9.8 | 124 | 3.64 | 206 |
| 215 | 11/3/2007 | 19.59 | 14.17 | 11.9 | 148 | 1.54 | 207 |
| 223 | 3/14/2010 | 21.37 | 15.39 | 10.8 | 131 | 0.52 | 207 |
| 224 | 9/4/2010 | 17.90 | 15.09 | 14.4 | 152 | 0.23 | 207 |

Figure B9. BOUSS-2D grid for storms coming from 165–195 deg (S) sector.

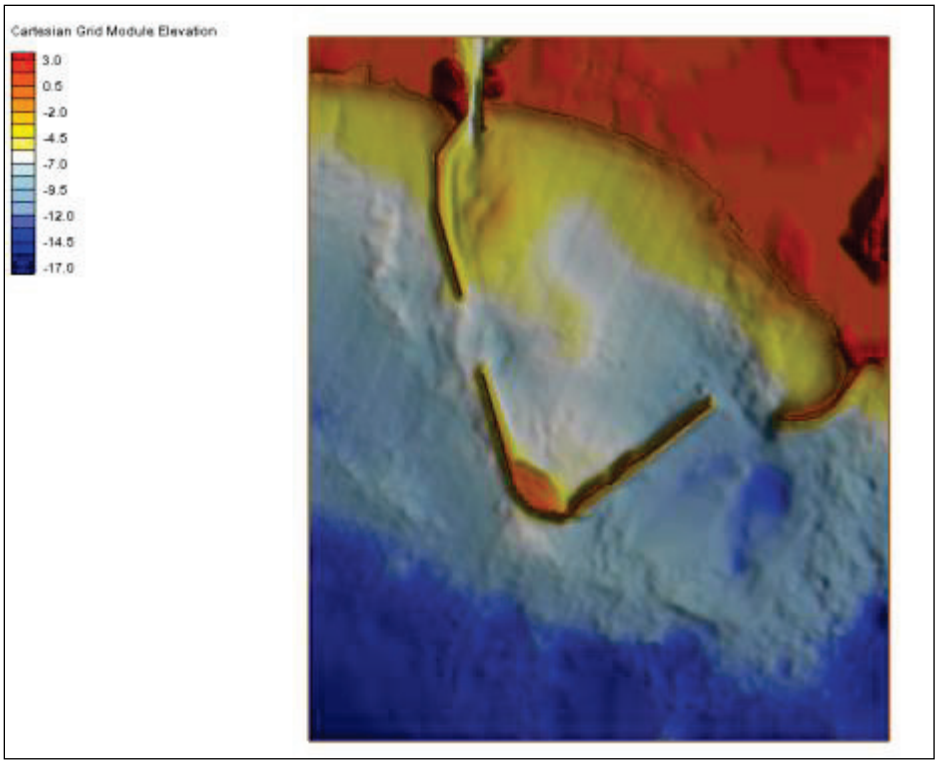


Figure B10. BOUSS-2D grid for storms coming from 130–165 deg (SE) sector.

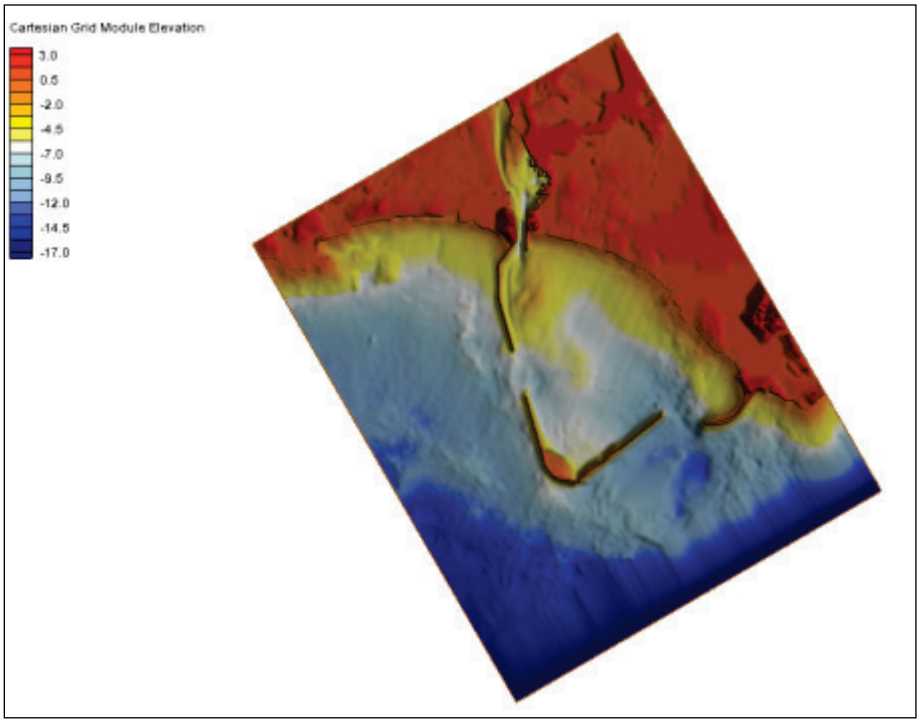

Figure B11. BOUSS-2D grid for storms coming from 195-230 deg (SW) sector.

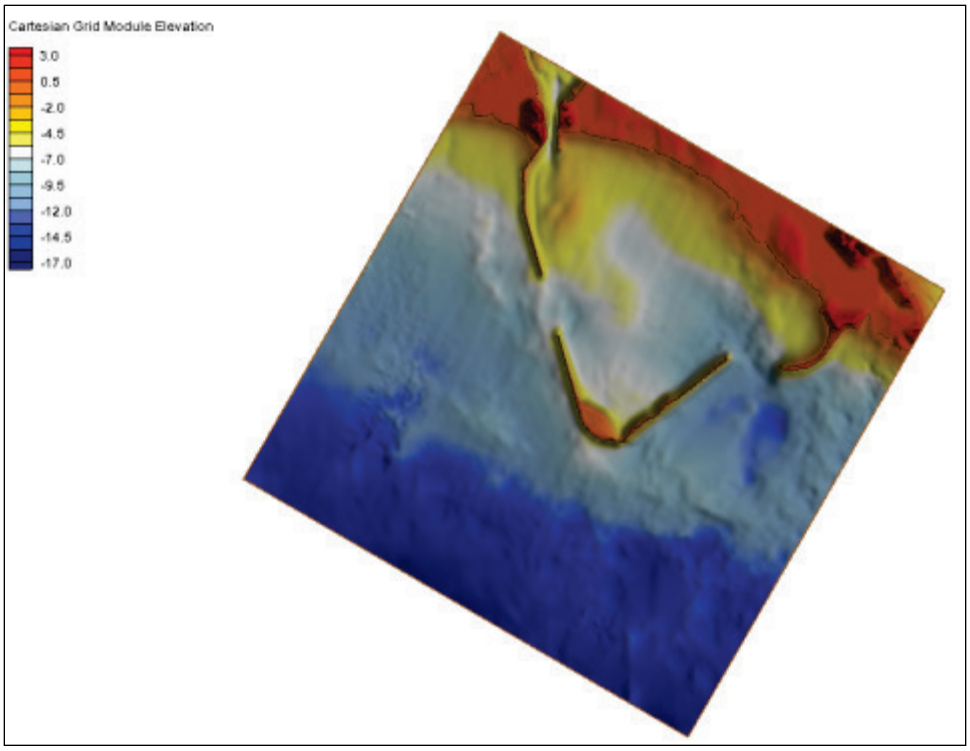


### B.4.2 Representation of structures in model grids

The breakwaters around Point Judith Harbor appear as smooth structures in Figures B9 through B11. The three-dimensional (3D) images displayed in Figures B12 through B14 show more details of these structures, revealing irregular shapes and varying side slopes along different segments. The images reveal gaps in parts of structures. The crest elevations vary irregularly. The variability in the crest elevations affects wave overtopping along the breakwater segments. This can be seen clearly in the animations of each storm that were generated as part of this study.

The irregular geometries, intermittently wet and dry porous sections, and structural complexities of breakwaters pose computational challenges to numerical models. Calculating the interaction of waves with such highly irregular structures required refining model grids several times while retaining the local variation in the bathymetry around breakwaters. Details of the bathymetry and structures were considered in these numerical simulations. The fully nonlinear Boussinesq formulation option available in BOUSS-2D with the wave-induced turbulence closure scheme was required. Since no nearshore wave measurements were available to validate the model, the BOUSS-2D settings were determined by trial-and-error runs.

Figure B12. 3D image of West Shore Arm and Main breakwaters and main channel area. Interior and exterior bathymetries in the vicinity of structures are also shown.

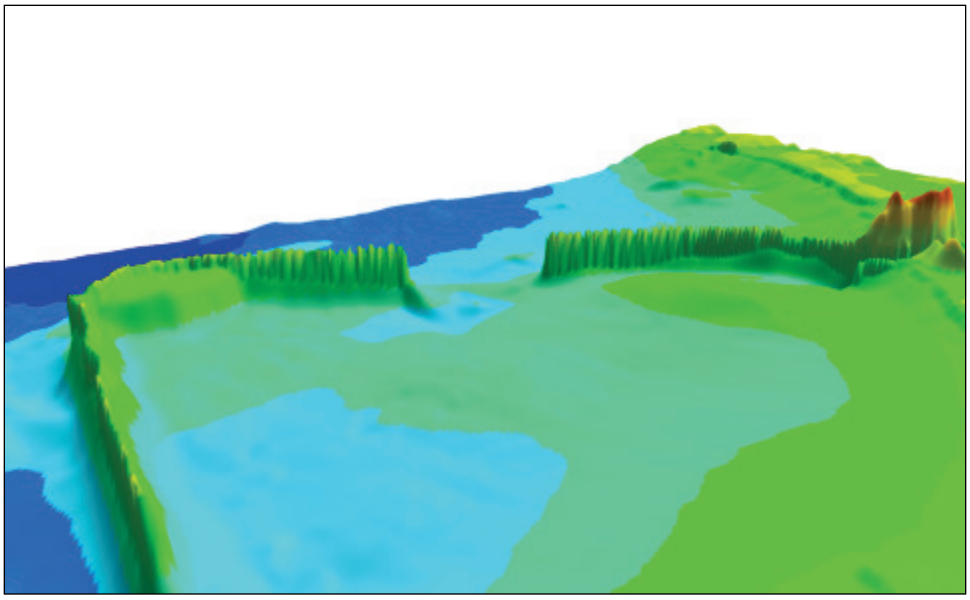

Figure B13. 3D image of Main and West Shore Arm breakwaters and interior and exterior bathymetries in the vicinity of structures.

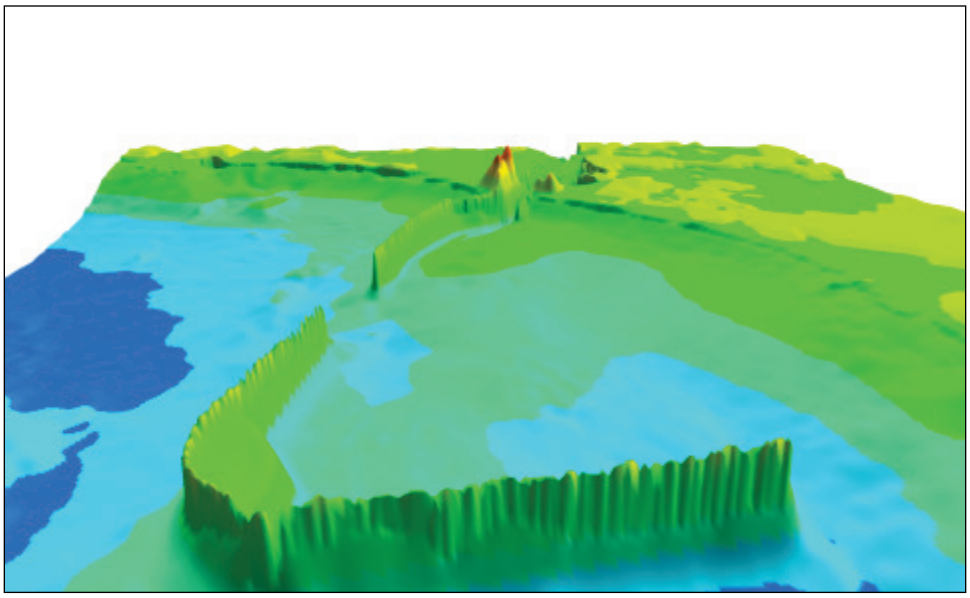

Figure B14. 3D image of East Shore Arm on left, West Shore Arm on right, and Main breakwaters as well as interior and exterior bathymetries near structures.

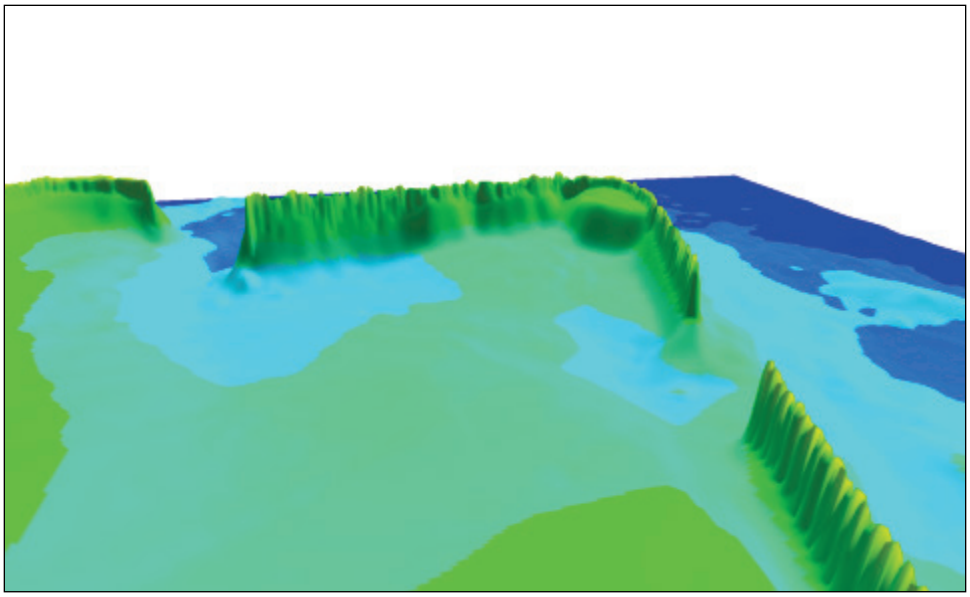

In Table B3, the GROW-FAB offshore peak wave height associated with the storm is listed as is the input wave condition and grid point number at the offshore boundary condition.

BOUSS-2D model results were saved at the same 204 stations where CMS-Wave results were saved. BOUSS-2D outputs time-varying sea surface elevation ($\eta$) and 2D velocities ($u$, $v$) at each grid point. Wave spectra were computed from these time-series data, and wave parameters of engineering interest were calculated ($H_{m0}$, $T_p$, and $\theta$) at 204 save points. These calculated wave parameters for each of the 20 storms were provided to the project team as tabulated data.

An example of the 2D spatial variation of significant wave height for storm 32 is shown in Figure B15 near the peak of the storm. Storm 32 is from the SE sector and consequently high wave heights occur outside the harbor on the ocean side of exterior breakwaters. The breakwaters intercept these large waves, reducing wave energy substantially throughout the harbor. Figure B15 shows large waves entering the sheltered area through the east gap between the Main and East Shore Arm breakwaters. Most of the harbor interior remains well sheltered. The wave energy that does enter the sheltered area could potentially cause mooring problems to vessels seeking shelter inside the harbor of refuge and erosion of the shoreline along the north boundary of the harbor. Given that a majority of storms approach Point Judith Harbor from the southeast sector, one option to

reduce wave energy within the harbor of refuge would be to close or narrow the east gap. In general, for all 20 storms simulated, BOUSS-2D model results indicated comparatively less wave energy gets into the harbor through the west gap since the west entrance to the harbor is somewhat sheltered.

Figure B15. Spatial variation of significant wave height (Hs) for Storm 32.

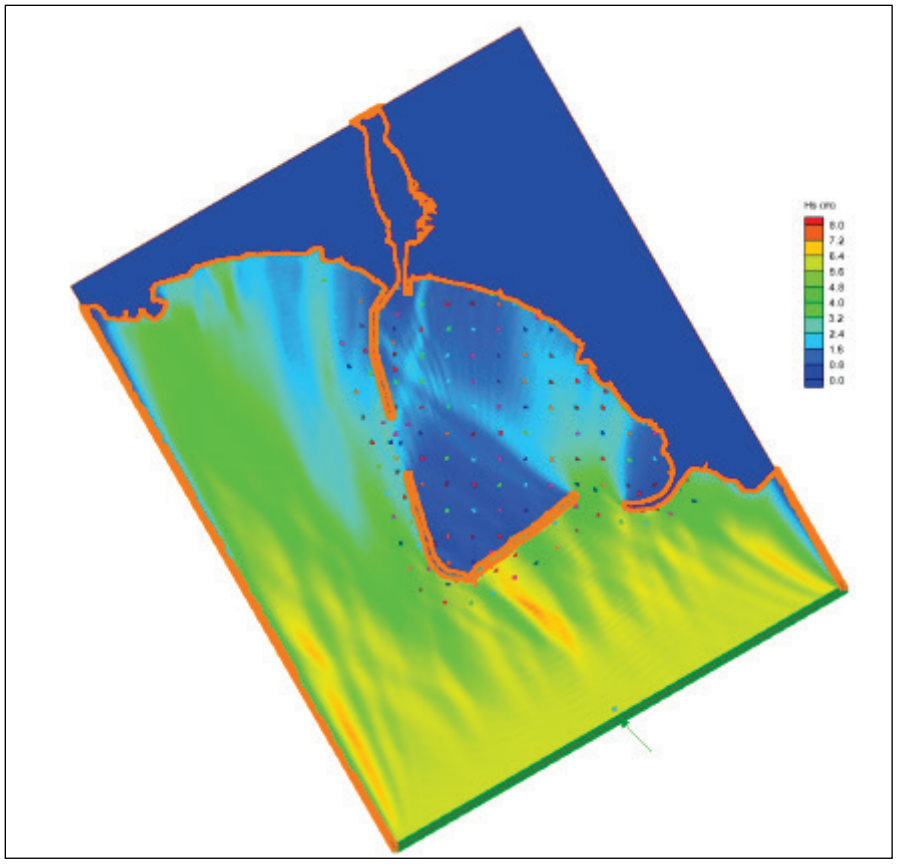

Model results indicated that waves entering the west gap move through the channel near the entrance and then shoal shoreward just east of the channel. The waves appear to shoal on the dredged mound just east of the channel and can be seen as light-blue area extending northward from the west entrance in Figure B15. These higher waves may cause erosion of the northern shoreline to the east of the channel.

# Appendix C: Point Judith Wave and Water Level Climate Analysis[1]

## C.1 Historical waves and water levels

As stated earlier, measured and predicted water level data were obtained from National Oceanic and Atmospheric Administration (NOAA), National Ocean Service (NOS), for the period 1930–2011 for stations 8455083, Narragansett Pier, RI, and 8452660, Newport, RI. The tidal statistics for station 8452660 were listed in Table A1.

The ocean wave climate, and in particular the high-energy waves generated by severe storms, are the primary forcing for coastal structures such as breakwaters, jetties, and levees. The wave climate in extratropical regions can be very energetic due to the high frequency of winter storms, which are typically large and intense. Also, large storms can occur multiple times within a single winter season and in close succession. Coastal structures face the risk of being damaged by large waves associated with these severe events. Projects dealing with coastal structures often require extensive review and analysis of data to accurately represent the wave climate. Accurate assessment of potential long-term trends and the computation of extremal statistics of wave and water level parameters are critical to the success of any engineering analysis of these structures. The variables usually considered include but are not limited to wave height, wave period, wave direction, wind speed, wind direction, storm duration, surge, and time of year. Wave power is also considered in the following analysis. Tidal variations must be modeled but are not random and can be accurately predicted. Time of year is important if storms are being simulated statistically because often the most severe storms are more likely to occur at the same time of year as the highest spring tides, creating a higher probability for larger waves in depth-limited breaking areas.

In the following sections, the offshore wave data used for this study are described. Then, significant storms in this data set are identified, and the extreme values of the parameters wave height, peak period, wave direction, wave power, wind speed, storm duration, storm surge, storm

[1] Authored by Jeffrey Melby and Norberto Nadal-Caraballo

hydrograph shape parameters, and month of occurrence are quantified for the significant storms. An extremal analysis is performed by fitting marginal distribution functions to each set of empirical probabilities of these parameters. The complex joint statistical relationships between the parameters are also quantified through joint probability analysis.

## C.2 Data sources

For this study, the offshore wave conditions are based on the GROW-FAB hindcast while the nearshore wave conditions are based on the CMS-Wave wave transformation results, as discussed earlier. Extremal analysis was conducted for both the offshore and nearshore conditions as discussed in the following. Water levels are based on the Newport, RI, tide gage.

## C.3 Extremal analysis toolkit

In this study, the numerical extremal statistical toolkit StormSim, developed at ERDC-CHL (Melby and Nadal-Caraballo 2009) was used for statistical analysis of the wave climate. The generalized toolkit is a suite of Matlab scripts with capabilities to do the following:

1. Plot numerical simulation and measurements and validate numerical models or assimilate data into simulations.
2. Identify storms in the offshore wave height time-series using peaks-over-threshold (POT) method, and isolate or compute important parameters and merge water level data with wave data.
3. Compute and plot wave power index as a function of time. Here, power index is defined as $(H_{mo})^2 \times$ storm duration, computed from POT analysis.
4. Fit marginal parametric distributions to empirical probability distributions for important parameters such as significant wave height, peak wave period, wave direction, wave power, wind speed, storm duration, storm surge, storm hydrograph shape parameters, and month of occurrence.
5. Compute correlations between parameters and fit joint probability distributions.
6. Employ Monte Carlo Simulation (MCS) technique to simulate future life-cycles of offshore storms based on a Gaussian Copula Model (GCM).
7. Develop SLR scenarios using criteria set forth in USACE (2011) with the addition of probabilistic characterization of the various scenarios.
8. Transform offshore waves to nearshore using table-lookup surrogate model and precomputed transformation coefficients.

## C.4 Peaks-over-threshold analysis

The POT censoring technique is widely used for identification of extreme values in time-series of wave climate data. The main concern is that the POT method suffers from lack of general guidance for its application (Lang et al. 1999). The sampled peak exceedances must be independent and identically distributed (i.i.d.), and their occurrences should be described by a Poisson process (Luceño et al. 2006).

When applying the POT technique, the most significant parameters are (1) the time lag required for the extreme events to be considered i.i.d., often referred to as interevent time, $\tau$, (2) the number of individual storms per year which is usually referred to as sample intensity, $\lambda$, and (3) $H_{th}$, the threshold wave height. The StormSim software performs several analyses to determine the optimal interevent time and sample intensity and to objectively select $H_{th}$.

The optimal interevent time is determined from autocorrelation analysis. Figure C1 shows $H_{m0}$ autocorrelation as a function of interevent time, computed for different threshold percentiles (i.e., 90% to 99.5%). Then the interevent time is selected to minimize the autocorrelation of wave height. An interevent time of 48 hr was chosen for Point Judith. In this way, the peaks selected are independent and not likely to be multiple peaks of a single storm.

Figure C1. Autocorrelation function for different $H_{m0}$ threshold percentiles.

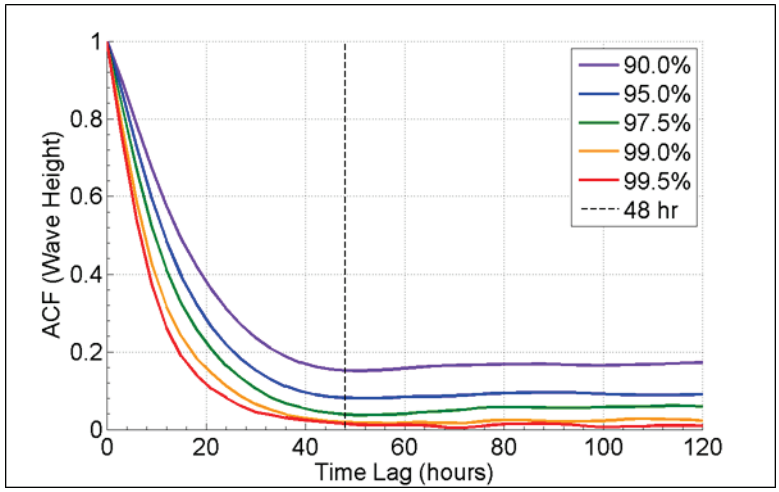

The ideal sample intensity is determined by analysis of the 100 and 500 yr $H_{m0}$ return periods (RP) resulting from a range of sample intensity values. Figure C2 shows predicted $H_{m0}$ for RP = 100 and 500 yr, as a function of sample intensity. These wave heights, normalized by $\tilde{H}_{m0}$, are plotted in Figure C3 where $\tilde{H}_{m0}$ is the predicted $H_{m0}$ averaged for all sample intensities between 10 and 20 storms/yr. This analysis aims to select the smallest sample intensity that meets the following criterion: $H_{m0} / \tilde{H}_{m0} \leq 1.1$, considering RP = 100 and 500 yr. The optimal sample intensity for Point Judith was determined to be $\lambda$ = 4 storms/yr (illustrated in Figure C3 by a dashed vertical line).

Figure C2. Predicted offshore wave heights ($H_{m0}$) as a function of sample intensity ($\lambda$).

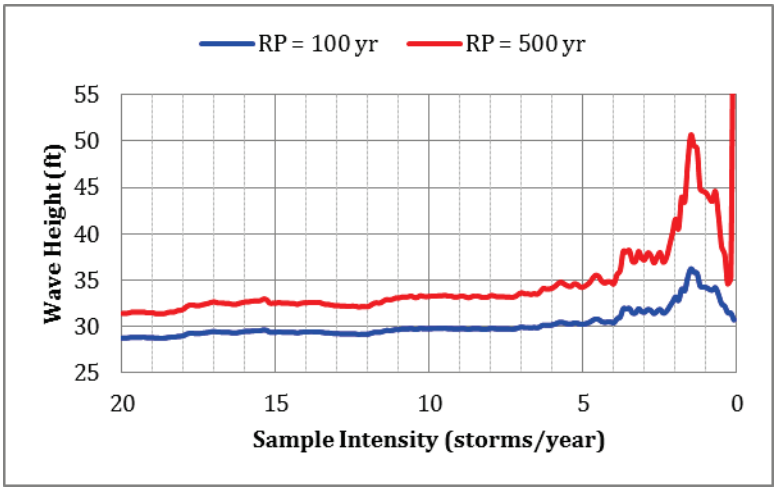


Figure C3. Normalized offshore wave heights as a function of sample intensity.

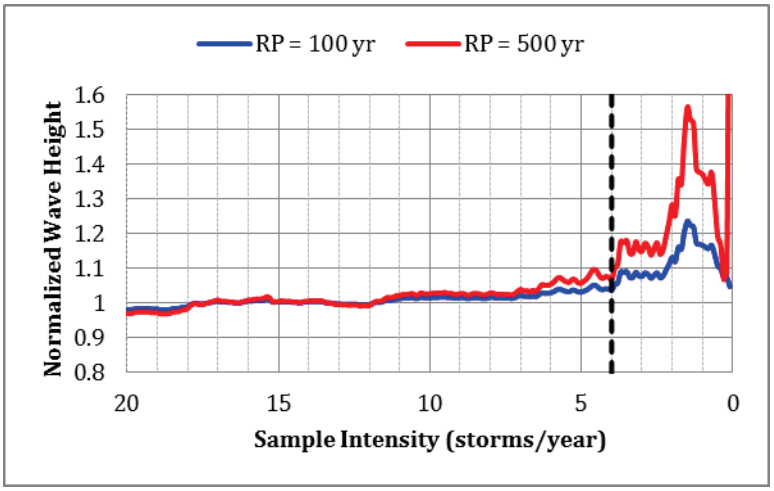

For the GROW-FAB hindcast, 225 storms were identified over the 57 yr record length with $\tau$ = 48 hr and $\lambda$ = 4 storms/yr. Figure C4 shows how $H_{th}$ varies as a function of sample intensity. The final $H_{th}$ for Point Judith was determined to be 15.4 ft, which corresponds to $\lambda$ = 4 storms/yr.

Figure C4. Offshore wave height threshold as a function of sample intensity.

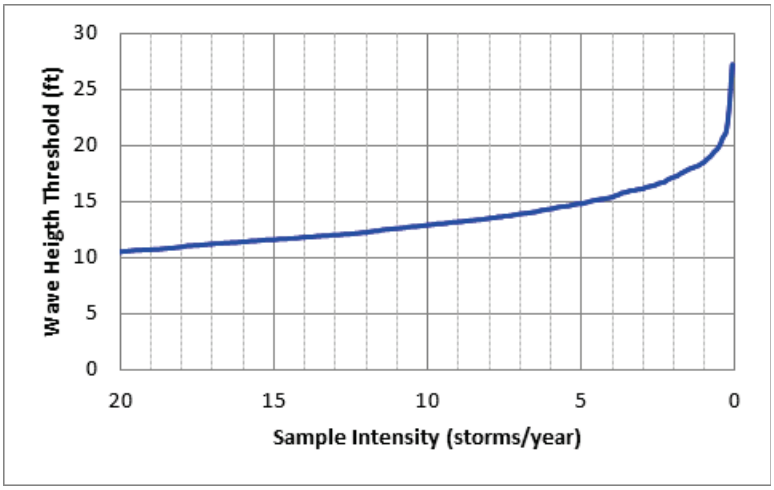


Table C1 lists the peak wave parameters for all 225 storms. The storm duration, $D_S$, is the duration over the threshold wave height. Storm power index, PI = $(H_{m0})^2 \times D_S$, is a measure of the intensity of a storm. The storm surge was computed by subtracting the predicted water level from the measured water level at the Newport tide gage. NaN, or not a number, indicates that data are not available for those dates. The storms are ordered by wave height, sorted in order from high to low. Figures C5 and C6 show time-series of offshore wave parameters. Intense storm clustering can be seen around 1960 and in the early 1990s. The recent decade has been relatively less severe for storm intensity.

Table C1. Summary of historical offshore storm wave peak values from GROW hindcast in rank order of decreasing wave heights.

| Storm | Date | $H_{m0}$ (ft) | Storm Duration (hrs) | Power Index (ft²*hr) | $T_p$ (sec) | Dir (Az. deg) | Surge (ft) | Water Level (ft, MSL) | | | |
|---|---|---|---|---|---|---|---|---|---|---|---|
| | | | | | | | | synoptic | avg | min | max |
| 1 | 8/19/91 18:00 | 33.00 | 9 | 9798 | 12.2 | 177 | 5.12 | 7.59 | 1.92 | -0.08 | 7.59 |
| 2 | 8/31/54 15:00 | 27.87 | 12 | 9324 | 11.4 | 174 | 7.93 | 10.21 | 2.81 | -0.79 | 10.61 |
| 3 | 9/11/54 18:00 | 27.63 | 15 | 11450 | 11.8 | 146 | NaN | NaN | NaN | NaN | NaN |

| Storm | Date | $H_{m0}$ (ft) | Storm Duration (hrs) | Power Index (ft²*hr) | $T_p$ (sec) | Dir (Az. deg) | Surge (ft) | Water Level (ft, MSL) | | | |
|---|---|---|---|---|---|---|---|---|---|---|---|
| | | | | | | | | synoptic | avg | min | max |
| 4 | 9/12/60 21:00 | 27.34 | 15 | 11212 | 11.0 | 155 | 4.38 | 6.21 | 2.15 | 0.01 | 6.51 |
| 5 | 9/27/85 18:00 | 27.24 | 15 | 11131 | 11.3 | 170 | 4.41 | 3.49 | 2.33 | -0.57 | 5.04 |
| 6 | 9/21/61 12:00 | 25.55 | 15 | 9793 | 11.0 | 119 | 2.34 | 5.41 | 2.17 | -0.19 | 5.61 |
| 7 | 12/12/92 0:00 | 24.62 | 75 | 45447 | 12.0 | 103 | 2.80 | 5.56 | 3.13 | 0.14 | 6.23 |
| 8 | 8/10/76 9:00 | 24.10 | 15 | 8715 | 11.1 | 174 | 1.44 | 2.33 | 1.83 | -0.80 | 4.37 |
| 9 | 3/7/62 6:00 | 23.68 | 51 | 28593 | 12.0 | 85 | 1.96 | 0.71 | 2.99 | -0.09 | 6.21 |
| 10 | 1/31/66 0:00 | 23.37 | 36 | 19661 | 11.3 | 209 | 2.85 | 0.21 | 1.55 | -1.39 | 5.31 |
| 11 | 9/17/99 6:00 | 23.32 | 15 | 8155 | 11.2 | 196 | 2.41 | 1.13 | 1.82 | -0.37 | 4.41 |
| 12 | 1/9/78 15:00 | 22.18 | 42 | 20665 | 10.7 | 168 | 2.51 | 3.16 | 1.50 | -2.43 | 7.19 |
| 13 | 3/14/93 9:00 | 22.13 | 30 | 14695 | 12.8 | 194 | 3.77 | 1.21 | 1.08 | -2.21 | 5.75 |
| 14 | 3/5/71 9:00 | 22.06 | 27 | 13144 | 10.6 | 243 | 3.30 | -0.92 | 0.71 | -1.52 | 4.72 |
| 15 | 10/31/91 6:00 | 21.91 | 36 | 17286 | 8.8 | 54 | 3.61 | 4.26 | 3.75 | 1.78 | 7.08 |
| 16 | 3/14/10 3:00 | 21.37 | 21 | 9591 | 10.8 | 110 | 2.47 | 2.26 | 2.87 | 0.65 | 5.03 |
| 17 | 3/20/58 18:00 | 21.21 | 21 | 9448 | 10.8 | 86 | 2.10 | 1.21 | 2.55 | -0.09 | 5.51 |
| 18 | 1/26/78 21:00 | 21.17 | 30 | 13447 | 11.1 | 204 | 2.59 | 2.46 | 1.75 | -1.21 | 5.70 |
| 19 | 12/24/94 3:00 | 21.12 | 15 | 6692 | 9.2 | 52 | 3.39 | 5.33 | 2.39 | 0.14 | 5.33 |
| 20 | 3/29/84 15:00 | 20.86 | 27 | 11748 | 10.9 | 96 | 2.76 | 3.12 | 2.96 | 0.63 | 5.05 |
| 21 | 2/2/76 18:00 | 20.81 | 18 | 7793 | 10.0 | 222 | 2.76 | -0.76 | 0.80 | -2.88 | 6.33 |
| 22 | 12/2/74 9:00 | 20.75 | 15 | 6461 | 10.1 | 102 | 2.76 | 1.20 | 2.42 | -0.62 | 7.06 |
| 23 | 2/19/72 15:00 | 20.61 | 15 | 6372 | 11.0 | 98 | 2.94 | 2.78 | 2.86 | -0.10 | 6.18 |
| 24 | 10/25/80 21:00 | 20.52 | 27 | 11374 | 10.2 | 137 | 2.38 | -0.48 | 1.80 | -2.11 | 5.90 |
| 25 | 3/6/59 21:00 | 20.17 | 12 | 4881 | 10.6 | 178 | 1.74 | 3.31 | 1.50 | -0.89 | 4.51 |

| Storm | Date | $H_{m0}$ (ft) | Storm Duration (hrs) | Power Index ($ft^2$*hr) | $T_p$ (sec) | Dir (Az. deg) | Surge (ft) | Water Level (ft, MSL) | | | |
|---|---|---|---|---|---|---|---|---|---|---|---|
| | | | | | | | | synoptic | avg | min | max |
| 26 | 1/8/96 12:00 | 20.16 | 15 | 6099 | 10.7 | 78 | 2.80 | 2.19 | 2.53 | 0.25 | 5.93 |
| 27 | 11/30/63 18:00 | 20.16 | 18 | 7314 | 10.1 | 211 | 2.26 | -1.69 | 1.79 | -1.89 | 7.01 |
| 28 | 2/4/72 12:00 | 20.05 | 18 | 7238 | 10.1 | 211 | 3.22 | 1.64 | 1.79 | -0.88 | 5.60 |
| 29 | 3/3/94 12:00 | 19.91 | 12 | 4758 | 9.8 | 105 | 2.34 | 1.29 | 2.44 | -0.42 | 4.91 |
| 30 | 11/12/95 9:00 | 19.89 | 12 | 4747 | 10.5 | 165 | 2.06 | 2.33 | 1.89 | -0.57 | 4.09 |
| 31 | 6/22/72 21:00 | 19.87 | 12 | 4737 | 10.4 | 149 | 1.95 | 5.30 | 2.63 | 0.83 | 5.51 |
| 32 | 2/2/81 21:00 | 19.73 | 12 | 4673 | 10.7 | 181 | 1.08 | 0.09 | 1.36 | -0.91 | 3.80 |
| 33 | 1/24/92 3:00 | 19.68 | 9 | 3486 | 10.4 | 175 | 1.80 | 5.71 | 2.05 | -0.29 | 5.71 |
| 34 | 12/17/70 12:00 | 19.65 | 9 | 3475 | 9.8 | 104 | 2.69 | 2.14 | 2.31 | 0.44 | 5.73 |
| 35 | 7/14/96 0:00 | 19.62 | 9 | 3465 | 10.7 | 185 | 1.34 | 1.39 | 1.93 | -0.10 | 4.90 |
| 36 | 11/3/07 21:00 | 19.59 | 12 | 4604 | 8.2 | 59 | 0.86 | 3.40 | 2.15 | 0.48 | 3.88 |
| 37 | 1/23/66 18:00 | 19.44 | 12 | 4536 | 10.3 | 103 | 2.81 | 0.91 | 2.69 | 0.61 | 5.11 |
| 38 | 3/23/73 0:00 | 19.43 | 30 | 11325 | 11.6 | 65 | NaN | NaN | NaN | NaN | NaN |
| 39 | 12/18/00 6:00 | 19.39 | 18 | 6770 | 9.9 | 222 | 2.11 | 2.96 | 1.50 | -1.54 | 4.63 |
| 40 | 1/25/79 6:00 | 19.33 | 12 | 4486 | 9.7 | 108 | 2.71 | 5.95 | 2.72 | 0.34 | 5.98 |
| 41 | 12/7/83 15:00 | 19.22 | 18 | 6649 | 10.0 | 241 | 2.55 | 2.56 | 1.56 | -1.26 | 4.76 |
| 42 | 2/3/73 3:00 | 19.16 | 9 | 3304 | 10.5 | 175 | 1.68 | 3.11 | 1.96 | -0.07 | 4.44 |
| 43 | 1/12/80 9:00 | 19.06 | 15 | 5448 | 10.5 | 196 | 0.91 | 0.66 | 0.78 | -1.75 | 3.57 |
| 44 | 1/22/79 0:00 | 19.05 | 12 | 4356 | 10.9 | 189 | 2.09 | 1.49 | 2.62 | 0.64 | 4.74 |
| 45 | 4/16/07 9:00 | 19.04 | 12 | 4350 | 10.3 | 138 | 2.96 | 5.10 | 3.07 | -0.05 | 6.66 |
| 46 | 10/25/05 15:00 | 19.01 | 15 | 5420 | 10.5 | 75 | 2.74 | 3.23 | 3.26 | 1.65 | 5.37 |

| Storm | Date | $H_{m0}$ (ft) | Storm Duration (hrs) | Power Index ($ft^2$*hr) | $T_p$ (sec) | Dir (Az. deg) | Surge (ft) | Water Level (ft, MSL) | | | |
|---|---|---|---|---|---|---|---|---|---|---|---|
| | | | | | | | | synoptic | avg | min | max |
| 47 | 3/22/80 21:00 | 18.94 | 24 | 8610 | 11.3 | 70 | 1.65 | 4.30 | 2.48 | 0.29 | 5.20 |
| 48 | 3/3/69 6:00 | 18.91 | 12 | 4291 | 10.0 | 71 | 1.53 | 1.41 | 2.21 | 0.15 | 4.24 |
| 49 | 11/12/68 18:00 | 18.88 | 18 | 6417 | 9.9 | 100 | 2.98 | 3.69 | 2.34 | -0.37 | 5.82 |
| 50 | 12/30/97 21:00 | 18.82 | 18 | 6375 | 10.1 | 223 | 2.28 | 0.20 | 1.90 | -1.37 | 5.53 |
| 51 | 6/4/07 18:00 | 18.73 | 6 | 2105 | 10.5 | 172 | 1.50 | 2.50 | 2.63 | 0.57 | 4.64 |
| 52 | 11/26/72 18:00 | 18.72 | 9 | 3155 | 10.4 | 178 | 2.37 | 4.68 | 2.24 | 0.41 | 5.62 |
| 53 | 1/23/87 12:00 | 18.65 | 18 | 6264 | 9.8 | 215 | 3.32 | 0.53 | 2.33 | 0.24 | 6.58 |
| 54 | 2/7/78 0:00 | 18.65 | 12 | 4173 | 10.2 | 78 | 3.09 | 3.24 | 2.58 | -0.59 | 6.37 |
| 55 | 12/3/86 12:00 | 18.57 | 15 | 5174 | 10.1 | 151 | 1.56 | 5.14 | 2.08 | -0.55 | 6.29 |
| 56 | 12/6/68 3:00 | 18.56 | 12 | 4134 | 9.8 | 238 | 1.86 | 0.78 | 1.02 | -1.61 | 3.97 |
| 57 | 12/8/59 0:00 | 18.55 | 21 | 7223 | 10.3 | 212 | 1.80 | 0.31 | 1.71 | -0.79 | 4.61 |
| 58 | 1/30/71 12:00 | 18.48 | 6 | 2050 | 9.7 | 208 | NaN | NaN | NaN | NaN | NaN |
| 59 | 3/27/92 9:00 | 18.48 | 9 | 3074 | 10.1 | 148 | 1.73 | 4.02 | 1.97 | 0.63 | 4.42 |
| 60 | 3/30/74 21:00 | 18.46 | 12 | 4091 | 9.8 | 100 | 1.58 | 3.83 | 2.31 | -0.29 | 4.82 |
| 61 | 4/28/67 18:00 | 18.42 | 27 | 9160 | 8.6 | 43 | 1.71 | 2.11 | 1.97 | 0.11 | 4.51 |
| 62 | 2/13/85 0:00 | 18.38 | 12 | 4054 | 9.5 | 119 | 2.35 | 3.28 | 2.58 | 0.86 | 4.60 |
| 63 | 2/11/73 18:00 | 18.35 | 21 | 7068 | 8.4 | 39 | 1.97 | 3.61 | 2.40 | 0.15 | 5.39 |
| 64 | 2/12/81 3:00 | 18.27 | 12 | 4007 | 10.4 | 179 | 1.09 | -1.53 | 0.68 | -1.65 | 3.83 |
| 65 | 1/11/77 0:00 | 18.27 | 27 | 9013 | 10.5 | 186 | 2.55 | 2.14 | 1.26 | -1.73 | 5.20 |
| 66 | 1/16/65 18:00 | 18.24 | 12 | 3994 | 9.4 | 55 | 0.86 | -0.49 | 1.54 | -1.29 | 5.21 |
| 67 | 3/7/63 3:00 | 18.23 | 9 | 2992 | 9.9 | 232 | 1.54 | -0.09 | 1.48 | -0.69 | 4.81 |
| 68 | 12/25/66 21:00 | 18.20 | 15 | 4968 | 9.7 | 248 | 2.46 | -1.49 | 1.02 | -2.09 | 4.11 |

| Storm | Date | $H_{m0}$ (ft) | Storm Duration (hrs) | Power Index (ft²*hr) | $T_p$ (sec) | Dir (Az. deg) | Surge (ft) | Water Level (ft, MSL) | | | |
|---|---|---|---|---|---|---|---|---|---|---|---|
| | | | | | | | | synoptic | avg | min | max |
| 69 | 10/29/06 9:00 | 18.16 | 36 | 11872 | 9.8 | 237 | 3.02 | 3.17 | 2.20 | -0.61 | 6.24 |
| 70 | 12/27/57 0:00 | 18.12 | 9 | 2955 | 9.6 | 160 | 1.99 | 2.81 | 1.51 | -0.79 | 3.71 |
| 71 | 4/4/75 6:00 | 18.12 | 18 | 5910 | 9.8 | 234 | 0.69 | 1.00 | 1.77 | 0.18 | 3.39 |
| 72 | 4/3/70 3:00 | 18.11 | 21 | 6888 | 10.4 | 198 | 2.46 | 1.47 | 1.60 | -1.44 | 4.93 |
| 73 | 2/14/71 6:00 | 18.11 | 9 | 2952 | 10.5 | 183 | NaN | NaN | NaN | NaN | NaN |
| 74 | 1/29/98 0:00 | 18.10 | 12 | 3933 | 9.8 | 65 | 1.61 | 0.42 | 2.33 | -0.57 | 5.81 |
| 75 | 11/14/03 3:00 | 18.08 | 15 | 4905 | 9.7 | 249 | 1.60 | -0.60 | 1.13 | -0.81 | 4.09 |
| 76 | 2/5/98 18:00 | 18.05 | 21 | 6840 | 10.5 | 71 | 2.11 | 1.92 | 2.83 | 0.88 | 5.17 |
| 77 | 1/9/56 18:00 | 18.00 | 30 | 9719 | 11.4 | 75 | 1.96 | 3.91 | 2.74 | 1.11 | 5.01 |
| 78 | 2/4/61 15:00 | 18.00 | 18 | 5831 | 9.8 | 97 | 1.80 | 3.21 | 1.89 | -0.69 | 4.91 |
| 79 | 2/15/60 3:00 | 17.99 | 18 | 5827 | 9.8 | 226 | 2.15 | 2.61 | 1.34 | -1.69 | 5.71 |
| 80 | 2/4/70 0:00 | 17.99 | 42 | 13591 | 12.7 | 176 | 2.11 | 3.58 | 1.62 | -1.37 | 4.93 |
| 81 | 12/25/78 21:00 | 17.95 | 27 | 8702 | 9.7 | 232 | 2.60 | 2.33 | 1.48 | -1.10 | 5.23 |
| 82 | 11/15/95 0:00 | 17.95 | 9 | 2901 | 9.9 | 91 | 2.09 | 2.60 | 2.70 | 0.59 | 4.94 |
| 83 | 1/5/82 0:00 | 17.93 | 6 | 1929 | 9.5 | 171 | 1.77 | 2.73 | 1.73 | -1.75 | 4.36 |
| 84 | 9/4/10 3:00 | 17.90 | 9 | 2885 | 15.0 | 153 | 1.45 | 1.96 | 2.54 | 0.72 | 4.46 |
| 85 | 2/12/06 12:00 | 17.80 | 6 | 1901 | 9.0 | 80 | 2.33 | 2.68 | 2.23 | 0.01 | 5.55 |
| 86 | 12/31/62 15:00 | 17.80 | 30 | 9500 | 8.8 | 286 | 0.19 | 2.31 | 0.61 | -2.19 | 3.11 |
| 87 | 2/19/60 9:00 | 17.77 | 33 | 10419 | 9.8 | 122 | 2.95 | 1.11 | 1.63 | -0.79 | 5.71 |
| 88 | 3/4/99 18:00 | 17.76 | 12 | 3786 | 10.3 | 201 | 1.79 | -0.78 | 1.34 | -1.06 | 4.68 |
| 89 | 12/7/62 21:00 | 17.76 | 15 | 4729 | 9.8 | 217 | 1.93 | 1.31 | 1.90 | -0.79 | 4.61 |
| 90 | 3/22/01 3:00 | 17.75 | 15 | 4724 | 9.7 | 100 | 1.41 | 1.74 | 2.31 | 0.38 | 4.57 |
| 91 | 11/2/73 3:00 | 17.71 | 12 | 3765 | 9.7 | 242 | 0.89 | -0.19 | 1.02 | -1.21 | 3.49 |

| Storm | Date | $H_{m0}$ (ft) | Storm Duration (hrs) | Power Index ($ft^2$*hr) | $T_p$ *(sec)* | Dir (Az. deg) | Surge (ft) | Water Level (ft, MSL) | | | |
|---|---|---|---|---|---|---|---|---|---|---|---|
| | | | | | | | | synoptic | avg | min | max |
| 92 | 12/17/74 3:00 | 17.70 | 9 | 2821 | 9.8 | 128 | 1.94 | 5.00 | 2.31 | 0.14 | 5.04 |
| 93 | 10/20/96 3:00 | 17.68 | 15 | 4687 | 9.8 | 91 | 2.25 | 1.98 | 3.10 | 1.08 | 5.74 |
| 94 | 9/2/96 9:00 | 17.60 | 15 | 4644 | 10.4 | 65 | 0.89 | 1.60 | 2.15 | -0.19 | 4.85 |
| 95 | 1/25/10 21:00 | 17.58 | 9 | 2782 | 10.5 | 170 | 2.40 | 3.35 | 2.47 | 0.29 | 4.50 |
| 96 | 4/5/84 21:00 | 17.58 | 9 | 2781 | 9.8 | 146 | 1.52 | 1.37 | 2.22 | 0.26 | 4.46 |
| 97 | 3/5/93 3:00 | 17.57 | 9 | 2777 | 9.7 | 88 | 1.64 | 2.27 | 2.22 | 0.47 | 4.82 |
| 98 | 11/9/72 0:00 | 17.56 | 6 | 1851 | 9.2 | 115 | 2.59 | 1.55 | 2.80 | 0.89 | 5.47 |
| 99 | 2/16/58 12:00 | 17.55 | 9 | 2773 | 9.7 | 99 | 2.77 | 1.91 | 2.03 | -0.39 | 5.41 |
| 100 | 11/21/89 15:00 | 17.51 | 12 | 3678 | 9.4 | 263 | 1.09 | 1.44 | 1.26 | -0.53 | 3.38 |
| 101 | 3/9/08 9:00 | 17.50 | 12 | 3676 | 9.9 | 228 | 1.31 | -0.63 | 1.30 | -1.91 | 5.27 |
| 102 | 1/13/64 21:00 | 17.46 | 9 | 2744 | 9.7 | 73 | 2.07 | 3.91 | 2.07 | 0.01 | 4.51 |
| 103 | 3/13/59 15:00 | 17.42 | 18 | 5461 | 9.6 | 248 | 2.30 | 0.71 | 1.42 | -1.59 | 4.71 |
| 104 | 12/29/68 3:00 | 17.41 | 6 | 1819 | 10.1 | 193 | 1.43 | 3.87 | 1.49 | -0.64 | 3.87 |
| 105 | 3/28/58 3:00 | 17.40 | 15 | 4544 | 10.7 | 62 | 1.61 | 1.91 | 2.56 | 1.21 | 4.41 |
| 106 | 2/26/56 3:00 | 17.35 | 9 | 2708 | 10.0 | 218 | 0.49 | 1.01 | 0.96 | -2.59 | 4.81 |
| 107 | 1/27/71 9:00 | 17.30 | 21 | 6283 | 9.8 | 244 | NaN | NaN | NaN | NaN | NaN |
| 108 | 11/29/03 18:00 | 17.26 | 15 | 4471 | 9.7 | 231 | 1.58 | 3.37 | 1.54 | -0.88 | 4.87 |
| 109 | 12/16/72 21:00 | 17.25 | 39 | 11601 | 9.6 | 246 | 1.59 | 1.07 | 0.78 | -2.14 | 4.15 |
| 110 | 12/5/57 12:00 | 17.22 | 12 | 3557 | 8.4 | 21 | 1.19 | 2.01 | 2.35 | 0.01 | 4.71 |
| 111 | 3/20/75 6:00 | 17.21 | 6 | 1777 | 9.7 | 148 | 1.12 | 2.23 | 1.93 | 0.06 | 3.97 |
| 112 | 9/3/72 15:00 | 17.20 | 9 | 2664 | 9.9 | 106 | 1.08 | 0.86 | 2.17 | 0.41 | 3.95 |
| 113 | 1/28/63 3:00 | 17.20 | 9 | 2662 | 9.4 | 245 | 0.07 | -2.19 | 0.13 | -2.19 | 3.01 |

| Storm | Date | $H_{m0}$ (ft) | Storm Duration (hrs) | Power Index (ft²*hr) | $T_p$ (sec) | Dir (Az. deg) | Surge (ft) | Water Level (ft, MSL) | | | |
|---|---|---|---|---|---|---|---|---|---|---|---|
| | | | | | | | | synoptic | avg | min | max |
| 114 | 2/12/93 18:00 | 17.19 | 6 | 1773 | 9.7 | 93 | 1.81 | 3.73 | 2.18 | -0.55 | 5.01 |
| 115 | 1/16/80 0:00 | 17.17 | 27 | 7956 | 8.5 | 47 | 0.87 | 3.46 | 1.73 | -0.04 | 4.10 |
| 116 | 12/17/07 6:00 | 17.13 | 24 | 7039 | 9.3 | 240 | 2.36 | 0.63 | 1.46 | -1.16 | 5.52 |
| 117 | 11/16/81 6:00 | 17.10 | 18 | 5263 | 9.8 | 102 | 0.79 | 2.64 | 2.21 | -0.01 | 4.95 |
| 118 | 12/21/93 21:00 | 17.07 | 21 | 6122 | 10.3 | 181 | 2.01 | 1.31 | 1.77 | -0.61 | 4.51 |
| 119 | 3/14/80 6:00 | 17.06 | 6 | 1746 | 9.3 | 104 | 1.54 | 2.55 | 1.18 | -2.23 | 5.51 |
| 120 | 2/7/80 21:00 | 17.04 | 15 | 4357 | 8.2 | 48 | 0.96 | 0.95 | 1.86 | -0.28 | 3.88 |
| 121 | 1/5/80 21:00 | 17.00 | 12 | 3469 | 8.7 | 50 | 1.11 | 1.80 | 1.87 | -0.69 | 4.33 |
| 122 | 11/8/77 12:00 | 16.95 | 12 | 3448 | 10.0 | 105 | 1.43 | 1.46 | 2.54 | 0.25 | 5.20 |
| 123 | 12/27/10 3:00 | 16.93 | 6 | 1720 | 9.6 | 66 | 2.30 | 3.18 | 2.09 | -0.37 | 5.63 |
| 124 | 1/2/69 0:00 | 16.92 | 9 | 2576 | 9.1 | 260 | 0.48 | 0.23 | 0.43 | -2.23 | 3.45 |
| 125 | 2/14/72 0:00 | 16.92 | 6 | 1718 | 9.4 | 139 | 1.94 | 5.30 | 2.02 | -0.61 | 5.30 |
| 126 | 12/17/73 21:00 | 16.91 | 18 | 5149 | 10.7 | 162 | 1.75 | 2.39 | 1.37 | -1.14 | 4.41 |
| 127 | 2/23/74 18:00 | 16.88 | 9 | 2565 | 9.4 | 244 | 0.67 | -1.90 | 0.46 | -2.07 | 2.94 |
| 128 | 9/7/08 6:00 | 16.86 | 3 | 853 | 9.8 | 199 | 1.20 | 3.84 | 2.02 | 0.30 | 3.91 |
| 129 | 12/20/09 9:00 | 16.82 | 9 | 2546 | 8.5 | 56 | 1.71 | 3.66 | 2.52 | 0.51 | 4.87 |
| 130 | 1/5/94 0:00 | 16.75 | 9 | 2526 | 10.5 | 198 | 2.05 | 2.13 | 1.91 | -1.12 | 4.96 |
| 131 | 1/3/60 18:00 | 16.74 | 6 | 1680 | 9.7 | 192 | 2.45 | 0.81 | 1.63 | -1.69 | 5.91 |
| 132 | 1/7/62 12:00 | 16.68 | 6 | 1669 | 9.6 | 188 | 1.16 | 3.51 | 1.76 | -0.69 | 5.11 |
| 133 | 12/6/81 15:00 | 16.67 | 21 | 5838 | 8.2 | 311 | 0.60 | 3.06 | 1.54 | -0.48 | 3.57 |
| 134 | 3/31/87 21:00 | 16.66 | 6 | 1665 | 10.1 | 165 | 1.17 | 3.31 | 2.03 | -0.24 | 4.64 |
| 135 | 4/7/71 6:00 | 16.65 | 6 | 1663 | 9.5 | 83 | 1.80 | 0.74 | 1.73 | -0.71 | 4.48 |

| Storm | Date | $H_{m0}$ (ft) | Storm Duration (hrs) | Power Index (ft²*hr) | $T_p$ (sec) | Dir (Az. deg) | Surge (ft) | Water Level (ft, MSL) | | | |
|---|---|---|---|---|---|---|---|---|---|---|---|
| | | | | | | | | synoptic | avg | min | max |
| 136 | 1/26/87 21:00 | 16.65 | 9 | 2494 | 8.5 | 45 | 1.41 | 1.07 | 2.02 | -0.21 | 5.04 |
| 137 | 10/15/55 0:00 | 16.64 | 9 | 2493 | 9.8 | 109 | 1.74 | 2.71 | 2.90 | 0.41 | 5.51 |
| 138 | 3/9/05 6:00 | 16.64 | 12 | 3324 | 8.7 | 272 | 1.60 | 0.16 | 1.40 | -1.96 | 4.76 |
| 139 | 12/21/73 18:00 | 16.63 | 9 | 2490 | 10.3 | 171 | 1.64 | 2.58 | 1.34 | -1.05 | 3.79 |
| 140 | 11/29/54 21:00 | 16.62 | 6 | 1657 | 9.2 | 243 | NaN | NaN | NaN | NaN | NaN |
| 141 | 3/28/55 0:00 | 16.60 | 18 | 4963 | 9.4 | 252 | NaN | NaN | NaN | NaN | NaN |
| 142 | 1/19/06 3:00 | 16.57 | 15 | 4121 | 9.5 | 232 | 2.20 | 2.49 | 1.50 | -1.01 | 4.79 |
| 143 | 8/29/58 15:00 | 16.56 | 3 | 823 | 12.8 | 139 | 0.14 | 2.01 | 1.62 | -0.59 | 3.81 |
| 144 | 11/26/83 3:00 | 16.53 | 6 | 1640 | 9.2 | 253 | 2.33 | -0.08 | 1.80 | -1.10 | 5.86 |
| 145 | 1/16/61 0:00 | 16.52 | 12 | 3276 | 9.8 | 81 | 1.67 | 0.91 | 1.95 | -0.79 | 5.81 |
| 146 | 1/20/78 18:00 | 16.52 | 6 | 1637 | 9.5 | 86 | 2.15 | 2.30 | 1.88 | -0.60 | 4.66 |
| 147 | 11/28/93 21:00 | 16.52 | 6 | 1637 | 9.7 | 162 | 1.78 | 0.23 | 2.08 | -0.14 | 4.54 |
| 148 | 1/3/99 21:00 | 16.47 | 6 | 1628 | 9.4 | 145 | 1.92 | 0.44 | 1.83 | -1.18 | 5.04 |
| 149 | 10/15/03 18:00 | 16.47 | 9 | 2441 | 9.5 | 229 | 2.38 | 2.53 | 2.17 | 0.37 | 4.26 |
| 150 | 12/16/05 15:00 | 16.45 | 3 | 811 | 8.9 | 135 | 2.20 | 2.84 | 1.96 | -0.33 | 5.49 |
| 151 | 12/12/60 15:00 | 16.39 | 12 | 3225 | 9.4 | 55 | 1.85 | 2.41 | 2.07 | 0.51 | 3.81 |
| 152 | 1/2/64 9:00 | 16.38 | 6 | 1610 | 9.6 | 219 | 1.17 | -0.89 | 1.01 | -1.39 | 4.61 |
| 153 | 10/22/88 12:00 | 16.38 | 6 | 1609 | 9.5 | 120 | 1.81 | 4.15 | 2.47 | -0.03 | 5.98 |
| 154 | 2/26/65 0:00 | 16.37 | 15 | 4022 | 9.7 | 161 | 2.32 | 3.11 | 1.94 | -0.29 | 4.41 |
| 155 | 2/10/69 18:00 | 16.37 | 6 | 1609 | 8.1 | 324 | 2.05 | 1.65 | 1.87 | 0.30 | 4.37 |
| 156 | 2/12/83 6:00 | 16.37 | 9 | 2413 | 8.9 | 61 | 2.02 | 1.99 | 1.72 | -0.60 | 4.11 |
| 157 | 2/24/98 12:00 | 16.36 | 6 | 1607 | 9.5 | 75 | 2.25 | 2.01 | 2.69 | 0.51 | 5.44 |

| Storm | Date | $H_{m0}$ (ft) | Storm Duration (hrs) | Power Index ($ft^2$*hr) | $T_p$ (sec) | Dir (Az. deg) | Surge (ft) | Water Level (ft, MSL) | | | |
|---|---|---|---|---|---|---|---|---|---|---|---|
| | | | | | | | | synoptic | avg | min | max |
| 158 | 10/21/76 9:00 | 16.34 | 6 | 1602 | 9.6 | 177 | 2.11 | -0.56 | 1.72 | -1.41 | 5.07 |
| 159 | 3/1/68 21:00 | 16.31 | 9 | 2393 | 8.0 | 291 | 1.56 | 2.61 | 1.67 | -1.01 | 4.68 |
| 160 | 3/23/77 0:00 | 16.30 | 3 | 797 | 9.4 | 117 | 2.13 | 0.99 | 1.92 | -0.16 | 5.44 |
| 161 | 12/16/81 21:00 | 16.29 | 6 | 1593 | 8.9 | 250 | 1.67 | -1.01 | 0.97 | -1.54 | 4.35 |
| 162 | 12/15/03 3:00 | 16.29 | 6 | 1593 | 9.2 | 112 | NaN | NaN | NaN | NaN | NaN |
| 163 | 6/14/66 6:00 | 16.28 | 3 | 795 | 10.4 | 152 | 0.01 | 1.61 | 1.38 | 0.01 | 2.91 |
| 164 | 11/29/58 6:00 | 16.28 | 3 | 795 | 9.0 | 172 | 2.53 | 2.61 | 1.33 | -2.19 | 4.61 |
| 165 | 10/8/65 9:00 | 16.26 | 3 | 793 | 9.1 | 158 | 1.37 | 3.81 | 2.18 | 0.21 | 4.21 |
| 166 | 2/12/55 12:00 | 16.25 | 6 | 1585 | 9.3 | 244 | NaN | NaN | NaN | NaN | NaN |
| 167 | 10/16/02 21:00 | 16.24 | 3 | 792 | 9.6 | 119 | 2.23 | 1.49 | 2.75 | 0.81 | 5.36 |
| 168 | 12/26/69 18:00 | 16.21 | 3 | 789 | 9.6 | 119 | 2.24 | 2.38 | 2.75 | 0.61 | 4.71 |
| 169 | 1/28/96 0:00 | 16.20 | 3 | 787 | 9.4 | 164 | 1.75 | 0.87 | 1.17 | -0.78 | 3.56 |
| 170 | 1/15/92 9:00 | 16.17 | 6 | 1569 | 9.0 | 253 | 1.77 | 1.31 | 1.53 | -0.34 | 4.36 |
| 171 | 3/22/99 15:00 | 16.15 | 9 | 2347 | 9.8 | 165 | 1.72 | -0.07 | 1.88 | -0.46 | 4.96 |
| 172 | 1/8/09 12:00 | 16.14 | 6 | 1562 | 9.1 | 231 | 0.87 | -0.25 | 1.03 | -1.38 | 3.91 |
| 173 | 12/21/60 21:00 | 16.13 | 3 | 780 | 9.6 | 169 | 1.00 | -0.69 | 1.55 | -0.99 | 5.31 |
| 174 | 1/6/59 3:00 | 16.11 | 24 | 6225 | 8.5 | 284 | 0.73 | 1.21 | -0.16 | -2.79 | 3.21 |
| 175 | 2/26/60 9:00 | 16.10 | 6 | 1555 | 9.0 | 119 | 2.02 | 5.41 | 1.86 | -0.99 | 5.41 |
| 176 | 11/7/63 18:00 | 16.09 | 6 | 1554 | 9.2 | 125 | 1.40 | 5.01 | 2.51 | 0.61 | 5.01 |
| 177 | 9/24/64 0:00 | 16.09 | 6 | 1553 | 14.0 | 128 | 0.40 | 3.91 | 2.02 | -0.09 | 4.51 |
| 178 | 1/14/02 0:00 | 16.08 | 6 | 1551 | 8.9 | 259 | 0.80 | 2.84 | 1.16 | -1.94 | 4.40 |

| Storm | Date | $H_{m0}$ (ft) | Storm Duration (hrs) | Power Index ($ft^2$*hr) | $T_p$ (sec) | Dir (Az. deg) | Surge (ft) | Water Level (ft, MSL) | | | |
|---|---|---|---|---|---|---|---|---|---|---|---|
| | | | | | | | | synoptic | avg | min | max |
| 179 | 10/29/08 6:00 | 16.08 | 6 | 1551 | 9.6 | 242 | 1.67 | 1.42 | 2.13 | -0.58 | 5.19 |
| 180 | 1/20/96 3:00 | 16.07 | 6 | 1550 | 10.5 | 180 | 2.22 | -1.32 | 1.82 | -1.32 | 6.18 |
| 181 | 3/24/68 15:00 | 16.07 | 6 | 1549 | 9.4 | 228 | 0.00 | -0.60 | 0.71 | -1.28 | 2.97 |
| 182 | 2/16/67 21:00 | 16.06 | 6 | 1548 | 9.2 | 244 | 0.63 | -1.09 | 0.71 | -1.89 | 2.71 |
| 183 | 1/29/94 0:00 | 16.04 | 3 | 772 | 10.4 | 181 | 1.32 | -0.33 | 1.54 | -1.29 | 4.84 |
| 184 | 11/2/97 0:00 | 16.02 | 6 | 1540 | 9.6 | 128 | 2.34 | 5.33 | 2.70 | 0.30 | 5.85 |
| 185 | 2/24/89 18:00 | 15.97 | 12 | 3061 | 8.2 | 40 | 0.84 | 1.91 | 1.90 | -0.24 | 3.98 |
| 186 | 3/18/73 6:00 | 15.95 | 6 | 1526 | 9.7 | 211 | NaN | NaN | NaN | NaN | NaN |
| 187 | 12/9/73 18:00 | 15.95 | 6 | 1526 | 9.5 | 113 | 1.41 | 4.35 | 1.92 | -0.69 | 4.95 |
| 188 | 3/11/04 12:00 | 15.95 | 6 | 1526 | 8.0 | 45 | 1.18 | 3.02 | 2.17 | -0.16 | 4.93 |
| 189 | 1/4/92 18:00 | 15.94 | 6 | 1525 | 9.1 | 97 | 1.45 | 3.01 | 2.27 | 0.10 | 4.38 |
| 190 | 1/23/05 15:00 | 15.94 | 15 | 3812 | 8.0 | 32 | 2.13 | 3.70 | 2.69 | 0.81 | 4.99 |
| 191 | 4/3/05 6:00 | 15.94 | 3 | 762 | 9.2 | 142 | 1.91 | 4.74 | 2.73 | 1.39 | 5.42 |
| 192 | 1/24/98 3:00 | 15.94 | 3 | 762 | 9.5 | 134 | 1.77 | 1.82 | 2.34 | 0.63 | 4.10 |
| 193 | 2/4/95 21:00 | 15.94 | 15 | 3809 | 9.4 | 123 | 2.51 | 0.15 | 1.98 | -0.40 | 5.01 |
| 194 | 2/4/69 9:00 | 15.93 | 6 | 1523 | 8.9 | 258 | 1.37 | 2.22 | 0.98 | -1.62 | 3.51 |
| 195 | 2/12/88 15:00 | 15.91 | 6 | 1519 | 9.4 | 109 | 1.89 | 2.11 | 2.19 | 0.19 | 4.34 |
| 196 | 10/14/84 18:00 | 15.89 | 12 | 3031 | 9.5 | 89 | 0.69 | 1.02 | 2.34 | 0.88 | 4.30 |
| 197 | 12/2/06 3:00 | 15.88 | 3 | 757 | 9.0 | 207 | 1.33 | 0.60 | 1.72 | -0.81 | 4.09 |
| 198 | 12/12/00 18:00 | 15.88 | 6 | 1513 | 8.8 | 233 | 1.61 | 1.16 | 1.30 | -1.94 | 6.17 |
| 199 | 1/26/75 6:00 | 15.87 | 18 | 4535 | 9.2 | 211 | 1.72 | 1.63 | 1.47 | -2.12 | 5.19 |
| 200 | 2/26/61 12:00 | 15.85 | 12 | 3015 | 9.8 | 201 | 1.55 | 1.21 | 1.67 | -0.19 | 3.71 |

| Storm | Date | $H_{m0}$ (ft) | Storm Duration (hrs) | Power Index ($ft^2$*hr) | $T_p$ (sec) | Dir (Az. deg) | Surge (ft) | Water Level (ft, MSL) | | | |
|---|---|---|---|---|---|---|---|---|---|---|---|
| | | | | | | | | synoptic | avg | min | max |
| 201 | 12/18/78 6:00 | 15.84 | 9 | 2257 | 8.9 | 264 | 1.06 | 0.48 | 0.83 | -0.96 | 3.74 |
| 202 | 4/1/97 12:00 | 15.83 | 6 | 1504 | 8.1 | 24 | 1.98 | 3.06 | 2.80 | 1.13 | 4.79 |
| 203 | 1/9/66 9:00 | 15.83 | 6 | 1504 | 8.4 | 285 | 0.95 | 1.31 | 1.37 | -2.39 | 5.31 |
| 204 | 12/19/77 18:00 | 15.83 | 6 | 1503 | 9.5 | 76 | 1.76 | 3.18 | 2.78 | 1.04 | 4.72 |
| 205 | 2/14/66 3:00 | 15.80 | 3 | 749 | 9.5 | 177 | 1.45 | 3.01 | 1.56 | 0.11 | 3.61 |
| 206 | 1/3/79 3:00 | 15.79 | 3 | 748 | 10.0 | 182 | 0.92 | 2.55 | 1.27 | -1.01 | 4.73 |
| 207 | 10/17/77 15:00 | 15.78 | 6 | 1494 | 9.5 | 210 | 1.61 | 3.13 | 1.70 | -1.04 | 4.72 |
| 208 | 12/7/76 21:00 | 15.76 | 3 | 746 | 9.3 | 165 | 1.44 | -0.41 | 1.63 | -0.53 | 3.67 |
| 209 | 2/17/03 21:00 | 15.76 | 3 | 745 | 9.5 | 82 | 1.34 | 0.37 | 1.61 | -1.26 | 4.84 |
| 210 | 4/7/82 9:00 | 15.75 | 6 | 1489 | 8.1 | 298 | 1.26 | 0.23 | 1.12 | -1.70 | 3.69 |
| 211 | 1/28/67 15:00 | 15.73 | 6 | 1486 | 9.6 | 219 | 1.87 | 5.01 | 2.16 | -0.49 | 5.31 |
| 212 | 11/12/90 9:00 | 15.73 | 3 | 743 | 9.1 | 253 | -0.10 | -0.03 | 0.60 | -1.67 | 2.43 |
| 213 | 3/2/66 9:00 | 15.71 | 6 | 1481 | 9.0 | 250 | 1.33 | 0.41 | 1.37 | -0.59 | 3.81 |
| 214 | 3/12/92 6:00 | 15.63 | 3 | 733 | 9.1 | 239 | 1.75 | 2.69 | 1.75 | 0.01 | 4.16 |
| 215 | 2/28/58 9:00 | 15.60 | 3 | 730 | 9.1 | 104 | 2.08 | 2.51 | 2.24 | 0.81 | 3.81 |
| 216 | 11/16/89 21:00 | 15.59 | 3 | 730 | 9.2 | 177 | 1.46 | -0.21 | 1.94 | -0.23 | 5.27 |
| 217 | 9/7/79 0:00 | 15.57 | 3 | 728 | 9.5 | 209 | 1.64 | 4.55 | 2.04 | -0.75 | 5.18 |
| 218 | 11/27/97 15:00 | 15.55 | 6 | 1451 | 8.7 | 271 | 0.86 | 1.47 | 1.63 | -1.05 | 4.37 |
| 219 | 10/24/59 21:00 | 15.52 | 3 | 722 | 9.6 | 131 | 1.21 | 1.41 | 2.37 | 1.11 | 4.31 |
| 220 | 12/27/04 6:00 | 15.52 | 3 | 722 | 11.7 | 60 | 1.76 | 3.25 | 2.01 | -0.74 | 5.07 |
| 221 | 1/12/87 3:00 | 15.52 | 3 | 722 | 8.8 | 267 | 1.35 | -0.57 | 1.54 | -0.57 | 3.95 |
| 222 | 1/28/66 12:00 | 15.49 | 3 | 719 | 8.1 | 291 | 1.33 | 0.11 | 1.22 | -1.19 | 3.81 |
| 223 | 9/30/01 21:00 | 15.48 | 9 | 2156 | 10.5 | 70 | 1.23 | 2.21 | 2.68 | 0.73 | 4.63 |

| Storm | Date | $H_{m0}$ (ft) | Storm Duration (hrs) | Power Index (ft²*hr) | $T_p$ (sec) | Dir (Az. deg) | Surge (ft) | Water Level (ft, MSL) | | | |
|---|---|---|---|---|---|---|---|---|---|---|---|
| | | | | | | | | synoptic | avg | min | max |
| 224 | 1/10/64 0:00 | 15.40 | 3 | 711 | 8.9 | 135 | 1.56 | 1.61 | 1.52 | -1.69 | 3.61 |
| 225 | 3/13/68 12:00 | 15.39 | 3 | 711 | 9.7 | 185 | 1.17 | 0.77 | 1.22 | -1.79 | 4.33 |

Figure C5. Time-series of offshore GROW wave height and wave period.

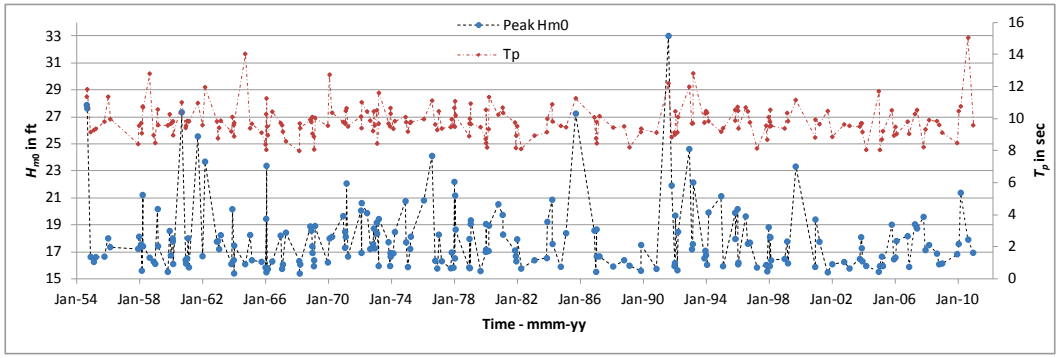


Figure C6. Time series of offshore GROW wave power and storm duration.

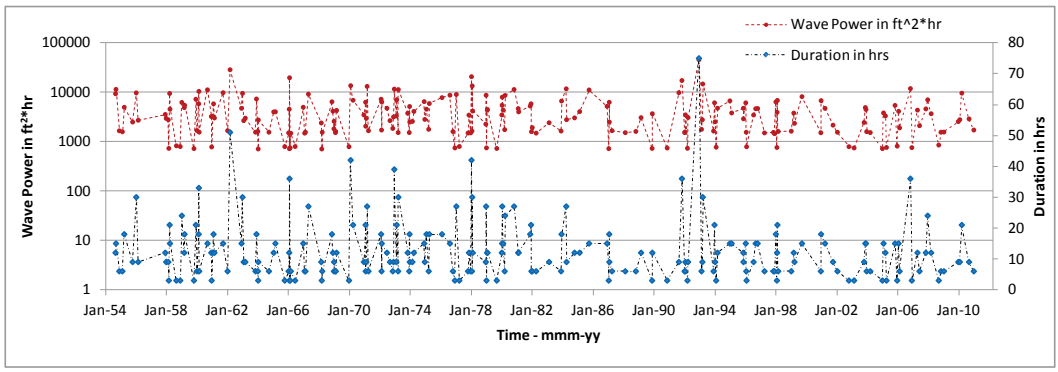


Events in the NOAA HURDAT, HURricane DATabases, combined with the Dredging Research Program surge database (Scheffner et al. 1994) for the node closest to Point Judith are listed in Table C2. If Newport-measured peak water levels were available, they are also listed. Upon reviewing these modeled results, it was concluded that the historical events represented in Table C1 were statistically inclusive of the pre-1954 hurricanes listed in Table C2, so there was no need to add these early storms.

Table C2. HURDAT database of hurricanes near Point Judith Harbor of Refuge.

| Peak Date | Storm | Time of Peak Surge | Modeled Peak Surge (ft) | Peak Surge from Newport Gage (ft) |
|---|---|---|---|---|
| 15-Sep-1904 | NOT_NAMED | 11:20 | 4.3 | N/A |
| 17-Sep-1936 | NOT_NAMED | 15:20 | 3.3 | 1.0 |
| 15-Sep-1938 | NOT_NAMED | 13:45 | 7.1 | N/A |
| 14-Sep-1944 | NOT_NAMED | 22:10 | 5.9 | 7.2 |
| 31-Aug-1954 | CAROL | 2:45 | 4.7 | 7.9 |
| 11-Sep-1954 | EDNA | 12:20 | 3.0 | N/A |
| 7-Sep-1960 | DONNA | 11:10 | 5.9 | 4.4 |
| 22-Sep-1985 | GLORIA | 14:00 | 5.4 | 4.4 |
| 19-Aug-1991 | BOB | 17:20 | 7.0 | 5.1 |
| 8-Oct-1996 | JOSEPHINE | 12:05 | 2.9 | 1.7 |
| 15-Sep-1999 | FLOYD | 5:10 | 2.1 | 2.4 |

## C.5 Marginal distributions of offshore waves and measured water level parameters

Extremal analysis of the wave hindcast and water level data was performed by fitting probabilistic distributions to parameters associated with storm peaks for storms listed in Table C1. The Generalized Pareto Distribution (GPD) was found to provide the best fit for most parameters. StormSim was used to fit GPDs to wave height, peak wave period, power index, surge, and water level data. The normal distribution is used to fit wave direction. Monthly frequency of storms was modeled with a Beta distribution. The GPD equation is given by

$$F(x) = 1 - \left(1 + \frac{k(x-\mu)}{\sigma}\right)^{-1/k} \tag{C1}$$

where $x$ is the random variable and $\mu$, $\sigma$, and $k$ are best-fit coefficients. The PDF and CDF of the normal distribution are, respectively,

$$f(x) = \frac{1}{\sigma\sqrt{2\pi}} \cdot \exp\left[-\frac{1}{2}\left(\frac{(x-\mu)^2}{\sigma^2}\right)\right] \tag{C2}$$

$$F(x) = \left[1 + erf\left(\frac{x-\mu}{\sqrt{2\sigma^2}}\right)\right] \tag{C3}$$

The Beta distribution is given by

$$F(x) = \frac{\int_0^x t^{\alpha-1}(1-t)^{\beta-1}\,dt}{\int_0^1 t^{\alpha-1}(1-t)^{\beta-1}\,dt} \tag{C4}$$

The best-fit distributions are shown in Figures C7 through C13. The best-fit coefficients are shown on each figure. Figure C7 shows the wave height ($H_{m0}$) empirical distribution with the best-fit GPD. The last point near 33 ft is located at a return period of 57 yr because this is the record length. It is likely that this is a lower probability event than is reflected by its plotting position. Melby et al. (2012) discuss the impact of record length and show that for extratropical storms, extreme values determined from the parametric GPD are more reliable than the empirical distribution values. Figure C8 shows wave height predictions from different probability distributions, including GPD, generalized extreme value (GEV), Weibull, Lognormal, and Gumbel, for comparison purposes. For this study, it was found that the predictions made by the Weibull, Lognormal, and Gumbel distributions were similar but underestimated $H_{m0}$. Conversely, the GEV distribution overestimated the extreme values.

Figure C7. Offshore wave height best-fit GPD with POT data.

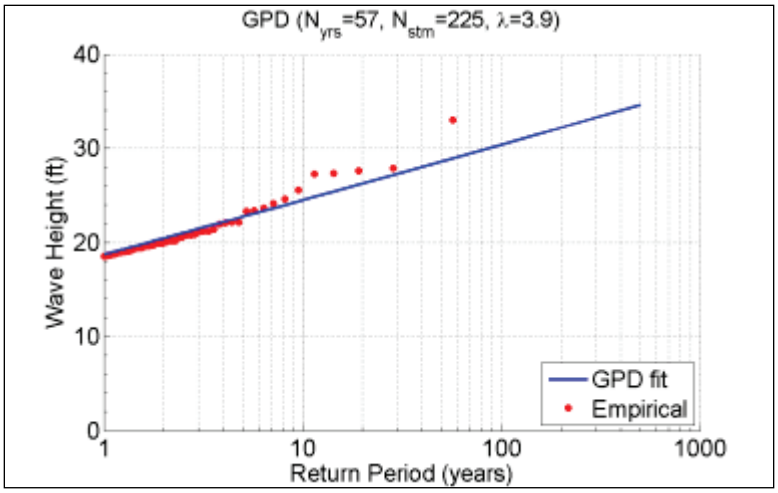

Figure C8. Comparison of wave heights predictions from different probability distributions.

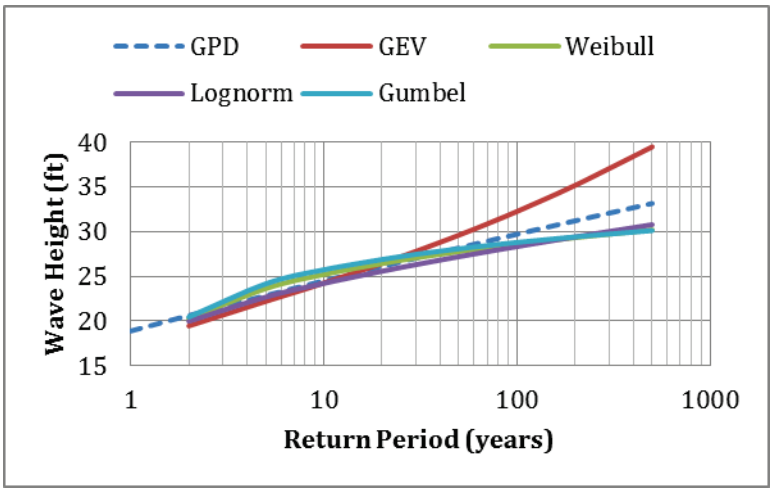


Figure C9. Offshore wave peak period best-fit GPD with POT data.

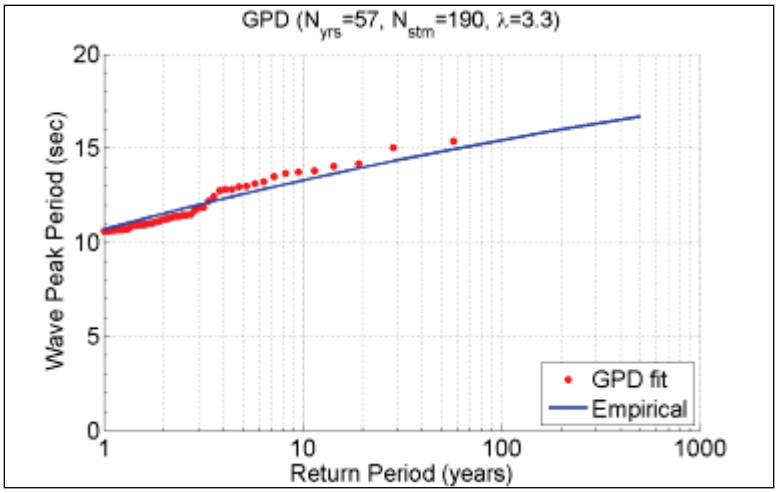


Figure C10. Offshore storm duration best-fit GPD with POT data.

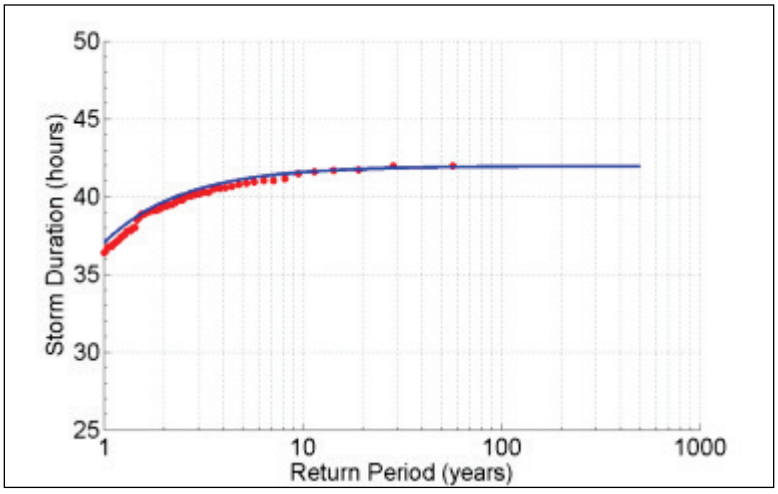

Figure C11. Storm surge best-fit GPD with POT data.

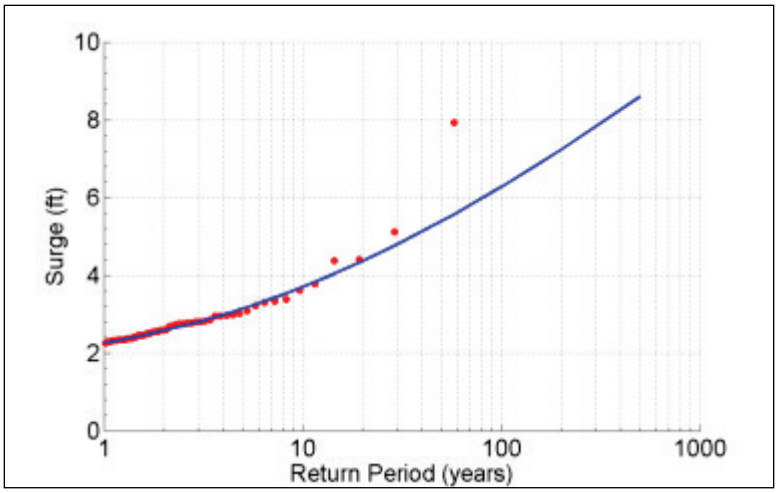


Figure C12. Mean total water level best-fit GPD with POT data.

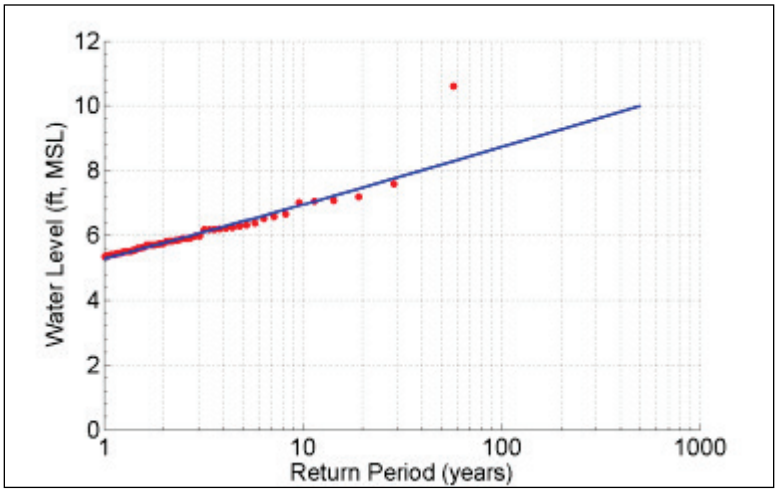


Figure C13. Monthly frequency of storms best-fit Beta distribution with POT data.

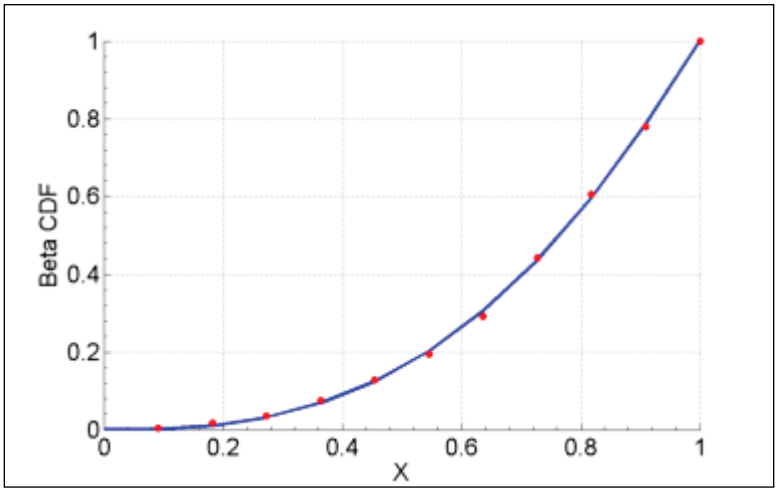

## C.6 Joint probability distributions of offshore waves and measured water level parameters

### C.6.1 Bivariate normal distribution

Joint probability distributions were used to model the dependence between storms parameters and to compute the return periods for all conditions evaluated as part of this study. This required computing correlations between the various wave and water level parameters. The Bivariate Normal distribution (BVN) was used to provide a fitted surface to the joint probability analysis relations between the parameters. The BVN probability density function is given as

$$f(x,y) = \frac{1}{2\pi\sigma_x\sigma_y\sqrt{1-\rho^2}} \cdot \exp\left[-\frac{1}{2(1-\rho^2)}\left(\frac{(x-\mu_x)^2}{\sigma_x^2} - \frac{2\rho(x-\mu_x)(y-\mu_y)}{\sigma_x\sigma_y} + \frac{(y-\mu_y)^2}{\sigma_y^2}\right)\right] \quad \text{(C.5)}$$

where $\mu_x$ and $\mu_y$ = marginal means, $\sigma_x$ and $\sigma_y$ = marginal variances, and $\rho$ = correlation between $x$ and $y$.

In the case of the BVN, the conditional probability distribution for either $x$ or $y$ is also normally distributed. For example, the conditional probability of $x$, given a known value of $y$, can be computed using Equation C5. The conditional mean and variance of $x$ are given by

$$\mu_{x/y} = \mu_x + \rho\,\mu_x \frac{(y-\mu_y)}{\sigma_y} \quad \text{(C.6)}$$

$$\sigma_{x/y} = \sigma_x\sqrt{1-\rho^2} \quad \text{(C.7)}$$

For the computation of return period conditions, $H_{m0}$ is determined from its marginal distribution. Secondary parameters (e.g., peak wave period, wave direction, surge, water level) are determined from the BVN conditional distribution given a known value of $H_{m0}$.

### C.6.2 Gaussian Copula Model

The GCM is used as part of the MCS to generate the synthetic extratropical storms while maintaining the correlations between simulated storm parameters. In other words, the GCM is capable of describing the marginal distribution of each parameter and the dependence structure among all parameters. The bivariate GCM can expressed as

$$C_\rho(x,y) = \Phi_\rho\left(\Phi^{-1}(x), \Phi^{-1}(y)\right) \quad \text{(C.8)}$$

where $\rho$ = correlation matrix between $x$ and y, $\Phi$ = joint cumulative distribution function of the bivariate normal distribution, and $\Phi^{-1}$ = inverse cumulative distribution function of the standard normal distribution.

## C.7 Wave transformation to nearshore

As described in Appendix B, CMS-Wave was used to transform waves to nearshore. Historical wave conditions were transformed. In addition, a matrix of transformation coefficients was generated by running thousands of CMS-Wave runs covering a more extensive and more finely discretized parameter space than is represented by the historical conditions. This matrix of transformation coefficients was used to transform synthetic storm events that included SLR or that were generated using the MCS. A Matlab script for interpolating within this table was developed and used to transform all synthetic-storm wave conditions to nearshore.

## C.8 Waves and water levels for project design

The joint probabilistic model was used to develop design alternatives for the breakwater. Table C3 lists the CMS-Wave stations and associated datum depths that are opposite the 500 ft reaches shown in Figure 3. The wave and water level conditions associated with the various return periods for the CMS-Wave Stations along the seaward side of the Main breakwater are listed in Appendix D. For the conditions listed, the wave height was chosen from the wave height marginal distribution, then the other parameters were selected as mean values associated with each return period from the bivariate normal distribution. Water level was selected slightly differently. For water level, three different values corresponding to varied quartiles were selected: $\mu$, $\mu+\sigma$, and $\mu+2\sigma$, where $\mu$ is the mean and $\sigma$ is the standard deviation. In this way, the sensitivity of the design to varied water levels could be ascertained.

Table C3. CMS-Wave stations associated with specific breakwater reaches and datum depths.

| Breakwater Reach Stationing | CMS-Wave Station | Station Datum Depth, ft, MSL |
|---|---|---|
| 0+00 – 5+00 | 35 | 22.9 |
| 5+00 – 10+00 | 35 | 22.9 |
| 10+00 – 15+00 | 36 | 21.2 |
| 15+00 – 20+00 | 37 | 22.9 |
| 20+00 – 25+00 | 38 | 22.2 |
| 25+00 – 30+00 | 39 | 20.6 |
| 30+00 – 35+00 | 40 | 27.7 |
| 35+00 – 40+00 | 41 | 30.6 |
| 40+00 – 45+00 | 41 | 30.6 |
| 45+00 – 50+00 | 42 | 31.2 |
| 50+00 – 55+00 | 43 | 31.6 |
| 55+00 – 60+00 | 44 | 32.6 |
| 60+00 – 67+00 | 45 | 32.9 |

## C.9 Wave diffraction

Waves commonly diffract through inlets and around ends of breakwaters to enter protected areas in the lee of breakwaters. Waves also overtop structures and pass through breaches in structures. These waves can be thought of as diffracting into the lee if the wave crests overtop sporadically in space and time. This is most often the case. The transmitted wave height in the sheltered area is typically the primary design parameter for determining the breakwater crest height, and so it is the critical criterion for assessing the functional performance of the structure. Thus, one of the most important tasks in the life-cycle analysis is computation of the diffracted wave energy in the lee of the structure.

As discussed in Appendix B, the most severe 20 storms in Table C1 were modeled using a high-fidelity Boussinesq model. The model included overtopping of the breakwater using the present breakwater condition. The model output wave conditions on the CMS-Wave grid.

Wave diffraction is expressed in terms of a wave diffraction coefficient, $K_{d,}$ where

$$K_d = \frac{H_d}{H_i} \tag{C.9}$$

and

$H_d$ = diffracted $H_{m0}$ at a point in lee of breakwater
$H_i$ = incident $H_{m0}$ just seaward of inlet or just leeward of breakwater.

StormSim contains a generalized surrogate diffraction tool constructed from thousands of high-fidelity hydrodynamic model results on an idealized bay with flat bottom and assuming infinitely thin vertical breakwaters. An example of a diffraction nomograph created from this table is shown in Figure C14 for the case of waves transmitted through a gap of width $B$. The $K_d$ contours are given as a function of normalized distance along structure ($x$) and leeward of structure ($y$). The StormSim surrogate diffraction model was used to compute transmitted waves at CMS-Wave save stations. The results of the table lookup were compared to the Boussinesq results for the 20 most severe storms. Over the save stations that were away from shore, the average difference was approximately 10%. Nearshore, the difference was larger because of reflection, wave breaking and complex nearshore currents that are modeled in the Boussinesq model but are not present in the surrogate model. Comparing to wave transmission computed using the CMS-Wave model, the average difference over all save points was 6%. The CMS-Wave model approximates diffraction by smoothing the wave energy. Because this model does not include all of the nearshore wave reflection and complex wave phenomenon, it may be a better metric for validating the surrogate model. Given the relatively low error of the surrogate model, it was decided this low-fidelity model was reasonably accurate for determining wave transmission into the sheltered area for all historical and MCS storms.

Figure C14. Diffraction coefficients with axes normalized by gap width.

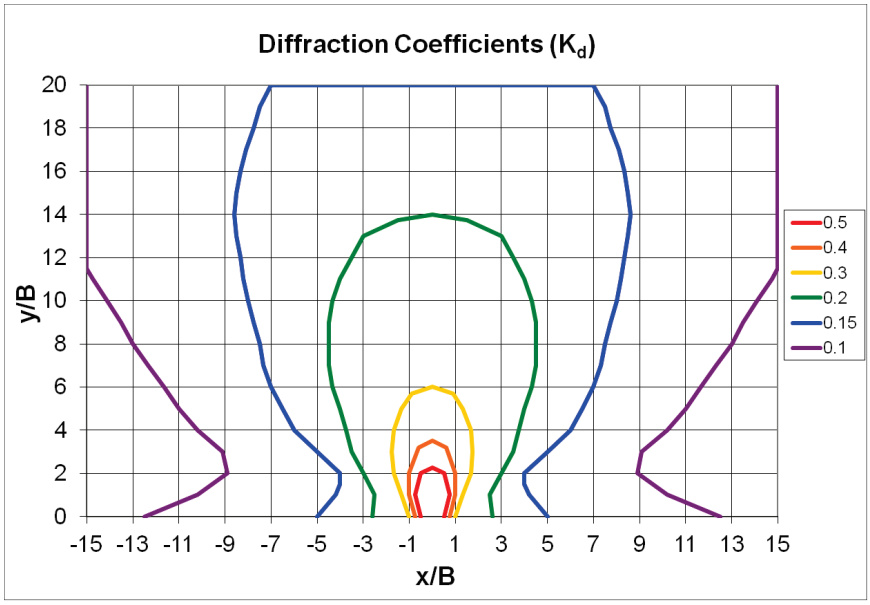

# Appendix D: Return Period Wave Conditions for Near-Breakwater CMS-Wave Stations[1]

Table D1. Extremal joint probability analysis results for CMS-Wave output Station 26.

| Return Period | Hm0 | Storm Duration | Power Index | Tp | Dir | Surge at Storm Peak | Water Level |
|---|---|---|---|---|---|---|---|
| (years) | (ft) | (hrs) | (ft2*hr) | (sec) | (Az. deg.) | (ft) | (ft, MSL) |
| 5 | 7.0 | 33.9 | 1649 | 10.4 | 210 | 4.5 | 7.7 |
| 10 | 7.3 | 34.4 | 1847 | 10.7 | 211 | 4.8 | 7.9 |
| 25 | 7.7 | 34.9 | 2088 | 11.0 | 213 | 5.2 | 8.2 |
| 50 | 8.0 | 35.3 | 2253 | 11.2 | 214 | 5.5 | 8.3 |
| 75 | 8.1 | 35.5 | 2344 | 11.3 | 215 | 5.6 | 8.4 |
| 100 | 8.2 | 35.6 | 2405 | 11.4 | 215 | 5.7 | 8.5 |
| 200 | 8.4 | 35.9 | 2544 | 11.6 | 216 | 6.0 | 8.6 |
| 500 | 8.6 | 36.2 | 2708 | 11.8 | 217 | 6.3 | 8.8 |

Figure D1. Wave height $H_{m0}$ marginal empirical distribution and best-fit GPD for CMS-Wave station 26.

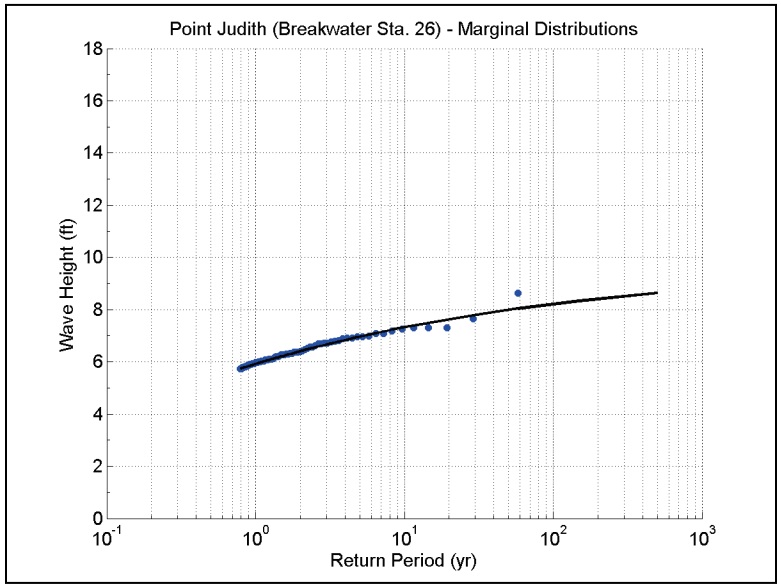


[1] Authored by Jeffrey Melby and Norberto Nadal-Caraballo

Figure D2. Wave period $T_p$ marginal empirical distribution and best-fit GPD for CMS-Wave station 26.

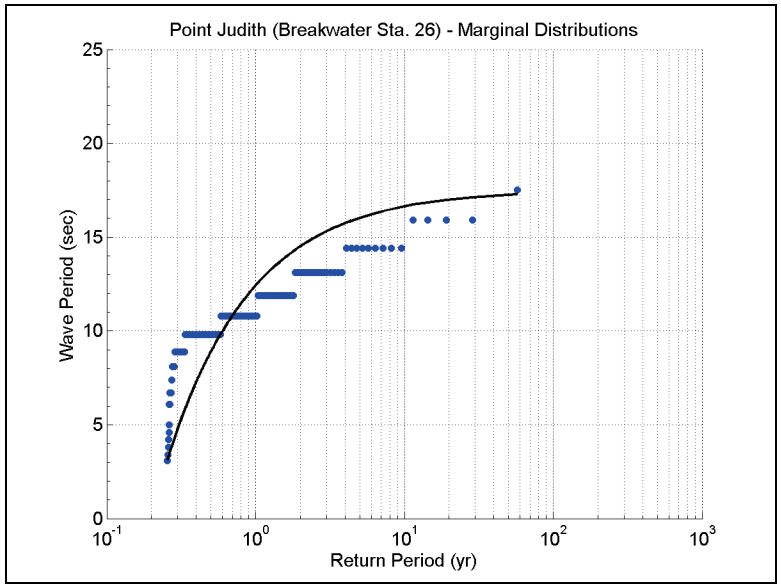


Figure D3. Wave direction marginal empirical distribution and best-fit normal distribution for CMS-Wave station 26.

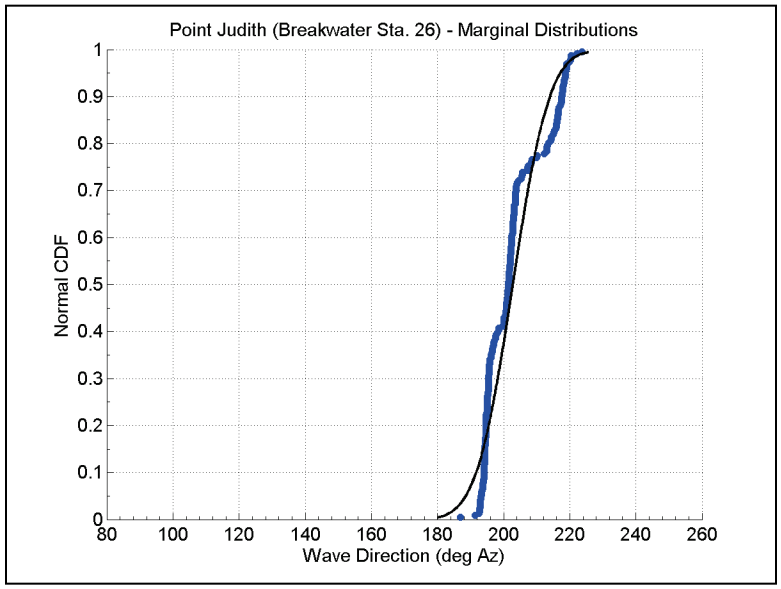

Table D2. Extremal joint probability analysis results for CMS-Wave output Station 27.

| Return Period | Hm0 | Storm Duration | Power Index | Tp | Dir | Surge at Storm Peak | Water Level |
|---|---|---|---|---|---|---|---|
| (years) | (ft) | (hrs) | (ft2*hr) | (sec) | (Az. deg.) | (ft) | (ft, MSL) |
| 5 | 8.0 | 34.0 | 2181 | 8.4 | 210 | 4.4 | 7.6 |
| 10 | 8.3 | 34.5 | 2384 | 8.3 | 212 | 4.7 | 7.8 |
| 25 | 8.6 | 35.0 | 2575 | 8.2 | 215 | 5.0 | 8.0 |
| 50 | 8.7 | 35.4 | 2676 | 8.1 | 216 | 5.2 | 8.1 |
| 75 | 8.8 | 35.5 | 2724 | 8.1 | 217 | 5.3 | 8.1 |
| 100 | 8.8 | 35.7 | 2753 | 8.1 | 217 | 5.4 | 8.2 |
| 200 | 8.8 | 36.0 | 2811 | 8.0 | 219 | 5.6 | 8.2 |
| 500 | 8.9 | 36.3 | 2869 | 7.9 | 220 | 5.8 | 8.3 |

Table D3. Extremal joint probability analysis results for CMS-Wave output Station 28.

| Return Period | Hm0 | Storm Duration | Power Index | Tp | Dir | Surge at Storm Peak | Water Level |
|---|---|---|---|---|---|---|---|
| (years) | (ft) | (hrs) | (ft2*hr) | (sec) | (Az. deg.) | (ft) | (ft, MSL) |
| 5 | 8.6 | 34.2 | 2546 | 6.3 | 219 | 3.9 | 7.0 |
| 10 | 9.0 | 34.7 | 2798 | 5.9 | 221 | 3.9 | 7.0 |
| 25 | 9.2 | 35.2 | 3009 | 5.5 | 225 | 3.9 | 6.8 |
| 50 | 9.3 | 35.6 | 3111 | 5.2 | 227 | 3.9 | 6.7 |
| 75 | 9.4 | 35.8 | 3156 | 5.1 | 228 | 3.9 | 6.7 |
| 100 | 9.4 | 36.0 | 3183 | 5.0 | 229 | 3.9 | 6.6 |
| 200 | 9.4 | 36.3 | 3236 | 4.8 | 231 | 3.9 | 6.5 |
| 500 | 9.5 | 36.6 | 3288 | 4.5 | 233 | 3.9 | 6.4 |

Table D4. Extremal joint probability analysis results for CMS-Wave output Station 29.

| Return Period | Hm0 | Storm Duration | Power Index | Tp | Dir | Surge at Storm Peak | Water Level |
|---|---|---|---|---|---|---|---|
| (years) | (ft) | (hrs) | (ft2*hr) | (sec) | (Az. deg.) | (ft) | (ft, MSL) |
| 5 | 8.7 | 34.3 | 2585 | 6.7 | 221 | 3.9 | 7.0 |
| 10 | 9.1 | 34.8 | 2876 | 6.3 | 224 | 3.9 | 7.0 |
| 25 | 9.4 | 35.4 | 3144 | 5.9 | 227 | 3.9 | 6.9 |
| 50 | 9.6 | 35.7 | 3284 | 5.6 | 230 | 3.9 | 6.8 |
| 75 | 9.7 | 35.9 | 3348 | 5.5 | 231 | 3.9 | 6.7 |
| 100 | 9.7 | 36.1 | 3387 | 5.4 | 232 | 3.9 | 6.7 |
| 200 | 9.8 | 36.4 | 3465 | 5.2 | 234 | 3.9 | 6.6 |
| 500 | 9.8 | 36.8 | 3541 | 4.9 | 236 | 3.9 | 6.5 |

Table D5. Extremal joint probability analysis results for CMS-Wave output Station 30.

| Return Period | $H_{m0}$ | Storm Duration | Power Index | $T_p$ | Dir | Surge at Storm Peak | Water Level |
|---|---|---|---|---|---|---|---|
| (years) | (ft) | (hrs) | (ft²*hr) | (sec) | (Az. deg.) | (ft) | (ft, MSL) |
| 5 | 8.8 | 34.5 | 2656 | 7.0 | 221 | 3.9 | 7.1 |
| 10 | 9.2 | 35.0 | 2991 | 6.7 | 224 | 4.0 | 7.1 |
| 25 | 9.6 | 35.6 | 3319 | 6.4 | 227 | 4.0 | 7.0 |
| 50 | 9.9 | 36.0 | 3500 | 6.1 | 229 | 4.0 | 6.9 |
| 75 | 9.9 | 36.3 | 3586 | 6.0 | 231 | 4.1 | 6.9 |
| 100 | 10.0 | 36.4 | 3639 | 5.9 | 231 | 4.1 | 6.8 |
| 200 | 10.1 | 36.7 | 3747 | 5.7 | 233 | 4.1 | 6.7 |
| 500 | 10.2 | 37.1 | 3854 | 5.5 | 236 | 4.1 | 6.6 |

Table D6. Extremal joint probability analysis results for CMS-Wave output Station 31.

| Return Period | $H_{m0}$ | Storm Duration | Power Index | $T_p$ | Dir | Surge at Storm Peak | Water Level |
|---|---|---|---|---|---|---|---|
| (years) | (ft) | (hrs) | (ft²*hr) | (sec) | (Az. deg.) | (ft) | (ft, MSL) |
| 5 | 8.8 | 34.5 | 2665 | 7.0 | 216 | 4.0 | 7.2 |
| 10 | 9.2 | 35.0 | 2975 | 6.6 | 219 | 4.1 | 7.2 |
| 25 | 9.6 | 35.6 | 3275 | 6.3 | 222 | 4.2 | 7.2 |
| 50 | 9.8 | 36.0 | 3439 | 6.1 | 224 | 4.2 | 7.1 |
| 75 | 9.8 | 36.3 | 3517 | 6.0 | 225 | 4.2 | 7.1 |
| 100 | 9.9 | 36.4 | 3565 | 5.9 | 226 | 4.3 | 7.0 |
| 200 | 10.0 | 36.7 | 3661 | 5.7 | 228 | 4.3 | 7.0 |
| 500 | 10.1 | 37.1 | 3757 | 5.5 | 230 | 4.4 | 6.9 |

Table D7. Extremal joint probability analysis results for CMS-Wave output Station 32.

| Return Period | $H_{m0}$ | Storm Duration | Power Index | $T_p$ | Dir | Surge at Storm Peak | Water Level |
|---|---|---|---|---|---|---|---|
| (years) | (ft) | (hrs) | (ft²*hr) | (sec) | (Az. deg.) | (ft) | (ft, MSL) |
| 5 | 8.8 | 34.5 | 2670 | 7.6 | 218 | 4.1 | 7.3 |
| 10 | 9.3 | 35.0 | 3020 | 7.4 | 221 | 4.2 | 7.3 |
| 25 | 9.8 | 35.6 | 3388 | 7.2 | 224 | 4.3 | 7.3 |
| 50 | 10.0 | 36.0 | 3608 | 7.0 | 226 | 4.4 | 7.3 |
| 75 | 10.1 | 36.2 | 3716 | 6.9 | 227 | 4.5 | 7.3 |
| 100 | 10.2 | 36.4 | 3785 | 6.8 | 228 | 4.5 | 7.3 |
| 200 | 10.3 | 36.7 | 3929 | 6.7 | 230 | 4.6 | 7.2 |
| 500 | 10.5 | 37.1 | 4078 | 6.5 | 232 | 4.6 | 7.2 |

Table D8. Extremal joint probability analysis results for CMS-Wave output Station 33.

| Return Period | Hm0 | Storm Duration | Power Index | Tp | Dir | Surge at Storm Peak | Water Level |
|---|---|---|---|---|---|---|---|
| (years) | (ft) | (hrs) | (ft2*hr) | (sec) | (Az. deg.) | (ft) | (ft, MSL) |
| 5 | 8.8 | 34.6 | 2662 | 8.4 | 222 | 3.9 | 7.1 |
| 10 | 9.3 | 35.1 | 3066 | 8.3 | 225 | 4.0 | 7.1 |
| 25 | 9.9 | 35.7 | 3535 | 8.2 | 229 | 4.0 | 7.0 |
| 50 | 10.3 | 36.2 | 3841 | 8.1 | 231 | 4.0 | 6.9 |
| 75 | 10.5 | 36.4 | 4001 | 8.1 | 232 | 4.0 | 6.9 |
| 100 | 10.6 | 36.5 | 4108 | 8.0 | 233 | 4.1 | 6.8 |
| 200 | 10.9 | 36.8 | 4340 | 8.0 | 235 | 4.1 | 6.7 |
| 500 | 11.1 | 37.2 | 4600 | 7.9 | 237 | 4.1 | 6.6 |

Figure D4. Wave height $H_{m0}$ marginal empirical distribution and best-fit GPD for CMS-Wave station 33.

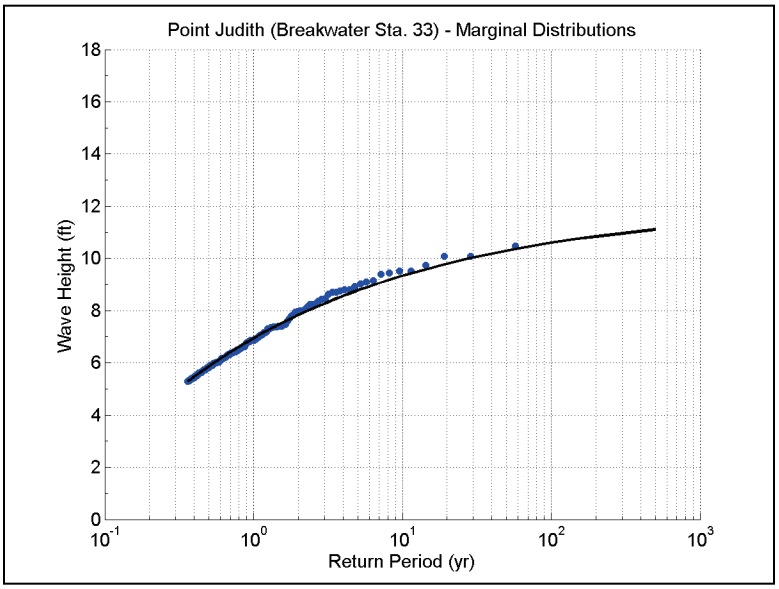

Figure D5. Wave period $T_p$ marginal empirical distribution and best-fit GPD for CMS-Wave station 33.

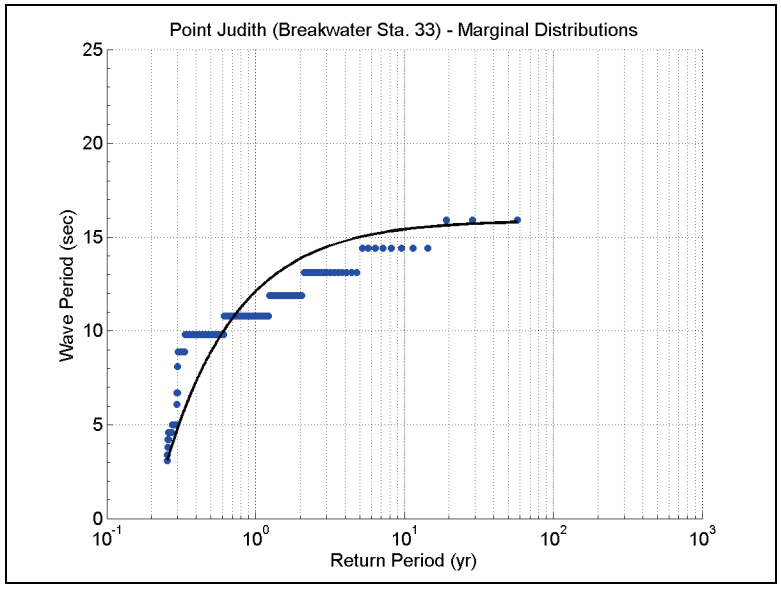


Figure D6. Wave direction marginal empirical distribution and best-fit normal distribution for CMS-Wave station 33.

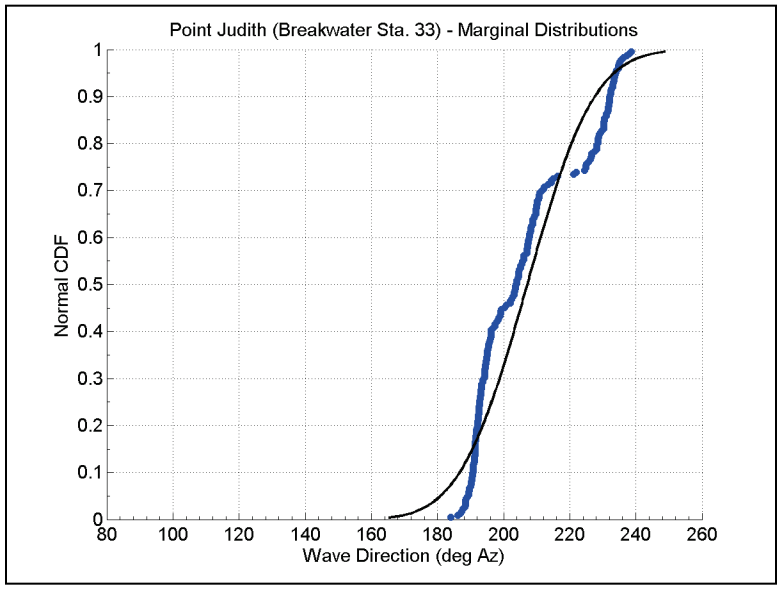

Table D9. Extremal joint probability analysis results for CMS-Wave output Station 34.

| Return Period | Hm0 | Storm Duration | Power Index | Tp | Dir | Surge at Storm Peak | Water Level |
|---|---|---|---|---|---|---|---|
| (years) | (ft) | (hrs) | (ft2*hr) | (sec) | (Az. deg.) | (ft) | (ft, MSL) |
| 5 | 9.3 | 34.7 | 3003 | 7.9 | 223 | 3.9 | 7.1 |
| 10 | 9.8 | 35.3 | 3403 | 7.7 | 226 | 3.9 | 7.0 |
| 25 | 10.3 | 35.9 | 3821 | 7.5 | 229 | 3.9 | 6.9 |
| 50 | 10.6 | 36.4 | 4068 | 7.4 | 232 | 4.0 | 6.8 |
| 75 | 10.7 | 36.6 | 4189 | 7.3 | 233 | 4.0 | 6.8 |
| 100 | 10.8 | 36.7 | 4266 | 7.3 | 234 | 4.0 | 6.7 |
| 200 | 10.9 | 37.1 | 4425 | 7.1 | 236 | 4.0 | 6.6 |
| 500 | 11.1 | 37.5 | 4589 | 7.0 | 239 | 4.0 | 6.5 |

Table D10. Extremal joint probability analysis results for CMS-Wave output Station 35.

| Return Period | Hm0 | Storm Duration | Power Index | Tp | Dir | Surge at Storm Peak | Water Level |
|---|---|---|---|---|---|---|---|
| (years) | (ft) | (hrs) | (ft2*hr) | (sec) | (Az. deg.) | (ft) | (ft, MSL) |
| 5 | 9.5 | 34.7 | 3123 | 8.1 | 219 | 3.9 | 7.1 |
| 10 | 10.0 | 35.3 | 3531 | 7.9 | 221 | 3.9 | 7.0 |
| 25 | 10.5 | 36.0 | 3954 | 7.7 | 225 | 4.0 | 6.9 |
| 50 | 10.7 | 36.4 | 4202 | 7.6 | 227 | 4.0 | 6.9 |
| 75 | 10.9 | 36.6 | 4324 | 7.6 | 228 | 4.0 | 6.8 |
| 100 | 10.9 | 36.8 | 4401 | 7.5 | 229 | 4.0 | 6.8 |
| 200 | 11.1 | 37.1 | 4560 | 7.4 | 231 | 4.0 | 6.7 |
| 500 | 11.2 | 37.5 | 4723 | 7.3 | 233 | 4.0 | 6.5 |

Table D11. Extremal joint probability analysis results for CMS-Wave output Station 36.

| Return Period | $H_{m0}$ | Storm Duration | Power Index | $T_p$ | Dir | Surge at Storm Peak | Water Level |
|---|---|---|---|---|---|---|---|
| (years) | (ft) | (hrs) | ($ft^2$*hr) | (sec) | (Az. deg.) | (ft) | (ft, MSL) |
| 5 | 9.7 | 34.6 | 3260 | 8.6 | 216 | 4.3 | 7.5 |
| 10 | 10.2 | 35.2 | 3639 | 8.6 | 218 | 4.5 | 7.6 |
| 25 | 10.6 | 35.8 | 4042 | 8.5 | 221 | 4.8 | 7.7 |
| 50 | 10.9 | 36.2 | 4284 | 8.4 | 223 | 4.9 | 7.8 |
| 75 | 11.0 | 36.4 | 4404 | 8.4 | 224 | 5.0 | 7.8 |
| 100 | 11.1 | 36.6 | 4482 | 8.4 | 225 | 5.1 | 7.9 |
| 200 | 11.2 | 36.9 | 4644 | 8.3 | 226 | 5.2 | 7.9 |
| 500 | 11.4 | 37.3 | 4814 | 8.3 | 228 | 5.4 | 7.9 |

Table D12. Extremal joint probability analysis results for CMS-Wave output Station 37.

| Return Period | Hm0 | Storm Duration | Power Index | Tp | Dir | Surge at Storm Peak | Water Level |
|---|---|---|---|---|---|---|---|
| (years) | (ft) | (hrs) | (ft2*hr) | (sec) | (Az. deg.) | (ft) | (ft, MSL) |
| 5 | 10.1 | 34.3 | 3481 | 10.7 | 203 | 4.5 | 7.6 |
| 10 | 10.6 | 34.8 | 3890 | 11.1 | 205 | 4.8 | 7.9 |
| 25 | 11.1 | 35.4 | 4348 | 11.5 | 206 | 5.2 | 8.2 |
| 50 | 11.4 | 35.8 | 4638 | 11.7 | 207 | 5.4 | 8.3 |
| 75 | 11.5 | 36.0 | 4788 | 11.9 | 208 | 5.6 | 8.4 |
| 100 | 11.6 | 36.1 | 4886 | 12.0 | 208 | 5.7 | 8.5 |
| 200 | 11.8 | 36.5 | 5097 | 12.2 | 209 | 5.9 | 8.6 |
| 500 | 12.0 | 36.8 | 5328 | 12.5 | 210 | 6.2 | 8.7 |

Table D13. Extremal joint probability analysis results for CMS-Wave output Station 38.

| Return Period | Hm0 | Storm Duration | Power Index | Tp | Dir | Surge at Storm Peak | Water Level |
|---|---|---|---|---|---|---|---|
| (years) | (ft) | (hrs) | (ft2*hr) | (sec) | (Az. deg.) | (ft) | (ft, MSL) |
| 5 | 11.5 | 33.4 | 4446 | 12.9 | 180 | 4.5 | 7.7 |
| 10 | 12.1 | 33.8 | 4946 | 13.6 | 179 | 5.0 | 8.1 |
| 25 | 12.7 | 34.2 | 5551 | 14.2 | 178 | 5.6 | 8.6 |
| 50 | 13.1 | 34.5 | 5965 | 14.6 | 178 | 6.1 | 9.0 |
| 75 | 13.4 | 34.7 | 6191 | 14.9 | 177 | 6.3 | 9.2 |
| 100 | 13.5 | 34.8 | 6344 | 15.0 | 177 | 6.5 | 9.3 |
| 200 | 13.8 | 35.0 | 6689 | 15.3 | 176 | 6.9 | 9.6 |
| 500 | 14.2 | 35.3 | 7096 | 15.7 | 175 | 7.5 | 10.0 |

Table D14. Extremal joint probability analysis results for CMS-Wave output Station 39.

| Return Period | Hm0 | Storm Duration | Power Index | Tp | Dir | Surge At Storm Peak | Water Level |
|---|---|---|---|---|---|---|---|
| (years) | (ft) | (hrs) | (ft2*hr) | (sec) | (Az. deg.) | (ft) | (ft, MSL) |
| 5 | 13.0 | 33.3 | 5640 | 12.5 | 154 | 4.6 | 7.7 |
| 10 | 13.6 | 33.6 | 6240 | 13.0 | 151 | 5.0 | 8.1 |
| 25 | 14.2 | 34.0 | 6895 | 13.7 | 148 | 5.5 | 8.5 |
| 50 | 14.6 | 34.3 | 7300 | 14.1 | 146 | 5.9 | 8.8 |
| 75 | 14.8 | 34.4 | 7505 | 14.3 | 145 | 6.1 | 8.9 |
| 100 | 14.9 | 34.5 | 7639 | 14.4 | 144 | 6.2 | 9.0 |
| 200 | 15.1 | 34.7 | 7922 | 14.8 | 142 | 6.6 | 9.3 |
| 500 | 15.3 | 35.0 | 8226 | 15.1 | 140 | 7.0 | 9.5 |

Table D15. Extremal joint probability analysis results for CMS-Wave output Station 40.

| Return Period | Hm0 | Storm Duration | Power Index | Tp | Dir | Surge at Storm Peak | Water Level |
|---|---|---|---|---|---|---|---|
| (years) | (ft) | (hrs) | (ft2*hr) | (sec) | (Az. deg.) | (ft) | (ft, MSL) |
| 5 | 14.0 | 33.0 | 6518 | 12.0 | 136 | 4.5 | 7.6 |
| 10 | 14.6 | 33.3 | 7150 | 12.4 | 132 | 4.7 | 7.8 |
| 25 | 15.2 | 33.7 | 7745 | 12.9 | 128 | 5.1 | 8.0 |
| 50 | 15.4 | 33.9 | 8063 | 13.2 | 125 | 5.3 | 8.2 |
| 75 | 15.5 | 34.0 | 8210 | 13.3 | 124 | 5.4 | 8.2 |
| 100 | 15.6 | 34.1 | 8300 | 13.4 | 123 | 5.5 | 8.3 |
| 200 | 15.7 | 34.3 | 8480 | 13.7 | 120 | 5.7 | 8.4 |
| 500 | 15.8 | 34.6 | 8655 | 13.9 | 117 | 6.0 | 8.5 |

Table D16. Extremal joint probability analysis results for CMS-Wave output Station 41.

| Return Period | Hm0 | Storm Duration | Power Index | Tp | Dir | Surge at Storm Peak | Water Level |
|---|---|---|---|---|---|---|---|
| (years) | (ft) | (hrs) | (ft2*hr) | (sec) | (Az. deg.) | (ft) | (ft, MSL) |
| 5 | 14.1 | 32.4 | 6417 | 11.7 | 134 | 4.4 | 7.6 |
| 10 | 14.7 | 32.6 | 6993 | 12.1 | 130 | 4.7 | 7.8 |
| 25 | 15.3 | 32.8 | 7626 | 12.6 | 126 | 5.1 | 8.0 |
| 50 | 15.6 | 32.9 | 8020 | 12.9 | 124 | 5.3 | 8.2 |
| 75 | 15.8 | 33.0 | 8221 | 13.0 | 122 | 5.4 | 8.2 |
| 100 | 15.9 | 33.1 | 8352 | 13.1 | 121 | 5.5 | 8.3 |
| 200 | 16.1 | 33.2 | 8632 | 13.4 | 119 | 5.7 | 8.4 |
| 500 | 16.4 | 33.3 | 8934 | 13.6 | 116 | 6.0 | 8.5 |

Figure D7. Wave height $H_{m0}$ marginal empirical distribution and best-fit GPD for CMS-Wave station 41.

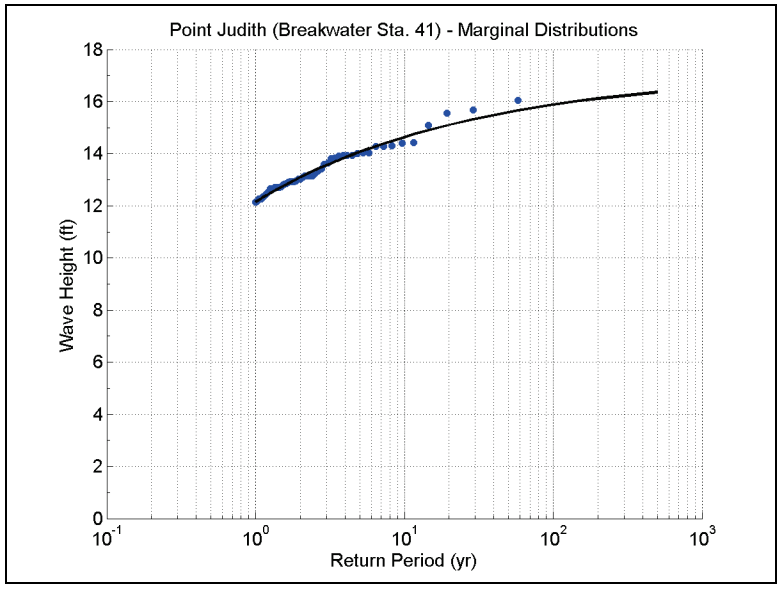


Figure D8. Wave period $T_p$ marginal empirical distribution and best-fit GPD for CMS-Wave station 41.

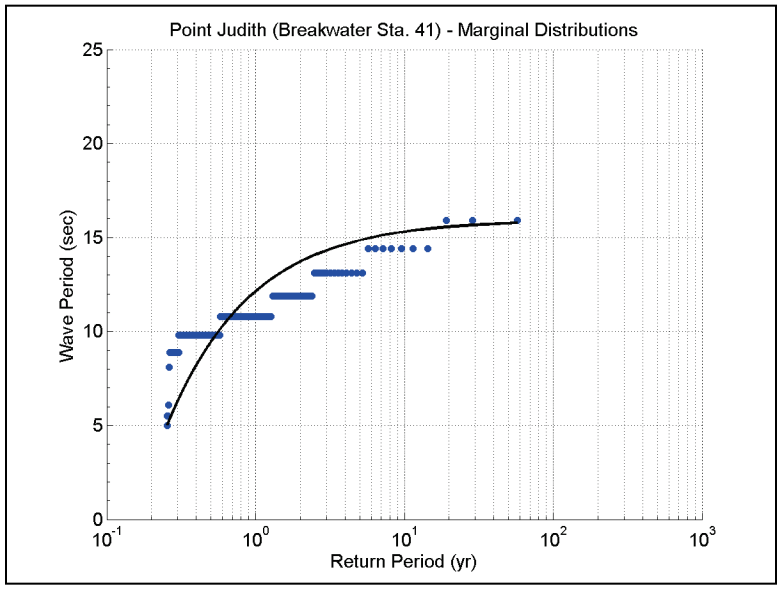

Figure D9. Wave direction marginal empirical distribution and best-fit normal distribution for CMS-Wave station 41.

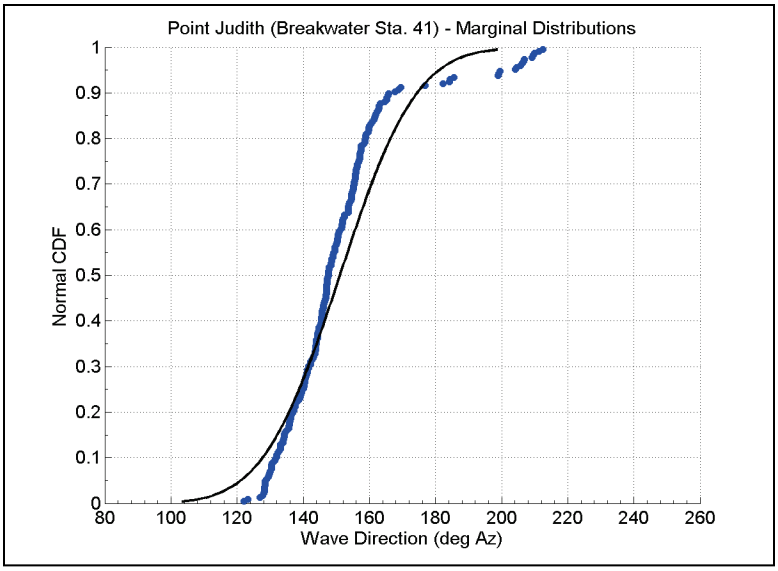


Table D17. Extremal joint probability analysis results for CMS-Wave output Station 42.

| Return Period | Hm0 | Storm Duration | Power Index | Tp | Dir | Surge at Storm Peak | Water Level |
|---|---|---|---|---|---|---|---|
| (years) | (ft) | (hrs) | (ft2*hr) | (sec) | (Az. deg.) | (ft) | (ft, MSL) |
| 5 | 13.8 | 32.3 | 6168 | 11.9 | 134 | 4.5 | 7.6 |
| 10 | 14.4 | 32.5 | 6778 | 12.3 | 131 | 4.7 | 7.8 |
| 25 | 15.1 | 32.7 | 7399 | 12.8 | 128 | 5.1 | 8.0 |
| 50 | 15.4 | 32.8 | 7757 | 13.1 | 125 | 5.3 | 8.2 |
| 75 | 15.5 | 32.9 | 7930 | 13.2 | 124 | 5.4 | 8.2 |
| 100 | 15.6 | 32.9 | 8038 | 13.3 | 123 | 5.5 | 8.3 |
| 200 | 15.8 | 33.0 | 8261 | 13.6 | 121 | 5.7 | 8.4 |
| 500 | 16.0 | 33.2 | 8484 | 13.9 | 118 | 6.0 | 8.5 |

Table D18. Extremal joint probability analysis results for CMS-Wave output Station 43.

| Return Period | Hm0 | Storm Duration | Power Index | Tp | Dir | Surge at Storm Peak | Water Level |
|---|---|---|---|---|---|---|---|
| (years) | (ft) | (hrs) | (ft2*hr) | (sec) | (Az. deg.) | (ft) | (ft, MSL) |
| 5 | 13.5 | 32.2 | 5882 | 12.1 | 136 | 4.5 | 7.6 |
| 10 | 14.2 | 32.3 | 6515 | 12.6 | 133 | 4.7 | 7.8 |
| 25 | 14.9 | 32.5 | 7175 | 13.1 | 129 | 5.1 | 8.0 |
| 50 | 15.2 | 32.6 | 7563 | 13.4 | 127 | 5.3 | 8.2 |
| 75 | 15.4 | 32.6 | 7753 | 13.6 | 126 | 5.4 | 8.2 |
| 100 | 15.5 | 32.7 | 7873 | 13.7 | 125 | 5.5 | 8.3 |
| 200 | 15.7 | 32.8 | 8122 | 14.0 | 123 | 5.7 | 8.4 |
| 500 | 16.0 | 32.9 | 8376 | 14.2 | 121 | 6.0 | 8.5 |

Table D19. Extremal joint probability analysis results for CMS-Wave output Station 44.

| Return Period | Hm0 | Storm Duration | Power Index | Tp | Dir | Surge at Storm Peak | Water Level |
|---|---|---|---|---|---|---|---|
| (years) | (ft) | (hrs) | (ft2*hr) | (sec) | (Az. deg.) | (ft) | (ft, MSL) |
| 5 | 12.8 | 32.1 | 5291 | 11.9 | 140 | 4.5 | 7.6 |
| 10 | 13.5 | 32.2 | 5906 | 12.3 | 137 | 4.8 | 7.9 |
| 25 | 14.2 | 32.4 | 6564 | 12.8 | 135 | 5.1 | 8.1 |
| 50 | 14.6 | 32.5 | 6959 | 13.1 | 133 | 5.3 | 8.2 |
| 75 | 14.8 | 32.5 | 7157 | 13.3 | 132 | 5.5 | 8.3 |
| 100 | 15.0 | 32.6 | 7283 | 13.4 | 131 | 5.6 | 8.4 |
| 200 | 15.2 | 32.7 | 7547 | 13.7 | 129 | 5.8 | 8.5 |
| 500 | 15.5 | 32.8 | 7821 | 13.9 | 127 | 6.1 | 8.6 |

Table D20. Extremal joint probability analysis results for CMS-Wave output Station 45.

| Return Period | Hm0 | Storm Duration | Power Index | Tp | Dir | Surge at Storm Peak | Water Level |
|---|---|---|---|---|---|---|---|
| (years) | (ft) | (hrs) | (ft2*hr) | (sec) | (Az. deg.) | (ft) | (ft, MSL) |
| 5 | 12.3 | 32.1 | 4840 | 12.0 | 146 | 4.5 | 7.6 |
| 10 | 13.0 | 32.3 | 5445 | 12.5 | 144 | 4.8 | 7.9 |
| 25 | 13.7 | 32.4 | 6075 | 13.0 | 141 | 5.1 | 8.1 |
| 50 | 14.1 | 32.5 | 6444 | 13.3 | 140 | 5.4 | 8.3 |
| 75 | 14.3 | 32.6 | 6625 | 13.5 | 139 | 5.5 | 8.3 |
| 100 | 14.4 | 32.6 | 6739 | 13.6 | 138 | 5.6 | 8.4 |
| 200 | 14.6 | 32.7 | 6974 | 13.8 | 137 | 5.9 | 8.5 |
| 500 | 14.8 | 32.8 | 7212 | 14.1 | 135 | 6.1 | 8.7 |

Figure D10. Wave height $H_{m0}$ marginal empirical distribution and best-fit GPD for CMS-Wave station 45.

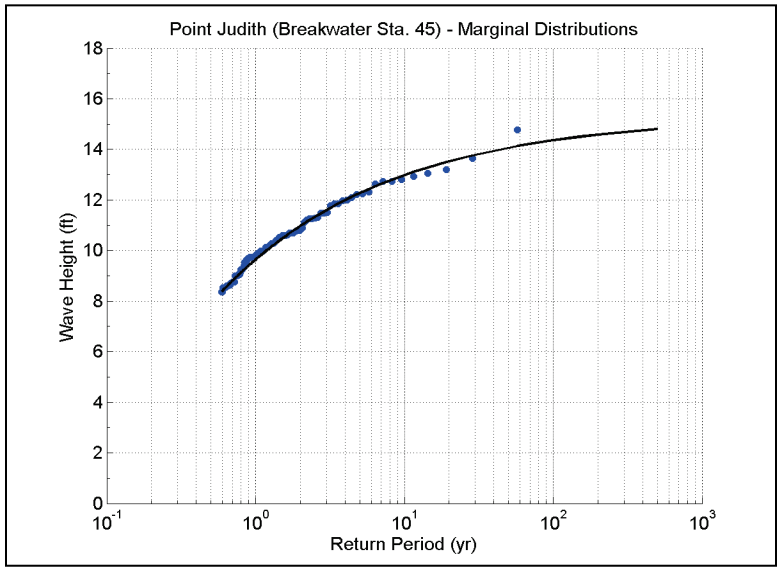

Figure D11. Wave period $T_p$ marginal empirical distribution and best-fit GPD for CMS-Wave station 45.

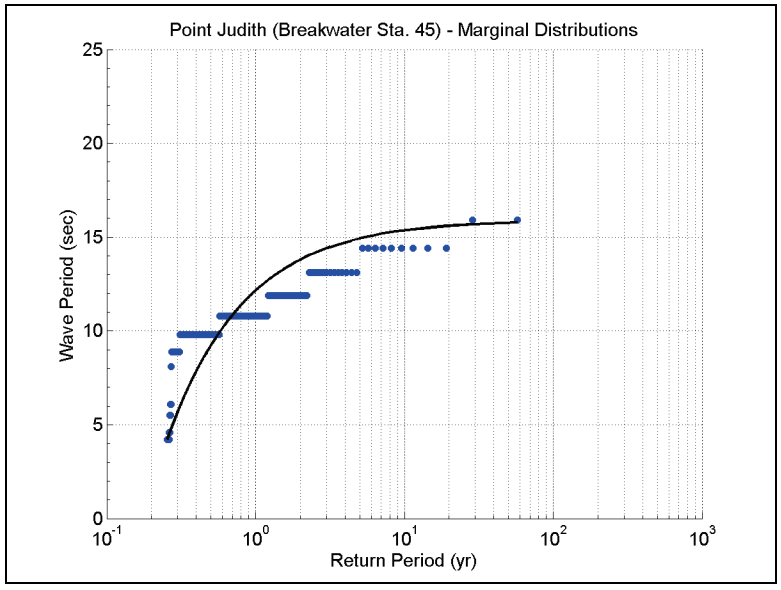


Figure D12. Wave direction marginal empirical distribution and best-fit normal distribution for CMS-Wave station 45.

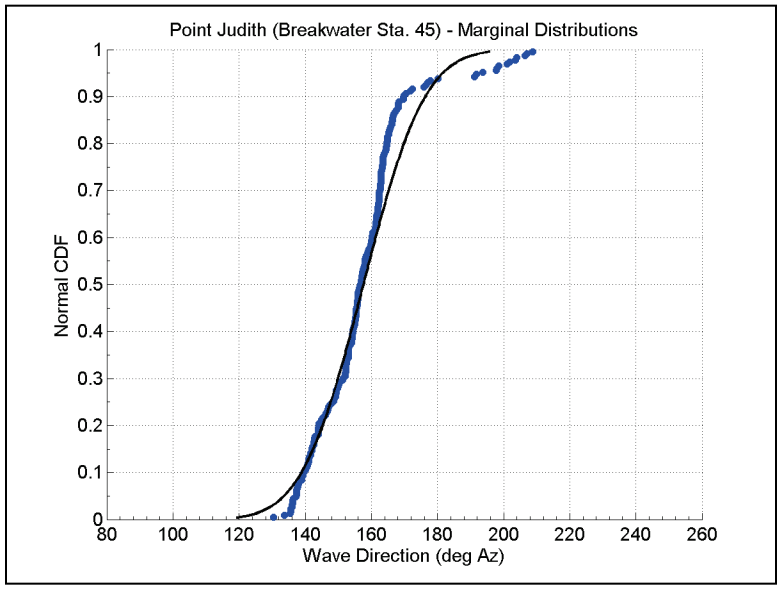

Table D21. Extremal joint probability analysis results for CMS-Wave output Station 46.

| Return Period | Hm0 | Storm Duration | Power Index | Tp | Dir | Surge at Storm Peak | Water Level |
|---|---|---|---|---|---|---|---|
| (years) | (ft) | (hrs) | (ft2*hr) | (sec) | (Az. deg.) | (ft) | (ft, MSL) |
| 5 | 10.1 | 32.4 | 3296 | 13.0 | 164 | 4.5 | 7.7 |
| 10 | 10.8 | 32.6 | 3771 | 13.7 | 162 | 4.9 | 8.0 |
| 25 | 11.5 | 32.8 | 4327 | 14.5 | 161 | 5.4 | 8.4 |
| 50 | 11.9 | 33.0 | 4695 | 14.9 | 160 | 5.7 | 8.6 |
| 75 | 12.2 | 33.1 | 4889 | 15.1 | 160 | 5.9 | 8.7 |
| 100 | 12.3 | 33.1 | 5019 | 15.3 | 159 | 6.0 | 8.8 |
| 200 | 12.6 | 33.3 | 5303 | 15.6 | 159 | 6.3 | 9.0 |
| 500 | 13.0 | 33.4 | 5624 | 15.9 | 158 | 6.7 | 9.2 |

# Appendix E: Main Breakwater Stability and Damage Analysis and Wave Transmission for Historical Wave Conditions[1]

## E.1 BreakwaterSim

A computational environment BWSim (Melby 2009, 2010), developed at ERDC-CHL, was used for analyzing the structural and functional performance of the Main breakwater. The model consists of a suite of Matlab scripts to compute structure damage progression, wave transmission by overtopping, and wave transmission into the protected embayment. The computational methods are described in the following sections.

## E.2 Stable seaside armor size

Stable armor stone size is computed here based on return period wave and water level conditions given in the previous sections. In this report, seaside armor stability is computed based on Melby and Kobayashi (2011). The maximum wave momentum flux is highly nonlinear for nonlinear waves (i.e., steep waves in shallow water). This corresponds to the case where armor stability is at its minimum. Melby and Hughes (2004) described a nonlinear wave momentum flux using a numerical Fourier solution. The resulting approximate relation was found to be

$$\left(\frac{M_F}{\rho_w g h^2}\right)_{\max} = A_0 \left(\frac{h}{g T_m^2}\right)^{-A_1}$$

$$A_0 = 0.639 \left(\frac{H_{m0}}{h}\right)^{2.026} \tag{E1}$$

$$A_1 = 0.180 \left(\frac{H_{m0}}{h}\right)^{-0.391}$$

[1] Authored by Jeffrey Melby and Norberto Nadal-Caraballo

Where $H_{m0}$ is the significant wave height, $h$ is the local water depth, $T_m$ is the mean wave period, $M_f$ is the momentum flux, $\rho_w$ is the density of water, and $g$ is the acceleration of gravity. A nonlinear approximation for momentum flux is important because stability is at its minimum when the incident wave is the most nonlinear.

Two stability equations resulted from the fit to data using Equation E1. The recommended equations for stability are

$$N_m = \frac{1}{a_m}\left(\frac{S}{K_s\sqrt{N_z}}\right)^{0.2} \tag{E2}$$

and

$$N_m = \left(\frac{(M_F/\gamma_w h^2)_{\max}}{(S_r - 1)}\right)^{1/2} \frac{h}{D_{n50}} \tag{E3}$$

Plunging waves:

$$a_m = \frac{1}{5P^{0.18}\sqrt{\cot\theta}} \qquad s_m \geq s_{mc} \tag{E4}$$

Surging waves:

$$a_m = \frac{s_m^{P/3}}{5P^{0.18}(\cot\theta)^{0.5-P}s_m^{-P/3}} \quad s_m < s_{mc} \tag{E5}$$

$$s_m = H_{m0}/L_{m,} \qquad s_{mc} = -0.0035\cot\theta + 0.028 \tag{E6}$$

Solving for the stable stone size yields

$$D_{n50} = ha_m\left(\frac{S}{K_s\sqrt{N_z}}\right)^{-1/5}\left(\frac{(M_F/\gamma_w h^2)_{\max}}{\Delta}\right)^{1/2} \tag{E7}$$

Here, $D_{n50} = (V_{50})^{1/3}$ = nominal stone size, $V_{50} = M_{50}/\rho_r$ = median volume of armor stone, $M_{50}$ = median mass, cot θ = structure seaward slope, $\Delta = S_r - 1$, $S_r = \rho_r/\rho_w$ = relative specific gravity of armor stone, $\rho_r$ = density of stone, $\rho_w$ = density of water that the structure is in, $N_m$ is the momentum flux

stability number, $P$ = notional permeability of the structure, $S = A_e/(D_{n50})^2$ = normalized eroded area, $A_e$ = eroded area, and $N_z$ = storm duration/$T_m$. $S$ and $A_e$ are illustrated in Figure E1. $K_s$ = 1.3 is an empirical parameter to account for accelerated damage that occurs with constant wave conditions, $\gamma_w$ is the specific weight of water, θ is the seaside structure slope, and $s_m$ is the local wave steepness. Damage levels given by $S$ = 1 to 3 represent the start of damage and correspond to Hudson's (1959) $D$ = 0 to 5%. For an impermeable dike, $P$ = 0.1. For a traditional multilayer breakwater, $P$ = 0.4 – 0.6. However, with sand tightening and repeated damage of the Point Judith structures, a permeability of near 0.4 can be expected.

Figure E1. Illustration of damage parameters.

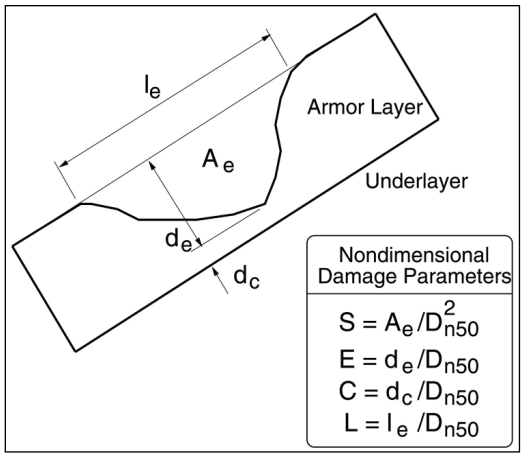


The stable seaside armor sizes for various return periods were computed for all reaches. This yielded a wide variety of armor sizes for the many permutations of parameters. The number of armor weights was reduced to two for each alternative corresponding to the maximum stone weights for west and east legs of the Main breakwater and mean water level from the joint probability distribution. The final list is shown in Table E1. For these calculations, armor stone relative specific gravity $S_r$ = 2.69 corresponding to granite, and zero damage $S$ = 2 were assumed. These required stone sizes are generally greater than the existing 12–15 ton armor stone used on the last two rehabilitations. Note that the equations listed above are derived from mean fits to data and are not necessarily conservative. For these large USACE projects, the goal is typically identification of the alternative that produces the highest positive benefit-to-cost ratio. Therefore, these stone sizes are somewhat arbitrary and are simply inputs to the risk analysis. In this type of analysis, the return period simply provides some context for the alternative but is not a primary design parameter. That is, the goal here is not to design to a specific return period

such as 50 or 100 yr. The goal is to determine which of these alternatives has the lowest risk and produces the highest net benefit. Here, risk is defined as the product of the probability of consequences and the cost of those consequences.

Table E1. Seaside median stone weights in tons for various alternatives and return periods for mean plus two standard deviations water level.

| Alternative | BW Reach | Return Period (Years) | | | | | | | |
|---|---|---|---|---|---|---|---|---|---|
| | | 5 | 10 | 25 | 50 | 75 | 100 | 200 | 500 |
| 1 | 0+00 – 20+00 | 7 | 8 | 9 | 10 | 10 | 10 | 11 | 12 |
| | 20+00 – 67+00 | 16 | 18 | 20 | 21 | 22 | 23 | 24 | 25 |
| 2 | 0+00 – 20+00 | 4 | 5 | 5 | 6 | 6 | 6 | 6 | 7 |
| | 20+00 – 67+00 | 9 | 10 | 11 | 12 | 12 | 12 | 13 | 14 |
| 3 | 0+00 – 20+00 | 7 | 8 | 9 | 10 | 10 | 10 | 11 | 12 |
| | 20+00 – 67+00 | 16 | 18 | 20 | 21 | 22 | 23 | 24 | 25 |
| 4 | 0+00 – 20+00 | 4 | 5 | 5 | 6 | 6 | 6 | 6 | 7 |
| | 20+00 – 67+00 | 9 | 10 | 11 | 12 | 12 | 13 | 13 | 14 |

## E.3 Stable leeside armor size

Stability equations were given by Van Gent and Pozueta (2004) for leeside stability. Melby (2009) revised these equations to be in a similar form to the seaside equations as follows:

$$D_{n50} = a_{ls}\left(\frac{S_{ls}}{K_{ls}\sqrt{N_z}}\right)^{-1/r}\left(\frac{u_{1\%}T_{m-1,0}}{125\sqrt{\Delta}}\right) \tag{E8}$$

$$a_{ls} = (\cot\varphi)^{-2.5/r}[1+10\cdot\exp(-R_{c-rear}/H_s)]^{1/r} \tag{E9}$$

where $S_{ls}$ is the leeside damage, $r$ = 6 for constant wave conditions, $T_{m\text{-}1,0}$ = $m_{\text{-}1}/m_0$ of incident spectrum, $T_{m\text{-}1,0} \sim T_p$ /1.1 for a JONSWAP incident wave spectrum, $R_{c\text{-}rear}$ = freeboard of leeside edge of crest, cot $\phi$ = leeside slope, $u_{1\%}$ = maximum crest velocity exceeded by 1% of the waves, $H_s = H_{m0}$ of incident wave spectrum, $K_{ls}$ and $r$ are empirical fit parameters, and $(D_n)_{ls}$ and $\Delta_{ls}$ are the nominal stone size and density parameter for the leeside armor, respectively. A leeside stability number, $N_{ls}$, is introduced where

$$N_{ls} = \left( \frac{u_{1\%} T_{m-1,0}}{125(D_n \sqrt{\Delta})_{ls}} \right) = \frac{1}{a_{ls}} \left( \frac{S_{ls}}{K_{ls} \sqrt{N_z}} \right)^{1/r} \tag{E10}$$

Then, the single storm leeside damage for constant wave conditions can be expressed as

$$S_{ls} = K_{ls} \sqrt{N_z} \left( a_{ls} N_{ls} \right)^r \tag{E11}$$

The $n^{\text{th}}$ moment of the incident wave energy density spectrum is given by

$$m_n = \int_0^\infty f^n S(f) df \tag{E12}$$

The crest velocity exceeded by 1% of the waves is given by

$$\frac{u_{1\%}}{\sqrt{g H_s}} = \frac{1.7 (\gamma_{f-C})^{0.5} \left( \frac{z_{1\%} - R_c}{\gamma_f H_s} \right)^{0.5}}{\left( 1 + 0.1 \frac{B_c}{H_s} \right)} \tag{E13}$$

where $\gamma_{f\text{-}C}$ = friction factor on crest, $\gamma_f$ = friction factor on seaward slope, $R_c$ = freeboard of seaside crest, $B_c$ = breakwater crest width, and $z_{1\%}$ = runup exceeded by 1% of waves. The friction coefficients and runup can be computed by Equations 14 and 15, respectively:

$$\gamma_f = \gamma_{f-C} = \begin{cases} 0.55 & \xi_{s,-1} \le 2 \\ 0.05625 * (\xi_{s,-1} - 2) + 0.55 & 2 < \xi_{s,-1} < 10 \\ 1.0 & \xi_{s,-1} \ge 10 \end{cases} \tag{E14}$$

$$\frac{z_{1\%}}{\gamma H_s} = \begin{cases} c_0 \xi_{s,-1} & for\ \xi_{s,-1} \le p \\ c_1 - c_2 / \xi_{s,-1} & for\ \xi_{s,-1} > p \end{cases} \tag{E15}$$

Here $c_2 = 0.25\ c_1^2/c_0$, $p = 0.5\ c_1/c_0$, and $\gamma = \gamma_f$ = reduction factor for roughness and angular wave attack. The Iribarren parameter based on the first negative moment wave period is

$$\xi_{s,-1} = \frac{\tan\theta}{\sqrt{\frac{H_s}{L_{m-1,0}}}} \tag{E16}$$

where

$$L_{m-1,0} = \frac{gT_{m-1,0}^2}{2\pi} \tag{E17}$$

and $c_0 = 1.45$ and $c_1 = 5.1$ for $z_{1\%}$. For the Point Judith structures, Equation E15 becomes

$$\frac{z_{1\%}}{H_s} = \begin{cases} 1.45\xi_{s,-1} & for\ \xi_{s,-1} \le 1.76 \\ 5.10 - 4.485/\xi_{s,-1} & for\ \xi_{s,-1} > 1.76 \end{cases} \tag{E18}$$

The stable leeside armor sizes are listed in Table E2 for various return period wave and water level conditions. The leeside stone weights are significantly greater than historically used on the structure for most alternatives. This is a consequence of the relatively low crest height. The importance of the leeside armor stone will be shown in following sections.

Table E2. Leeside median stone weights in tons for various alternatives and return periods for mean plus two standard deviation water level.

| Alternative | BW Reach | Return Period (Years) | | | | | | | |
|---|---|---|---|---|---|---|---|---|---|
| | | 5 | 10 | 25 | 50 | 75 | 100 | 200 | 500 |
| 1 | 0+00 – 20+00 | 9 | 11 | 14 | 17 | 18 | 19 | 22 | 25 |
| | 20+00 – 67+00 | 22 | 29 | 39 | 47 | 52 | 56 | 65 | 77 |
| 2 | 0+00 – 20+00 | 6 | 8 | 10 | 12 | 13 | 14 | 16 | 18 |
| | 20+00 – 67+00 | 16 | 21 | 28 | 35 | 38 | 41 | 48 | 57 |
| 3 | 0+00 – 20+00 | 4 | 5 | 7 | 9 | 10 | 10 | 12 | 14 |
| | 20+00 – 67+00 | 12 | 17 | 23 | 28 | 31 | 33 | 39 | 48 |
| 4 | 0+00 – 20+00 | 3 | 3 | 5 | 6 | 6 | 7 | 8 | 9 |
| | 20+00 – 67+00 | 8 | 11 | 15 | 19 | 21 | 23 | 27 | 33 |

## E.4 Seaside armor accumulated damage

An illustration of seaside damage on a rubble mound structure is shown in Figure E2, indicated by numbers 1 and 2. Condition 1 illustrates damage initiation that occurs as armor is displaced near the still water line but has

not extended into the filter layers. Condition 2 illustrates extensive damage over the entire active zone of the seaward side extending into the filter layers and even into the core and crest. Herein, it is assumed that once seaside damage reaches condition 2, the structure has no capacity and will breach during the storm that caused it to be in condition 2.

Figure E2. Illustration of damage on a rubble mound structure (USACE 2002).

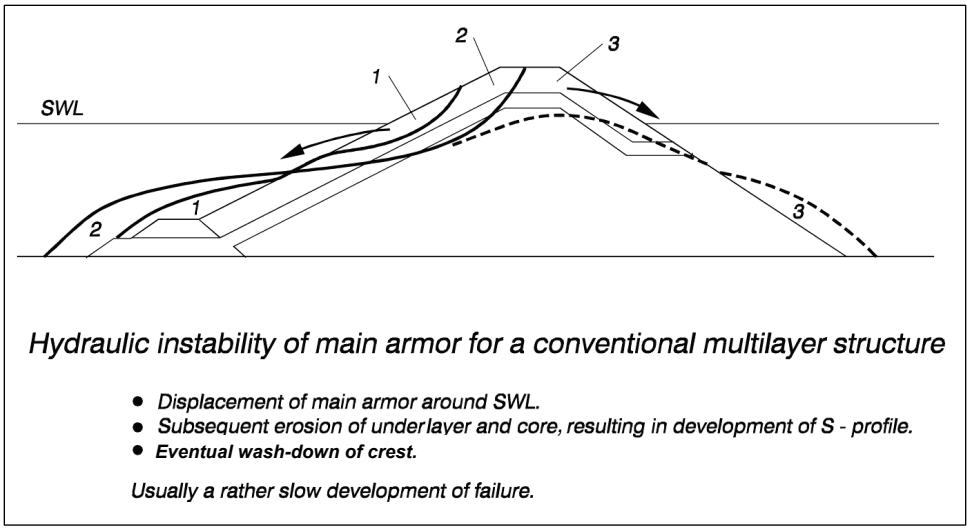


Although Equation E2 includes damage $S$, the damage is for constant wave conditions. The Coastal Engineering Manual (USACE 2002) provides equations from Melby and Kobayashi (1998) and Melby (1999) to predict the normalized eroded cross-sectional area as a function of time for varying wave and water level conditions. Melby and Kobayashi (1999) modified these equations to allow nonzero initial damage values. Recently, Melby and Kobayashi (2011) integrated the momentum flux stability equations given above using the Hypothesis-of-Equivalency to yield new equations that are more robust. The seaside damage relations are given as

$$\overline{S}(t_n) = \sqrt{N_{ze} + (N_z)_n}\,(a_m N_m)_n^5 \tag{E19}$$

$$a_m = \frac{1}{5P^{0.18}\sqrt{\cot\theta}} \qquad s_m \geq s_{mc} \tag{E20}$$

$$a_m = \frac{s_m^{P/3}}{5P^{0.18}(\cot\theta)^{0.5-P}} \quad s_m < s_{mc} \tag{E21}$$

$$(N_z)_n = \frac{t_n - t_{n-1}}{(T_m)_n} \tag{E22}$$

$$N_{ze} = \left( \frac{S_{n-1}}{(a_m N_m)_n^5} \right)^2 \tag{E23}$$

where $\overline{S}(t_n) = \overline{A}_e / D_{n50}^2$ is the mean damage at time $t_n$, $\overline{A}_e$ is the mean eroded cross-sectional area, and $N_m$ is the stability number given in Equations E2 and E3. Note that $S$ can be thought of as the number of stones displaced from a $D_{n50}$-wide cross section. The standard deviation of $S$ was given as a function of the mean $\overline{S}$ by the relation $\sigma_S = 0.5\,\overline{S}^{\,0.65}$. This quartile describes the alongshore variability of damage. Also given were relations for maximum depth of erosion, minimum remaining cover depth, and length of the eroded hole. The maximum eroded depth is $d_e$, minimum remaining cover depth is $d_c$, and maximum eroded length is $l_e$. These three parameters are normalized to obtain $E = d_e/D_{n50}$, $C = d_c/D_{n50}$, and $L = l_e/D_{n50}$. Melby and Kobayashi (2011) expressed the key profile parameters as a function of the mean damage as follows: $\overline{E} = 0.46\,\overline{S}^{\,0.5}$, $\overline{C} = C_o - 0.1\,\overline{S}$, and $\overline{L} = 0.44\,\overline{S}^{\,0.5}$ where $C_o$ is the initial armor layer thickness.

For this study, the wave and water level conditions are given in 3 hr increments, so $t_n - t_{n\text{-}1}$ = 3 hr or 10800 seconds (sec). For application of Equations E19 through E23, the life-cycle of storm conditions are incremented, calculating the zero-damage stability number at each time-step using Equations E2 through E6. If the zero-damage stability number is exceeded, then the accumulated damage is computed using Equations E19 through E23.

## E.5 Leeside armor accumulated damage

Leeside damage is illustrated in Figure E3. Damage begins on the rear crest and erodes seaward through the crest.

Figure E3. Illustration of leeside erosion of a rubble mound breakwater cross section.

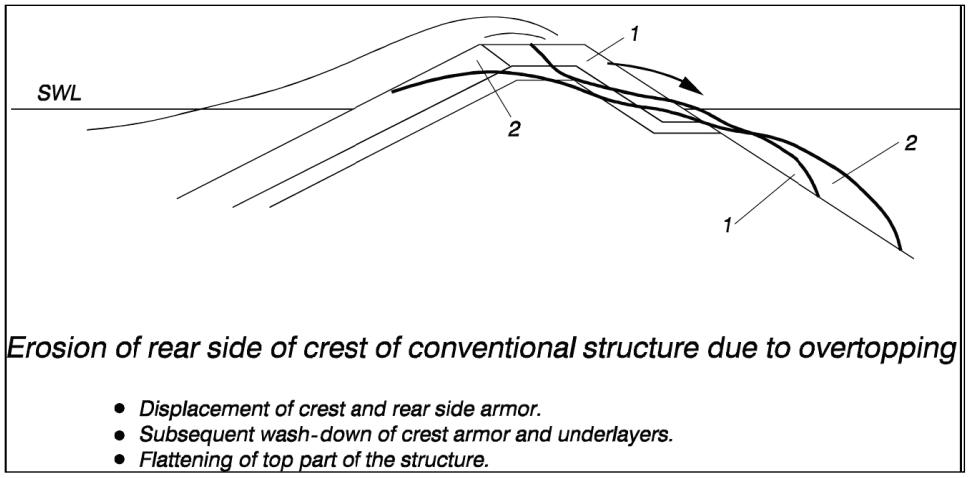


To develop an equation for time-dependent leeside damage, Equation E11 is differentiated to determine the rate of damage for a storm segment of approximately constant wave conditions and then integrated over some arbitrary time segment from $t_n$ to $t_{n+1}$. The Hypothesis-of-Equivalency is adopted again to yield Equations E24 and E25 for leeside erosion similar to Equations E19 through E23.

$$\bar{S}_{ls}(t_n) = K_{ls}\sqrt{(N_{ze})_{ls} + (N_z)_n}\,(a_{ls}N_{ls})^r \tag{E24}$$

$$(N_{ze})_{ls} = \left(\frac{\bar{S}(t_n)}{K_{ls}(a_{ls}N_{ls})^r}\right)^2 \tag{E25}$$

where $(N_z)_n$ is defined by Equation E22, $a_{ls}$ by Equation E9, and $N_{ls}$ by Equation E10.

## E.6 Accumulated crest height erosion

The previous equations give no prediction of crest height reduction as damage progresses into severe states.

### E.6.1 Seaside crest erosion

Generally, seaside erosion progresses slowly with damage distributed over a significant portion of the seaside slope as shown in Figure E2. The damage progresses in a predictable way according to Equations E25 through E29 until the underlayer is exposed through a hole roughly $D_{n50}$ in

size at roughly $\overline{S} \approx 20$ and $S_{max} \approx 30$ (Melby 1999). At that point, damage progresses much more rapidly through the crest of the structure until the profile approaches an equilibrium breached profile where the average crest height is reduced to approximately the MSL. Once this ultimate damage level occurs, the structure footprint is usually much larger than the original, and the structure consists of a wide, low berm that is still efficient at dissipating wave energy. This type of structure is shown in Figures 8 through 16 in the main text of this report. Subsequent repairs built on top of the heavily damaged sections retain the increased wave dissipating characteristics of the wide berm if the berm is not removed, and therefore may provide a more reliable structure than the original even though similar sized armor is used. In addition, if the repair is back to the original crest elevation, it is likely that the structure will provide increased wave protection over the original because of the wide, shallow, sloping berm. This is the case for the Point Judith breakwater.

In this study it assumed that if the seaside damage level reaches $\overline{S} \approx 20$ for a given reach, the crest height is immediately reduced to MSL following that storm. However, predicted seaside *S* did not reach this level for the historical storms at the Point Judith Main breakwater. This suggests that the dominant crest height reduction was from overtopping waves eroding the crest and leeside.

### E.6.2 Leeside crest erosion

For leeside erosion, the situation is significantly different than on the seaside. For low-crested structures, like Point Judith breakwaters, leeside erosion begins on the leeside corner of the crest and just below this level where the plunging overtopping waves attack the loose and mostly unrestrained armor stone. The damage progresses rapidly and forms a notch on the leeside crest. This notch will progress rapidly through the crest to the seaward side of the structure because the damage is highly concentrated.

Herein the method of Ahrens (1989) is adopted to compute crest height reduction for low-crested structures. The crest height at each time-step is computed as follows:

$$h_c = K_{cr}\sqrt{\frac{A_t}{\exp(aN_s^*)}} \tag{E26}$$

$$a = -.028 + 0.045c + 0.034(h_c / h) - (6e^{-9}B_n^2) \tag{E27}$$

$$N_s^* = \frac{H_s^{2/3}L_p^{1/3}}{\Delta D_{n50}} \tag{E28}$$

$$B_n = \frac{A_t}{D_{n50}^2} \tag{E29}$$

$$c = \frac{A_t}{h_c^2} \tag{E30}$$

$$A_t = h_c(B + h_c \cot\alpha) \tag{E31}$$

where the time dependency for crest height and wave parameters is assumed, $h_c$ = total damaged crest height of structure from toe, $L_p$ is the local wave length computed using linear wave theory and $T_p$, $h$ is the toe depth, $h_c$' = total undamaged crest height of structure from toe, $A_t$ = area of structure enclosed by symmetric trapezoid, $B$ = crest width, and $B_n$ = bulk stability number. Here, $H_{m0}$ is used for $H_s$. At each time-step, the crest height $h_c(t_n)$ from the previous time-step is used. Coefficient $K_{cr}$ is an empirical factor that was calibrated to force the predicted crest height to agree with the historical damage at Point Judith, including the rehabilitation in 1984. The average value of the empirical factor is $K_{cr}$ = 0.853. The value varied by reach in this study. The values for the eight reaches starting at 0+25 were $K_{cr}$ = 0.853, 0.8514, 0.8624, 0.8421, 0.857, 0.8541, 0.8497, and 0.853. This value varied primarily because the starting condition of each reach was unknown with a wide relic structure which is significantly different from the structure geometry for which these relations were developed. Note that, at each time-step, $h_c$ from Equation E26 can be higher or lower than the crest height at the previous time-step. For the life-cycle study, the lower of $h_c(t_n)$ or $h_c(t_{n-1})$ is used, where $h_c(t_n)$ is the crest height at the present time estimated from Equation E26 and $h_c(t_{n-1})$ is the crest height at the previous time step.

## E.7 Wave overtopping transmission

For a low-crested structure like the Point Judith Main breakwater, wave transmission into the lee from wave overtopping is common at the as-built crest height. Wave overtopping transmission is worse for heavily damaged sections that have lowered crest elevations. Wave overtopping transmission describes the transformation of spectral wave height from the seaside of the breakwater, $(H_{m0})_i$, to the leeside of the structure, $(H_{m0})_t$. Overtopping transmission $C_t = (H_{m0})_t/(H_{m0})_i$ is computed using the following relations:

$$C_t = \left(0.031\frac{H_{m0}}{D_{n50}} - 0.24\right)\frac{R_c}{D_{n50}} + b \tag{E34}$$

Conventional multilayer rubble mound structure:

$$0.75 \le C_t \le 0.075 \tag{E35}$$

$$b = -5.42 s_{op} + 0.0323\frac{H_{m0}}{D_{n50}} - 0.0017\left(\frac{B}{D_{n50}}\right)^{1.84} + 0.51 \tag{E36}$$

Reef-type rubble mound structure:

$$0.60 \le C_t \le 0.15 \tag{E37}$$

$$b = -2.6 s_{op} - 0.05\frac{H_{m0}}{D_{n50}} + 0.85 \tag{E38}$$

where $D_{n50}$ is the seaside stone size, $s_{op} = H_{m0}/L_{op}$ and $L_{op} = gT_p^2/2\pi$. For the condition where the structure crest is at the design height, the structure is considered a conventional structure.

# Appendix F: Detailed Life-Cycle Modeling Results[1]

In Tables F1 through F15, in column "Alt," the number is *alternative.return period*. Damage values given are $\mu_S+\sigma_S$ (mean + 1 standard deviation) of $S = A_e/D_{n50}^2$.

[1] Authored by Jeffrey Melby and Norberto Nadal-Caraballo

Table F1. Predicted seaside damage from BWSim at end of 57 yr life cycle between 2014 and 2071 with SLR scenario 1.

| Alt | Sta 6 | Sta 7 | Sta 8 | Sta 9 | Sta 10 | Sta 11 | Sta 12 | Sta 13 |
|---|---|---|---|---|---|---|---|---|
| 1.1 | 3.1 | 5.1 | 5.9 | 5.9 | 5.2 | 4.7 | 3.8 | 2.9 |
| 1.2 | 2.7 | 4.5 | 5.3 | 5.3 | 4.6 | 4.2 | 3.4 | 2.6 |
| 1.3 | 2.2 | 3.7 | 4.4 | 4.4 | 3.8 | 3.5 | 2.8 | 2.2 |
| 1.4 | 2.0 | 3.3 | 3.9 | 3.9 | 3.5 | 3.2 | 2.5 | 2.0 |
| 1.5 | 1.9 | 3.0 | 3.6 | 3.6 | 3.2 | 3.0 | 2.3 | 1.9 |
| 1.6 | 1.9 | 3.0 | 3.6 | 3.6 | 3.2 | 3.0 | 2.3 | 1.9 |
| 1.7 | 1.7 | 2.8 | 3.3 | 3.3 | 3.0 | 2.7 | 2.1 | 1.8 |
| 1.8 | 1.6 | 2.5 | 3.0 | 3.0 | 2.7 | 2.4 | 1.9 | 1.7 |
| 2.1 | 3.4 | 5.4 | 6.3 | 6.3 | 5.5 | 5.0 | 4.0 | 3.2 |
| 2.2 | 2.7 | 4.4 | 5.3 | 5.3 | 4.5 | 4.1 | 3.3 | 2.6 |
| 2.3 | 2.2 | 3.7 | 4.3 | 4.3 | 3.8 | 3.5 | 2.8 | 2.1 |
| 2.4 | 1.9 | 3.1 | 3.6 | 3.6 | 3.3 | 3.0 | 2.3 | 1.9 |
| 2.5 | 1.9 | 3.1 | 3.6 | 3.6 | 3.3 | 3.0 | 2.3 | 1.9 |
| 2.6 | 1.9 | 3.1 | 3.6 | 3.6 | 3.3 | 3.0 | 2.3 | 1.9 |
| 2.7 | 1.6 | 2.6 | 3.1 | 3.1 | 2.8 | 2.5 | 2.0 | 1.7 |
| 2.8 | 1.6 | 2.6 | 3.1 | 3.1 | 2.8 | 2.5 | 2.0 | 1.7 |
| 3.1 | 3.1 | 5.1 | 5.9 | 5.9 | 5.2 | 4.7 | 3.8 | 2.9 |
| 3.2 | 2.7 | 4.5 | 5.3 | 5.3 | 4.6 | 4.2 | 3.4 | 2.6 |
| 3.3 | 2.2 | 3.7 | 4.4 | 4.4 | 3.8 | 3.5 | 2.8 | 2.2 |
| 3.4 | 2.0 | 3.3 | 3.9 | 3.9 | 3.5 | 3.2 | 2.5 | 2.0 |
| 3.5 | 1.9 | 3.0 | 3.6 | 3.6 | 3.2 | 3.0 | 2.3 | 1.9 |
| 3.6 | 1.9 | 3.0 | 3.6 | 3.6 | 3.2 | 3.0 | 2.3 | 1.9 |
| 3.7 | 1.7 | 2.8 | 3.3 | 3.3 | 3.0 | 2.7 | 2.1 | 1.8 |
| 3.8 | 1.6 | 2.5 | 3.0 | 3.0 | 2.7 | 2.4 | 1.9 | 1.7 |
| 4.1 | 3.4 | 5.4 | 6.3 | 6.3 | 5.5 | 5.0 | 4.0 | 3.2 |
| 4.2 | 2.7 | 4.4 | 5.3 | 5.3 | 4.5 | 4.1 | 3.3 | 2.6 |
| 4.3 | 2.2 | 3.7 | 4.3 | 4.3 | 3.8 | 3.5 | 2.8 | 2.1 |
| 4.4 | 1.9 | 3.1 | 3.6 | 3.6 | 3.3 | 3.0 | 2.3 | 1.9 |
| 4.5 | 1.9 | 3.1 | 3.6 | 3.6 | 3.3 | 3.0 | 2.3 | 1.9 |
| 4.6 | 1.9 | 3.1 | 3.6 | 3.6 | 3.3 | 3.0 | 2.3 | 1.9 |
| 4.7 | 1.6 | 2.6 | 3.1 | 3.1 | 2.8 | 2.5 | 2.0 | 1.7 |
| 4.8 | 1.6 | 2.6 | 3.1 | 3.1 | 2.8 | 2.5 | 2.0 | 1.7 |

Table F2. Predicted leeside damage from BWSim at end of 57 yr life cycle between 2014 and 2071 with SLR scenario 1.

| Alt | Sta 6 | Sta 7 | Sta 8 | Sta 9 | Sta 10 | Sta 11 | Sta 12 | Sta 13 |
|---|---|---|---|---|---|---|---|---|
| 1.1 | 7.3 | 7.9 | 8.3 | 8.6 | 7.7 | 7.3 | 6.5 | 5.8 |
| 1.2 | 6.0 | 6.6 | 6.8 | 6.8 | 6.4 | 6.0 | 5.4 | 4.8 |
| 1.3 | 4.2 | 4.8 | 5.1 | 5.1 | 4.7 | 4.5 | 3.8 | 3.4 |
| 1.4 | 1.8 | 4.1 | 4.5 | 4.5 | 4.0 | 3.7 | 0.0 | 0.0 |
| 1.5 | 0.0 | 3.6 | 4.0 | 4.0 | 3.5 | 0.0 | 0.0 | 0.0 |
| 1.6 | 0.0 | 0.0 | 0.0 | 0.0 | 0.0 | 0.0 | 0.0 | 0.0 |
| 1.7 | 0.0 | 0.0 | 0.0 | 0.0 | 0.0 | 0.0 | 0.0 | 0.0 |
| 1.8 | 0.0 | 0.0 | 0.0 | 0.0 | 0.0 | 0.0 | 0.0 | 0.0 |
| 2.1 | 6.6 | 8.2 | 8.4 | 12.6 | 8.2 | 8.3 | 6.6 | 5.3 |
| 2.2 | 5.6 | 5.9 | 6.2 | 8.0 | 5.9 | 5.6 | 5.0 | 4.3 |
| 2.3 | 3.9 | 4.2 | 4.6 | 5.0 | 4.2 | 3.8 | 3.4 | 0.0 |
| 2.4 | 0.0 | 0.0 | 3.7 | 3.7 | 0.0 | 0.0 | 0.0 | 0.0 |
| 2.5 | 0.0 | 0.0 | 0.0 | 0.0 | 0.0 | 0.0 | 0.0 | 0.0 |
| 2.6 | 0.0 | 0.0 | 0.0 | 0.0 | 0.0 | 0.0 | 0.0 | 0.0 |
| 2.7 | 0.0 | 0.0 | 0.0 | 0.0 | 0.0 | 0.0 | 0.0 | 0.0 |
| 2.8 | 0.0 | 0.0 | 0.0 | 0.0 | 0.0 | 0.0 | 0.0 | 0.0 |
| 3.1 | 2.8 | 3.4 | 3.4 | 5.1 | 3.2 | 3.2 | 3.0 | 2.0 |
| 3.2 | 1.6 | 2.0 | 2.6 | 3.4 | 2.0 | 2.3 | 1.6 | 1.0 |
| 3.3 | 1.0 | 1.0 | 1.1 | 1.8 | 1.0 | 1.0 | 1.0 | 0.0 |
| 3.4 | 0.0 | 1.0 | 1.0 | 1.0 | 1.0 | 1.0 | 0.0 | 0.0 |
| 3.5 | 0.0 | 0.0 | 0.0 | 1.0 | 0.0 | 0.0 | 0.0 | 0.0 |
| 3.6 | 0.0 | 0.0 | 0.0 | 0.0 | 0.0 | 0.0 | 0.0 | 0.0 |
| 3.7 | 0.0 | 0.0 | 0.0 | 0.0 | 0.0 | 0.0 | 0.0 | 0.0 |
| 3.8 | 0.0 | 0.0 | 0.0 | 0.0 | 0.0 | 0.0 | 0.0 | 0.0 |
| 4.1 | 2.0 | 4.9 | 5.1 | 10.2 | 4.8 | 4.8 | 3.6 | 1.6 |
| 4.2 | 1.4 | 2.9 | 3.0 | 4.9 | 2.8 | 2.8 | 1.8 | 1.0 |
| 4.3 | 0.0 | 1.0 | 1.0 | 2.6 | 1.0 | 1.0 | 0.0 | 0.0 |
| 4.4 | 0.0 | 0.0 | 0.0 | 0.0 | 0.0 | 0.0 | 0.0 | 0.0 |
| 4.5 | 0.0 | 0.0 | 0.0 | 0.0 | 0.0 | 0.0 | 0.0 | 0.0 |
| 4.6 | 0.0 | 0.0 | 0.0 | 0.0 | 0.0 | 0.0 | 0.0 | 0.0 |
| 4.7 | 0.0 | 0.0 | 0.0 | 0.0 | 0.0 | 0.0 | 0.0 | 0.0 |
| 4.8 | 0.0 | 0.0 | 0.0 | 0.0 | 0.0 | 0.0 | 0.0 | 0.0 |

Table F3. Predicted free board in feet, MSL, from BWSim at end of 57 yr life cycle between 2014 and 2071 with SLR scenario 1.

| Alt | Sta 6 | Sta 7 | Sta 8 | Sta 9 | Sta 10 | Sta 11 | Sta 12 | Sta 13 |
|---|---|---|---|---|---|---|---|---|
| 1.1 | 8.26 | 8.26 | 8.26 | 8.09 | 8.26 | 8.26 | 8.26 | 8.26 |
| 1.2 | 8.26 | 8.26 | 8.26 | 8.26 | 8.26 | 8.26 | 8.26 | 8.26 |
| 1.3 | 8.26 | 8.26 | 8.26 | 8.26 | 8.26 | 8.26 | 8.26 | 8.26 |
| 1.4 | 8.26 | 8.26 | 8.26 | 8.26 | 8.26 | 8.26 | 8.26 | 8.26 |
| 1.5 | 8.26 | 8.26 | 8.26 | 8.26 | 8.26 | 8.26 | 8.26 | 8.26 |
| 1.6 | 8.26 | 8.26 | 8.26 | 8.26 | 8.26 | 8.26 | 8.26 | 8.26 |
| 1.7 | 8.26 | 8.26 | 8.26 | 8.26 | 8.26 | 8.26 | 8.26 | 8.26 |
| 1.8 | 8.26 | 8.26 | 8.26 | 8.26 | 8.26 | 8.26 | 8.26 | 8.26 |
| 2.1 | 8.26 | 7.58 | 7.64 | 5.12 | 7.38 | 7.15 | 7.62 | 8.26 |
| 2.2 | 8.26 | 8.26 | 8.26 | 7.04 | 8.20 | 8.20 | 8.26 | 8.26 |
| 2.3 | 8.26 | 8.26 | 8.26 | 7.91 | 8.26 | 8.26 | 8.26 | 8.26 |
| 2.4 | 8.26 | 8.26 | 8.26 | 8.26 | 8.26 | 8.26 | 8.26 | 8.26 |
| 2.5 | 8.26 | 8.26 | 8.26 | 8.26 | 8.26 | 8.26 | 8.26 | 8.26 |
| 2.6 | 8.26 | 8.26 | 8.26 | 8.26 | 8.26 | 8.26 | 8.26 | 8.26 |
| 2.7 | 8.26 | 8.26 | 8.26 | 8.26 | 8.26 | 8.26 | 8.26 | 8.26 |
| 2.8 | 8.26 | 8.26 | 8.26 | 8.26 | 8.26 | 8.26 | 8.26 | 8.26 |
| 3.1 | 14.26 | 13.96 | 14.23 | 12.73 | 13.94 | 13.76 | 13.73 | 14.26 |
| 3.2 | 14.26 | 14.23 | 14.26 | 13.05 | 14.25 | 14.01 | 13.96 | 14.26 |
| 3.3 | 14.26 | 14.26 | 14.26 | 13.64 | 14.26 | 14.26 | 14.26 | 14.26 |
| 3.4 | 14.26 | 14.26 | 14.26 | 13.90 | 14.26 | 14.26 | 14.26 | 14.26 |
| 3.5 | 14.26 | 14.26 | 14.26 | 14.14 | 14.26 | 14.26 | 14.26 | 14.26 |
| 3.6 | 14.26 | 14.26 | 14.26 | 14.14 | 14.26 | 14.26 | 14.26 | 14.26 |
| 3.7 | 14.26 | 14.26 | 14.26 | 14.26 | 14.26 | 14.26 | 14.26 | 14.26 |
| 3.8 | 14.26 | 14.26 | 14.26 | 14.26 | 14.26 | 14.26 | 14.26 | 14.26 |
| 4.1 | 14.26 | 11.66 | 11.72 | 6.20 | 11.46 | 10.99 | 11.71 | 14.26 |
| 4.2 | 14.26 | 13.11 | 13.30 | 10.57 | 13.03 | 12.78 | 13.36 | 14.26 |
| 4.3 | 14.26 | 14.05 | 14.15 | 12.45 | 14.04 | 13.89 | 14.17 | 14.26 |
| 4.4 | 14.26 | 14.26 | 14.26 | 13.47 | 14.26 | 14.26 | 14.26 | 14.26 |
| 4.5 | 14.26 | 14.26 | 14.26 | 13.47 | 14.26 | 14.26 | 14.26 | 14.26 |
| 4.6 | 14.26 | 14.26 | 14.26 | 13.47 | 14.26 | 14.26 | 14.26 | 14.26 |
| 4.7 | 14.26 | 14.26 | 14.26 | 14.13 | 14.26 | 14.26 | 14.26 | 14.26 |
| 4.8 | 14.26 | 14.26 | 14.26 | 14.13 | 14.26 | 14.26 | 14.26 | 14.26 |

Table F4. Predicted seaside damage from BWSim at end of 57 yr life cycle between 2014 and 2071 with SLR scenario 2.

| Alt | Sta 6 | Sta 7 | Sta 8 | Sta 9 | Sta 10 | Sta 11 | Sta 12 | Sta 13 |
|---|---|---|---|---|---|---|---|---|
| 1.1 | 3.1 | 5.1 | 5.9 | 5.9 | 5.2 | 4.7 | 3.8 | 2.9 |
| 1.2 | 2.8 | 4.5 | 5.4 | 5.4 | 4.7 | 4.3 | 3.5 | 2.7 |
| 1.3 | 2.2 | 3.7 | 4.4 | 4.4 | 3.8 | 3.6 | 2.8 | 2.2 |
| 1.4 | 2.0 | 3.4 | 4.0 | 4.0 | 3.5 | 3.3 | 2.5 | 2.0 |
| 1.5 | 1.9 | 3.1 | 3.6 | 3.6 | 3.2 | 3.0 | 2.3 | 1.9 |
| 1.6 | 1.9 | 3.1 | 3.6 | 3.6 | 3.2 | 3.0 | 2.3 | 1.9 |
| 1.7 | 1.7 | 2.8 | 3.3 | 3.3 | 3.0 | 2.7 | 2.1 | 1.8 |
| 1.8 | 1.6 | 2.5 | 3.1 | 3.1 | 2.7 | 2.4 | 1.9 | 1.7 |
| 2.1 | 3.4 | 5.5 | 6.3 | 6.3 | 5.5 | 5.0 | 4.0 | 3.2 |
| 2.2 | 2.7 | 4.4 | 5.3 | 5.3 | 4.6 | 4.2 | 3.4 | 2.6 |
| 2.3 | 2.2 | 3.7 | 4.4 | 4.4 | 3.8 | 3.5 | 2.8 | 2.2 |
| 2.4 | 1.9 | 3.1 | 3.7 | 3.7 | 3.3 | 3.0 | 2.3 | 1.9 |
| 2.5 | 1.9 | 3.1 | 3.7 | 3.7 | 3.3 | 3.0 | 2.3 | 1.9 |
| 2.6 | 1.9 | 3.1 | 3.7 | 3.7 | 3.3 | 3.0 | 2.3 | 1.9 |
| 2.7 | 1.7 | 2.6 | 3.1 | 3.1 | 2.8 | 2.5 | 2.0 | 1.7 |
| 2.8 | 1.7 | 2.6 | 3.1 | 3.1 | 2.8 | 2.5 | 2.0 | 1.7 |
| 3.1 | 3.1 | 5.1 | 5.9 | 5.9 | 5.2 | 4.7 | 3.8 | 2.9 |
| 3.2 | 2.8 | 4.5 | 5.4 | 5.4 | 4.7 | 4.3 | 3.5 | 2.7 |
| 3.3 | 2.2 | 3.7 | 4.4 | 4.4 | 3.8 | 3.6 | 2.8 | 2.2 |
| 3.4 | 2.0 | 3.4 | 4.0 | 4.0 | 3.5 | 3.3 | 2.5 | 2.0 |
| 3.5 | 1.9 | 3.1 | 3.6 | 3.6 | 3.2 | 3.0 | 2.3 | 1.9 |
| 3.6 | 1.9 | 3.1 | 3.6 | 3.6 | 3.2 | 3.0 | 2.3 | 1.9 |
| 3.7 | 1.7 | 2.8 | 3.3 | 3.3 | 3.0 | 2.7 | 2.1 | 1.8 |
| 3.8 | 1.6 | 2.5 | 3.1 | 3.1 | 2.7 | 2.4 | 1.9 | 1.7 |
| 4.1 | 3.4 | 5.5 | 6.3 | 6.3 | 5.5 | 5.0 | 4.0 | 3.2 |
| 4.2 | 2.7 | 4.4 | 5.3 | 5.3 | 4.6 | 4.2 | 3.4 | 2.6 |
| 4.3 | 2.2 | 3.7 | 4.4 | 4.4 | 3.8 | 3.5 | 2.8 | 2.2 |
| 4.4 | 1.9 | 3.1 | 3.7 | 3.7 | 3.3 | 3.0 | 2.3 | 1.9 |
| 4.5 | 1.9 | 3.1 | 3.7 | 3.7 | 3.3 | 3.0 | 2.3 | 1.9 |
| 4.6 | 1.9 | 3.1 | 3.7 | 3.7 | 3.3 | 3.0 | 2.3 | 1.9 |
| 4.7 | 1.7 | 2.6 | 3.1 | 3.1 | 2.8 | 2.5 | 2.0 | 1.7 |
| 4.8 | 1.7 | 2.6 | 3.1 | 3.1 | 2.8 | 2.5 | 2.0 | 1.7 |

Table F5. Predicted leeside damage from BWSim at end of 57 yr life cycle between 2014 and 2071 with SLR scenario 2.

| Alt | Sta 6 | Sta 7 | Sta 8 | Sta 9 | Sta 10 | Sta 11 | Sta 12 | Sta 13 |
|---|---|---|---|---|---|---|---|---|
| 1.1 | 7.8 | 8.3 | 8.9 | 9.2 | 8.0 | 7.6 | 6.8 | 6.2 |
| 1.2 | 6.4 | 6.9 | 7.3 | 7.3 | 6.7 | 6.4 | 5.8 | 5.2 |
| 1.3 | 4.8 | 5.2 | 5.5 | 5.5 | 5.0 | 4.8 | 4.1 | 3.7 |
| 1.4 | 2.0 | 4.4 | 4.8 | 4.8 | 4.4 | 4.2 | 2.1 | 0.0 |
| 1.5 | 0.0 | 4.0 | 4.4 | 4.4 | 4.0 | 0.0 | 0.0 | 0.0 |
| 1.6 | 0.0 | 0.0 | 0.0 | 0.0 | 0.0 | 0.0 | 0.0 | 0.0 |
| 1.7 | 0.0 | 0.0 | 0.0 | 0.0 | 0.0 | 0.0 | 0.0 | 0.0 |
| 1.8 | 0.0 | 0.0 | 0.0 | 0.0 | 0.0 | 0.0 | 0.0 | 0.0 |
| 2.1 | 7.0 | 8.7 | 9.0 | 13.3 | 8.7 | 8.7 | 7.1 | 5.7 |
| 2.2 | 6.0 | 6.3 | 6.5 | 8.5 | 6.3 | 6.0 | 5.3 | 4.5 |
| 2.3 | 4.2 | 4.8 | 5.0 | 5.4 | 4.5 | 4.4 | 3.6 | 1.3 |
| 2.4 | 0.0 | 0.0 | 4.0 | 4.0 | 0.0 | 0.0 | 0.0 | 0.0 |
| 2.5 | 0.0 | 0.0 | 0.0 | 0.0 | 0.0 | 0.0 | 0.0 | 0.0 |
| 2.6 | 0.0 | 0.0 | 0.0 | 0.0 | 0.0 | 0.0 | 0.0 | 0.0 |
| 2.7 | 0.0 | 0.0 | 0.0 | 0.0 | 0.0 | 0.0 | 0.0 | 0.0 |
| 2.8 | 0.0 | 0.0 | 0.0 | 0.0 | 0.0 | 0.0 | 0.0 | 0.0 |
| 3.1 | 3.1 | 3.5 | 3.6 | 5.4 | 3.4 | 3.3 | 3.0 | 2.2 |
| 3.2 | 1.9 | 2.6 | 3.0 | 3.6 | 2.4 | 2.5 | 2.0 | 1.1 |
| 3.3 | 1.0 | 1.1 | 1.3 | 2.1 | 1.1 | 1.1 | 1.0 | 0.2 |
| 3.4 | 0.0 | 1.0 | 1.0 | 1.0 | 1.0 | 1.0 | 0.0 | 0.0 |
| 3.5 | 0.0 | 0.0 | 1.0 | 1.0 | 0.0 | 0.0 | 0.0 | 0.0 |
| 3.6 | 0.0 | 0.0 | 0.0 | 0.0 | 0.0 | 0.0 | 0.0 | 0.0 |
| 3.7 | 0.0 | 0.0 | 0.0 | 0.0 | 0.0 | 0.0 | 0.0 | 0.0 |
| 3.8 | 0.0 | 0.0 | 0.0 | 0.0 | 0.0 | 0.0 | 0.0 | 0.0 |
| 4.1 | 2.3 | 5.2 | 5.4 | 11.0 | 5.2 | 5.1 | 3.9 | 1.8 |
| 4.2 | 1.6 | 3.1 | 3.2 | 5.1 | 3.1 | 3.0 | 1.9 | 1.0 |
| 4.3 | 0.0 | 1.0 | 1.0 | 2.7 | 1.0 | 1.0 | 0.0 | 0.0 |
| 4.4 | 0.0 | 0.0 | 0.0 | 0.0 | 0.0 | 0.0 | 0.0 | 0.0 |
| 4.5 | 0.0 | 0.0 | 0.0 | 0.0 | 0.0 | 0.0 | 0.0 | 0.0 |
| 4.6 | 0.0 | 0.0 | 0.0 | 0.0 | 0.0 | 0.0 | 0.0 | 0.0 |
| 4.7 | 0.0 | 0.0 | 0.0 | 0.0 | 0.0 | 0.0 | 0.0 | 0.0 |
| 4.8 | 0.0 | 0.0 | 0.0 | 0.0 | 0.0 | 0.0 | 0.0 | 0.0 |

Table F6. Predicted free board in feet, MSL, from BWSim at end of 57 yr life cycle between 2014 and 2071 with SLR scenario 2.

| Alt | Sta 6 | Sta 7 | Sta 8 | Sta 9 | Sta 10 | Sta 11 | Sta 12 | Sta 13 |
|---|---|---|---|---|---|---|---|---|
| 1.1 | 8.26 | 8.26 | 8.26 | 8.08 | 8.26 | 8.26 | 8.26 | 8.26 |
| 1.2 | 8.26 | 8.26 | 8.26 | 8.26 | 8.26 | 8.26 | 8.26 | 8.26 |
| 1.3 | 8.26 | 8.26 | 8.26 | 8.26 | 8.26 | 8.26 | 8.26 | 8.26 |
| 1.4 | 8.26 | 8.26 | 8.26 | 8.26 | 8.26 | 8.26 | 8.26 | 8.26 |
| 1.5 | 8.26 | 8.26 | 8.26 | 8.26 | 8.26 | 8.26 | 8.26 | 8.26 |
| 1.6 | 8.26 | 8.26 | 8.26 | 8.26 | 8.26 | 8.26 | 8.26 | 8.26 |
| 1.7 | 8.26 | 8.26 | 8.26 | 8.26 | 8.26 | 8.26 | 8.26 | 8.26 |
| 1.8 | 8.26 | 8.26 | 8.26 | 8.26 | 8.26 | 8.26 | 8.26 | 8.26 |
| 2.1 | 8.26 | 7.57 | 7.63 | 5.08 | 7.37 | 7.09 | 7.61 | 8.26 |
| 2.2 | 8.26 | 8.26 | 8.26 | 6.98 | 8.19 | 8.19 | 8.26 | 8.26 |
| 2.3 | 8.26 | 8.26 | 8.26 | 7.90 | 8.26 | 8.26 | 8.26 | 8.26 |
| 2.4 | 8.26 | 8.26 | 8.26 | 8.26 | 8.26 | 8.26 | 8.26 | 8.26 |
| 2.5 | 8.26 | 8.26 | 8.26 | 8.26 | 8.26 | 8.26 | 8.26 | 8.26 |
| 2.6 | 8.26 | 8.26 | 8.26 | 8.26 | 8.26 | 8.26 | 8.26 | 8.26 |
| 2.7 | 8.26 | 8.26 | 8.26 | 8.26 | 8.26 | 8.26 | 8.26 | 8.26 |
| 2.8 | 8.26 | 8.26 | 8.26 | 8.26 | 8.26 | 8.26 | 8.26 | 8.26 |
| 3.1 | 14.26 | 13.95 | 14.23 | 12.73 | 13.94 | 13.76 | 13.73 | 14.26 |
| 3.2 | 14.26 | 14.22 | 14.26 | 13.05 | 14.25 | 14.01 | 13.96 | 14.26 |
| 3.3 | 14.26 | 14.26 | 14.26 | 13.63 | 14.26 | 14.26 | 14.26 | 14.26 |
| 3.4 | 14.26 | 14.26 | 14.26 | 13.90 | 14.26 | 14.26 | 14.26 | 14.26 |
| 3.5 | 14.26 | 14.26 | 14.26 | 14.14 | 14.26 | 14.26 | 14.26 | 14.26 |
| 3.6 | 14.26 | 14.26 | 14.26 | 14.14 | 14.26 | 14.26 | 14.26 | 14.26 |
| 3.7 | 14.26 | 14.26 | 14.26 | 14.26 | 14.26 | 14.26 | 14.26 | 14.26 |
| 3.8 | 14.26 | 14.26 | 14.26 | 14.26 | 14.26 | 14.26 | 14.26 | 14.26 |
| 4.1 | 14.26 | 11.62 | 11.70 | 6.06 | 11.39 | 10.99 | 11.68 | 14.26 |
| 4.2 | 14.26 | 13.10 | 13.29 | 10.58 | 13.02 | 12.72 | 13.31 | 14.26 |
| 4.3 | 14.26 | 14.04 | 14.14 | 12.39 | 14.03 | 13.88 | 14.17 | 14.26 |
| 4.4 | 14.26 | 14.26 | 14.26 | 13.46 | 14.26 | 14.26 | 14.26 | 14.26 |
| 4.5 | 14.26 | 14.26 | 14.26 | 13.46 | 14.26 | 14.26 | 14.26 | 14.26 |
| 4.6 | 14.26 | 14.26 | 14.26 | 13.46 | 14.26 | 14.26 | 14.26 | 14.26 |
| 4.7 | 14.26 | 14.26 | 14.26 | 14.13 | 14.26 | 14.26 | 14.26 | 14.26 |
| 4.8 | 14.26 | 14.26 | 14.26 | 14.13 | 14.26 | 14.26 | 14.26 | 14.26 |

Table F7. Predicted seaside damage from BWSim at end of 57 yr life cycle between 2014 and 2071 with SLR scenario 3.

| Alt | Sta 6 | Sta 7 | Sta 8 | Sta 9 | Sta 10 | Sta 11 | Sta 12 | Sta 13 |
|---|---|---|---|---|---|---|---|---|
| 1.1 | 3.2 | 5.1 | 6.0 | 6.0 | 5.2 | 4.7 | 3.8 | 3.0 |
| 1.2 | 2.8 | 4.5 | 5.4 | 5.4 | 4.7 | 4.3 | 3.5 | 2.7 |
| 1.3 | 2.3 | 3.7 | 4.4 | 4.4 | 3.9 | 3.6 | 2.8 | 2.2 |
| 1.4 | 2.1 | 3.4 | 4.0 | 4.0 | 3.5 | 3.3 | 2.6 | 2.0 |
| 1.5 | 1.9 | 3.1 | 3.6 | 3.6 | 3.3 | 3.0 | 2.3 | 1.9 |
| 1.6 | 1.9 | 3.1 | 3.6 | 3.6 | 3.3 | 3.0 | 2.3 | 1.9 |
| 1.7 | 1.7 | 2.8 | 3.3 | 3.3 | 3.0 | 2.7 | 2.1 | 1.8 |
| 1.8 | 1.6 | 2.5 | 3.1 | 3.1 | 2.7 | 2.4 | 1.9 | 1.7 |
| 2.1 | 3.5 | 5.5 | 6.3 | 6.3 | 5.5 | 5.0 | 4.0 | 3.2 |
| 2.2 | 2.8 | 4.4 | 5.3 | 5.3 | 4.6 | 4.2 | 3.4 | 2.6 |
| 2.3 | 2.3 | 3.7 | 4.4 | 4.4 | 3.8 | 3.6 | 2.8 | 2.2 |
| 2.4 | 1.9 | 3.1 | 3.7 | 3.7 | 3.3 | 3.0 | 2.4 | 1.9 |
| 2.5 | 1.9 | 3.1 | 3.7 | 3.7 | 3.3 | 3.0 | 2.4 | 1.9 |
| 2.6 | 1.9 | 3.1 | 3.7 | 3.7 | 3.3 | 3.0 | 2.4 | 1.9 |
| 2.7 | 1.7 | 2.6 | 3.1 | 3.1 | 2.8 | 2.5 | 2.0 | 1.7 |
| 2.8 | 1.7 | 2.6 | 3.1 | 3.1 | 2.8 | 2.5 | 2.0 | 1.7 |
| 3.1 | 3.2 | 5.1 | 6.0 | 6.0 | 5.2 | 4.7 | 3.8 | 3.0 |
| 3.2 | 2.8 | 4.5 | 5.4 | 5.4 | 4.7 | 4.3 | 3.5 | 2.7 |
| 3.3 | 2.3 | 3.7 | 4.4 | 4.4 | 3.9 | 3.6 | 2.8 | 2.2 |
| 3.4 | 2.1 | 3.4 | 4.0 | 4.0 | 3.5 | 3.3 | 2.6 | 2.0 |
| 3.5 | 1.9 | 3.1 | 3.6 | 3.6 | 3.3 | 3.0 | 2.3 | 1.9 |
| 3.6 | 1.9 | 3.1 | 3.6 | 3.6 | 3.3 | 3.0 | 2.3 | 1.9 |
| 3.7 | 1.7 | 2.8 | 3.3 | 3.3 | 3.0 | 2.7 | 2.1 | 1.8 |
| 3.8 | 1.6 | 2.5 | 3.1 | 3.1 | 2.7 | 2.4 | 1.9 | 1.7 |
| 4.1 | 3.5 | 5.5 | 6.3 | 6.3 | 5.5 | 5.0 | 4.0 | 3.2 |
| 4.2 | 2.8 | 4.4 | 5.3 | 5.3 | 4.6 | 4.2 | 3.4 | 2.6 |
| 4.3 | 2.3 | 3.7 | 4.4 | 4.4 | 3.8 | 3.6 | 2.8 | 2.2 |
| 4.4 | 1.9 | 3.1 | 3.7 | 3.7 | 3.3 | 3.0 | 2.4 | 1.9 |
| 4.5 | 1.9 | 3.1 | 3.7 | 3.7 | 3.3 | 3.0 | 2.4 | 1.9 |
| 4.6 | 1.9 | 3.1 | 3.7 | 3.7 | 3.3 | 3.0 | 2.4 | 1.9 |
| 4.7 | 1.7 | 2.6 | 3.1 | 3.1 | 2.8 | 2.5 | 2.0 | 1.7 |
| 4.8 | 1.7 | 2.6 | 3.1 | 3.1 | 2.8 | 2.5 | 2.0 | 1.7 |

Table F8. Predicted leeside damage from BWSim at end of 57 yr life cycle between 2014 and 2071 with SLR scenario 3.

| Alt | Sta 6 | Sta 7 | Sta 8 | Sta 9 | Sta 10 | Sta 11 | Sta 12 | Sta 13 |
|---|---|---|---|---|---|---|---|---|
| 1.1 | 8.0 | 8.5 | 9.1 | 9.6 | 8.3 | 7.9 | 7.0 | 6.4 |
| 1.2 | 6.6 | 7.2 | 7.4 | 7.4 | 6.9 | 6.5 | 5.9 | 5.4 |
| 1.3 | 5.2 | 5.4 | 5.6 | 5.6 | 5.2 | 5.0 | 4.3 | 3.7 |
| 1.4 | 2.2 | 4.7 | 4.9 | 4.9 | 4.4 | 4.3 | 2.2 | 0.0 |
| 1.5 | 0.0 | 4.3 | 4.5 | 4.5 | 4.3 | 2.2 | 0.0 | 0.0 |
| 1.6 | 0.0 | 0.0 | 0.0 | 0.0 | 0.0 | 0.0 | 0.0 | 0.0 |
| 1.7 | 0.0 | 0.0 | 0.0 | 0.0 | 0.0 | 0.0 | 0.0 | 0.0 |
| 1.8 | 0.0 | 0.0 | 0.0 | 0.0 | 0.0 | 0.0 | 0.0 | 0.0 |
| 2.1 | 7.3 | 9.0 | 9.4 | 13.8 | 9.1 | 9.0 | 7.3 | 5.8 |
| 2.2 | 6.1 | 6.6 | 6.8 | 8.8 | 6.4 | 6.1 | 5.5 | 4.7 |
| 2.3 | 4.5 | 4.9 | 5.1 | 5.5 | 4.8 | 4.5 | 3.7 | 1.7 |
| 2.4 | 0.0 | 0.0 | 4.3 | 4.3 | 0.0 | 0.0 | 0.0 | 0.0 |
| 2.5 | 0.0 | 0.0 | 0.0 | 0.0 | 0.0 | 0.0 | 0.0 | 0.0 |
| 2.6 | 0.0 | 0.0 | 0.0 | 0.0 | 0.0 | 0.0 | 0.0 | 0.0 |
| 2.7 | 0.0 | 0.0 | 0.0 | 0.0 | 0.0 | 0.0 | 0.0 | 0.0 |
| 2.8 | 0.0 | 0.0 | 0.0 | 0.0 | 0.0 | 0.0 | 0.0 | 0.0 |
| 3.1 | 3.1 | 3.8 | 3.9 | 5.6 | 3.6 | 3.5 | 3.1 | 2.3 |
| 3.2 | 2.2 | 2.8 | 3.0 | 3.9 | 2.4 | 2.6 | 2.1 | 1.1 |
| 3.3 | 1.0 | 1.1 | 1.5 | 2.5 | 1.1 | 1.1 | 1.0 | 0.2 |
| 3.4 | 0.0 | 1.0 | 1.0 | 1.3 | 1.0 | 1.0 | 0.0 | 0.0 |
| 3.5 | 0.0 | 0.0 | 1.0 | 1.0 | 0.0 | 0.0 | 0.0 | 0.0 |
| 3.6 | 0.0 | 0.0 | 0.0 | 0.0 | 0.0 | 0.0 | 0.0 | 0.0 |
| 3.7 | 0.0 | 0.0 | 0.0 | 0.0 | 0.0 | 0.0 | 0.0 | 0.0 |
| 3.8 | 0.0 | 0.0 | 0.0 | 0.0 | 0.0 | 0.0 | 0.0 | 0.0 |
| 4.1 | 2.7 | 5.4 | 5.6 | 11.3 | 5.3 | 5.3 | 4.0 | 2.1 |
| 4.2 | 1.6 | 3.2 | 3.2 | 5.2 | 3.1 | 3.0 | 2.1 | 1.1 |
| 4.3 | 0.0 | 1.0 | 1.0 | 2.8 | 1.0 | 1.0 | 0.0 | 0.0 |
| 4.4 | 0.0 | 0.0 | 0.0 | 0.0 | 0.0 | 0.0 | 0.0 | 0.0 |
| 4.5 | 0.0 | 0.0 | 0.0 | 0.0 | 0.0 | 0.0 | 0.0 | 0.0 |
| 4.6 | 0.0 | 0.0 | 0.0 | 0.0 | 0.0 | 0.0 | 0.0 | 0.0 |
| 4.7 | 0.0 | 0.0 | 0.0 | 0.0 | 0.0 | 0.0 | 0.0 | 0.0 |
| 4.8 | 0.0 | 0.0 | 0.0 | 0.0 | 0.0 | 0.0 | 0.0 | 0.0 |

Table F9. Predicted free board in feet, MSL, from BWSim at end of 57 yr life cycle between 2014 and 2071 with SLR scenario 3.

| Alt | Sta 6 | Sta 7 | Sta 8 | Sta 9 | Sta 10 | Sta 11 | Sta 12 | Sta 13 |
|---|---|---|---|---|---|---|---|---|
| 1.1 | 8.26 | 8.26 | 8.26 | 8.08 | 8.26 | 8.26 | 8.26 | 8.26 |
| 1.2 | 8.26 | 8.26 | 8.26 | 8.26 | 8.26 | 8.26 | 8.26 | 8.26 |
| 1.3 | 8.26 | 8.26 | 8.26 | 8.26 | 8.26 | 8.26 | 8.26 | 8.26 |
| 1.4 | 8.26 | 8.26 | 8.26 | 8.26 | 8.26 | 8.26 | 8.26 | 8.26 |
| 1.5 | 8.26 | 8.26 | 8.26 | 8.26 | 8.26 | 8.26 | 8.26 | 8.26 |
| 1.6 | 8.26 | 8.26 | 8.26 | 8.26 | 8.26 | 8.26 | 8.26 | 8.26 |
| 1.7 | 8.26 | 8.26 | 8.26 | 8.26 | 8.26 | 8.26 | 8.26 | 8.26 |
| 1.8 | 8.26 | 8.26 | 8.26 | 8.26 | 8.26 | 8.26 | 8.26 | 8.26 |
| 2.1 | 8.26 | 7.57 | 7.63 | 5.06 | 7.37 | 7.06 | 7.57 | 8.26 |
| 2.2 | 8.26 | 8.26 | 8.26 | 6.94 | 8.19 | 8.19 | 8.26 | 8.26 |
| 2.3 | 8.26 | 8.26 | 8.26 | 7.90 | 8.26 | 8.26 | 8.26 | 8.26 |
| 2.4 | 8.26 | 8.26 | 8.26 | 8.26 | 8.26 | 8.26 | 8.26 | 8.26 |
| 2.5 | 8.26 | 8.26 | 8.26 | 8.26 | 8.26 | 8.26 | 8.26 | 8.26 |
| 2.6 | 8.26 | 8.26 | 8.26 | 8.26 | 8.26 | 8.26 | 8.26 | 8.26 |
| 2.7 | 8.26 | 8.26 | 8.26 | 8.26 | 8.26 | 8.26 | 8.26 | 8.26 |
| 2.8 | 8.26 | 8.26 | 8.26 | 8.26 | 8.26 | 8.26 | 8.26 | 8.26 |
| 3.1 | 14.26 | 13.95 | 14.23 | 12.73 | 13.93 | 13.76 | 13.73 | 14.26 |
| 3.2 | 14.26 | 14.22 | 14.26 | 13.05 | 14.25 | 14.01 | 13.96 | 14.26 |
| 3.3 | 14.26 | 14.26 | 14.26 | 13.63 | 14.26 | 14.26 | 14.26 | 14.26 |
| 3.4 | 14.26 | 14.26 | 14.26 | 13.90 | 14.26 | 14.26 | 14.26 | 14.26 |
| 3.5 | 14.26 | 14.26 | 14.26 | 14.14 | 14.26 | 14.26 | 14.26 | 14.26 |
| 3.6 | 14.26 | 14.26 | 14.26 | 14.14 | 14.26 | 14.26 | 14.26 | 14.26 |
| 3.7 | 14.26 | 14.26 | 14.26 | 14.26 | 14.26 | 14.26 | 14.26 | 14.26 |
| 3.8 | 14.26 | 14.26 | 14.26 | 14.26 | 14.26 | 14.26 | 14.26 | 14.26 |
| 4.1 | 14.26 | 11.59 | 11.70 | 5.97 | 11.35 | 10.97 | 11.65 | 14.26 |
| 4.2 | 14.26 | 13.10 | 13.29 | 10.59 | 13.02 | 12.69 | 13.28 | 14.26 |
| 4.3 | 14.26 | 14.04 | 14.14 | 12.36 | 14.03 | 13.88 | 14.17 | 14.26 |
| 4.4 | 14.26 | 14.26 | 14.26 | 13.46 | 14.26 | 14.26 | 14.26 | 14.26 |
| 4.5 | 14.26 | 14.26 | 14.26 | 13.46 | 14.26 | 14.26 | 14.26 | 14.26 |
| 4.6 | 14.26 | 14.26 | 14.26 | 13.46 | 14.26 | 14.26 | 14.26 | 14.26 |
| 4.7 | 14.26 | 14.26 | 14.26 | 14.13 | 14.26 | 14.26 | 14.26 | 14.26 |
| 4.8 | 14.26 | 14.26 | 14.26 | 14.13 | 14.26 | 14.26 | 14.26 | 14.26 |

Table F10. Predicted seaside damage from BWSim at end of 57 yr life cycle between 2014 and 2071 with SLR scenario 4.

| Alt | Sta 6 | Sta 7 | Sta 8 | Sta 9 | Sta 10 | Sta 11 | Sta 12 | Sta 13 |
|---|---|---|---|---|---|---|---|---|
| 1.1 | 3.3 | 5.2 | 6.0 | 6.0 | 5.2 | 4.7 | 3.9 | 3.0 |
| 1.2 | 2.9 | 4.6 | 5.4 | 5.4 | 4.7 | 4.3 | 3.5 | 2.7 |
| 1.3 | 2.3 | 3.8 | 4.4 | 4.4 | 3.9 | 3.6 | 2.9 | 2.3 |
| 1.4 | 2.1 | 3.4 | 4.0 | 4.0 | 3.5 | 3.3 | 2.6 | 2.0 |
| 1.5 | 2.0 | 3.1 | 3.7 | 3.7 | 3.3 | 3.0 | 2.4 | 1.9 |
| 1.6 | 2.0 | 3.1 | 3.7 | 3.7 | 3.3 | 3.0 | 2.4 | 1.9 |
| 1.7 | 1.8 | 2.9 | 3.4 | 3.4 | 3.0 | 2.8 | 2.1 | 1.8 |
| 1.8 | 1.7 | 2.5 | 3.1 | 3.1 | 2.8 | 2.4 | 2.0 | 1.7 |
| 2.1 | 3.6 | 5.5 | 6.4 | 6.4 | 5.6 | 5.0 | 4.1 | 3.3 |
| 2.2 | 2.8 | 4.5 | 5.3 | 5.3 | 4.6 | 4.2 | 3.4 | 2.6 |
| 2.3 | 2.3 | 3.7 | 4.4 | 4.4 | 3.9 | 3.6 | 2.8 | 2.3 |
| 2.4 | 2.0 | 3.2 | 3.7 | 3.7 | 3.3 | 3.1 | 2.4 | 2.0 |
| 2.5 | 2.0 | 3.2 | 3.7 | 3.7 | 3.3 | 3.1 | 2.4 | 2.0 |
| 2.6 | 2.0 | 3.2 | 3.7 | 3.7 | 3.3 | 3.1 | 2.4 | 2.0 |
| 2.7 | 1.7 | 2.6 | 3.2 | 3.2 | 2.9 | 2.6 | 2.0 | 1.7 |
| 2.8 | 1.7 | 2.6 | 3.2 | 3.2 | 2.9 | 2.6 | 2.0 | 1.7 |
| 3.1 | 3.3 | 5.2 | 6.0 | 6.0 | 5.2 | 4.7 | 3.9 | 3.0 |
| 3.2 | 2.9 | 4.6 | 5.4 | 5.4 | 4.7 | 4.3 | 3.5 | 2.7 |
| 3.3 | 2.3 | 3.8 | 4.4 | 4.4 | 3.9 | 3.6 | 2.9 | 2.3 |
| 3.4 | 2.1 | 3.4 | 4.0 | 4.0 | 3.5 | 3.3 | 2.6 | 2.0 |
| 3.5 | 2.0 | 3.1 | 3.7 | 3.7 | 3.3 | 3.0 | 2.4 | 1.9 |
| 3.6 | 2.0 | 3.1 | 3.7 | 3.7 | 3.3 | 3.0 | 2.4 | 1.9 |
| 3.7 | 1.8 | 2.9 | 3.4 | 3.4 | 3.0 | 2.8 | 2.1 | 1.8 |
| 3.8 | 1.7 | 2.5 | 3.1 | 3.1 | 2.8 | 2.4 | 2.0 | 1.7 |
| 4.1 | 3.6 | 5.5 | 6.4 | 6.4 | 5.6 | 5.0 | 4.1 | 3.3 |
| 4.2 | 2.8 | 4.5 | 5.3 | 5.3 | 4.6 | 4.2 | 3.4 | 2.6 |
| 4.3 | 2.3 | 3.7 | 4.4 | 4.4 | 3.9 | 3.6 | 2.8 | 2.3 |
| 4.4 | 2.0 | 3.2 | 3.7 | 3.7 | 3.3 | 3.1 | 2.4 | 2.0 |
| 4.5 | 2.0 | 3.2 | 3.7 | 3.7 | 3.3 | 3.1 | 2.4 | 2.0 |
| 4.6 | 2.0 | 3.2 | 3.7 | 3.7 | 3.3 | 3.1 | 2.4 | 2.0 |
| 4.7 | 1.7 | 2.6 | 3.2 | 3.2 | 2.9 | 2.6 | 2.0 | 1.7 |
| 4.8 | 1.7 | 2.6 | 3.2 | 3.2 | 2.9 | 2.6 | 2.0 | 1.7 |

Table F11. Predicted leeside damage from BWSim at end of 57 yr life cycle between 2014 and 2071 with SLR scenario 4.

| Alt | Sta 6 | Sta 7 | Sta 8 | Sta 9 | Sta 10 | Sta 11 | Sta 12 | Sta 13 |
|---|---|---|---|---|---|---|---|---|
| 1.1 | 8.8 | 9.5 | 10.0 | 10.3 | 9.2 | 8.4 | 7.6 | 6.9 |
| 1.2 | 7.3 | 7.8 | 8.0 | 8.0 | 7.5 | 7.2 | 6.5 | 5.9 |
| 1.3 | 5.6 | 6.0 | 6.2 | 6.2 | 5.7 | 5.4 | 4.9 | 4.2 |
| 1.4 | 3.1 | 5.2 | 5.4 | 5.4 | 5.0 | 4.9 | 2.8 | 2.2 |
| 1.5 | 2.8 | 4.8 | 5.0 | 5.0 | 4.6 | 2.8 | 1.8 | 0.0 |
| 1.6 | 0.0 | 2.7 | 3.2 | 3.2 | 2.3 | 2.2 | 0.0 | 0.0 |
| 1.7 | 0.0 | 0.0 | 0.0 | 0.0 | 0.0 | 0.0 | 0.0 | 0.0 |
| 1.8 | 0.0 | 0.0 | 0.0 | 0.0 | 0.0 | 0.0 | 0.0 | 0.0 |
| 2.1 | 8.0 | 10.0 | 10.3 | 15.1 | 10.1 | 9.9 | 8.1 | 6.4 |
| 2.2 | 6.7 | 7.1 | 7.4 | 9.8 | 7.0 | 6.7 | 6.0 | 5.3 |
| 2.3 | 5.3 | 5.4 | 5.7 | 6.1 | 5.2 | 5.1 | 4.4 | 2.4 |
| 2.4 | 0.0 | 2.9 | 4.9 | 4.9 | 4.5 | 2.2 | 1.8 | 0.0 |
| 2.5 | 0.0 | 0.0 | 2.2 | 2.2 | 0.0 | 0.0 | 0.0 | 0.0 |
| 2.6 | 0.0 | 0.0 | 0.0 | 0.0 | 0.0 | 0.0 | 0.0 | 0.0 |
| 2.7 | 0.0 | 0.0 | 0.0 | 0.0 | 0.0 | 0.0 | 0.0 | 0.0 |
| 2.8 | 0.0 | 0.0 | 0.0 | 0.0 | 0.0 | 0.0 | 0.0 | 0.0 |
| 3.1 | 3.5 | 4.3 | 4.3 | 5.9 | 4.2 | 4.1 | 3.5 | 2.5 |
| 3.2 | 2.4 | 2.9 | 3.2 | 4.4 | 2.6 | 2.6 | 2.4 | 1.7 |
| 3.3 | 1.7 | 1.6 | 1.9 | 2.6 | 1.7 | 1.9 | 1.5 | 0.2 |
| 3.4 | 0.2 | 1.0 | 1.5 | 1.7 | 1.3 | 1.3 | 0.2 | 0.0 |
| 3.5 | 0.0 | 0.2 | 1.0 | 1.0 | 0.2 | 0.2 | 0.0 | 0.0 |
| 3.6 | 0.0 | 0.0 | 0.0 | 0.2 | 0.0 | 0.0 | 0.0 | 0.0 |
| 3.7 | 0.0 | 0.0 | 0.0 | 0.0 | 0.0 | 0.0 | 0.0 | 0.0 |
| 3.8 | 0.0 | 0.0 | 0.0 | 0.0 | 0.0 | 0.0 | 0.0 | 0.0 |
| 4.1 | 3.0 | 5.9 | 6.1 | 12.4 | 6.0 | 5.9 | 4.6 | 2.3 |
| 4.2 | 2.4 | 3.6 | 3.7 | 5.7 | 3.4 | 3.5 | 2.3 | 1.5 |
| 4.3 | 0.2 | 1.5 | 1.5 | 3.2 | 1.5 | 1.5 | 0.2 | 0.0 |
| 4.4 | 0.0 | 0.0 | 0.0 | 0.9 | 0.0 | 0.0 | 0.0 | 0.0 |
| 4.5 | 0.0 | 0.0 | 0.0 | 0.0 | 0.0 | 0.0 | 0.0 | 0.0 |
| 4.6 | 0.0 | 0.0 | 0.0 | 0.0 | 0.0 | 0.0 | 0.0 | 0.0 |
| 4.7 | 0.0 | 0.0 | 0.0 | 0.0 | 0.0 | 0.0 | 0.0 | 0.0 |
| 4.8 | 0.0 | 0.0 | 0.0 | 0.0 | 0.0 | 0.0 | 0.0 | 0.0 |

Table F12. Predicted free board in feet, MSL, from BWSim at end of 57 yr life cycle between 2014 and 2071 with SLR scenario 4.

| Alt | Sta 6 | Sta 7 | Sta 8 | Sta 9 | Sta 10 | Sta 11 | Sta 12 | Sta 13 |
|---|---|---|---|---|---|---|---|---|
| 1.1 | 8.26 | 8.26 | 8.26 | 8.08 | 8.26 | 8.26 | 8.26 | 8.26 |
| 1.2 | 8.26 | 8.26 | 8.26 | 8.26 | 8.26 | 8.26 | 8.26 | 8.26 |
| 1.3 | 8.26 | 8.26 | 8.26 | 8.26 | 8.26 | 8.26 | 8.26 | 8.26 |
| 1.4 | 8.26 | 8.26 | 8.26 | 8.26 | 8.26 | 8.26 | 8.26 | 8.26 |
| 1.5 | 8.26 | 8.26 | 8.26 | 8.26 | 8.26 | 8.26 | 8.26 | 8.26 |
| 1.6 | 8.26 | 8.26 | 8.26 | 8.26 | 8.26 | 8.26 | 8.26 | 8.26 |
| 1.7 | 8.26 | 8.26 | 8.26 | 8.26 | 8.26 | 8.26 | 8.26 | 8.26 |
| 1.8 | 8.26 | 8.26 | 8.26 | 8.26 | 8.26 | 8.26 | 8.26 | 8.26 |
| 2.1 | 8.26 | 7.56 | 7.62 | 5.05 | 7.31 | 6.98 | 7.50 | 8.26 |
| 2.2 | 8.26 | 8.26 | 8.26 | 6.87 | 8.19 | 8.18 | 8.26 | 8.26 |
| 2.3 | 8.26 | 8.26 | 8.26 | 7.90 | 8.26 | 8.26 | 8.26 | 8.26 |
| 2.4 | 8.26 | 8.26 | 8.26 | 8.26 | 8.26 | 8.26 | 8.26 | 8.26 |
| 2.5 | 8.26 | 8.26 | 8.26 | 8.26 | 8.26 | 8.26 | 8.26 | 8.26 |
| 2.6 | 8.26 | 8.26 | 8.26 | 8.26 | 8.26 | 8.26 | 8.26 | 8.26 |
| 2.7 | 8.26 | 8.26 | 8.26 | 8.26 | 8.26 | 8.26 | 8.26 | 8.26 |
| 2.8 | 8.26 | 8.26 | 8.26 | 8.26 | 8.26 | 8.26 | 8.26 | 8.26 |
| 3.1 | 14.26 | 13.95 | 14.22 | 12.73 | 13.93 | 13.76 | 13.73 | 14.26 |
| 3.2 | 14.26 | 14.22 | 14.26 | 13.05 | 14.25 | 14.01 | 13.96 | 14.26 |
| 3.3 | 14.26 | 14.26 | 14.26 | 13.63 | 14.26 | 14.26 | 14.26 | 14.26 |
| 3.4 | 14.26 | 14.26 | 14.26 | 13.89 | 14.26 | 14.26 | 14.26 | 14.26 |
| 3.5 | 14.26 | 14.26 | 14.26 | 14.14 | 14.26 | 14.26 | 14.26 | 14.26 |
| 3.6 | 14.26 | 14.26 | 14.26 | 14.14 | 14.26 | 14.26 | 14.26 | 14.26 |
| 3.7 | 14.26 | 14.26 | 14.26 | 14.26 | 14.26 | 14.26 | 14.26 | 14.26 |
| 3.8 | 14.26 | 14.26 | 14.26 | 14.26 | 14.26 | 14.26 | 14.26 | 14.26 |
| 4.1 | 14.26 | 11.56 | 11.63 | 5.83 | 11.26 | 10.90 | 11.57 | 14.26 |
| 4.2 | 14.26 | 13.09 | 13.28 | 10.62 | 12.95 | 12.61 | 13.22 | 14.26 |
| 4.3 | 14.26 | 14.04 | 14.13 | 12.29 | 14.02 | 13.88 | 14.17 | 14.26 |
| 4.4 | 14.26 | 14.26 | 14.26 | 13.45 | 14.26 | 14.26 | 14.26 | 14.26 |
| 4.5 | 14.26 | 14.26 | 14.26 | 13.45 | 14.26 | 14.26 | 14.26 | 14.26 |
| 4.6 | 14.26 | 14.26 | 14.26 | 13.45 | 14.26 | 14.26 | 14.26 | 14.26 |
| 4.7 | 14.26 | 14.26 | 14.26 | 14.12 | 14.26 | 14.26 | 14.26 | 14.26 |
| 4.8 | 14.26 | 14.26 | 14.26 | 14.12 | 14.26 | 14.26 | 14.26 | 14.26 |

Table F13. Predicted seaside damage from BWSim at end of 57 yr life cycle between 2014 and 2071 with SLR scenario 5.

| Alt | Sta 6 | Sta 7 | Sta 8 | Sta 9 | Sta 10 | Sta 11 | Sta 12 | Sta 13 |
|---|---|---|---|---|---|---|---|---|
| 1.1 | 3.3 | 5.2 | 6.0 | 6.0 | 5.3 | 4.8 | 3.9 | 3.0 |
| 1.2 | 3.0 | 4.6 | 5.4 | 5.4 | 4.8 | 4.3 | 3.5 | 2.7 |
| 1.3 | 2.4 | 3.8 | 4.5 | 4.5 | 3.9 | 3.6 | 2.9 | 2.3 |
| 1.4 | 2.1 | 3.4 | 4.0 | 4.0 | 3.6 | 3.4 | 2.6 | 2.0 |
| 1.5 | 2.0 | 3.1 | 3.7 | 3.7 | 3.3 | 3.0 | 2.4 | 2.0 |
| 1.6 | 2.0 | 3.1 | 3.7 | 3.7 | 3.3 | 3.0 | 2.4 | 2.0 |
| 1.7 | 1.8 | 2.9 | 3.4 | 3.4 | 3.1 | 2.8 | 2.2 | 1.8 |
| 1.8 | 1.7 | 2.6 | 3.1 | 3.1 | 2.8 | 2.5 | 2.0 | 1.7 |
| 2.1 | 3.6 | 5.6 | 6.4 | 6.4 | 5.6 | 5.1 | 4.1 | 3.3 |
| 2.2 | 2.9 | 4.5 | 5.3 | 5.3 | 4.7 | 4.2 | 3.5 | 2.7 |
| 2.3 | 2.4 | 3.8 | 4.4 | 4.4 | 3.9 | 3.6 | 2.9 | 2.3 |
| 2.4 | 2.0 | 3.2 | 3.7 | 3.7 | 3.3 | 3.1 | 2.4 | 2.0 |
| 2.5 | 2.0 | 3.2 | 3.7 | 3.7 | 3.3 | 3.1 | 2.4 | 2.0 |
| 2.6 | 2.0 | 3.2 | 3.7 | 3.7 | 3.3 | 3.1 | 2.4 | 2.0 |
| 2.7 | 1.7 | 2.7 | 3.2 | 3.2 | 2.9 | 2.6 | 2.0 | 1.7 |
| 2.8 | 1.7 | 2.7 | 3.2 | 3.2 | 2.9 | 2.6 | 2.0 | 1.7 |
| 3.1 | 3.3 | 5.2 | 6.0 | 6.0 | 5.3 | 4.8 | 3.9 | 3.0 |
| 3.2 | 3.0 | 4.6 | 5.4 | 5.4 | 4.8 | 4.3 | 3.5 | 2.7 |
| 3.3 | 2.4 | 3.8 | 4.5 | 4.5 | 3.9 | 3.6 | 2.9 | 2.3 |
| 3.4 | 2.1 | 3.4 | 4.0 | 4.0 | 3.6 | 3.4 | 2.6 | 2.0 |
| 3.5 | 2.0 | 3.1 | 3.7 | 3.7 | 3.3 | 3.0 | 2.4 | 2.0 |
| 3.6 | 2.0 | 3.1 | 3.7 | 3.7 | 3.3 | 3.0 | 2.4 | 2.0 |
| 3.7 | 1.8 | 2.9 | 3.4 | 3.4 | 3.1 | 2.8 | 2.2 | 1.8 |
| 3.8 | 1.7 | 2.6 | 3.1 | 3.1 | 2.8 | 2.5 | 2.0 | 1.7 |
| 4.1 | 3.6 | 5.6 | 6.4 | 6.4 | 5.6 | 5.1 | 4.1 | 3.3 |
| 4.2 | 2.9 | 4.5 | 5.3 | 5.3 | 4.7 | 4.2 | 3.5 | 2.7 |
| 4.3 | 2.4 | 3.8 | 4.4 | 4.4 | 3.9 | 3.6 | 2.9 | 2.3 |
| 4.4 | 2.0 | 3.2 | 3.7 | 3.7 | 3.3 | 3.1 | 2.4 | 2.0 |
| 4.5 | 2.0 | 3.2 | 3.7 | 3.7 | 3.3 | 3.1 | 2.4 | 2.0 |
| 4.6 | 2.0 | 3.2 | 3.7 | 3.7 | 3.3 | 3.1 | 2.4 | 2.0 |
| 4.7 | 1.7 | 2.7 | 3.2 | 3.2 | 2.9 | 2.6 | 2.0 | 1.7 |
| 4.8 | 1.7 | 2.7 | 3.2 | 3.2 | 2.9 | 2.6 | 2.0 | 1.7 |

Table F14. Predicted leeside damage from BWSim at end of 57 yr life cycle between 2014 and 2071 with SLR scenario 5.

| Alt | Sta 6 | Sta 7 | Sta 8 | Sta 9 | Sta 10 | Sta 11 | Sta 12 | Sta 13 |
|---|---|---|---|---|---|---|---|---|
| 1.1 | 9.7 | 10.4 | 10.8 | 11.2 | 10.0 | 9.4 | 8.3 | 7.4 |
| 1.2 | 7.9 | 8.4 | 9.0 | 9.0 | 8.2 | 7.7 | 7.0 | 6.6 |
| 1.3 | 6.2 | 6.6 | 6.8 | 6.8 | 6.5 | 6.1 | 5.3 | 4.9 |
| 1.4 | 4.4 | 5.7 | 6.0 | 6.0 | 5.5 | 5.3 | 4.6 | 2.8 |
| 1.5 | 3.4 | 5.3 | 5.5 | 5.5 | 5.0 | 4.9 | 2.8 | 2.2 |
| 1.6 | 3.3 | 3.3 | 3.6 | 3.6 | 3.3 | 3.1 | 2.2 | 0.0 |
| 1.7 | 0.0 | 0.0 | 1.4 | 1.4 | 0.0 | 0.0 | 0.0 | 0.0 |
| 1.8 | 0.0 | 0.0 | 0.0 | 0.0 | 0.0 | 0.0 | 0.0 | 0.0 |
| 2.1 | 9.0 | 11.0 | 11.3 | 16.5 | 11.2 | 11.1 | 9.0 | 7.0 |
| 2.2 | 7.4 | 7.8 | 8.0 | 10.8 | 7.7 | 7.3 | 6.7 | 5.9 |
| 2.3 | 5.8 | 6.0 | 6.3 | 6.8 | 5.9 | 5.6 | 5.0 | 2.9 |
| 2.4 | 3.4 | 5.1 | 5.4 | 5.4 | 5.0 | 3.2 | 2.3 | 2.2 |
| 2.5 | 1.3 | 2.4 | 2.4 | 2.4 | 2.4 | 2.4 | 1.3 | 0.0 |
| 2.6 | 0.0 | 0.0 | 2.4 | 2.4 | 1.3 | 1.3 | 0.0 | 0.0 |
| 2.7 | 0.0 | 0.0 | 0.0 | 0.0 | 0.0 | 0.0 | 0.0 | 0.0 |
| 2.8 | 0.0 | 0.0 | 0.0 | 0.0 | 0.0 | 0.0 | 0.0 | 0.0 |
| 3.1 | 3.9 | 4.6 | 4.7 | 6.6 | 4.5 | 4.4 | 3.7 | 2.9 |
| 3.2 | 2.9 | 3.4 | 3.6 | 4.7 | 3.0 | 3.2 | 2.6 | 2.0 |
| 3.3 | 2.2 | 2.2 | 2.5 | 3.0 | 2.0 | 2.1 | 1.8 | 1.5 |
| 3.4 | 1.2 | 1.7 | 1.8 | 2.1 | 1.7 | 1.7 | 0.9 | 0.2 |
| 3.5 | 0.2 | 0.9 | 1.7 | 1.7 | 0.9 | 0.9 | 0.2 | 0.0 |
| 3.6 | 0.0 | 0.2 | 0.9 | 0.9 | 0.2 | 0.2 | 0.0 | 0.0 |
| 3.7 | 0.0 | 0.0 | 0.0 | 0.0 | 0.0 | 0.0 | 0.0 | 0.0 |
| 3.8 | 0.0 | 0.0 | 0.0 | 0.0 | 0.0 | 0.0 | 0.0 | 0.0 |
| 4.1 | 3.3 | 6.6 | 6.8 | 13.5 | 6.6 | 6.5 | 5.0 | 2.5 |
| 4.2 | 2.7 | 4.1 | 4.2 | 6.5 | 4.1 | 4.0 | 2.7 | 1.8 |
| 4.3 | 1.2 | 1.9 | 2.1 | 3.6 | 1.8 | 2.0 | 0.9 | 0.2 |
| 4.4 | 0.0 | 0.2 | 0.9 | 1.2 | 0.2 | 0.2 | 0.0 | 0.0 |
| 4.5 | 0.0 | 0.0 | 0.2 | 1.2 | 0.0 | 0.0 | 0.0 | 0.0 |
| 4.6 | 0.0 | 0.0 | 0.0 | 0.2 | 0.0 | 0.0 | 0.0 | 0.0 |
| 4.7 | 0.0 | 0.0 | 0.0 | 0.0 | 0.0 | 0.0 | 0.0 | 0.0 |
| 4.8 | 0.0 | 0.0 | 0.0 | 0.0 | 0.0 | 0.0 | 0.0 | 0.0 |

Table F15. Predicted free board in feet, MSL, from BWSim at end of 57 yr life cycle between 2014 and 2071 with SLR scenario 5.

| Alt | Sta 6 | Sta 7 | Sta 8 | Sta 9 | Sta 10 | Sta 11 | Sta 12 | Sta 13 |
|---|---|---|---|---|---|---|---|---|
| 1.1 | 8.26 | 8.26 | 8.26 | 8.08 | 8.26 | 8.26 | 8.26 | 8.26 |
| 1.2 | 8.26 | 8.26 | 8.26 | 8.26 | 8.26 | 8.26 | 8.26 | 8.26 |
| 1.3 | 8.26 | 8.26 | 8.26 | 8.26 | 8.26 | 8.26 | 8.26 | 8.26 |
| 1.4 | 8.26 | 8.26 | 8.26 | 8.26 | 8.26 | 8.26 | 8.26 | 8.26 |
| 1.5 | 8.26 | 8.26 | 8.26 | 8.26 | 8.26 | 8.26 | 8.26 | 8.26 |
| 1.6 | 8.26 | 8.26 | 8.26 | 8.26 | 8.26 | 8.26 | 8.26 | 8.26 |
| 1.7 | 8.26 | 8.26 | 8.26 | 8.26 | 8.26 | 8.26 | 8.26 | 8.26 |
| 1.8 | 8.26 | 8.26 | 8.26 | 8.26 | 8.26 | 8.26 | 8.26 | 8.26 |
| 2.1 | 8.26 | 7.55 | 7.60 | 5.02 | 7.23 | 6.90 | 7.43 | 8.26 |
| 2.2 | 8.26 | 8.25 | 8.26 | 6.80 | 8.18 | 8.18 | 8.26 | 8.26 |
| 2.3 | 8.26 | 8.26 | 8.26 | 7.89 | 8.26 | 8.26 | 8.26 | 8.26 |
| 2.4 | 8.26 | 8.26 | 8.26 | 8.26 | 8.26 | 8.26 | 8.26 | 8.26 |
| 2.5 | 8.26 | 8.26 | 8.26 | 8.26 | 8.26 | 8.26 | 8.26 | 8.26 |
| 2.6 | 8.26 | 8.26 | 8.26 | 8.26 | 8.26 | 8.26 | 8.26 | 8.26 |
| 2.7 | 8.26 | 8.26 | 8.26 | 8.26 | 8.26 | 8.26 | 8.26 | 8.26 |
| 2.8 | 8.26 | 8.26 | 8.26 | 8.26 | 8.26 | 8.26 | 8.26 | 8.26 |
| 3.1 | 14.26 | 13.95 | 14.22 | 12.72 | 13.93 | 13.76 | 13.73 | 14.26 |
| 3.2 | 14.26 | 14.22 | 14.26 | 13.05 | 14.25 | 14.01 | 13.96 | 14.26 |
| 3.3 | 14.26 | 14.26 | 14.26 | 13.63 | 14.26 | 14.26 | 14.26 | 14.26 |
| 3.4 | 14.26 | 14.26 | 14.26 | 13.89 | 14.26 | 14.26 | 14.26 | 14.26 |
| 3.5 | 14.26 | 14.26 | 14.26 | 14.14 | 14.26 | 14.26 | 14.26 | 14.26 |
| 3.6 | 14.26 | 14.26 | 14.26 | 14.14 | 14.26 | 14.26 | 14.26 | 14.26 |
| 3.7 | 14.26 | 14.26 | 14.26 | 14.26 | 14.26 | 14.26 | 14.26 | 14.26 |
| 3.8 | 14.26 | 14.26 | 14.26 | 14.26 | 14.26 | 14.26 | 14.26 | 14.26 |
| 4.1 | 14.26 | 11.48 | 11.56 | 5.75 | 11.17 | 10.78 | 11.50 | 14.26 |
| 4.2 | 14.26 | 13.04 | 13.24 | 10.61 | 12.87 | 12.54 | 13.15 | 14.26 |
| 4.3 | 14.26 | 14.03 | 14.13 | 12.22 | 14.02 | 13.87 | 14.17 | 14.26 |
| 4.4 | 14.26 | 14.26 | 14.26 | 13.45 | 14.26 | 14.26 | 14.26 | 14.26 |
| 4.5 | 14.26 | 14.26 | 14.26 | 13.45 | 14.26 | 14.26 | 14.26 | 14.26 |
| 4.6 | 14.26 | 14.26 | 14.26 | 13.45 | 14.26 | 14.26 | 14.26 | 14.26 |
| 4.7 | 14.26 | 14.26 | 14.26 | 14.12 | 14.26 | 14.26 | 14.26 | 14.26 |
| 4.8 | 14.26 | 14.26 | 14.26 | 14.12 | 14.26 | 14.26 | 14.26 | 14.26 |

Table F16. Predicted mean of peak storm $H_{m0}$ in feet from BWSim at consequence locations over 57 yr life cycle between 2014 and 2071 with SLR scenario 1.

| Alt .RP | 129 | 132 | 135 | 147 | 166 | 170 | 172 | 185 | 195 | 196 | 198 | 203 |
|---|---|---|---|---|---|---|---|---|---|---|---|---|
| 1.1 | 3.0 | 3.4 | 4.0 | 2.2 | 3.3 | 3.7 | 4.4 | 3.7 | 3.8 | 3.4 | 3.6 | 3.4 |
| 1.2 | 3.0 | 3.4 | 4.0 | 2.2 | 3.3 | 3.7 | 4.4 | 3.7 | 3.8 | 3.4 | 3.6 | 3.4 |
| 1.3 | 3.0 | 3.4 | 4.0 | 2.2 | 3.3 | 3.7 | 4.4 | 3.7 | 3.8 | 3.4 | 3.6 | 3.4 |
| 1.4 | 3.0 | 3.4 | 4.0 | 2.2 | 3.3 | 3.7 | 4.4 | 3.7 | 3.8 | 3.4 | 3.6 | 3.4 |
| 1.5 | 3.0 | 3.4 | 4.0 | 2.2 | 3.3 | 3.7 | 4.4 | 3.7 | 3.8 | 3.4 | 3.6 | 3.4 |
| 1.6 | 3.0 | 3.4 | 4.0 | 2.2 | 3.3 | 3.7 | 4.4 | 3.7 | 3.8 | 3.4 | 3.6 | 3.4 |
| 1.7 | 3.0 | 3.4 | 4.0 | 2.2 | 3.3 | 3.7 | 4.4 | 3.7 | 3.8 | 3.4 | 3.6 | 3.4 |
| 1.8 | 3.0 | 3.4 | 4.0 | 2.2 | 3.3 | 3.7 | 4.4 | 3.7 | 3.8 | 3.4 | 3.6 | 3.4 |
| 2.1 | 3.8 | 4.1 | 4.6 | 3.8 | 4.2 | 4.2 | 4.5 | 4.3 | 4.1 | 4.0 | 4.2 | 4.0 |
| 2.2 | 3.7 | 4.0 | 4.6 | 3.8 | 4.2 | 4.2 | 4.5 | 4.3 | 4.1 | 4.0 | 4.1 | 4.0 |
| 2.3 | 3.6 | 4.0 | 4.6 | 3.7 | 4.1 | 4.1 | 4.5 | 4.2 | 4.1 | 3.9 | 4.1 | 3.9 |
| 2.4 | 3.6 | 3.9 | 4.5 | 3.6 | 4.1 | 4.0 | 4.4 | 4.2 | 4.0 | 3.9 | 4.0 | 3.8 |
| 2.5 | 3.6 | 3.9 | 4.5 | 3.6 | 4.1 | 4.0 | 4.4 | 4.2 | 4.0 | 3.9 | 4.0 | 3.8 |
| 2.6 | 3.6 | 3.9 | 4.5 | 3.6 | 4.1 | 4.0 | 4.4 | 4.2 | 4.0 | 3.9 | 4.0 | 3.8 |
| 2.7 | 3.6 | 3.9 | 4.5 | 3.6 | 4.1 | 4.0 | 4.4 | 4.2 | 4.0 | 3.9 | 4.0 | 3.8 |
| 2.8 | 3.5 | 3.8 | 4.4 | 3.4 | 3.9 | 3.9 | 4.4 | 4.1 | 4.0 | 3.8 | 3.9 | 3.7 |
| 3.1 | 2.9 | 3.2 | 3.9 | 1.7 | 3.0 | 3.6 | 4.4 | 3.5 | 3.7 | 3.2 | 3.5 | 3.3 |
| 3.2 | 2.9 | 3.2 | 3.9 | 1.7 | 3.0 | 3.6 | 4.4 | 3.5 | 3.7 | 3.2 | 3.5 | 3.3 |
| 3.3 | 2.9 | 3.2 | 3.9 | 1.6 | 3.0 | 3.6 | 4.4 | 3.5 | 3.7 | 3.2 | 3.5 | 3.3 |
| 3.4 | 2.9 | 3.2 | 3.9 | 1.6 | 3.0 | 3.6 | 4.4 | 3.5 | 3.7 | 3.2 | 3.5 | 3.3 |
| 3.5 | 2.9 | 3.2 | 3.9 | 1.6 | 3.0 | 3.6 | 4.4 | 3.5 | 3.7 | 3.2 | 3.5 | 3.3 |
| 3.6 | 2.9 | 3.2 | 3.9 | 1.6 | 3.0 | 3.6 | 4.4 | 3.5 | 3.7 | 3.2 | 3.5 | 3.3 |
| 3.7 | 2.9 | 3.2 | 3.9 | 1.6 | 3.0 | 3.6 | 4.4 | 3.5 | 3.7 | 3.2 | 3.5 | 3.3 |
| 3.8 | 2.9 | 3.2 | 3.9 | 1.6 | 3.0 | 3.6 | 4.4 | 3.5 | 3.7 | 3.2 | 3.5 | 3.3 |
| 4.1 | 3.8 | 4.0 | 4.6 | 3.8 | 4.2 | 4.2 | 4.5 | 4.3 | 4.1 | 4.0 | 4.2 | 4.0 |
| 4.2 | 3.7 | 4.0 | 4.6 | 3.8 | 4.2 | 4.2 | 4.5 | 4.3 | 4.1 | 4.0 | 4.1 | 3.9 |
| 4.3 | 3.6 | 4.0 | 4.6 | 3.8 | 4.2 | 4.2 | 4.5 | 4.3 | 4.1 | 3.9 | 4.1 | 3.9 |
| 4.4 | 3.5 | 3.9 | 4.5 | 3.6 | 4.1 | 4.0 | 4.4 | 4.2 | 4.0 | 3.9 | 4.0 | 3.8 |
| 4.5 | 3.5 | 3.9 | 4.5 | 3.6 | 4.1 | 4.0 | 4.4 | 4.2 | 4.0 | 3.9 | 4.0 | 3.8 |
| 4.6 | 3.5 | 3.9 | 4.5 | 3.6 | 4.1 | 4.0 | 4.4 | 4.2 | 4.0 | 3.9 | 4.0 | 3.8 |
| 4.7 | 3.5 | 3.9 | 4.5 | 3.6 | 4.1 | 4.0 | 4.4 | 4.2 | 4.0 | 3.9 | 4.0 | 3.8 |
| 4.8 | 3.5 | 3.8 | 4.5 | 3.5 | 4.0 | 4.0 | 4.4 | 4.1 | 4.0 | 3.8 | 4.0 | 3.8 |

Table F17. Predicted mean of peak storm $H_{m0}$ in feet from BWSim at consequence locations over 57 yr life cycle between 2014 and 2071 with SLR scenario 2.

| Alt .RP | 129 | 132 | 135 | 147 | 166 | 170 | 172 | 185 | 195 | 196 | 198 | 203 |
|---|---|---|---|---|---|---|---|---|---|---|---|---|
| 1.1 | 3.1 | 3.4 | 4.0 | 2.2 | 3.3 | 3.7 | 4.4 | 3.7 | 3.8 | 3.4 | 3.6 | 3.4 |
| 1.2 | 3.1 | 3.4 | 4.0 | 2.2 | 3.3 | 3.7 | 4.4 | 3.7 | 3.8 | 3.4 | 3.6 | 3.4 |
| 1.3 | 3.1 | 3.4 | 4.0 | 2.2 | 3.3 | 3.7 | 4.4 | 3.7 | 3.8 | 3.4 | 3.6 | 3.4 |
| 1.4 | 3.1 | 3.4 | 4.0 | 2.2 | 3.3 | 3.7 | 4.4 | 3.7 | 3.8 | 3.4 | 3.6 | 3.4 |
| 1.5 | 3.1 | 3.4 | 4.0 | 2.2 | 3.3 | 3.7 | 4.4 | 3.7 | 3.8 | 3.4 | 3.6 | 3.4 |
| 1.6 | 3.1 | 3.4 | 4.0 | 2.2 | 3.3 | 3.7 | 4.4 | 3.7 | 3.8 | 3.4 | 3.6 | 3.4 |
| 1.7 | 3.1 | 3.4 | 4.0 | 2.2 | 3.3 | 3.7 | 4.4 | 3.7 | 3.8 | 3.4 | 3.6 | 3.4 |
| 1.8 | 3.1 | 3.4 | 4.0 | 2.2 | 3.3 | 3.7 | 4.4 | 3.7 | 3.8 | 3.4 | 3.6 | 3.4 |
| 2.1 | 3.8 | 4.1 | 4.7 | 3.9 | 4.3 | 4.2 | 4.5 | 4.4 | 4.1 | 4.1 | 4.2 | 4.0 |
| 2.2 | 3.8 | 4.1 | 4.6 | 3.9 | 4.3 | 4.2 | 4.5 | 4.3 | 4.1 | 4.0 | 4.2 | 4.0 |
| 2.3 | 3.7 | 4.0 | 4.6 | 3.8 | 4.2 | 4.2 | 4.5 | 4.3 | 4.1 | 4.0 | 4.1 | 3.9 |
| 2.4 | 3.6 | 3.9 | 4.5 | 3.7 | 4.1 | 4.0 | 4.5 | 4.2 | 4.0 | 3.9 | 4.1 | 3.9 |
| 2.5 | 3.6 | 3.9 | 4.5 | 3.7 | 4.1 | 4.0 | 4.5 | 4.2 | 4.0 | 3.9 | 4.1 | 3.9 |
| 2.6 | 3.6 | 3.9 | 4.5 | 3.7 | 4.1 | 4.0 | 4.5 | 4.2 | 4.0 | 3.9 | 4.1 | 3.9 |
| 2.7 | 3.6 | 3.9 | 4.5 | 3.7 | 4.1 | 4.0 | 4.5 | 4.2 | 4.0 | 3.9 | 4.1 | 3.9 |
| 2.8 | 3.5 | 3.9 | 4.5 | 3.5 | 4.0 | 3.9 | 4.4 | 4.1 | 4.0 | 3.8 | 4.0 | 3.8 |
| 3.1 | 2.9 | 3.2 | 3.9 | 1.7 | 3.0 | 3.6 | 4.4 | 3.5 | 3.7 | 3.2 | 3.5 | 3.3 |
| 3.2 | 2.9 | 3.2 | 3.9 | 1.7 | 3.0 | 3.6 | 4.4 | 3.5 | 3.7 | 3.2 | 3.5 | 3.3 |
| 3.3 | 2.9 | 3.2 | 3.9 | 1.6 | 3.0 | 3.6 | 4.4 | 3.5 | 3.7 | 3.2 | 3.5 | 3.3 |
| 3.4 | 2.9 | 3.2 | 3.9 | 1.6 | 3.0 | 3.6 | 4.4 | 3.5 | 3.7 | 3.2 | 3.5 | 3.3 |
| 3.5 | 2.9 | 3.2 | 3.9 | 1.6 | 3.0 | 3.6 | 4.4 | 3.5 | 3.7 | 3.2 | 3.5 | 3.3 |
| 3.6 | 2.9 | 3.2 | 3.9 | 1.6 | 3.0 | 3.6 | 4.4 | 3.5 | 3.7 | 3.2 | 3.5 | 3.3 |
| 3.7 | 2.9 | 3.2 | 3.9 | 1.6 | 3.0 | 3.6 | 4.4 | 3.5 | 3.7 | 3.2 | 3.5 | 3.3 |
| 3.8 | 2.9 | 3.2 | 3.9 | 1.6 | 3.0 | 3.6 | 4.4 | 3.5 | 3.7 | 3.2 | 3.5 | 3.3 |
| 4.1 | 3.8 | 4.1 | 4.6 | 3.9 | 4.3 | 4.2 | 4.5 | 4.4 | 4.1 | 4.1 | 4.2 | 4.0 |
| 4.2 | 3.7 | 4.0 | 4.6 | 3.9 | 4.2 | 4.2 | 4.5 | 4.3 | 4.1 | 4.0 | 4.2 | 4.0 |
| 4.3 | 3.7 | 4.0 | 4.6 | 3.8 | 4.2 | 4.2 | 4.5 | 4.3 | 4.1 | 4.0 | 4.1 | 3.9 |
| 4.4 | 3.6 | 3.9 | 4.5 | 3.6 | 4.1 | 4.1 | 4.5 | 4.2 | 4.0 | 3.9 | 4.1 | 3.8 |
| 4.5 | 3.6 | 3.9 | 4.5 | 3.6 | 4.1 | 4.1 | 4.5 | 4.2 | 4.0 | 3.9 | 4.1 | 3.8 |
| 4.6 | 3.6 | 3.9 | 4.5 | 3.6 | 4.1 | 4.1 | 4.5 | 4.2 | 4.0 | 3.9 | 4.1 | 3.8 |
| 4.7 | 3.6 | 3.9 | 4.5 | 3.6 | 4.1 | 4.1 | 4.5 | 4.2 | 4.0 | 3.9 | 4.1 | 3.8 |
| 4.8 | 3.5 | 3.9 | 4.5 | 3.5 | 4.0 | 4.0 | 4.4 | 4.1 | 4.0 | 3.8 | 4.0 | 3.8 |

Table F18. Predicted mean of peak storm $H_{m0}$ in feet from BWSim at consequence locations over 57 yr life cycle between 2014 and 2071 with SLR scenario 3.

| Alt .RP | 129 | 132 | 135 | 147 | 166 | 170 | 172 | 185 | 195 | 196 | 198 | 203 |
|---|---|---|---|---|---|---|---|---|---|---|---|---|
| 1.1 | 3.1 | 3.4 | 4.0 | 2.3 | 3.3 | 3.7 | 4.4 | 3.7 | 3.8 | 3.4 | 3.7 | 3.4 |
| 1.2 | 3.1 | 3.4 | 4.0 | 2.3 | 3.3 | 3.7 | 4.4 | 3.7 | 3.8 | 3.4 | 3.7 | 3.4 |
| 1.3 | 3.1 | 3.4 | 4.0 | 2.3 | 3.3 | 3.7 | 4.4 | 3.7 | 3.8 | 3.4 | 3.7 | 3.4 |
| 1.4 | 3.1 | 3.4 | 4.0 | 2.3 | 3.3 | 3.7 | 4.4 | 3.7 | 3.8 | 3.4 | 3.7 | 3.4 |
| 1.5 | 3.1 | 3.4 | 4.0 | 2.3 | 3.3 | 3.7 | 4.4 | 3.7 | 3.8 | 3.4 | 3.7 | 3.4 |
| 1.6 | 3.1 | 3.4 | 4.0 | 2.3 | 3.3 | 3.7 | 4.4 | 3.7 | 3.8 | 3.4 | 3.7 | 3.4 |
| 1.7 | 3.1 | 3.4 | 4.0 | 2.3 | 3.3 | 3.7 | 4.4 | 3.7 | 3.8 | 3.4 | 3.7 | 3.4 |
| 1.8 | 3.1 | 3.4 | 4.0 | 2.3 | 3.3 | 3.7 | 4.4 | 3.7 | 3.8 | 3.4 | 3.7 | 3.4 |
| 2.1 | 3.9 | 4.1 | 4.7 | 3.9 | 4.3 | 4.3 | 4.5 | 4.4 | 4.2 | 4.1 | 4.2 | 4.1 |
| 2.2 | 3.8 | 4.1 | 4.7 | 3.9 | 4.3 | 4.2 | 4.5 | 4.4 | 4.1 | 4.1 | 4.2 | 4.0 |
| 2.3 | 3.7 | 4.0 | 4.6 | 3.8 | 4.2 | 4.2 | 4.5 | 4.3 | 4.1 | 4.0 | 4.1 | 3.9 |
| 2.4 | 3.6 | 4.0 | 4.6 | 3.7 | 4.1 | 4.1 | 4.5 | 4.2 | 4.0 | 3.9 | 4.1 | 3.9 |
| 2.5 | 3.6 | 4.0 | 4.6 | 3.7 | 4.1 | 4.1 | 4.5 | 4.2 | 4.0 | 3.9 | 4.1 | 3.9 |
| 2.6 | 3.6 | 4.0 | 4.6 | 3.7 | 4.1 | 4.1 | 4.5 | 4.2 | 4.0 | 3.9 | 4.1 | 3.9 |
| 2.7 | 3.6 | 4.0 | 4.6 | 3.7 | 4.1 | 4.1 | 4.5 | 4.2 | 4.0 | 3.9 | 4.1 | 3.9 |
| 2.8 | 3.5 | 3.9 | 4.5 | 3.5 | 4.0 | 3.9 | 4.4 | 4.1 | 4.0 | 3.8 | 4.0 | 3.8 |
| 3.1 | 2.9 | 3.2 | 3.9 | 1.7 | 3.0 | 3.6 | 4.4 | 3.5 | 3.7 | 3.2 | 3.5 | 3.3 |
| 3.2 | 2.9 | 3.2 | 3.9 | 1.7 | 3.0 | 3.6 | 4.4 | 3.5 | 3.7 | 3.2 | 3.5 | 3.3 |
| 3.3 | 2.9 | 3.2 | 3.9 | 1.6 | 3.0 | 3.6 | 4.4 | 3.5 | 3.7 | 3.2 | 3.5 | 3.3 |
| 3.4 | 2.9 | 3.2 | 3.9 | 1.6 | 3.0 | 3.6 | 4.4 | 3.5 | 3.7 | 3.2 | 3.5 | 3.3 |
| 3.5 | 2.9 | 3.2 | 3.9 | 1.6 | 3.0 | 3.6 | 4.4 | 3.5 | 3.7 | 3.2 | 3.5 | 3.3 |
| 3.6 | 2.9 | 3.2 | 3.9 | 1.6 | 3.0 | 3.6 | 4.4 | 3.5 | 3.7 | 3.2 | 3.5 | 3.3 |
| 3.7 | 2.9 | 3.2 | 3.9 | 1.6 | 3.0 | 3.6 | 4.4 | 3.5 | 3.7 | 3.2 | 3.5 | 3.3 |
| 3.8 | 2.9 | 3.2 | 3.9 | 1.6 | 3.0 | 3.6 | 4.4 | 3.5 | 3.7 | 3.2 | 3.5 | 3.3 |
| 4.1 | 3.8 | 4.1 | 4.7 | 3.9 | 4.3 | 4.3 | 4.5 | 4.4 | 4.2 | 4.1 | 4.2 | 4.0 |
| 4.2 | 3.7 | 4.0 | 4.6 | 3.9 | 4.3 | 4.2 | 4.5 | 4.4 | 4.1 | 4.0 | 4.2 | 4.0 |
| 4.3 | 3.7 | 4.0 | 4.6 | 3.9 | 4.2 | 4.2 | 4.5 | 4.3 | 4.1 | 4.0 | 4.2 | 4.0 |
| 4.4 | 3.6 | 3.9 | 4.6 | 3.7 | 4.1 | 4.1 | 4.5 | 4.2 | 4.1 | 3.9 | 4.1 | 3.9 |
| 4.5 | 3.6 | 3.9 | 4.6 | 3.7 | 4.1 | 4.1 | 4.5 | 4.2 | 4.1 | 3.9 | 4.1 | 3.9 |
| 4.6 | 3.6 | 3.9 | 4.6 | 3.7 | 4.1 | 4.1 | 4.5 | 4.2 | 4.1 | 3.9 | 4.1 | 3.9 |
| 4.7 | 3.6 | 3.9 | 4.6 | 3.7 | 4.1 | 4.1 | 4.5 | 4.2 | 4.1 | 3.9 | 4.1 | 3.9 |
| 4.8 | 3.5 | 3.9 | 4.5 | 3.6 | 4.0 | 4.0 | 4.4 | 4.2 | 4.0 | 3.8 | 4.0 | 3.8 |

Table F19. Predicted mean of peak storm $H_{m0}$ in feet from BWSim at consequence locations over 57 yr life cycle between 2014 and 2071 with SLR scenario 4.

| Alt .RP | 129 | 132 | 135 | 147 | 166 | 170 | 172 | 185 | 195 | 196 | 198 | 203 |
|---|---|---|---|---|---|---|---|---|---|---|---|---|
| 1.1 | 3.1 | 3.4 | 4.1 | 2.3 | 3.3 | 3.7 | 4.4 | 3.7 | 3.8 | 3.4 | 3.7 | 3.5 |
| 1.2 | 3.1 | 3.4 | 4.1 | 2.3 | 3.3 | 3.7 | 4.4 | 3.7 | 3.8 | 3.4 | 3.7 | 3.5 |
| 1.3 | 3.1 | 3.4 | 4.1 | 2.3 | 3.3 | 3.7 | 4.4 | 3.7 | 3.8 | 3.4 | 3.7 | 3.5 |
| 1.4 | 3.1 | 3.4 | 4.1 | 2.3 | 3.3 | 3.7 | 4.4 | 3.7 | 3.8 | 3.4 | 3.7 | 3.5 |
| 1.5 | 3.1 | 3.4 | 4.1 | 2.3 | 3.3 | 3.7 | 4.4 | 3.7 | 3.8 | 3.4 | 3.7 | 3.5 |
| 1.6 | 3.1 | 3.4 | 4.1 | 2.3 | 3.3 | 3.7 | 4.4 | 3.7 | 3.8 | 3.4 | 3.7 | 3.5 |
| 1.7 | 3.1 | 3.4 | 4.1 | 2.3 | 3.3 | 3.7 | 4.4 | 3.7 | 3.8 | 3.4 | 3.7 | 3.5 |
| 1.8 | 3.1 | 3.4 | 4.1 | 2.3 | 3.3 | 3.7 | 4.4 | 3.7 | 3.8 | 3.4 | 3.7 | 3.5 |
| 2.1 | 3.9 | 4.2 | 4.7 | 4.0 | 4.4 | 4.3 | 4.5 | 4.4 | 4.2 | 4.2 | 4.3 | 4.1 |
| 2.2 | 3.8 | 4.1 | 4.7 | 4.0 | 4.3 | 4.3 | 4.5 | 4.4 | 4.2 | 4.1 | 4.2 | 4.1 |
| 2.3 | 3.8 | 4.1 | 4.7 | 3.9 | 4.3 | 4.2 | 4.5 | 4.4 | 4.1 | 4.0 | 4.2 | 4.0 |
| 2.4 | 3.7 | 4.0 | 4.6 | 3.8 | 4.2 | 4.1 | 4.5 | 4.3 | 4.1 | 4.0 | 4.1 | 3.9 |
| 2.5 | 3.7 | 4.0 | 4.6 | 3.8 | 4.2 | 4.1 | 4.5 | 4.3 | 4.1 | 4.0 | 4.1 | 3.9 |
| 2.6 | 3.7 | 4.0 | 4.6 | 3.8 | 4.2 | 4.1 | 4.5 | 4.3 | 4.1 | 4.0 | 4.1 | 3.9 |
| 2.7 | 3.7 | 4.0 | 4.6 | 3.8 | 4.2 | 4.1 | 4.5 | 4.3 | 4.1 | 4.0 | 4.1 | 3.9 |
| 2.8 | 3.6 | 3.9 | 4.5 | 3.6 | 4.1 | 4.0 | 4.4 | 4.2 | 4.0 | 3.9 | 4.0 | 3.8 |
| 3.1 | 2.9 | 3.2 | 3.9 | 1.7 | 3.0 | 3.6 | 4.4 | 3.5 | 3.7 | 3.2 | 3.5 | 3.3 |
| 3.2 | 2.9 | 3.2 | 3.9 | 1.7 | 3.0 | 3.6 | 4.4 | 3.5 | 3.7 | 3.2 | 3.5 | 3.3 |
| 3.3 | 2.9 | 3.2 | 3.9 | 1.7 | 3.0 | 3.6 | 4.4 | 3.5 | 3.7 | 3.2 | 3.5 | 3.3 |
| 3.4 | 2.9 | 3.2 | 3.9 | 1.7 | 3.0 | 3.6 | 4.4 | 3.5 | 3.7 | 3.2 | 3.5 | 3.3 |
| 3.5 | 2.9 | 3.2 | 3.9 | 1.7 | 3.0 | 3.6 | 4.4 | 3.5 | 3.7 | 3.2 | 3.5 | 3.3 |
| 3.6 | 2.9 | 3.2 | 3.9 | 1.7 | 3.0 | 3.6 | 4.4 | 3.5 | 3.7 | 3.2 | 3.5 | 3.3 |
| 3.7 | 2.9 | 3.2 | 3.9 | 1.7 | 3.0 | 3.6 | 4.4 | 3.5 | 3.7 | 3.2 | 3.5 | 3.3 |
| 3.8 | 2.9 | 3.2 | 3.9 | 1.7 | 3.0 | 3.6 | 4.4 | 3.5 | 3.7 | 3.2 | 3.5 | 3.3 |
| 4.1 | 3.9 | 4.1 | 4.7 | 4.0 | 4.4 | 4.3 | 4.5 | 4.4 | 4.2 | 4.1 | 4.3 | 4.1 |
| 4.2 | 3.8 | 4.1 | 4.7 | 4.0 | 4.3 | 4.3 | 4.5 | 4.4 | 4.2 | 4.1 | 4.2 | 4.0 |
| 4.3 | 3.7 | 4.1 | 4.7 | 4.0 | 4.3 | 4.3 | 4.5 | 4.4 | 4.2 | 4.0 | 4.2 | 4.0 |
| 4.4 | 3.6 | 4.0 | 4.6 | 3.8 | 4.2 | 4.1 | 4.5 | 4.3 | 4.1 | 3.9 | 4.1 | 3.9 |
| 4.5 | 3.6 | 4.0 | 4.6 | 3.8 | 4.2 | 4.1 | 4.5 | 4.3 | 4.1 | 3.9 | 4.1 | 3.9 |
| 4.6 | 3.6 | 4.0 | 4.6 | 3.8 | 4.2 | 4.1 | 4.5 | 4.3 | 4.1 | 3.9 | 4.1 | 3.9 |
| 4.7 | 3.6 | 4.0 | 4.6 | 3.8 | 4.2 | 4.1 | 4.5 | 4.3 | 4.1 | 3.9 | 4.1 | 3.9 |
| 4.8 | 3.6 | 3.9 | 4.5 | 3.7 | 4.1 | 4.0 | 4.4 | 4.2 | 4.0 | 3.9 | 4.0 | 3.8 |

Table F20. Predicted mean of peak storm $H_{m0}$ in feet from BWSim at consequence locations over 57 yr life cycle between 2014 and 2071 with SLR scenario 5.

| Alt .RP | 129 | 132 | 135 | 147 | 166 | 170 | 172 | 185 | 195 | 196 | 198 | 203 |
|---|---|---|---|---|---|---|---|---|---|---|---|---|
| 1.1 | 3.1 | 3.5 | 4.1 | 2.4 | 3.4 | 3.8 | 4.4 | 3.7 | 3.8 | 3.5 | 3.7 | 3.5 |
| 1.2 | 3.1 | 3.5 | 4.1 | 2.4 | 3.4 | 3.8 | 4.4 | 3.7 | 3.8 | 3.5 | 3.7 | 3.5 |
| 1.3 | 3.1 | 3.5 | 4.1 | 2.4 | 3.4 | 3.8 | 4.4 | 3.7 | 3.8 | 3.5 | 3.7 | 3.5 |
| 1.4 | 3.1 | 3.5 | 4.1 | 2.4 | 3.4 | 3.8 | 4.4 | 3.7 | 3.8 | 3.5 | 3.7 | 3.5 |
| 1.5 | 3.1 | 3.5 | 4.1 | 2.4 | 3.4 | 3.8 | 4.4 | 3.7 | 3.8 | 3.5 | 3.7 | 3.5 |
| 1.6 | 3.1 | 3.5 | 4.1 | 2.4 | 3.4 | 3.8 | 4.4 | 3.7 | 3.8 | 3.5 | 3.7 | 3.5 |
| 1.7 | 3.1 | 3.5 | 4.1 | 2.4 | 3.4 | 3.8 | 4.4 | 3.7 | 3.8 | 3.5 | 3.7 | 3.5 |
| 1.8 | 3.1 | 3.5 | 4.1 | 2.4 | 3.4 | 3.8 | 4.4 | 3.7 | 3.8 | 3.5 | 3.7 | 3.5 |
| 2.1 | 4.0 | 4.3 | 4.8 | 4.1 | 4.4 | 4.4 | 4.5 | 4.5 | 4.2 | 4.2 | 4.3 | 4.2 |
| 2.2 | 3.9 | 4.2 | 4.8 | 4.1 | 4.4 | 4.3 | 4.5 | 4.5 | 4.2 | 4.2 | 4.3 | 4.1 |
| 2.3 | 3.8 | 4.1 | 4.7 | 4.0 | 4.3 | 4.3 | 4.5 | 4.4 | 4.2 | 4.1 | 4.2 | 4.0 |
| 2.4 | 3.7 | 4.1 | 4.6 | 3.9 | 4.2 | 4.1 | 4.5 | 4.3 | 4.1 | 4.0 | 4.2 | 4.0 |
| 2.5 | 3.7 | 4.1 | 4.6 | 3.9 | 4.2 | 4.1 | 4.5 | 4.3 | 4.1 | 4.0 | 4.2 | 4.0 |
| 2.6 | 3.7 | 4.1 | 4.6 | 3.9 | 4.2 | 4.1 | 4.5 | 4.3 | 4.1 | 4.0 | 4.2 | 4.0 |
| 2.7 | 3.7 | 4.1 | 4.6 | 3.9 | 4.2 | 4.1 | 4.5 | 4.3 | 4.1 | 4.0 | 4.2 | 4.0 |
| 2.8 | 3.6 | 4.0 | 4.6 | 3.7 | 4.1 | 4.0 | 4.4 | 4.2 | 4.0 | 3.9 | 4.1 | 3.9 |
| 3.1 | 2.9 | 3.2 | 3.9 | 1.7 | 3.1 | 3.6 | 4.4 | 3.5 | 3.8 | 3.3 | 3.5 | 3.3 |
| 3.2 | 2.9 | 3.2 | 3.9 | 1.7 | 3.0 | 3.6 | 4.4 | 3.5 | 3.7 | 3.2 | 3.5 | 3.3 |
| 3.3 | 2.9 | 3.2 | 3.9 | 1.7 | 3.0 | 3.6 | 4.4 | 3.5 | 3.7 | 3.2 | 3.5 | 3.3 |
| 3.4 | 2.9 | 3.2 | 3.9 | 1.7 | 3.0 | 3.6 | 4.4 | 3.5 | 3.7 | 3.2 | 3.5 | 3.3 |
| 3.5 | 2.9 | 3.2 | 3.9 | 1.7 | 3.0 | 3.6 | 4.4 | 3.5 | 3.7 | 3.2 | 3.5 | 3.3 |
| 3.6 | 2.9 | 3.2 | 3.9 | 1.7 | 3.0 | 3.6 | 4.4 | 3.5 | 3.7 | 3.2 | 3.5 | 3.3 |
| 3.7 | 2.9 | 3.2 | 3.9 | 1.7 | 3.0 | 3.6 | 4.4 | 3.5 | 3.7 | 3.2 | 3.5 | 3.3 |
| 3.8 | 2.9 | 3.2 | 3.9 | 1.7 | 3.0 | 3.6 | 4.4 | 3.5 | 3.7 | 3.2 | 3.5 | 3.3 |
| 4.1 | 4.0 | 4.2 | 4.7 | 4.1 | 4.4 | 4.3 | 4.5 | 4.5 | 4.2 | 4.2 | 4.3 | 4.1 |
| 4.2 | 3.8 | 4.1 | 4.7 | 4.1 | 4.4 | 4.3 | 4.5 | 4.5 | 4.2 | 4.1 | 4.3 | 4.1 |
| 4.3 | 3.8 | 4.1 | 4.7 | 4.0 | 4.4 | 4.3 | 4.5 | 4.4 | 4.2 | 4.1 | 4.2 | 4.0 |
| 4.4 | 3.7 | 4.0 | 4.6 | 3.9 | 4.2 | 4.2 | 4.5 | 4.3 | 4.1 | 4.0 | 4.2 | 3.9 |
| 4.5 | 3.7 | 4.0 | 4.6 | 3.9 | 4.2 | 4.2 | 4.5 | 4.3 | 4.1 | 4.0 | 4.2 | 3.9 |
| 4.6 | 3.7 | 4.0 | 4.6 | 3.9 | 4.2 | 4.2 | 4.5 | 4.3 | 4.1 | 4.0 | 4.2 | 3.9 |
| 4.7 | 3.7 | 4.0 | 4.6 | 3.9 | 4.2 | 4.2 | 4.5 | 4.3 | 4.1 | 4.0 | 4.2 | 3.9 |
| 4.8 | 3.6 | 4.0 | 4.6 | 3.8 | 4.2 | 4.1 | 4.5 | 4.3 | 4.1 | 3.9 | 4.1 | 3.9 |

Table F21. Predicted maximum of peak storm $H_{m0}$ in feet from BWSim at consequence locations over 57 yr life cycle between 2014 and 2071 with SLR scenario 1.

| Alt .RP | 129 | 132 | 135 | 147 | 166 | 170 | 172 | 185 | 195 | 196 | 198 | 203 |
|---|---|---|---|---|---|---|---|---|---|---|---|---|
| 1.1 | 7.1 | 7.5 | 7.7 | 5.9 | 6.2 | 7.0 | 8.0 | 6.9 | 7.0 | 7.3 | 7.2 | 7.1 |
| 1.2 | 7.1 | 7.5 | 7.7 | 5.9 | 6.2 | 7.0 | 8.0 | 6.9 | 7.0 | 7.3 | 7.2 | 7.1 |
| 1.3 | 7.1 | 7.5 | 7.7 | 5.9 | 6.2 | 7.0 | 8.0 | 6.9 | 7.0 | 7.3 | 7.2 | 7.1 |
| 1.4 | 7.1 | 7.5 | 7.7 | 5.9 | 6.2 | 7.0 | 8.0 | 6.9 | 7.0 | 7.3 | 7.2 | 7.1 |
| 1.5 | 7.1 | 7.5 | 7.7 | 5.9 | 6.2 | 7.0 | 8.0 | 6.9 | 7.0 | 7.3 | 7.2 | 7.1 |
| 1.6 | 7.1 | 7.5 | 7.7 | 5.9 | 6.2 | 7.0 | 8.0 | 6.9 | 7.0 | 7.3 | 7.2 | 7.1 |
| 1.7 | 7.1 | 7.5 | 7.7 | 5.9 | 6.2 | 7.0 | 8.0 | 6.9 | 7.0 | 7.3 | 7.2 | 7.1 |
| 1.8 | 7.1 | 7.5 | 7.7 | 5.9 | 6.2 | 7.0 | 8.0 | 6.9 | 7.0 | 7.3 | 7.2 | 7.1 |
| 2.1 | 8.0 | 8.3 | 8.5 | 7.5 | 7.4 | 7.7 | 8.2 | 7.8 | 7.5 | 8.1 | 7.9 | 7.9 |
| 2.2 | 7.9 | 8.3 | 8.5 | 7.5 | 7.4 | 7.7 | 8.2 | 7.8 | 7.5 | 8.0 | 7.9 | 7.8 |
| 2.3 | 7.8 | 8.2 | 8.5 | 7.5 | 7.4 | 7.7 | 8.2 | 7.8 | 7.5 | 8.0 | 7.8 | 7.8 |
| 2.4 | 7.7 | 8.1 | 8.4 | 7.4 | 7.3 | 7.5 | 8.1 | 7.7 | 7.4 | 7.9 | 7.7 | 7.7 |
| 2.5 | 7.7 | 8.1 | 8.4 | 7.4 | 7.3 | 7.5 | 8.1 | 7.7 | 7.4 | 7.9 | 7.7 | 7.7 |
| 2.6 | 7.7 | 8.1 | 8.4 | 7.4 | 7.3 | 7.5 | 8.1 | 7.7 | 7.4 | 7.9 | 7.7 | 7.7 |
| 2.7 | 7.7 | 8.1 | 8.4 | 7.4 | 7.3 | 7.5 | 8.1 | 7.7 | 7.4 | 7.9 | 7.7 | 7.7 |
| 2.8 | 7.5 | 8.0 | 8.3 | 7.2 | 7.2 | 7.3 | 8.0 | 7.5 | 7.2 | 7.7 | 7.6 | 7.6 |
| 3.1 | 5.9 | 6.3 | 6.9 | 4.4 | 6.0 | 6.5 | 7.9 | 6.1 | 6.6 | 6.3 | 6.4 | 6.3 |
| 3.2 | 5.8 | 6.3 | 6.8 | 4.2 | 6.0 | 6.4 | 7.9 | 6.1 | 6.6 | 6.2 | 6.4 | 6.2 |
| 3.3 | 5.8 | 6.2 | 6.7 | 4.0 | 6.0 | 6.4 | 7.9 | 6.0 | 6.6 | 6.2 | 6.3 | 6.2 |
| 3.4 | 5.8 | 6.2 | 6.7 | 4.0 | 6.0 | 6.4 | 7.9 | 6.0 | 6.6 | 6.2 | 6.3 | 6.2 |
| 3.5 | 5.8 | 6.2 | 6.7 | 4.0 | 6.0 | 6.4 | 7.9 | 6.0 | 6.6 | 6.2 | 6.3 | 6.2 |
| 3.6 | 5.8 | 6.2 | 6.7 | 4.0 | 6.0 | 6.4 | 7.9 | 6.0 | 6.6 | 6.2 | 6.3 | 6.2 |
| 3.7 | 5.8 | 6.2 | 6.7 | 4.0 | 6.0 | 6.4 | 7.9 | 6.0 | 6.6 | 6.2 | 6.3 | 6.2 |
| 3.8 | 5.8 | 6.2 | 6.7 | 4.0 | 6.0 | 6.4 | 7.9 | 6.0 | 6.6 | 6.2 | 6.3 | 6.2 |
| 4.1 | 7.7 | 7.9 | 8.4 | 7.5 | 7.4 | 7.7 | 8.2 | 7.8 | 7.5 | 7.8 | 7.8 | 7.7 |
| 4.2 | 7.5 | 7.9 | 8.3 | 7.5 | 7.4 | 7.7 | 8.2 | 7.8 | 7.5 | 7.7 | 7.7 | 7.6 |
| 4.3 | 7.4 | 7.8 | 8.3 | 7.5 | 7.4 | 7.7 | 8.2 | 7.8 | 7.5 | 7.7 | 7.7 | 7.6 |
| 4.4 | 7.3 | 7.7 | 8.3 | 7.4 | 7.4 | 7.5 | 8.1 | 7.7 | 7.4 | 7.6 | 7.6 | 7.5 |
| 4.5 | 7.2 | 7.7 | 8.3 | 7.4 | 7.4 | 7.5 | 8.1 | 7.7 | 7.4 | 7.6 | 7.6 | 7.4 |
| 4.6 | 7.2 | 7.7 | 8.3 | 7.4 | 7.4 | 7.5 | 8.1 | 7.7 | 7.4 | 7.6 | 7.6 | 7.4 |
| 4.7 | 7.2 | 7.7 | 8.3 | 7.4 | 7.4 | 7.5 | 8.1 | 7.7 | 7.3 | 7.6 | 7.6 | 7.4 |
| 4.8 | 7.1 | 7.6 | 8.2 | 7.4 | 7.3 | 7.3 | 8.0 | 7.5 | 7.2 | 7.5 | 7.5 | 7.3 |

Table F22. Predicted maximum of peak storm $H_{m0}$ in feet from BWSim at consequence locations over 57 yr life cycle between 2014 and 2071 with SLR scenario 2.

| Alt .RP | 129 | 132 | 135 | 147 | 166 | 170 | 172 | 185 | 195 | 196 | 198 | 203 |
|---|---|---|---|---|---|---|---|---|---|---|---|---|
| 1.1 | 7.2 | 7.6 | 7.8 | 6.0 | 6.3 | 7.1 | 8.0 | 7.0 | 7.1 | 7.4 | 7.3 | 7.3 |
| 1.2 | 7.2 | 7.6 | 7.8 | 6.0 | 6.3 | 7.1 | 8.0 | 7.0 | 7.1 | 7.4 | 7.3 | 7.3 |
| 1.3 | 7.2 | 7.6 | 7.8 | 6.0 | 6.3 | 7.1 | 8.0 | 7.0 | 7.1 | 7.4 | 7.3 | 7.3 |
| 1.4 | 7.2 | 7.6 | 7.8 | 6.0 | 6.3 | 7.1 | 8.0 | 7.0 | 7.1 | 7.4 | 7.3 | 7.3 |
| 1.5 | 7.2 | 7.6 | 7.8 | 6.0 | 6.3 | 7.1 | 8.0 | 7.0 | 7.1 | 7.4 | 7.3 | 7.3 |
| 1.6 | 7.2 | 7.6 | 7.8 | 6.0 | 6.3 | 7.1 | 8.0 | 7.0 | 7.1 | 7.4 | 7.3 | 7.3 |
| 1.7 | 7.2 | 7.6 | 7.8 | 6.0 | 6.3 | 7.1 | 8.0 | 7.0 | 7.1 | 7.4 | 7.3 | 7.3 |
| 1.8 | 7.2 | 7.6 | 7.8 | 6.0 | 6.3 | 7.1 | 8.0 | 7.0 | 7.1 | 7.4 | 7.3 | 7.3 |
| 2.1 | 8.1 | 8.5 | 8.6 | 7.6 | 7.5 | 7.8 | 8.2 | 7.9 | 7.6 | 8.2 | 8.0 | 8.0 |
| 2.2 | 8.0 | 8.4 | 8.6 | 7.6 | 7.5 | 7.8 | 8.2 | 7.9 | 7.6 | 8.2 | 8.0 | 8.0 |
| 2.3 | 7.9 | 8.3 | 8.6 | 7.6 | 7.5 | 7.8 | 8.2 | 7.9 | 7.6 | 8.1 | 7.9 | 7.9 |
| 2.4 | 7.8 | 8.3 | 8.5 | 7.6 | 7.4 | 7.6 | 8.1 | 7.8 | 7.4 | 8.0 | 7.8 | 7.8 |
| 2.5 | 7.8 | 8.3 | 8.5 | 7.6 | 7.4 | 7.6 | 8.1 | 7.8 | 7.4 | 8.0 | 7.8 | 7.8 |
| 2.6 | 7.8 | 8.3 | 8.5 | 7.6 | 7.4 | 7.6 | 8.1 | 7.8 | 7.4 | 8.0 | 7.8 | 7.8 |
| 2.7 | 7.8 | 8.3 | 8.5 | 7.6 | 7.4 | 7.6 | 8.1 | 7.8 | 7.4 | 8.0 | 7.8 | 7.8 |
| 2.8 | 7.7 | 8.1 | 8.4 | 7.4 | 7.3 | 7.4 | 8.1 | 7.6 | 7.3 | 7.9 | 7.7 | 7.7 |
| 3.1 | 6.0 | 6.4 | 7.0 | 4.5 | 6.0 | 6.5 | 7.9 | 6.2 | 6.7 | 6.4 | 6.5 | 6.4 |
| 3.2 | 6.0 | 6.4 | 6.9 | 4.3 | 6.0 | 6.5 | 7.9 | 6.2 | 6.7 | 6.3 | 6.5 | 6.3 |
| 3.3 | 5.9 | 6.3 | 6.8 | 4.2 | 6.0 | 6.5 | 7.9 | 6.1 | 6.6 | 6.3 | 6.4 | 6.3 |
| 3.4 | 5.9 | 6.3 | 6.8 | 4.2 | 6.0 | 6.5 | 7.9 | 6.1 | 6.6 | 6.3 | 6.4 | 6.3 |
| 3.5 | 5.9 | 6.3 | 6.8 | 4.2 | 6.0 | 6.5 | 7.9 | 6.1 | 6.6 | 6.3 | 6.4 | 6.3 |
| 3.6 | 5.9 | 6.3 | 6.8 | 4.2 | 6.0 | 6.5 | 7.9 | 6.1 | 6.6 | 6.3 | 6.4 | 6.3 |
| 3.7 | 5.9 | 6.3 | 6.8 | 4.2 | 6.0 | 6.5 | 7.9 | 6.1 | 6.6 | 6.3 | 6.4 | 6.3 |
| 3.8 | 5.9 | 6.3 | 6.8 | 4.2 | 6.0 | 6.5 | 7.9 | 6.1 | 6.6 | 6.3 | 6.4 | 6.3 |
| 4.1 | 7.8 | 8.1 | 8.5 | 7.6 | 7.5 | 7.8 | 8.2 | 7.9 | 7.6 | 8.0 | 7.9 | 7.8 |
| 4.2 | 7.6 | 8.0 | 8.5 | 7.6 | 7.5 | 7.8 | 8.2 | 7.9 | 7.6 | 7.9 | 7.8 | 7.7 |
| 4.3 | 7.5 | 7.9 | 8.4 | 7.6 | 7.5 | 7.8 | 8.2 | 7.9 | 7.5 | 7.8 | 7.8 | 7.7 |
| 4.4 | 7.4 | 7.9 | 8.4 | 7.6 | 7.5 | 7.6 | 8.1 | 7.8 | 7.4 | 7.7 | 7.7 | 7.6 |
| 4.5 | 7.4 | 7.8 | 8.4 | 7.6 | 7.5 | 7.6 | 8.1 | 7.8 | 7.4 | 7.7 | 7.7 | 7.6 |
| 4.6 | 7.4 | 7.8 | 8.4 | 7.6 | 7.5 | 7.6 | 8.1 | 7.8 | 7.4 | 7.7 | 7.7 | 7.6 |
| 4.7 | 7.3 | 7.8 | 8.4 | 7.6 | 7.5 | 7.6 | 8.1 | 7.8 | 7.4 | 7.7 | 7.7 | 7.5 |
| 4.8 | 7.2 | 7.7 | 8.3 | 7.5 | 7.4 | 7.4 | 8.1 | 7.6 | 7.3 | 7.6 | 7.6 | 7.4 |

Table F23. Predicted maximum of peak storm $H_{m0}$ ft from BWSim at consequence locations over 57 yr life cycle between 2014 and 2071 with SLR scenario 3.

| Alt .RP | 129 | 132 | 135 | 147 | 166 | 170 | 172 | 185 | 195 | 196 | 198 | 203 |
|---|---|---|---|---|---|---|---|---|---|---|---|---|
| 1.1 | 7.3 | 7.7 | 7.9 | 6.1 | 6.4 | 7.2 | 8.1 | 7.1 | 7.1 | 7.5 | 7.3 | 7.3 |
| 1.2 | 7.3 | 7.7 | 7.9 | 6.1 | 6.4 | 7.2 | 8.1 | 7.1 | 7.1 | 7.5 | 7.3 | 7.3 |
| 1.3 | 7.3 | 7.7 | 7.9 | 6.1 | 6.4 | 7.2 | 8.1 | 7.1 | 7.1 | 7.5 | 7.3 | 7.3 |
| 1.4 | 7.3 | 7.7 | 7.9 | 6.1 | 6.4 | 7.2 | 8.1 | 7.1 | 7.1 | 7.5 | 7.3 | 7.3 |
| 1.5 | 7.3 | 7.7 | 7.9 | 6.1 | 6.4 | 7.2 | 8.1 | 7.1 | 7.1 | 7.5 | 7.3 | 7.3 |
| 1.6 | 7.3 | 7.7 | 7.9 | 6.1 | 6.4 | 7.2 | 8.1 | 7.1 | 7.1 | 7.5 | 7.3 | 7.3 |
| 1.7 | 7.3 | 7.7 | 7.9 | 6.1 | 6.4 | 7.2 | 8.1 | 7.1 | 7.1 | 7.5 | 7.3 | 7.3 |
| 1.8 | 7.3 | 7.7 | 7.9 | 6.1 | 6.4 | 7.2 | 8.1 | 7.1 | 7.1 | 7.5 | 7.3 | 7.3 |
| 2.1 | 8.2 | 8.6 | 8.7 | 7.7 | 7.6 | 7.9 | 8.2 | 8.0 | 7.6 | 8.3 | 8.0 | 8.1 |
| 2.2 | 8.1 | 8.5 | 8.7 | 7.7 | 7.6 | 7.9 | 8.2 | 8.0 | 7.6 | 8.2 | 8.0 | 8.0 |
| 2.3 | 8.0 | 8.4 | 8.6 | 7.7 | 7.6 | 7.9 | 8.2 | 8.0 | 7.6 | 8.2 | 8.0 | 8.0 |
| 2.4 | 7.9 | 8.4 | 8.6 | 7.6 | 7.5 | 7.6 | 8.1 | 7.8 | 7.5 | 8.1 | 7.9 | 7.9 |
| 2.5 | 7.9 | 8.3 | 8.6 | 7.6 | 7.5 | 7.6 | 8.1 | 7.8 | 7.5 | 8.1 | 7.9 | 7.9 |
| 2.6 | 7.9 | 8.3 | 8.6 | 7.6 | 7.5 | 7.6 | 8.1 | 7.8 | 7.5 | 8.1 | 7.9 | 7.9 |
| 2.7 | 7.9 | 8.3 | 8.6 | 7.6 | 7.5 | 7.6 | 8.1 | 7.8 | 7.5 | 8.1 | 7.9 | 7.9 |
| 2.8 | 7.8 | 8.2 | 8.5 | 7.4 | 7.3 | 7.4 | 8.1 | 7.6 | 7.3 | 7.9 | 7.7 | 7.7 |
| 3.1 | 6.1 | 6.5 | 7.0 | 4.6 | 6.0 | 6.6 | 7.9 | 6.3 | 6.7 | 6.4 | 6.6 | 6.4 |
| 3.2 | 6.0 | 6.4 | 6.9 | 4.4 | 6.0 | 6.5 | 7.9 | 6.2 | 6.7 | 6.4 | 6.5 | 6.4 |
| 3.3 | 6.0 | 6.4 | 6.9 | 4.2 | 6.0 | 6.5 | 7.9 | 6.1 | 6.7 | 6.3 | 6.5 | 6.3 |
| 3.4 | 5.9 | 6.4 | 6.9 | 4.2 | 6.0 | 6.5 | 7.9 | 6.1 | 6.7 | 6.3 | 6.5 | 6.3 |
| 3.5 | 5.9 | 6.4 | 6.9 | 4.2 | 6.0 | 6.5 | 7.9 | 6.1 | 6.7 | 6.3 | 6.5 | 6.3 |
| 3.6 | 5.9 | 6.4 | 6.9 | 4.2 | 6.0 | 6.5 | 7.9 | 6.1 | 6.7 | 6.3 | 6.5 | 6.3 |
| 3.7 | 5.9 | 6.4 | 6.9 | 4.2 | 6.0 | 6.5 | 7.9 | 6.1 | 6.7 | 6.3 | 6.5 | 6.3 |
| 3.8 | 5.9 | 6.4 | 6.9 | 4.2 | 6.0 | 6.5 | 7.9 | 6.1 | 6.7 | 6.3 | 6.5 | 6.3 |
| 4.1 | 7.9 | 8.2 | 8.5 | 7.7 | 7.6 | 7.9 | 8.2 | 7.9 | 7.6 | 8.0 | 7.9 | 7.9 |
| 4.2 | 7.7 | 8.1 | 8.5 | 7.7 | 7.6 | 7.9 | 8.2 | 7.9 | 7.6 | 7.9 | 7.9 | 7.8 |
| 4.3 | 7.6 | 8.0 | 8.5 | 7.7 | 7.6 | 7.9 | 8.2 | 7.9 | 7.6 | 7.9 | 7.9 | 7.7 |
| 4.4 | 7.5 | 7.9 | 8.4 | 7.6 | 7.5 | 7.7 | 8.2 | 7.8 | 7.5 | 7.8 | 7.8 | 7.6 |
| 4.5 | 7.4 | 7.9 | 8.4 | 7.6 | 7.5 | 7.7 | 8.2 | 7.8 | 7.5 | 7.8 | 7.8 | 7.6 |
| 4.6 | 7.4 | 7.9 | 8.4 | 7.6 | 7.5 | 7.7 | 8.2 | 7.8 | 7.5 | 7.8 | 7.8 | 7.6 |
| 4.7 | 7.4 | 7.9 | 8.4 | 7.6 | 7.5 | 7.7 | 8.2 | 7.8 | 7.5 | 7.7 | 7.7 | 7.6 |
| 4.8 | 7.3 | 7.8 | 8.4 | 7.6 | 7.4 | 7.4 | 8.1 | 7.7 | 7.3 | 7.6 | 7.6 | 7.5 |

Table F24. Predicted maximum of peak storm $H_{m0}$ in feet from BWSim at consequence locations over 57 yr life cycle between 2014 and 2071 with SLR scenario 4.

| Alt .RP | 129 | 132 | 135 | 147 | 166 | 170 | 172 | 185 | 195 | 196 | 198 | 203 |
|---|---|---|---|---|---|---|---|---|---|---|---|---|
| 1.1 | 7.5 | 7.9 | 8.0 | 6.3 | 6.5 | 7.3 | 8.1 | 7.2 | 7.2 | 7.6 | 7.4 | 7.5 |
| 1.2 | 7.5 | 7.9 | 8.0 | 6.3 | 6.5 | 7.3 | 8.1 | 7.2 | 7.2 | 7.6 | 7.4 | 7.5 |
| 1.3 | 7.5 | 7.9 | 8.0 | 6.3 | 6.5 | 7.3 | 8.1 | 7.2 | 7.2 | 7.6 | 7.4 | 7.5 |
| 1.4 | 7.5 | 7.9 | 8.0 | 6.3 | 6.5 | 7.3 | 8.1 | 7.2 | 7.2 | 7.6 | 7.4 | 7.5 |
| 1.5 | 7.5 | 7.9 | 8.0 | 6.3 | 6.5 | 7.3 | 8.1 | 7.2 | 7.2 | 7.6 | 7.4 | 7.5 |
| 1.6 | 7.5 | 7.9 | 8.0 | 6.3 | 6.5 | 7.3 | 8.1 | 7.2 | 7.2 | 7.6 | 7.4 | 7.5 |
| 1.7 | 7.5 | 7.9 | 8.0 | 6.3 | 6.5 | 7.3 | 8.1 | 7.2 | 7.2 | 7.6 | 7.4 | 7.5 |
| 1.8 | 7.5 | 7.9 | 8.0 | 6.3 | 6.5 | 7.3 | 8.1 | 7.2 | 7.2 | 7.6 | 7.4 | 7.5 |
| 2.1 | 8.4 | 8.8 | 8.8 | 7.9 | 7.7 | 8.0 | 8.3 | 8.1 | 7.7 | 8.5 | 8.2 | 8.2 |
| 2.2 | 8.3 | 8.7 | 8.8 | 7.9 | 7.7 | 8.0 | 8.3 | 8.1 | 7.7 | 8.4 | 8.1 | 8.2 |
| 2.3 | 8.2 | 8.6 | 8.8 | 7.9 | 7.7 | 8.0 | 8.3 | 8.1 | 7.7 | 8.4 | 8.1 | 8.1 |
| 2.4 | 8.1 | 8.5 | 8.7 | 7.8 | 7.6 | 7.7 | 8.2 | 8.0 | 7.6 | 8.3 | 8.0 | 8.0 |
| 2.5 | 8.1 | 8.5 | 8.7 | 7.8 | 7.6 | 7.7 | 8.2 | 8.0 | 7.6 | 8.2 | 8.0 | 8.0 |
| 2.6 | 8.1 | 8.5 | 8.7 | 7.8 | 7.6 | 7.7 | 8.2 | 8.0 | 7.6 | 8.2 | 8.0 | 8.0 |
| 2.7 | 8.1 | 8.5 | 8.7 | 7.8 | 7.6 | 7.7 | 8.2 | 8.0 | 7.6 | 8.2 | 8.0 | 8.0 |
| 2.8 | 7.9 | 8.4 | 8.6 | 7.6 | 7.5 | 7.5 | 8.1 | 7.8 | 7.4 | 8.1 | 7.9 | 7.9 |
| 3.1 | 6.3 | 6.7 | 7.1 | 4.7 | 6.0 | 6.6 | 8.0 | 6.4 | 6.8 | 6.6 | 6.7 | 6.6 |
| 3.2 | 6.2 | 6.6 | 7.1 | 4.6 | 6.0 | 6.6 | 8.0 | 6.3 | 6.8 | 6.5 | 6.6 | 6.5 |
| 3.3 | 6.1 | 6.5 | 7.0 | 4.4 | 6.0 | 6.6 | 8.0 | 6.2 | 6.7 | 6.5 | 6.6 | 6.5 |
| 3.4 | 6.1 | 6.5 | 7.0 | 4.4 | 6.0 | 6.6 | 8.0 | 6.2 | 6.7 | 6.5 | 6.6 | 6.5 |
| 3.5 | 6.1 | 6.5 | 7.0 | 4.4 | 6.0 | 6.6 | 8.0 | 6.2 | 6.7 | 6.5 | 6.6 | 6.5 |
| 3.6 | 6.1 | 6.5 | 7.0 | 4.4 | 6.0 | 6.6 | 8.0 | 6.2 | 6.7 | 6.5 | 6.6 | 6.5 |
| 3.7 | 6.1 | 6.5 | 7.0 | 4.4 | 6.0 | 6.6 | 8.0 | 6.2 | 6.7 | 6.5 | 6.6 | 6.5 |
| 3.8 | 6.1 | 6.5 | 7.0 | 4.4 | 6.0 | 6.6 | 8.0 | 6.2 | 6.7 | 6.5 | 6.6 | 6.5 |
| 4.1 | 8.1 | 8.3 | 8.7 | 7.9 | 7.7 | 8.0 | 8.3 | 8.1 | 7.7 | 8.2 | 8.0 | 8.0 |
| 4.2 | 7.8 | 8.2 | 8.6 | 7.9 | 7.7 | 8.0 | 8.3 | 8.1 | 7.7 | 8.1 | 8.0 | 7.9 |
| 4.3 | 7.7 | 8.2 | 8.6 | 7.9 | 7.7 | 8.0 | 8.3 | 8.1 | 7.7 | 8.0 | 8.0 | 7.9 |
| 4.4 | 7.7 | 8.1 | 8.6 | 7.8 | 7.6 | 7.8 | 8.2 | 7.9 | 7.6 | 8.0 | 7.9 | 7.8 |
| 4.5 | 7.6 | 8.1 | 8.6 | 7.8 | 7.6 | 7.8 | 8.2 | 7.9 | 7.6 | 7.9 | 7.9 | 7.8 |
| 4.6 | 7.6 | 8.1 | 8.6 | 7.8 | 7.6 | 7.8 | 8.2 | 7.9 | 7.6 | 7.9 | 7.9 | 7.8 |
| 4.7 | 7.6 | 8.0 | 8.6 | 7.8 | 7.6 | 7.8 | 8.2 | 7.9 | 7.6 | 7.9 | 7.9 | 7.7 |
| 4.8 | 7.4 | 7.9 | 8.5 | 7.7 | 7.5 | 7.5 | 8.1 | 7.8 | 7.4 | 7.8 | 7.7 | 7.6 |

Table F25. Predicted maximum of peak storm $H_{m0}$ in feet from BWSim at consequence locations over 57 yr life cycle between 2014 and 2071 with SLR scenario 5.

| Alt .RP | 129 | 132 | 135 | 147 | 166 | 170 | 172 | 185 | 195 | 196 | 198 | 203 |
|---|---|---|---|---|---|---|---|---|---|---|---|---|
| 1.1 | 7.7 | 8.1 | 8.1 | 6.4 | 6.6 | 7.3 | 8.2 | 7.3 | 7.3 | 7.8 | 7.5 | 7.6 |
| 1.2 | 7.7 | 8.1 | 8.1 | 6.4 | 6.6 | 7.3 | 8.2 | 7.3 | 7.3 | 7.8 | 7.5 | 7.6 |
| 1.3 | 7.7 | 8.1 | 8.1 | 6.4 | 6.6 | 7.3 | 8.2 | 7.3 | 7.3 | 7.8 | 7.5 | 7.6 |
| 1.4 | 7.7 | 8.1 | 8.1 | 6.4 | 6.6 | 7.3 | 8.2 | 7.3 | 7.3 | 7.8 | 7.5 | 7.6 |
| 1.5 | 7.7 | 8.1 | 8.1 | 6.4 | 6.6 | 7.3 | 8.2 | 7.3 | 7.3 | 7.8 | 7.5 | 7.6 |
| 1.6 | 7.7 | 8.1 | 8.1 | 6.4 | 6.6 | 7.3 | 8.2 | 7.3 | 7.3 | 7.8 | 7.5 | 7.6 |
| 1.7 | 7.7 | 8.1 | 8.1 | 6.4 | 6.6 | 7.3 | 8.2 | 7.3 | 7.3 | 7.8 | 7.5 | 7.6 |
| 1.8 | 7.7 | 8.1 | 8.1 | 6.4 | 6.6 | 7.3 | 8.2 | 7.3 | 7.3 | 7.8 | 7.5 | 7.6 |
| 2.1 | 8.6 | 8.9 | 9.0 | 8.0 | 7.9 | 8.1 | 8.3 | 8.2 | 7.8 | 8.6 | 8.3 | 8.4 |
| 2.2 | 8.4 | 8.8 | 8.9 | 8.0 | 7.8 | 8.1 | 8.3 | 8.2 | 7.8 | 8.6 | 8.3 | 8.3 |
| 2.3 | 8.3 | 8.8 | 8.9 | 8.0 | 7.8 | 8.1 | 8.3 | 8.2 | 7.8 | 8.5 | 8.2 | 8.3 |
| 2.4 | 8.3 | 8.7 | 8.9 | 8.0 | 7.8 | 7.8 | 8.3 | 8.1 | 7.6 | 8.4 | 8.1 | 8.2 |
| 2.5 | 8.2 | 8.7 | 8.9 | 8.0 | 7.8 | 7.8 | 8.3 | 8.1 | 7.6 | 8.4 | 8.1 | 8.2 |
| 2.6 | 8.2 | 8.7 | 8.9 | 8.0 | 7.8 | 7.8 | 8.3 | 8.1 | 7.6 | 8.4 | 8.1 | 8.2 |
| 2.7 | 8.2 | 8.7 | 8.9 | 8.0 | 7.8 | 7.8 | 8.3 | 8.1 | 7.6 | 8.4 | 8.1 | 8.2 |
| 2.8 | 8.1 | 8.6 | 8.7 | 7.8 | 7.6 | 7.6 | 8.2 | 7.9 | 7.5 | 8.3 | 8.0 | 8.0 |
| 3.1 | 6.4 | 6.8 | 7.3 | 4.9 | 6.0 | 6.7 | 8.0 | 6.4 | 6.8 | 6.7 | 6.8 | 6.7 |
| 3.2 | 6.3 | 6.7 | 7.2 | 4.7 | 6.0 | 6.7 | 8.0 | 6.4 | 6.8 | 6.6 | 6.7 | 6.6 |
| 3.3 | 6.2 | 6.7 | 7.1 | 4.5 | 6.0 | 6.6 | 8.0 | 6.3 | 6.8 | 6.6 | 6.7 | 6.6 |
| 3.4 | 6.2 | 6.7 | 7.1 | 4.5 | 6.0 | 6.6 | 8.0 | 6.3 | 6.8 | 6.6 | 6.7 | 6.6 |
| 3.5 | 6.2 | 6.7 | 7.1 | 4.5 | 6.0 | 6.6 | 8.0 | 6.3 | 6.8 | 6.6 | 6.7 | 6.6 |
| 3.6 | 6.2 | 6.7 | 7.1 | 4.5 | 6.0 | 6.6 | 8.0 | 6.3 | 6.8 | 6.6 | 6.7 | 6.6 |
| 3.7 | 6.2 | 6.7 | 7.1 | 4.5 | 6.0 | 6.6 | 8.0 | 6.3 | 6.8 | 6.6 | 6.7 | 6.6 |
| 3.8 | 6.2 | 6.7 | 7.1 | 4.5 | 6.0 | 6.6 | 8.0 | 6.3 | 6.8 | 6.6 | 6.7 | 6.6 |
| 4.1 | 8.3 | 8.5 | 8.8 | 8.0 | 7.8 | 8.1 | 8.3 | 8.2 | 7.8 | 8.3 | 8.2 | 8.2 |
| 4.2 | 8.0 | 8.4 | 8.8 | 8.0 | 7.8 | 8.1 | 8.3 | 8.2 | 7.8 | 8.2 | 8.1 | 8.1 |
| 4.3 | 7.9 | 8.3 | 8.8 | 8.0 | 7.8 | 8.1 | 8.3 | 8.2 | 7.7 | 8.2 | 8.1 | 8.0 |
| 4.4 | 7.8 | 8.3 | 8.7 | 8.0 | 7.8 | 7.9 | 8.3 | 8.1 | 7.7 | 8.1 | 8.0 | 7.9 |
| 4.5 | 7.8 | 8.2 | 8.7 | 8.0 | 7.8 | 7.9 | 8.3 | 8.1 | 7.6 | 8.1 | 8.0 | 7.9 |
| 4.6 | 7.8 | 8.2 | 8.7 | 8.0 | 7.8 | 7.9 | 8.3 | 8.1 | 7.6 | 8.1 | 8.0 | 7.9 |
| 4.7 | 7.7 | 8.2 | 8.7 | 8.0 | 7.8 | 7.9 | 8.3 | 8.1 | 7.6 | 8.1 | 8.0 | 7.9 |
| 4.8 | 7.6 | 8.1 | 8.6 | 7.9 | 7.7 | 7.6 | 8.2 | 7.9 | 7.5 | 7.9 | 7.9 | 7.8 |

# REPORT DOCUMENTATION PAGE

*Form Approved*
*OMB No. 0704-0188*



| 1. REPORT DATE | 2. REPORT TYPE | 3. DATES COVERED *(From - To)* |
|---|---|---|
| August 2015 | Technical Report | |

**4. TITLE AND SUBTITLE**

Point Judith, Rhode Island, Breakwater Risk Assessment

**5a. CONTRACT NUMBER**

**5b. GRANT NUMBER**

**5c. PROGRAM ELEMENT NUMBER**

**6. AUTHOR(S)**

Jeffrey A. Melby, Norberto C. Nadal-Caraballo, and John Winkelman

**5d. PROJECT NUMBER**

**5e. TASK NUMBER**

**5f. WORK UNIT NUMBER**

**7. PERFORMING ORGANIZATION NAME(S) AND ADDRESS(ES)**

Coastal and Hydraulics Laboratory
U.S. Army Engineer and Development Center
3090 Halls Ferry Road
Vicksburg, MS 39180-6199

**8. PERFORMING ORGANIZATION REPORT NUMBER**

ERDC/CHL TR-15-13

**9. SPONSORING/MONITORING AGENCY NAME(S) AND ADDRESS(ES)**

U.S. Army Corps of Engineers
New England District
696 Virginia Road
Concord, MA 01742-2751

**10. SPONSOR/MONITOR'S ACRONYM(S)**

USACE NAE

**11. SPONSOR/MONITOR'S REPORT NUMBER(S)**

**12. DISTRIBUTION/AVAILABILITY STATEMENT**

Approved for public release; distribution is unlimited.

**13. SUPPLEMENTARY NOTES**

**14. ABSTRACT**

Point Judith breakwaters were built between 1891 and 1914. Three structures provide shelter for refuge, search and rescue operations, a commercial harbor, and a sandy, recreational shoreline. The Main breakwater is presently in a severely damaged state, and its functional efficiency compared to the as-built condition is unknown. This report provides a summary of a life-cycle risk assessment of the Point Judith Main breakwater. The report summarizes the Point Judith breakwater history, the present condition, the historical offshore wave climate in the area, nearshore wave and water level climate, probabilistic characteristics of the historical wave and water level climate, simulated breakwater damage and wave overtopping transmission, and resulting wave climate in the protected bay. Future sea level rise and its implications on structure performance are analyzed. Several rehabilitation alternatives are designed and then subjected to life cycles of storms with and without sea level rise. The results of the life-cycle study are discussed in the context of the future performance with and without rehabilitation.

| 15. SUBJECT TERMS | | |
|---|---|---|
| Risk | Life cycle | Storm |
| Breakwater | Damage | Probabilistic analysis |
| | Sea level change | |

| 16. SECURITY CLASSIFICATION OF: | | | 17. LIMITATION OF ABSTRACT | 18. NUMBER OF PAGES | 19a. NAME OF RESPONSIBLE PERSON |
|---|---|---|---|---|---|
| a. REPORT | b. ABSTRACT | c. THIS PAGE | | | Jeffrey A. Melby, PhD |
| Unclassified | Unclassified | Unclassified | Unlimited | 186 | **19b. TELEPHONE NUMBER** *(Include area code)* 601-634-2062 |